

**Mechanistic Investigation of the Transcriptional Coactivator Med25 and its
Protein-Protein Interaction Network**

by

Matthew S. Beyersdorf

A dissertation submitted in partial fulfillment
of the requirements for the degree of
Doctor of Philosophy
(Chemical Biology)
in the University of Michigan
2017

Doctoral Committee:

Professor Anna K. Mapp, Co-Chair
Professor David H. Sherman, Co-Chair
Professor Carol A. Fierke
Professor Janet Smith
Associate Professor Zaneta Nikolovska-Coleska

© Matthew S. Beyersdorf
msbeyers@umich.edu
ORCID iD: 0000-0002-9400-4234
All Rights Reserved, 2017

Acknowledgements

The road to a PhD offers a multitude of unique challenges and mental stresses. Completing this dissertation has been the most rewarding professional experience of my short life; I expect that it will remain to be so for a long time to come. I fought hard to get here and for that, I will forever be immensely proud. However, that all said, I could not have accomplished such a large feat without many people by my side along the way.

I would like to acknowledge and thank my two co-chairs – Professors Anna Mapp and David Sherman. They have been wonderful mentors and advocates for me throughout my time at Michigan. They allowed me to try out multiple research avenues and to grow independently as a research scientist and analytical thinker while always making sure that I kept the broader picture in mind. David taught me how to function and thrive within large teams and organizations. Anna has cultivated an incredible culture within her laboratory that I benefited tremendously from. Finally, as a mentor and leader, Anna displays the character, integrity, and compassion that I strive to emulate in my life.

I would like to acknowledge my other committee members – Professors Carol Fierke, Janet Smith, and Zaneta Nikolovska-Coleska. Their advice regarding both my research and my future career has been invaluable towards bettering my dissertation and expanding what I think is possible.

I would like to acknowledge my previous research advisor, Professor Chris Halkides at the University of North Carolina Wilmington. He taught me how to rigorously perform scientific research and the value of writing manuscripts as quickly as possible.

I would like to thank all my colleagues in both the Sherman and Mapp labs. Both sets of people have been incredibly wonderful peers and friends. Everyone has always

been willing to offer advice on research problems and, in many cases, provide direct research expertise. Dr. Ningkun Wang and Dr. Doug Hansen were terrific rotation mentors who taught me a great deal about the biochemistry of transcriptional coactivation domains and the challenges of organic synthesis and microbial fermentation, respectively. Dr. Ashu Tripathi was a critical collaborator in the natural products discovery pipeline who provided guidance throughout several junctures of my PhD. Dr. Steve Sturlis and Dr. Paul Bruno were fantastic colleagues who started the broader Med25 AcID project that has already been central to four doctorates, including their own, and will be central to many more in the future. Their early contributions to our understanding of this protein will always be a critical part of the Med25 story in the Mapp lab. I joined my two research labs with many wonderful peers and friends including freshly minted doctors from the Mapp lab - Andy Henderson and Cassie Joiner and future doctors from the Sherman lab – Matt DeMars, Aaron Koch, Shasha Li, and Jennifer Schmidt. I will miss working and laughing alongside each of them. Andy Henderson has been a true confidant in the Mapp lab; We spent countless hours complaining about and discussing big and small research problems and our lives and futures.

I would like to thank the entirety of the Chemical Biology program and especially the 2012-2013 cohort. My cohort has been quite close throughout our years here at Michigan and their friendship has meant a lot to me. We spent fake holidays and Super Bowls together, played board games and imbibed at each other's' houses, danced nights away at Live. We celebrated milestones – passing of candidacy exams, weddings, and now, successful doctoral defenses. Thanks for helping to brighten the cold winters.

I would like to acknowledge my family including those specifically unmentioned below for sticking by my side throughout all my triumphs and travails. My Dad and Mum have been incredibly supportive in this dream to attain a doctorate and raised me to enjoy hard work and to think critically about the world around me. I love them both so dearly and will always be there for them as they have been for me. My sisters have been equally supportive and loving my whole life. Janet is always a friend who is willing to sit and chat on the phone; Her laughter brings me so much happiness. Kate has inspired me daily. After college, she bravely moved by herself to the middle of Kansas in pursuit of her dreams. If my younger sister is that brave and determined, I better be as well. Lesley has been an emotional rock for everyone in my family at one point or another; She remains one of the warmest people that I know. It has been a blessing to live nearby Hillary and my amazing niece Caroline. I have loved spending time laughing and talking with both.

I would like to finally acknowledge my beautiful housemates – Lucy Huber and our three cats. Lucy is the funniest, wittiest, and most generous person that I have ever known. I don't think that I could have successfully navigated through this process without having her with me. The twenty-five minutes that we spent walking from our house to coffee and finally to Ithaca were the best moments of each day of graduate school during the final two years. When I think back on our time in Ann Arbor, I'll remember that she let me make up songs until we reached the park, that once every month we'd dramatically read the Old West Side News, and that we learned to love each other more than I thought possible during each of those wonderful commutes.

Tables of Contents

Acknowledgements	ii
List of Figures	ix
List of Tables	xiv
Abbreviations	xv
Abstract	xvii
Chapter One: Targeting protein-protein interactions involved in transcription	
A. Abstract	1
B. Protein-protein interactions in transcription	2
<i>Multidomain coactivator complexes</i>	<i>3</i>
<i>Transcriptional protein-protein interactions and disease</i>	<i>6</i>
<i>Features of transcriptional protein-protein interactions</i>	<i>7</i>
C. Small molecule modulation of transcriptional protein-protein interactions	9
<i>Difficulties in targeting transcriptional protein-protein interactions</i>	<i>9</i>
<i>Natural products to target transcriptional protein-protein interactions</i>	<i>10</i>
<i>Fragment screening to target transcriptional protein-protein interactions</i>	<i>13</i>
<i>Fragment screening using NMR methodologies</i>	<i>15</i>
D. Dissertation summary	17
E. References	19
Chapter Two: Investigation of Med25 AcID and its protein-protein network	
A. Abstract	29
B. Introduction	30
<i>Mediator subunit Med25 and AcID motif</i>	<i>30</i>
<i>Med25 AcID-activator protein-protein interactions</i>	<i>32</i>
<i>Role of electrostatic contacts in Med25 PPIs</i>	<i>34</i>
C. Results and discussion	34
<i>Characterization of the Med25 AcID-CBP protein-protein interaction</i>	<i>34</i>

<i>Characterization of the Med25 AcID-ATF6α protein-protein interaction...</i>	41
<i>Mutational analysis of Med25 to define binding models.....</i>	46
D. Conclusions and future directions	59
E. Materials and methods	62
F. References	72

Chapter Three: Defining binding mechanisms of Med25 AcID and its protein-protein interaction network using protein-observed ¹⁹F-NMR

A. Abstract	75
B. Introduction	76
<i>Limitations of ¹H, ¹⁵N-HSQC NMR in study of protein-protein interactions</i>	<i>76</i>
<i>Protein-observed ¹⁹F-NMR for study of protein-protein interactions</i>	<i>77</i>
<i>PrOF NMR for study of Med25 AcID and its protein-protein interaction network</i>	<i>78</i>
C. Results and discussion	
<i>Biochemical characterization of fluorinated Med25 variants</i>	<i>81</i>
<i>Assignment of 3FY resonances</i>	<i>86</i>
<i>PrOF NMR titrations with Med25-interacting peptides against 3FY Med25 AcID.....</i>	<i>88</i>
<i>PrOF NMR titrations with Med25-interacting peptides against 5FW Med25 AcID.....</i>	<i>99</i>
<i>Binding models for unique peptide interactions with Med25 AcID</i>	<i>102</i>
<i>Protein-observed ¹⁹F-NMR experiments demonstrate model of Med25 AcID inhibition induced by norstictic acid.....</i>	<i>111</i>
<i>PrOF NMR allows for characterization and development of a small molecule fragment that targets Med25 AcID.....</i>	<i>115</i>
D. Conclusions and future directions	123
E. Materials and methods	128
F. References	131

Chapter Four: Small molecule inhibition of Med25-activator interactions

A. Abstract	134
B. Introduction	135
<i>Difficulties in targeting protein-protein interactions</i>	135
<i>Natural products for the inhibition of protein-protein interactions</i>	135
<i>Molecular inhibition of Med25 AcID for study of disease</i>	136
<i>Initial success in demonstrating that Med25 can be targeted with small molecules</i>	138
C. Results and discussion	139
<i>NMR fragment screening allows for rapid discovery of weak-to-moderate affinity ligands</i>	139
<i>PrOF NMR presents a sensitive screening methodology for the discovery of small molecule fragments that target Med25 AcID</i>	140
<i>A naturally occurring lipopeptide demonstrates selective inhibition of Med25 AcID</i>	149
<i>The 34913 lipopeptide is an effective inhibitor of Med25 function in a cellular context</i>	157
D. Conclusions and future directions	161
E. Materials and methods	165
F. References	168

Chapter Five: Conclusions and future directions

A. Summary	172
B. Conclusions	173
C. Future Directions	176
<i>34913 lipopeptide will be used to study the role of Med25 in ATF6α transcriptional processes the unfolded protein response</i>	176
<i>The role of PTOV1 will be determined through the biochemical study of its AcID domains</i>	178
D. Materials and Methods	182
E. References	184

Appendix

A. The identification of a CBP-CBP protein-protein interaction presents a potential mechanism for the regulation of CBP function.....	186
B. An identified intramolecular salt bridge within Med25 AcID is likely important for Med25 function and stability	192
C. Garcinolic acid is an effective but non-selective inhibitor of Med25 AcID	195
D. Follow-up of a Natural Product Extracts screen against Med25-ERM ..	209
E. References.....	223

List of Figures

Figure 1.1. Model of transcriptional regulation.	3
Figure 1.2. The Mediator complex is a critical coactivator hub.	5
Figure 1.3. Structural organization of the hub coactivator CBP/p300.	6
Figure 1.4. Diversity of transcriptional protein-protein interactions.	8
Figure 1.5. Small molecule modulation of diverse classes of protein-protein interactions.	10
Figure 1.6. Examples of natural product small molecules.	12
Figure 2.1. Domain architecture of Med25 and the structure of the AcID motif.	31
Figure 2.2. Med25 AcID contains multiple binding sites.	33
Figure 2.3. Sequence alignment of CBP(20-44) and VP16(454-486).	35
Figure 2.4. Minimal Med25 AcID-interacting sequences of CBP.	36
Figure 2.5. Acetylated CBP(20-44) inhibits Med25 AcID interaction with Fluorescein-CBP(20-44).	37
Figure 2.6. ¹ H- ¹⁵ N-HSQC NMR spectra of Med25 AcID-CBP(20-44) complexes.	38
Figure 2.7. Chemical shift perturbations within Med25 AcID induced by saturating CBP(20-44) conditions.	39
Figure 2.8. Chemical shift perturbations within Med25 AcID induced by saturating CBP(20-44) conditions.	40
Figure 2.9. Sequence alignment of ATF6α(42-67) and VP16(423-448).	42
Figure 2.10. Minimal Med25 AcID-interacting sequences of ATF6α.	43
Figure 2.12. Chemical shift perturbations within Med25 AcID induced by saturating ATF6α conditions.	44
Figure 2.13. Chemical shift perturbations within Med25 AcID induced by saturating ATF6α conditions.	45
Figure 2.14. Mutagenesis at H1 site of Med25 AcID.	47
Figure 2.15. Mutagenesis at H2 site of Med25 AcID.	50
Figure 2.17 Mutagenesis to block H1 and H2 sites simultaneously.	53
Figure 2.18. Chemical shift perturbations within Med25 AcID induced by tethered VP16 G450C peptide.	56

Figure 2.19 Mutant Med25-G450C peptide complexes to block H1 and H2 sites simultaneously.	57
Figure 3.1. Representation of 3FY Med25 AcID.....	79
Figure 3.2. Representation of 5FW Med25 AcID.....	80
Figure 3.3. Mass spectrometry of fluorinated Med25 AcID variants.	82
Figure 3.4 Structural stability of fluorinated Med25 AcID variants.	83
Figure 3.5. ¹⁹ F-NMR spectra of fluorinated Med25 AcID variants.	85
Figure 3.6. Assignment of Y432 and Y528 resonances of 3FY Med25.	86
Figure 3.7. Assignment of Y487 and Y515 resonances of 3FY Med25.	88
Figure 3.8. PrOF NMR of 3FY Med25 AcID-VP16 H1 complexes.....	89
Figure 3.9. PrOF NMR of 3FY Med25 AcID-VP16 H2 complexes.....	91
Figure 3.10. PrOF NMR of 3FY Med25 AcID-VP16(438-490) complexes.....	92
Figure 3.11. PrOF NMR of 3FY Med25 AcID-ATF6 α (40-66) complexes.....	94
Figure 3.12. PrOF NMR of 3FY Med25 AcID-CBP(20-55) complexes.	95
Figure 3.13. PrOF NMR of 3FY Med25 AcID-ERM(38-68) complexes.....	97
Figure 3.14. PrOF NMR of 5FW Med25 AcID complexes.	100
Figure 3.15. PrOF NMR of 5FW Med25 AcID in complex with 1 eq ERM(38-68).	101
Figure 3.16. Model of the Med25 AcID-VP16 H1 PPI.	103
Figure 3.17. Model of the Med25 AcID-VP16 H2 PPI.	104
Figure 3.18. Model of the Med25 AcID-VP16(438-490) PPI.....	105
Figure 3.19. Model of the Med25 AcID-ERM PPI.....	107
Figure 3.20. Model of the Med25 AcID-ATF6 α PPI.....	109
Figure 3.21. Model of the Med25 AcID-CBP PPI.	110
Figure 3.22. Labeling of 3FY Med25 AcID with norstictic acid.	112
Figure 3.23. PrOF NMR of 3FY Med25 AcID labeled with norstictic acid.....	113
Figure 3.24. Model of norstictic acid labeling of Med25 AcID.....	115
Figure 3.25. Structures of fragment A6.	116
Figure 3.26. Mutant Med25-A6 complexes fail to block H1 and H2 sites simultaneously.	117
Figure 3.27. PrOF NMR of 3FY Med25 AcID labeled with VP16 G450C peptide or fragment A6.....	119

Figure 3.28. Structures of A6 derivatives.	121
Figure 3.29. PrOF NMR of 3FY Med25 AcID labeled with A6 or A6 derivatives.	122
Figure 3.30. PrOF NMR of Med25 AcID labeled with trifluoroacetone.	127
Figure 4.1. Depside and depsidones that target CBP KIX and Med25 AcID	138
Figure 4.2. Fragment EN300-51104 is a weak inhibitor of Med25 AcID.....	140
Figure 4.3. PrOF NMR of 3FY Med25 AcID in presence of EN300-51104.....	141
Figure 4.4. Generation of fragment library for PrOF NMR screening.	142
Figure 4.5. PrOF NMR of fragment mixtures not classified as hits.....	144
Figure 4.6. PrOF NMR of fragment mixtures classified as hits.....	145
Figure 4.7. Chemical shift perturbations of 3FY Med25 AcID residues in PrOF NMR fragment screening.....	146
Figure 4.8. Secondary screening of PrOF NMR fragment mixtures.	147
Figure 4.9. Structures of discovered fragments in PrOF NMR screen of Med25 AcID.	148
Figure 4.10. 34913 lipopeptide is a potent inhibitor of the Med25-ATF6 α PPI.	150
Figure 4.11. Inhibitory effects of 34913 lipopeptide against CBP KIX.	151
Figure 4.12. ^1H - ^{15}N -HSQC NMR spectra of Med25 AcID in complex with 34913 lipopeptide.....	152
Figure 4.13. Chemical shift perturbations within Med25 AcID induced by saturating 34913 lipopeptide.	153
Figure 4.14. Chemical shift perturbations induced by 34913 lipopeptide mapped on Med25 AcID.	155
Figure 4.15. Overlay of ATF6 α (40-66)-induced and 34913 lipopeptide-induced Med25 AcID chemical shifts in HSQC NMR.....	155
Figure 4.16. PrOF NMR of 3FY Med25 AcID in complex with 34913 lipopeptide.....	156
Figure 4.17. Inhibition of a Med25-dependent luciferase reporter by the 34913 lipopeptide.....	158
Figure 4.18. Inhibition of the Med25 AcID-ATF6 α PPI in a cellular context by the 34913 lipopeptide.....	160
Figure 4.19. Structures and activity of 34913 lipopeptide derivatives.....	164
Figure 5.1. Three critical activators bind Med25 AcID in three unique binding modes.	175
Figure 5.2. Activation of ATF6 α and GRP78.	177

Figure 5.3. Domain architecture of PTOV1 and structure of the AcID motif.	179
Figure 5.4. Production of PTOV1 AcID-A and AcID-B.....	181
Figure A.1. Sequence alignment of CBP(20-44) and VP16(454-486).	186
Figure A.2. CBP-derived peptides bind to the KIX domain of CBP.	187
Figure A.3. Chemical shift perturbations within CBP KIX induced by complexation with CBP(20-44).	188
Figure A.4. Chemical shift perturbations induced by CBP(20-44) mapped on CBP KIX.	189
Figure A.5. Proposed model for CBP regulation by the CBP-CBP interaction.	191
Figure A.6. Intramolecular salt bridge within Med25 AcID.....	193
Figure A.7. Garcinolic acid targets several transcriptional coactivation domains.	195
Figure A.8. ¹ H- ¹⁵ N-HSQC NMR spectra of Med25 AcID-garcinolic acid complexes. ..	198
Figure A.9. Chemical shift perturbations within Med25 AcID induced by saturating garcinolic acid conditions.	199
Figure A.10. Chemical shift perturbations induced by garcinolic acid mapped on Med25 AcID.	199
Figure A.11. PrOF NMR of 3FY Med25 AcID in complex with garcinolic acid.....	201
Figure A.12. ¹ H- ¹⁵ N-HSQC NMR spectra of CBP KIX-garcinolic acid complexes.	202
Figure A.13. Chemical shift perturbations within CBP KIX induced by saturating garcinolic acid conditions.	203
Figure A.14. Chemical shift perturbations induced by garcinolic acid mapped on CBP KIX.	204
Figure A.15. PrOF NMR of 3FY CBP KIX in complex with garcinolic acid.	206
Figure A.16. Garcinolic acid likely binds near the MLL site within CBP KIX.	207
Figure A.17. Workflow for the re-growth of NPE strains from the primary screen	212
Figure A.18. Inhibitory activity of selected Natural Product Extract Strains in Med25- dependent luciferase assay.....	213
Figure A.19. HPLC purification of 91085 C18-75:25.	216
Figure A.20. HPLC purification of 91085 C18-75:25/HPLC-22.....	217
Figure A.21 Cellular activity of 91085 C18-75:25/HPLC-22/HPLC-15.5 min.	218

Figure A.22 HPLC purifications of 91085 C18-75:25 are not reproducible from one growth of 91085 to the next.....	219
Figure A.23 Sequential HPLC purifications of 91085 C18-60:40.....	220
Figure A.24 Characterization of 91085 C18-60:40/HPLC-"28.5min"/HPLC-137.	221
Figure A.25 Comparison of stictic acid and norstictic acid.	222

List of Tables

Table 1.1. Examples of small molecules fragment modulators of protein-protein interactions.....	14
Table 3.1 Dissociation constants for Med25-interacting peptides to 3FY Med25 AcID.	83
Table A.1. Summary of the inhibitory effects of garcinolic acid.	196
Table A.2. Natural Product Extracts selected for initial follow-up after the NPE primary screen.	210
Table A.3. Analysis of inhibitory activity of re-grown NPE strains.	213
Table A.4. NPE strains grown at medium-scale.	214
Table A.5. Inhibitory activity of C18 fractionated NPE strains.	214

Abbreviations

HSQC	$^1\text{H}, ^{15}\text{N}$ -Heteronuclear single quantum coherence
ATF6 α	Activation transcription factor 6 α
AcID	Activator interaction domain
CBP	CREB-binding protein
CD	Circular dichroism
CH1	Cysteine-histidine rich 1
DBD	DNA-Binding Domain
DMEM	Dulbecco's modified eagle medium
DMSO	Dimethyl sulfoxide
DTT	Dithiothreitol
DNA	Deoxyribonucleic acid
E1A	Adenovirus-encoded E1A 13S protein
ESX	Epithelial specific transcription factor
FBS	Fetal bovine serum
FITC	Fluorescein isothiocyanate
FP	Fluorescence polarization
GST	Glutathione transferase
HEPES	4-(2-hydroxyethyl)-1-piperazineethanesulfonic acid
HPLC	High performance liquid chromatography
HSQC	Heteronuclear single quantum coherence spectroscopy
HTS	High throughput screen
IC ₅₀	Half-maximal inhibitory concentration

IPTG	Isopropyl- β -D-1-thiogalactopyranoside
KIX	Kinase-inducible domain interacting domain
LC-MS	Liquid chromatography mass spectrometry
MS	Mass spectrometry
Med25	Mediator subunit 25
MLL	Multi-lineage leukemia
MMP	Matrix metalloproteinase
mRNA	Messenger RNA
Ni-NTA	Nickel nitrilotriacetic acid
NMR	Nuclear magnetic resonance
PDB	Protein DataBank
PPI	Protein-protein interaction
PrOF	Protein-observed fluorine NMR
RAR α	Retinoic acid receptor α
RNA	Ribonucleic acid
RT-qPCR	Reverse transcription quantitative polymerase chain reaction
SDS-PAGE	Sodium dodecyl sulfate polyacrylamide gel electrophoresis
TAD	Transcriptional activation domain
VP16	Herpes simplex virus protein 16
VWA	Von Willebrand factor type A

Abstract

Regulation of transcription through protein complex assembly is critical for the maintenance of cellular homeostasis. Dysregulation of transcription is unexpectedly a cause or consequence of most human disease. Thus, there is significant therapeutic potential in discovering novel mechanisms to restore normal protein-protein interaction (PPI) networks in transcription. Targeting these transcriptional PPIs with small molecules has historically been challenging as the interactions occur over broad surface areas with relatively weak binding affinities. Within this dissertation, I describe two emergent strategies, namely natural products screening and protein-observed ^{19}F -NMR, that allowed for the identification of small molecule inhibitors of the activator interaction domain (AcID) of Med25, a critical coactivator protein in transcription.

Med25 AcID is a transcriptional coactivation domain that interacts with several transcriptional activators that have been implicated in cancer and disease, including the ETV/PEA3 family and the oxidative stress response factor ATF6 α . An overarching goal of this dissertation was to identify small molecule inhibition of Med25 AcID that will allow for future study of the role of Med25 in cancer processes such as metastasis and tumorigenesis.

This dissertation first describes the mechanistic details that define the interactions between Med25 AcID and its native protein partners to enable the identification of small molecules that selectively inhibit Med25 AcID. As demonstrated, the AcID motif interacts with each of its binding partners using discrete modes of molecular recognition. The significant differences between the interactions of Med25 AcID with the ERM and ATF6 α activators (*e.g.* differences in binding locations and relative dependence on electrostatic

interactions) highlight the diversity of molecular mechanisms through which Med25 AcID functions. Small molecule inhibitors of Med25 AcID were then identified, guided by these mechanistic details. Natural products discovery and protein-observed ^{19}F -NMR were leveraged to target Med25 AcID, which interacts with its protein partners over broad surface areas with relatively weak binding affinities. These two strategies have provided recent successes for other transcriptional PPIs. The 34913 lipopeptide, which exhibits effective inhibition of the Med25-ATF6 α PPI in a cellular context, and nine preliminary hit fragments were successfully identified using those strategies. Collectively, this dissertation represents a tremendous advance in the identification of small molecules that target a challenging transcriptional coactivator, Med25 AcID, that will allow for subsequent determination of the role of Med25 in disease.

Chapter One

Targeting protein-protein interactions involved in transcription

A. Abstract

Transcription, the central process that maintains normal homeostasis and cellular function, is tightly regulated through a series of protein-protein interactions (PPIs).¹ Unsurprisingly, dysregulation of transcription is often attributed to human disease, either by cause or effect.² Thus, there is a need for small molecules that can restore normal transcriptional output; targeting transcriptional PPIs represent a viable avenue towards this goal. However, targeting transcriptional PPIs is challenging to such an extent that these PPIs were once considered undruggable as they are typically transient in nature, are relatively low affinity interactions, and occur over large surface areas.^{3,4} While the discovery of small molecule modulators remains challenging, recent advances in chemical screening libraries and methodologies have made them tractable for small molecule intervention.

This introductory chapter will define the principles and regulatory mechanisms that underscore transcriptional PPIs and their roles in human disease. The features of transcriptional PPIs and the difficulties of targeting them with small molecules will be discussed. Finally, emergent strategies that leverage natural products discovery and fragment-based NMR screening to overcome the inherent challenges in modulating transcriptional PPIs will be discussed.

B. Protein-protein interactions in transcription

Protein-protein interactions (PPIs) between transcriptional activators and transcriptional coactivators are a key component of the regulatory network of transcription.^{1,5} The activator proteins are minimally composed of a DNA-binding domain (DBD) responsible for interaction at specific DNA promoter elements and a transcriptional activation domain (TAD) responsible for making contacts with transcriptional coactivators (Figure 1.1).⁶⁻⁸ The minimal assembly of these three elements (DNA, activator, and coactivator) at a specific gene promoter allows for subsequent localization of the pre-initiation complex and RNA Polymerase II.⁹ Following the recruitment of RNA Polymerase II, the gene will be transcribed into messenger RNA (mRNA) for future translation into protein.¹⁰ However, the multimeric assembly is much more complex than this simple model might suggest. Each of the transcriptional proteins make specific contacts with multiple binding partners and nearly half of all transcription factors have been computationally predicted to be intrinsically disordered, or lacking an ordered structure in solution.¹¹⁻¹⁴ Additionally, it has been suggested that a single activator may need to recruit multiple protein complexes to a promoter region to remodel chromatin structure prior to successful gene transcription.¹⁵

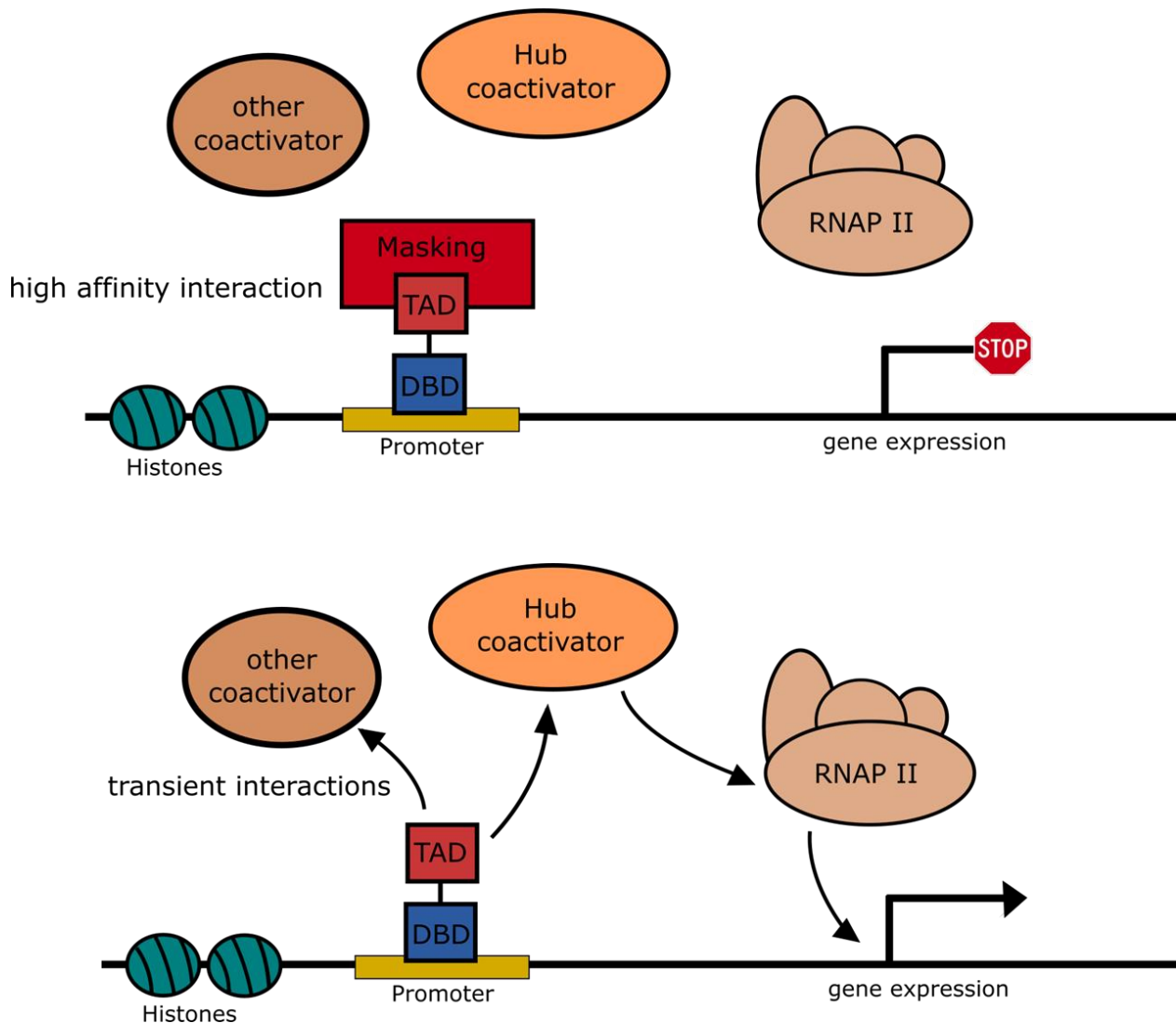


Figure 1.1. Model of transcriptional regulation. (A) A high-affinity interaction between masking proteins and DNA-bound transcriptional activation domains (TADs) suppresses TAD activity and subsequent transcription. (B) Transient interactions between TADs and coactivators, including hub coactivators, leads to recruitment of general transcription factors and RNA Polymerase II (RNAP II) and subsequent activation of transcription.

Multidomain coactivator complexes

Within transcriptional PPI networks, certain coactivators function as hub proteins or protein complexes that can bind to multiple proteins at either the same interface or at multiple interfaces simultaneously.^{16,17} Data suggest that hub proteins are capable of binding multiple proteins at multiple interfaces. High levels of structural plasticity allows

these proteins to exhibit multiple conformations to adapt towards differing partner proteins as needed.^{18,19} Additionally, coactivator hubs tend to contain few “hot spot” clusters at their binding interfaces and a high prevalence of α -helices at multifunctional interfaces.²⁰ To overcome these characteristics, coactivator hubs often bind activator partners following a post-translational modification of the activator or through allosteric communication between binding sites of the coactivator.^{21–23} Two critical and well-studied hubs that contain multiple binding interfaces include the Mediator complex and the master coactivator CBP/p300.^{24,25}

Recruitment of the Mediator complex, which consists of thirty-one protein subunits in humans, to DNA promoter regions is required for activated transcription of the majority of genes that code for proteins.^{26–28} This hub coactivator complex functions as a bridge that links multiple components of the transcriptional machinery through specific protein-protein interactions (Figure 1.2).^{25,29,30} The Mediator complex acts through contacts with transcriptional activators, general transcription factors, and RNA Polymerase II itself.^{31,32} Several Mediator-activator PPIs are important in the regulation of cellular homeostasis and thus have significant relevance in disease, including hormone and nuclear receptors (e.g. estrogen and androgen receptors) and the well-studied oncogenes p53 and ESX.^{33–37} Furthermore, the Mediator complex has been directly linked to several human diseases (e.g. cancer intellectual disability, Alzheimer’s disease).^{38–42}

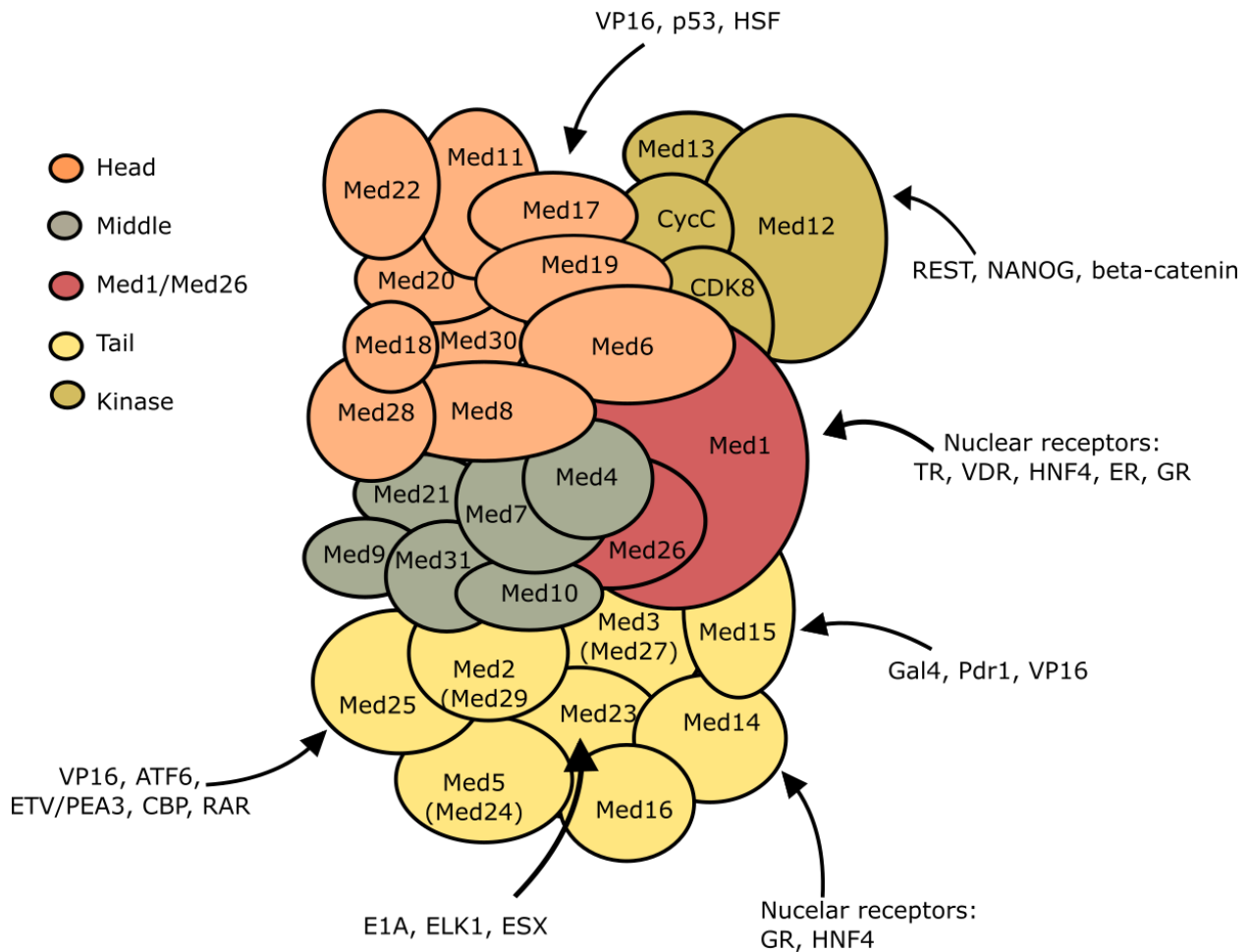


Figure 1.2. The Mediator complex is a critical coactivator hub. A composite image of the structure of the Mediator complex (human) showing the approximate relative location of each subunit. The Head, Middle, Tail, and Kinase modules are indicated by color; Med1 and Med26 are not always present in the complex. Protein binding partners for specific subunits are indicated. Figure adapted from Malik et. al (2010).

CBP/p300 represents a second example of a hub coactivator with multiple binding interfaces that can be occupied simultaneously (Figure 1.3).²⁴ CBP/p300 functions as a bridge between transcriptional activators and general transcription factors involved in the assembly of the pre-initiation complex.⁴³ Differing from the Mediator complex and its multiple protein subunits, CBP/p300 consists of multiple coactivator domains on a single polypeptide.^{44–46} However, like the Mediator complex, CBP/p300 makes several contacts

with transcriptional activators, such as p53, MLL, c-Jun, and HIF-1 α , that have been implicated in human diseases.^{47–51}

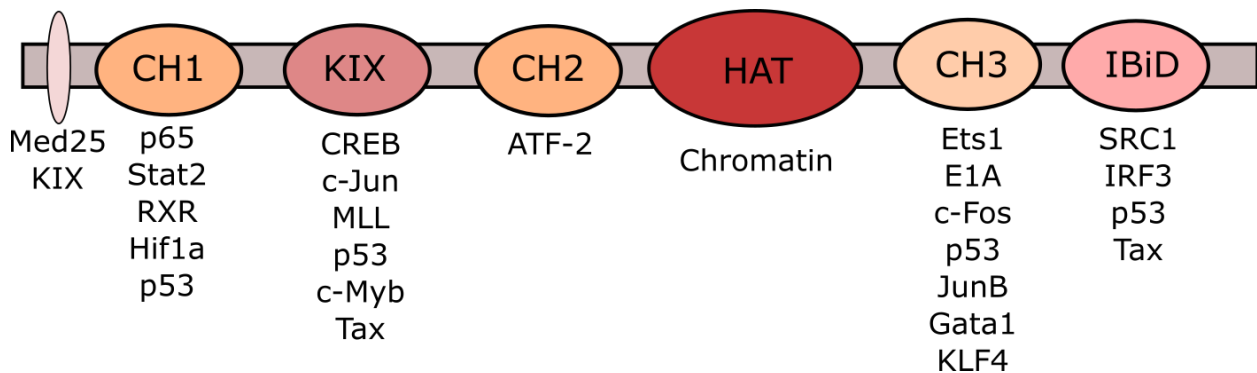


Figure 1.3. Structural organization of the hub coactivator CBP/p300. The domain organization of CBP/300 is shown. Protein binding partners for specific domains are indicated below the relevant domain. Figure adapted from Majmudar et. al (2012).

Transcriptional protein-protein interactions and disease

Due to the importance of transcription in cellular homeostasis, dysregulation of transcriptional PPIs is either a cause or effect of many human diseases.² Dysregulation of these processes occurs through several mechanisms including abnormally elevated or reduced expression of transcriptional proteins, the formation of fusion oncoproteins by chromosomal translocations, and genetic mutations within transcriptional proteins that elevate or reduce their activity.⁵² The transcriptional activator c-Myc represents an excellent example of an overexpressed activator in cancer.⁵³ Elevated expression levels of c-Myc lead to overexpression of oncoproteins involved in cell cycle and metabolic regulation.⁵⁴ Another example of the disease impact of overexpressed activators can be shown by the influences that the ETV/PEA3 family of activators (ETV1/ER81, ETV4/PEA3, and ETV5/ERM) play in cancer metastasis and tumorigenesis.^{55–57} These activators are amplified in concert with the Ras and PI3 kinase pathways and demonstrate high correlation with tumor invasion through the action of matrix metalloproteases.⁵⁸ With

respect to c-Myc and the ETV/PEA activators, elevated transcriptional activity occurs through an increase in the frequency of their interactions with coactivators and other transcription factors. Thus, the study and inhibition of these, and related PPIs represent an avenue to target and study disease processes.

Features of transcriptional protein-protein interactions

As described, transcriptional coactivators interact with multiple binding partners; the same is true for transcriptional activators through their TAD motifs. Most, if not all TADs are considered amphipathic, meaning that their primary structures consist of acidic and polar residues interspersed with hydrophobic amino acids, and are intrinsically disordered in solution.^{59,60,13} TADs tend to make specific contact with two classes of proteins, namely transcriptional coactivators and masking proteins (Figure 1.4).^{8,61} Masking proteins typically form specific and high affinity interactions with activators (nanomolar dissociation constants) for the purposes of suppressing, or 'masking', the activation of downstream gene production.⁶² Well-studied examples of activator interactions with masking proteins include p53-MDM2 and Gal4-Gal80.^{63,64} Crystal structures of both complexes have highlighted the importance of 'hot spot' residues, hydrophobic interactions, and small interaction interfaces that characterize masking-TAD PPIs.^{65,66} These features differ dramatically from activator-coactivator PPIs which are low-to-moderate affinity (micromolar dissociation constants) and occur over large interfaces (800-2500 Å²).⁶⁷⁻⁶⁹ These PPIs tend to involve a mechanism in which the activator and the coactivator undergo conformational changes upon binding.⁷⁰ In this scenario, the intrinsically disordered TAD adopts an α -helical structure upon binding to a coactivation

domain, causing the coactivator to allow for an induced fit between the activator and coactivator pair. For example, the activators pKID and Gcn4 are both intrinsically disordered prior to interaction with CBP/p300 KIX and Med15, respectively.^{71,72} Finally, activator-coactivator PPIs often exist in multiple “fuzzy” conformations and/or orientations, which is thought to be a critical determinant for the transiency and lack of specificity between these particular interacting partners.^{73,74}

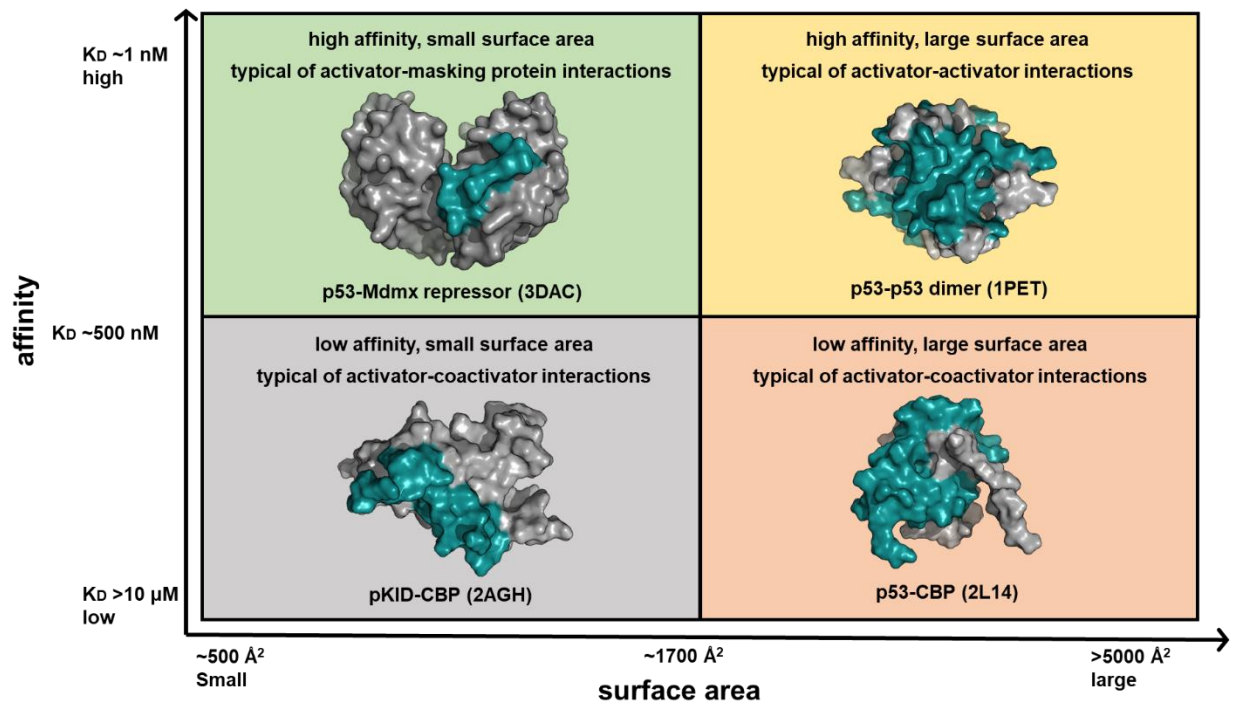


Figure 1.4. Diversity of transcriptional protein-protein interactions. PPIs can be classified according to the affinity and the surface area of the interaction. Examples found within transcription of all four classes of PPIs are shown. Figure adapted from Mapp et al. (2015).

C. Small molecule modulation of transcriptional protein-protein interactions

Difficulties in targeting transcriptional protein-protein interactions

Modulation of PPIs with small molecules has been historically challenging with significantly fewer than 0.01 % of all binary PPIs in the human cell having been successfully targeted.⁷⁵⁻⁷⁷ In fact, many PPIs, particularly those involving transcriptional proteins, have been previously classified as undruggable.^{3,4,78} The specific difficulty towards targeting transcriptional PPIs arises from inherent features of activator-coactivator PPIs, as described above. Examples of molecules that target unique classes of PPIs are provided in Figure 1.5.⁷⁹⁻⁸² Coactivator-activator interactions are transient with binding interactions that demonstrate weak affinity over large surface areas.^{68,69} Weak interactions occurring over large interfaces have traditionally been more challenging to target with small molecules, as fewer than four percent of known molecules that target PPI are represented by these characteristics.^{76,83} Targeting this class of PPI requires a structurally plastic and large molecule that can overcome the lack of 'hotspot' residues within the broad and poorly defined interface.⁸⁴ Additionally, due to their transient nature, the structural basis of many transcriptional PPIs have been poorly studied.⁸⁵ This fact has also significantly hampered the potential for small molecule discovery as the specific elements of individual PPIs (*e.g.* binding orientations, hydrophobic regions/clefts of binding interfaces) are unknown. As a result of these collective characteristics of transcriptional PPIs, traditional screening, medicinal chemistry efforts, and rational design methodologies have led to limited success towards the discovery of novel small molecule modulators.⁸⁶ Nevertheless, as described below, methodologies are being developed that demonstrate potential for the discovery of small molecules to target transcriptional PPIs.

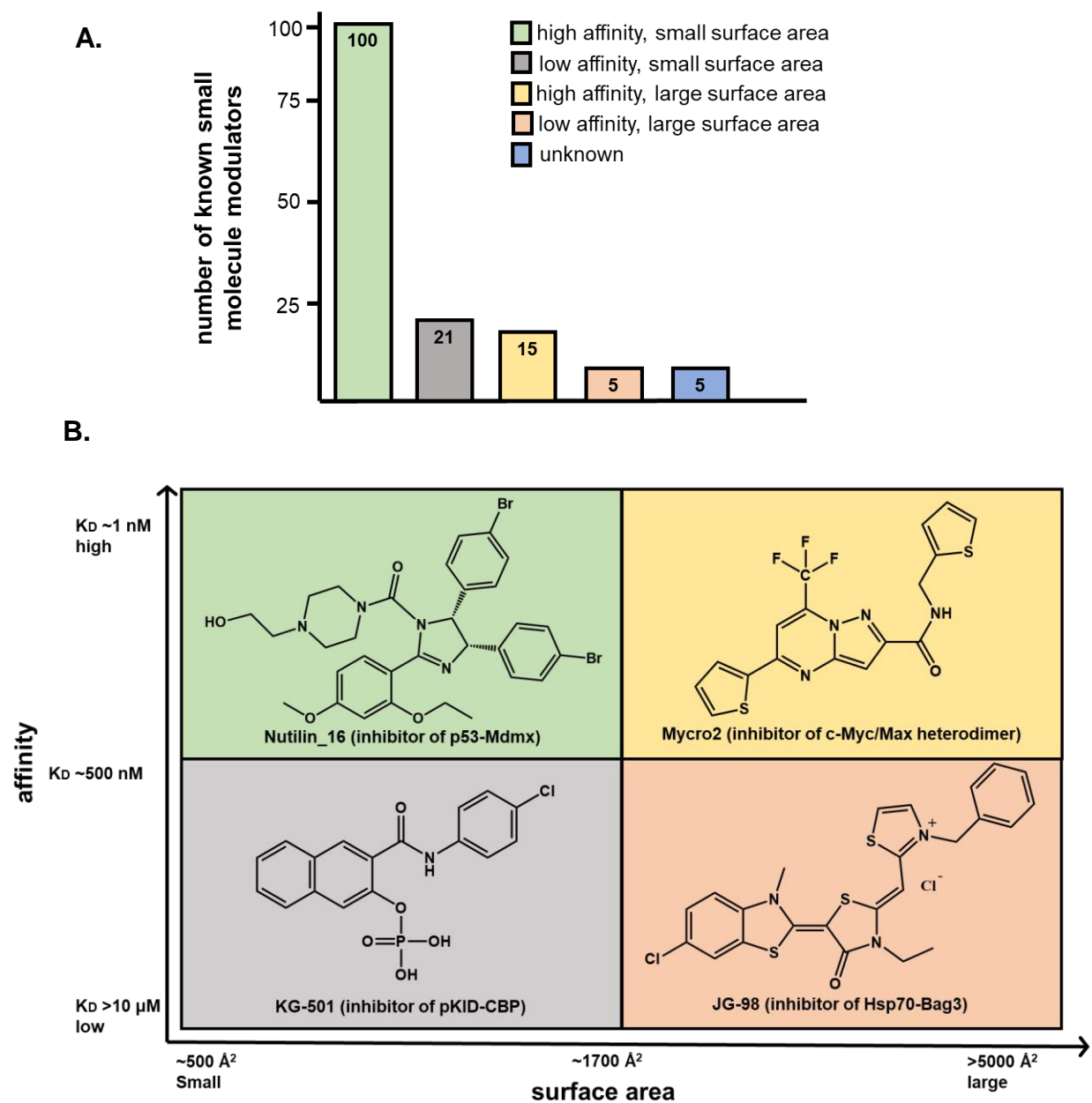


Figure 1.5. Small molecule modulation of diverse classes of protein-protein interactions. (A) Modulators of PPIs were categorized based on diverse classes of PPIs. An majority of known PPI modulators target PPIs with high affinity and small surface areas. (B) Examples of small molecules that target unique PPIs that represent each of the four PPI classes are provided. Figure adapted from Cesa et al. (2015).

Natural products to target transcriptional protein-protein interactions

Natural products discovery offer promise towards targeting transcriptional PPIs; several natural products have recently been developed as tool compounds to target PPIs

(Figure 1.6).⁸⁷⁻⁹¹ To highlight the broad utility of natural products, approximately 80% of all drugs available on the U.S. market in 2012 were natural products or derived from natural products.^{92,93} Natural product compounds derive great utility from their inherent structural complexity, ability to maintain high degrees of rigidity and chirality, and vast diversity of molecular structures and scaffolds.⁸⁷ In fact, nearly 40% of compounds represented in the Dictionary of Natural Products contain unique structural elements that are not otherwise represented in purely synthetic compounds.⁹⁵ Furthermore, it is thought that only a small fraction, particularly from the marine environment, of the total chemical matter that nature has designed has been identified by the scientific community suggesting that majority of potential compounds are still to be discovered.⁹⁶⁻⁹⁸ The discovery of these novel molecules should be forthcoming due to recent advances in fermentation, sample collection techniques, structural elucidation technologies, and increased exploration into the marine environment and other underutilized biological sources.^{99,100}

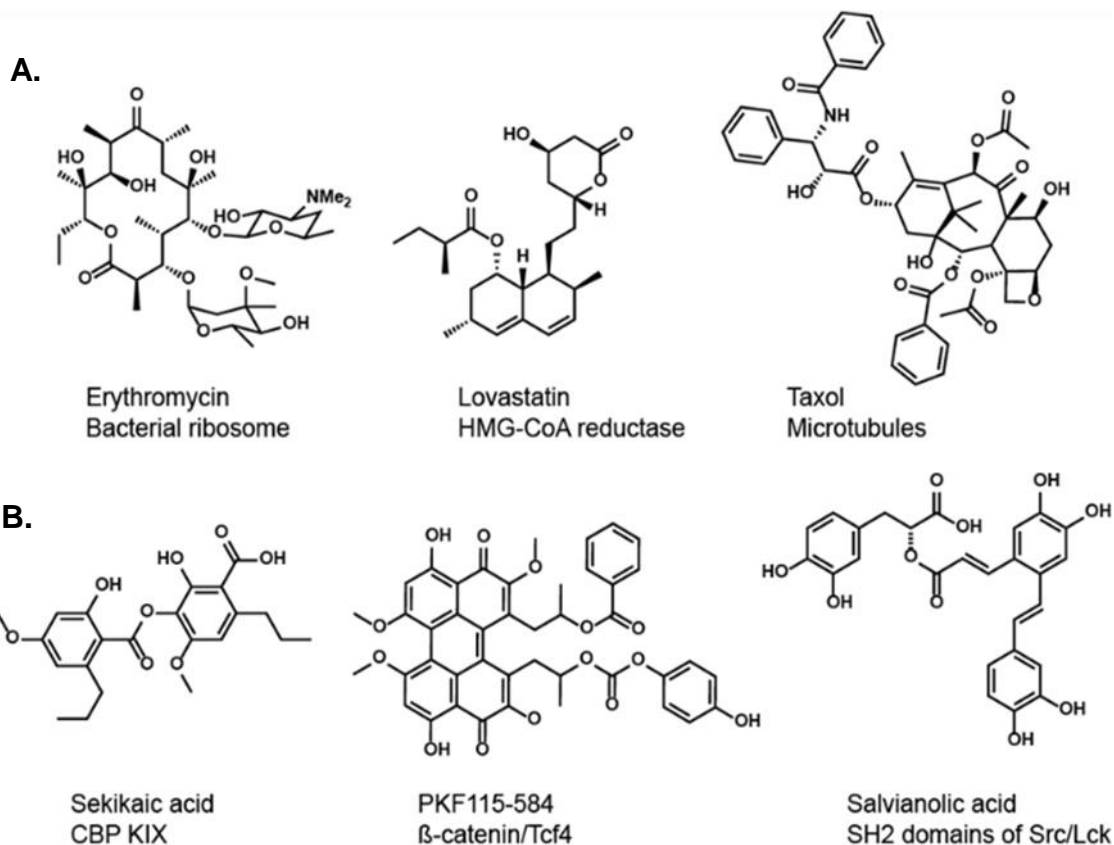


Figure 1.6. Examples of natural product small molecules. The field of natural products represents a broad range of structurally diverse molecules that have been (A) highly successful drugs and (B) capable of selectively inhibiting protein-protein interactions.

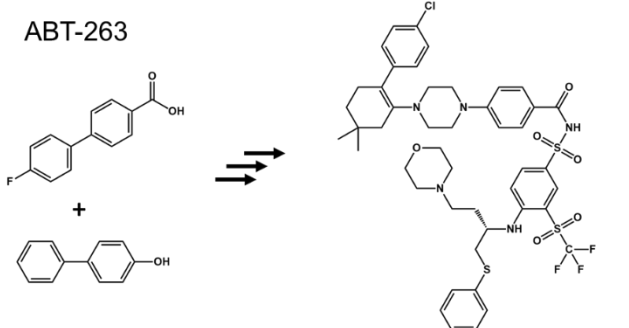
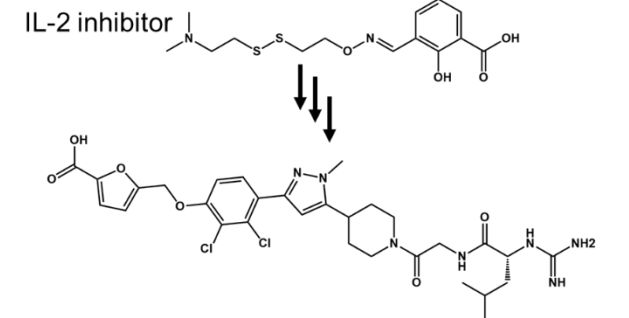
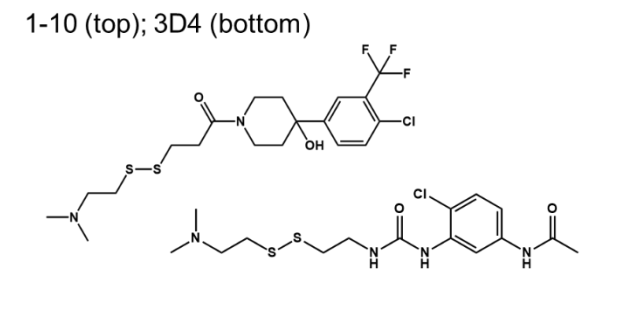
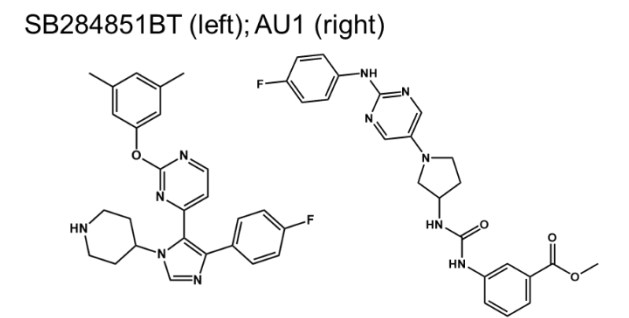
The discovery of lichen-derived natural products, sekikaic acid, and lobaric acid, that target CBP/p300 KIX represent an excellent example of the potential that natural products can provide for modulation of transcriptional PPIs. These molecules, which belong to a class of molecules known as depsides and depsidones, were identified using an iterative screening strategy against the CBP KIX-MLL PPI.^{87,101} While high-throughput screening of a traditional drug-like small molecule library (50,000+ compounds) had failed to identify inhibitors of this PPI, high-throughput screening of natural product extracts isolated from marine sediment-derived microbes, cyanobacteria, lichens, and sponges (16,320 total) provided sekikaic acid and lobaric acid, both of which are potent inhibitors

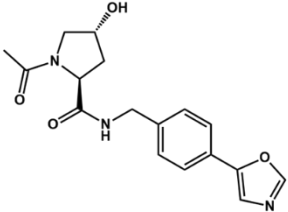
of CBP KIX-MLL (IC_{50} of 17 μ M and 25 μ M, respectively). Subsequent computational analysis of sekikaic acid revealed that its lowest energy suite of conformations demonstrate that the molecule adopts an orientation that mimics an amphipathic α -helix, suggesting that the depside class of natural products likely function as helical mimetics.

Fragment screening to target transcriptional protein-protein interactions

The screening of fragment-based libraries for the discovery of small molecule inhibitors of PPIs has become increasingly common since pioneering work in this area during the mid-1990s.^{102–105} Fragments are small molecules that typically obey a ‘Rule of Three’ (MW less than 300 Da, no more than three each of hydrogen bond donors and acceptors); though these rules are not strictly followed.^{106–108} There are several benefits of screening fragments instead of traditional chemical libraries.¹⁰⁹ Fragments can be screened at high concentrations due to their high solubility in aqueous solutions and their ability to maintain high ligand efficiency. Discovered fragments tend to rely more on hydrogen bond interactions with the protein-of-interest than traditional small molecules which rely more heavily on hydrophobic interactions.¹⁰⁴ Additionally, specific to the screening of PPIs, fragments are capable of interacting with one of the typically three to five regions critical for interaction with binding partners within a broad interface and have been successful in targeting highly dynamic regions within proteins.⁶⁸ Following initial fragment discovery against a target PPI, fragments can then be combined with other hot fragments or optimized into more potent compounds using structure-activity relationships.¹⁰² Examples of fragments that target PPIs are shown in Table 1.1.

Table 1.1. Examples of small molecules fragment modulators of protein-protein interactions. Fragments that modulate PPIs are shown; To demonstrate the power of fragment screening, ‘ABT-263’ and ‘IL-2 inhibitor’ are shown alongside the initial fragment(s) that lead to their discovery.

Compound	PPI interface(s)	Method of discovery
<p>ABT-263</p> 	<p>Bcl-2 family/BH3 family</p>	<p>protein-observed HSQC NMR Oltersdorf et al. (2005)</p>
<p>IL-2 inhibitor</p> 	<p>Interleukin-2/ Interleukin-2 receptor</p>	<p>Tethering Braisted et al. (2003)</p>
<p>1-10 (top); 3D4 (bottom)</p> 	<p>CBP KIX/MLL (1-10) CBP KIX/pKID (3D4)</p>	<p>Tethering Wang et al. (2013) Lodge et al. (2014)</p>
<p>SB284851BT (left); AU1 (right)</p> 	<p>Brd4 (SB284851BT) BPTF (AU1)</p>	<p>PrOF NMR Urlick et. al (2015)</p>

Compound	PPI interface(s)	Method of discovery
<p data-bbox="224 268 435 298">pVHL compound 4</p> 	<p data-bbox="912 373 1058 403">pVHL/HIF-1α</p>	<p data-bbox="1182 331 1383 394">Ligand-observed NMR</p> <p data-bbox="1182 428 1383 457">Dias et. al (2014)</p>

Fragment screening using NMR methodologies

While multiple methodologies (e.g. surface plasmon resonance and Tethering) have been successfully used for the screening of fragment libraries, protein-observed NMR methods have been the most commonly and effectively used, particularly against PPIs.^{110–117} First, NMR chemical shifts are extremely sensitive to their surrounding chemical environment, giving rise to an assay that is capable of efficient detection of weakly associating fragments (single-digit millimolar binding affinities). Secondly, NMR experiments allow for protein-ligand interactions to be determined in solution near physiological conditions and unrestricted by artificial matrices, offering a native, well-folded protein. NMR screening can provide a large amount of structural and biochemical characterization of protein-fragment interactions, even during the screening process itself. This structural and biochemical characterization can include determination of the binding location and binding affinity of the hit fragment towards the protein.^{118,119}

Most protein-observed NMR strategies for screening use two-dimensional heteronuclear single quantum correlation (HSQC) techniques that make use of ¹⁵N-¹H correlations in amide bonds or ¹³C-¹H bond correlations in methyl groups of amino acid side chains.¹²⁰ While HSQC protein NMR is most common and can provide the highest degree of structural information during the screening process, it does have serious

limitations. HSQC NMR requires a homogenous protein sample, long instrumental time (upwards of two hours per experiment), expensive isotopic reagents to produce ^{15}N -labeled or ^{13}C -labeled protein, and time-intensive analysis of the resultant two-dimensional NMR spectra. Additionally, with regards to ^1H , ^{15}N -HSQC, this method only detects chemical shift perturbations of amide N-H bonds, offering minimal, if any, insight into side chain interactions.

Protein-observed ^{19}F -NMR (PrOF NMR) represents an alternative NMR method for fragment screening. PrOF NMR requires the incorporation of ^{19}F through the integration of fluorinated amino acids into a protein-of-interest or through chemical modification to covalently label a residue onto the protein-of-interest with a fluorinated molecule.^{121,122} Relative to HSQC methodologies, PrOF NMR is desirable for its short experimental time (as short as five minutes per experiment), rapid analysis of one-dimensional spectra, and the ability to observe side chain interactions of a select number of residues.^{122,123} Inherent advantages also offered by the ^{19}F nucleus include its native isotopic abundance (100%), magnetic sensitivity (83% as sensitive as ^1H), and its low background signal in protein NMR (^{19}F does not occur naturally in proteins).¹²⁴ This strategy has been recently applied for the successful discovery of fragment-based inhibitors of the CBP/p300 KIX domain and its PPI network and as the orthogonal screening strategy against the SPRY-domain-containing SOCS box protein 2 and AMA1.^{125–127} Additionally, this methodology has been successfully applied for the simultaneous screening of two proteins of similar structure (BrdT and BPTF), indicating that PrOF NMR offers a tremendous opportunity for in-screen fragment filtering of protein selectivity.¹¹⁷

D. Thesis Summary

The subsequent chapters of this dissertation describe the protein-protein interaction network of the Mediator subunit Med25 and the discovery of small molecule inhibitors that target Med25-activator PPIs. Med25 functions through its activator interaction domain (AcID) to bridge transcriptional activators to the Mediator complex to enable activated transcription of their target gene products. Specifically, Med25 AcID interacts with transcriptional activators that include the herpes simplex viral activator VP16, the activator ERM/ETV5 (implicated in cancer progression and metastasis), and the hypoxic stress response activator ATF6 α (involved in the unfolded protein response).^{128–130} However, many questions regarding the selectivity of activators for unique Med25 binding sites and individual modes of molecular recognition remained unanswered prior to beginning this project.

This dissertation describes the discrete binding modes between Med25 AcID and its protein partners as well as the development of small molecule inhibitors of the AcID motif. These small molecules will be invariably useful towards the dissection of Med25 AcID function *in vitro* and in the cellular context as mechanistic probes in the elucidation of the role of Med25 in the regulation of transcriptional programs. Chapter Two describes the interaction between Med25 AcID and two of its protein partners, CBP and ATF6 α , using HSQC NMR. Additionally, this chapter describes a mutagenesis study that utilized protein mutagenesis coupled with fluorescence polarization assays to investigate Med25 AcID interactions with each of its native partners. Chapter Three expands upon the findings of Chapter Two to enable the generation of binding models that describe Med25 AcID and its interactions with discrete protein ligands using PrOF NMR of Med25 AcID.

Furthermore, this chapter leverages PrOF NMR to gain mechanistic understanding of Med25-small molecule interactions. Chapter Four describes the discovery of small molecule inhibitors of Med25 AcID. First, this chapter describes the identification of preliminary hit fragments using PrOF NMR of Med25 AcID to enable a rapid screening process. Finally, this chapter describes the identification and mechanism of action of a novel natural product that potently targets Med25 AcID and its PPI network.

E. References

1. Ptashne, M. & Gann, A. *Genes and Signals (2002) Genes and Signals*. ((Cold Spring Harbor Lab Press, 2002).
2. Lee, T. I. & Young, R. A. Transcriptional regulation and its misregulation in disease. *Cell* **152**, 1237–1251 (2013).
3. Yan, C. & Higgins, P. J. Drugging the undruggable: transcription therapy for cancer. *Biochim. Biophys. Acta* **1835**, 76–85 (2013).
4. Verdine, G. L. & Walensky, L. D. The challenge of drugging undruggable targets in cancer: lessons learned from targeting BCL-2 family members. *Clin. Cancer Res. Off. J. Am. Assoc. Cancer Res.* **13**, 7264–7270 (2007).
5. Ptashne, M. Gene regulation by proteins acting nearby and at a distance. *Nature* **322**, 697–701 (1986).
6. Ansari, A. Z., Mapp, A. K., Nguyen, D. H., Dervan, P. B. & Ptashne, M. Towards a minimal motif for artificial transcriptional activators. *Chem. Biol.* **8**, 583–592 (2001).
7. Ansari, A. Z. & Mapp, A. K. Modular design of artificial transcription factors. *Curr. Opin. Chem. Biol.* **6**, 765–772 (2002).
8. Mapp, A. K. & Ansari, A. Z. A TAD Further: Exogenous Control of Gene Activation. *ACS Chem. Biol.* **2**, 62–75 (2007).
9. Ptashne, M. & Gann, A. Transcriptional activation by recruitment. *Nature* **386**, 569–577 (1997).
10. Crick, F. Central Dogma of Molecular Biology. *Nature* **227**, 561–563 (1970).
11. Hermann, S., Berndt, K. D. & Wright, A. P. How Transcriptional Activators Bind Target Proteins. *J. Biol. Chem.* **276**, 40127–40132 (2001).
12. Henriques, J., Cragnell, C. & Skepö, M. Molecular Dynamics Simulations of Intrinsically Disordered Proteins: Force Field Evaluation and Comparison with Experiment. *J. Chem. Theory Comput.* **11**, 3420–3431 (2015).
13. Dyson, H. J. & Wright, P. E. Intrinsically unstructured proteins and their functions. *Nat. Rev. Mol. Cell Biol.* **6**, 197–208 (2005).
14. Dunker, A. K., Silman, I., Uversky, V. N. & Sussman, J. L. Function and structure of inherently disordered proteins. *Curr. Opin. Struct. Biol.* **18**, 756–764 (2008).
15. Peterson, C. L. & Workman, J. L. Promoter targeting and chromatin remodeling by the SWI/SNF complex. *Curr. Opin. Genet. Dev.* **10**, 187–192 (2000).

16. Keskin, O. & Nussinov, R. Similar binding sites and different partners: implications to shared proteins in cellular pathways. *Struct. Lond. Engl.* 1993 **15**, 341–354 (2007).
17. Singh, G. P., Ganapathi, M. & Dash, D. Role of intrinsic disorder in transient interactions of hub proteins. *Proteins* **66**, 761–765 (2007).
18. Schreiber, G. & Keating, A. E. Protein binding specificity versus promiscuity. *Curr. Opin. Struct. Biol.* **21**, 50–61 (2011).
19. Higurashi, M., Ishida, T. & Kinoshita, K. Identification of transient hub proteins and the possible structural basis for their multiple interactions. *Protein Sci. Publ. Protein Soc.* **17**, 72–78 (2008).
20. Kim, P. M., Sboner, A., Xia, Y. & Gerstein, M. The role of disorder in interaction networks: a structural analysis. *Mol. Syst. Biol.* **4**, 179 (2008).
21. Radhakrishnan, I. *et al.* Solution Structure of the KIX Domain of CBP Bound to the Transactivation Domain of CREB: A Model for Activator:Coactivator Interactions. *Cell* **91**, 741–752 (1997).
22. Goto, N. K., Zor, T., Martinez-Yamout, M., Dyson, H. J. & Wright, P. E. Cooperativity in Transcription Factor Binding to the Coactivator CREB-binding Protein (CBP) THE MIXED LINEAGE LEUKEMIA PROTEIN (MLL) ACTIVATION DOMAIN BINDS TO AN ALLOSTERIC SITE ON THE KIX DOMAIN. *J. Biol. Chem.* **277**, 43168–43174 (2002).
23. Westin, S. *et al.* Interactions controlling the assembly of nuclear-receptor heterodimers and co-activators. *Nature* **395**, 199–202 (1998).
24. Vo, N. & Goodman, R. H. CREB-binding Protein and p300 in Transcriptional Regulation. *J. Biol. Chem.* **276**, 13505–13508 (2001).
25. Poss, Z. C., Ebmeier, C. C. & Taatjes, D. J. The Mediator complex and transcription regulation. *Crit. Rev. Biochem. Mol. Biol.* **48**, 575–608 (2013).
26. Kelleher, R. J., Flanagan, P. M. & Kornberg, R. D. A novel mediator between activator proteins and the RNA polymerase II transcription apparatus. *Cell* **61**, 1209–1215 (1990).
27. Flanagan, P. M., Kelleher, R. J., Sayre, M. H., Tschochner, H. & Kornberg, R. D. A mediator required for activation of RNA polymerase II transcription in vitro. *Nature* **350**, 436–438 (1991).
28. Malik, S. & Roeder, R. G. The metazoan Mediator co-activator complex as an integrative hub for transcriptional regulation. *Nat. Rev. Genet.* **11**, 761–772 (2010).

29. Carlsten, J. O. P., Zhu, X. & Gustafsson, C. M. The multitasking Mediator complex. *Trends Biochem. Sci.* **38**, 531–537 (2013).
30. Ansari, S. A. *et al.* Mediator, TATA-binding protein, and RNA polymerase II contribute to low histone occupancy at active gene promoters in yeast. *J. Biol. Chem.* **289**, 14981–14995 (2014).
31. Cantin, G. T., Stevens, J. L. & Berk, A. J. Activation domain-mediator interactions promote transcription preinitiation complex assembly on promoter DNA. *Proc. Natl. Acad. Sci. U. S. A.* **100**, 12003–12008 (2003).
32. Ansari, S. A. & Morse, R. H. Mechanisms of Mediator complex action in transcriptional activation. *Cell. Mol. Life Sci. CMLS* **70**, 2743–2756 (2013).
33. Kang, Y. K., Guermah, M., Yuan, C.-X. & Roeder, R. G. The TRAP/Mediator coactivator complex interacts directly with estrogen receptors alpha and beta through the TRAP220 subunit and directly enhances estrogen receptor function in vitro. *Proc. Natl. Acad. Sci. U. S. A.* **99**, 2642–2647 (2002).
34. Vijayvargia, R., May, M. S. & Fondell, J. D. A coregulatory role for the mediator complex in prostate cancer cell proliferation and gene expression. *Cancer Res.* **67**, 4034–4041 (2007).
35. Taatjes, D. J., Schneider-Poetsch, T. & Tjian, R. Distinct conformational states of nuclear receptor-bound CRSP–Med complexes. *Nat. Struct. Mol. Biol.* **11**, 664–671 (2004).
36. Saldaña-Meyer, R. *et al.* CTCF regulates the human p53 gene through direct interaction with its natural antisense transcript, Wrap53. *Genes Dev.* **28**, 723–734 (2014).
37. Asada, S. *et al.* External control of Her2 expression and cancer cell growth by targeting a Ras-linked coactivator. *Proc. Natl. Acad. Sci.* **99**, 12747–12752 (2002).
38. Grueter, C. E. Mediator complex dependent regulation of cardiac development and disease. *Genomics Proteomics Bioinformatics* **11**, 151–157 (2013).
39. Spaeth, J. M., Kim, N. H. & Boyer, T. G. Mediator and human disease. *Semin. Cell Dev. Biol.* **22**, 776–787 (2011).
40. Turner, A. J., Belyaev, N. D. & Nalivaeva, N. N. Mediator: the missing link in amyloid precursor protein nuclear signalling. *EMBO Rep.* **12**, 180–181 (2011).
41. Philibert, R. A. & Madan, A. Role of MED12 in transcription and human behavior. *Pharmacogenomics* **8**, 909–916 (2007).

42. Janody, F. & Treisman, J. E. Requirements for mediator complex subunits distinguish three classes of Notch target genes at the *Drosophila* wing margin. *Dev. Dyn. Off. Publ. Am. Assoc. Anat.* **240**, 2051–2059 (2011).
43. Goodman, R. H. & Smolik, S. CBP/p300 in cell growth, transformation, and development. *Genes Dev.* **14**, 1553–1577 (2000).
44. De Guzman, R. N., Liu, H. Y., Martinez-Yamout, M., Dyson, H. J. & Wright, P. E. Solution structure of the TAZ2 (CH3) domain of the transcriptional adaptor protein CBP. *J. Mol. Biol.* **303**, 243–253 (2000).
45. De Guzman, R. N., Wojciak, J. M., Martinez-Yamout, M. A., Dyson, H. J. & Wright, P. E. CBP/p300 TAZ1 domain forms a structured scaffold for ligand binding. *Biochemistry (Mosc.)* **44**, 490–497 (2005).
46. Lin, C. H. *et al.* A small domain of CBP/p300 binds diverse proteins: solution structure and functional studies. *Mol. Cell* **8**, 581–590 (2001).
47. Livengood, J. A. *et al.* p53 Transcriptional activity is mediated through the SRC1-interacting domain of CBP/p300. *J. Biol. Chem.* **277**, 9054–9061 (2002).
48. Grossman, S. R. p300/CBP/p53 interaction and regulation of the p53 response. *Eur. J. Biochem.* **268**, 2773–2778 (2001).
49. Bannister, A. J., Oehler, T., Wilhelm, D., Angel, P. & Kouzarides, T. Stimulation of c-Jun activity by CBP: c-Jun residues Ser63/73 are required for CBP induced stimulation in vivo and CBP binding in vitro. *Oncogene* **11**, 2509–2514 (1995).
50. Wang, F. *et al.* Structures of KIX domain of CBP in complex with two FOXO3a transactivation domains reveal promiscuity and plasticity in coactivator recruitment. *Proc. Natl. Acad. Sci.* **109**, 6078–6083 (2012).
51. Dames, S. A., Martinez-Yamout, M., De Guzman, R. N., Dyson, H. J. & Wright, P. E. Structural basis for Hif-1 α /CBP recognition in the cellular hypoxic response. *Proc. Natl. Acad. Sci.* **99**, 5271–5276 (2002).
52. Nebert, D. W. Transcription factors and cancer: an overview. *Toxicology* **181**, 131–141 (2002).
53. Little, C. D., Nau, M. M., Carney, D. N., Gazdar, A. F. & Minna, J. D. Amplification and expression of the c-myc oncogene in human lung cancer cell lines. *Nature* **306**, 194–196 (1983).
54. Dang, C. V. c-Myc Target Genes Involved in Cell Growth, Apoptosis, and Metabolism. *Mol. Cell. Biol.* **19**, 1–11 (1999).

55. Aytes, A. *et al.* ETV4 promotes metastasis in response to activation of PI3-kinase and Ras signaling in a mouse model of advanced prostate cancer. *Proc. Natl. Acad. Sci.* **110**, E3506–E3515 (2013).
56. Pellicchia, A. *et al.* Overexpression of ETV4 is oncogenic in prostate cells through promotion of both cell proliferation and epithelial to mesenchymal transition. *Oncogenesis* **1**, e20 (2012).
57. de Launoit, Y. *et al.* The PEA3 group of ETS-related transcription factors. Role in breast cancer metastasis. *Adv. Exp. Med. Biol.* **480**, 107–116 (2000).
58. Firlej, V. *et al.* Reduced tumorigenesis in mouse mammary cancer cells following inhibition of Pea3- or Erm-dependent transcription. *J. Cell Sci.* **121**, 3393–3402 (2008).
59. Cress, W. D. & Triezenberg, S. J. Critical structural elements of the VP16 transcriptional activation domain. *Science* **251**, 87–90 (1991).
60. Regier, J. L., Shen, F. & Triezenberg, S. J. Pattern of aromatic and hydrophobic amino acids critical for one of two subdomains of the VP16 transcriptional activator. *Proc. Natl. Acad. Sci. U. S. A.* **90**, 883–887 (1993).
61. Pei, D., Zhang, Y. & Zheng, J. Regulation of p53: a collaboration between Mdm2 and Mdmx. *Oncotarget* **3**, 228–235 (2012).
62. Moll, U. M. & Petrenko, O. The MDM2-p53 Interaction. *Mol. Cancer Res.* **1**, 1001–1008 (2003).
63. Wade, M., Wang, Y. V. & Wahl, G. M. The p53 orchestra: Mdm2 and Mdmx set the tone. *Trends Cell Biol.* **20**, 299–309 (2010).
64. Lohr, D., Venkov, P. & Zlatanova, J. Transcriptional regulation in the yeast GAL gene family: a complex genetic network. *FASEB J. Off. Publ. Fed. Am. Soc. Exp. Biol.* **9**, 777–787 (1995).
65. Anil, B., Riedinger, C., Endicott, J. A. & Noble, M. E. M. The structure of an MDM2–Nutlin-3a complex solved by the use of a validated MDM2 surface-entropy reduction mutant. *Acta Crystallogr. D Biol. Crystallogr.* **69**, 1358–1366 (2013).
66. Kumar, P. R., Yu, Y., Sternglanz, R., Johnston, S. A. & Joshua-Tor, L. NADP Regulates the Yeast GAL Induction System. *Science* **319**, 1090–1092 (2008).
67. DeLano, W. L. Unraveling hot spots in binding interfaces: progress and challenges. *Curr. Opin. Struct. Biol.* **12**, 14–20 (2002).
68. Fuller, J. C., Burgoyne, N. J. & Jackson, R. M. Predicting druggable binding sites at the protein-protein interface. *Drug Discov. Today* **14**, 155–161 (2009).

69. Nooren, I. M. A. & Thornton, J. M. Structural characterisation and functional significance of transient protein-protein interactions. *J. Mol. Biol.* **325**, 991–1018 (2003).
70. Hammes, G. G., Chang, Y.-C. & Oas, T. G. Conformational selection or induced fit: a flux description of reaction mechanism. *Proc. Natl. Acad. Sci. U. S. A.* **106**, 13737–13741 (2009).
71. Sugase, K., Dyson, H. J. & Wright, P. E. Mechanism of coupled folding and binding of an intrinsically disordered protein. *Nature* **447**, 1021–1025 (2007).
72. Brzovic, P. S. *et al.* The acidic transcription activator Gcn4 binds the Mediator subunit Gal11/Med15 using a simple protein interface forming a fuzzy complex. *Mol. Cell* **44**, 942–953 (2011).
73. Sharma, R., Raduly, Z., Miskei, M. & Fuxreiter, M. Fuzzy complexes: Specific binding without complete folding. *FEBS Lett.* **589**, 2533–2542 (2015).
74. Scholes, N. S. & Weinzierl, R. O. J. Molecular Dynamics of ‘Fuzzy’ Transcriptional Activator-Coactivator Interactions. *PLoS Comput. Biol.* **12**, e1004935 (2016).
75. Overington, J. P., Al-Lazikani, B. & Hopkins, A. L. How many drug targets are there? *Nat. Rev. Drug Discov.* **5**, 993–996 (2006).
76. Thompson, A. D., Dugan, A., Gestwicki, J. E. & Mapp, A. K. Fine-Tuning Multiprotein Complexes Using Small Molecules. *ACS Chem. Biol.* **7**, 1311–1320 (2012).
77. Mapp, A. K., Pricer, R. & Sturlis, S. Targeting transcription is no longer a quixotic quest. *Nat. Chem. Biol.* **11**, 891–894 (2015).
78. Hopkins, A. L. & Groom, C. R. The druggable genome. *Nat. Rev. Drug Discov.* **1**, 727–730 (2002).
79. Klein, C. & Vassilev, L. T. Targeting the p53–MDM2 interaction to treat cancer. *Br. J. Cancer* **91**, 1415–1419 (2004).
80. Kiessling, A., Sperl, B., Hollis, A., Eick, D. & Berg, T. Selective inhibition of c-Myc/Max dimerization and DNA binding by small molecules. *Chem. Biol.* **13**, 745–751 (2006).
81. Best, J. L. *et al.* Identification of small-molecule antagonists that inhibit an activator: coactivator interaction. *Proc. Natl. Acad. Sci. U. S. A.* **101**, 17622–17627 (2004).
82. Li, X. *et al.* Validation of the Hsp70-Bag3 protein-protein interaction as a potential therapeutic target in cancer. *Mol. Cancer Ther.* **14**, 642–648 (2015).

83. Cesa, L. C., Mapp, A. K. & Gestwicki, J. E. Direct and Propagated Effects of Small Molecules on Protein–Protein Interaction Networks. *Front. Bioeng. Biotechnol.* **3**, (2015).
84. Mc, S. & Je, G. Features of protein-protein interactions that translate into potent inhibitors: topology, surface area and affinity., Features of Protein-Protein Interactions that Translate into Potent Inhibitors: Topology, Surface Area and Affinity. *Expert Rev. Mol. Med. Expert Rev. Mol. Med.* **14**, **14**, e16, e16–e16 (2012).
85. Perkins, J. R., Diboun, I., Dessailly, B. H., Lees, J. G. & Orengo, C. Transient Protein-Protein Interactions: Structural, Functional, and Network Properties. *Structure* **18**, 1233–1243 (2010).
86. Spencer, R. W. High-throughput screening of historic collections: observations on file size, biological targets, and file diversity. *Biotechnol. Bioeng.* **61**, 61–67 (1998).
87. Majmudar, C. Y. *et al.* Sekikaic Acid and Lobaric Acid Target a Dynamic Interface of the Coactivator CBP/p300. *Angew. Chem. Int. Ed.* **51**, 11258–11262 (2012).
88. Sperl, B., Seifert, M. H. J. & Berg, T. Natural product inhibitors of protein–protein interactions mediated by Src-family SH2 domains. *Bioorg. Med. Chem. Lett.* **19**, 3305–3309 (2009).
89. Hollis, A., Sperl, B., Gräber, M. & Berg, T. The Natural Product Betulinic Acid Inhibits C/EBP Family Transcription Factors. *ChemBioChem* **13**, 302–307 (2012).
90. Ardi, V. C., Alexander, L. D., Johnson, V. A. & McAlpine, S. R. Macrocycles That Inhibit the Binding between Heat Shock Protein 90 and TPR-Containing Proteins. *ACS Chem. Biol.* **6**, 1357–1366 (2011).
91. Lepourcelet, M. *et al.* Small-molecule antagonists of the oncogenic Tcf/ β -catenin protein complex. *Cancer Cell* **5**, 91–102 (2004).
92. Cragg, G. M. & Newman, D. J. Natural products: a continuing source of novel drug leads. *Biochim. Biophys. Acta* **1830**, 3670–3695 (2013).
93. Li, J. W.-H. & Vederas, J. C. Drug discovery and natural products: end of an era or an endless frontier? *Science* **325**, 161–165 (2009).
94. Dias, D. A., Urban, S. & Roessner, U. A historical overview of natural products in drug discovery. *Metabolites* **2**, 303–336 (2012).
95. Henkel, T., Brunne, R. M., Müller, H. & Reichel, F. Statistical Investigation into the Structural Complementarity of Natural Products and Synthetic Compounds. *Angew. Chem. Int. Ed.* **38**, 643–647 (1999).
96. Cragg, G. M., Grothaus, P. G. & Newman, D. J. Impact of Natural Products on Developing New Anti-Cancer Agents †. *Chem. Rev.* **109**, 3012–3043 (2009).

97. Harvey, A. L. Natural products as a screening resource. *Curr. Opin. Chem. Biol.* **11**, 480–484 (2007).
98. Bull, A. T. & Stach, J. E. M. Marine actinobacteria: new opportunities for natural product search and discovery. *Trends Microbiol.* **15**, 491–499 (2007).
99. Fenical, W. & Jensen, P. R. Developing a new resource for drug discovery: marine actinomycete bacteria. *Nat. Chem. Biol.* **2**, 666–673 (2006).
100. Molinski, T. F. Microscale methodology for structure elucidation of natural products. *Curr. Opin. Biotechnol.* **21**, 819–826 (2010).
101. Fischer, E. SYNTHESIS OF DEPSIDES, LICHEN-SUBSTANCES AND TANNINS. *J. Am. Chem. Soc.* **36**, 1170–1201 (1914).
102. Shuker, S. B., Hajduk, P. J., Meadows, R. P. & Fesik, S. W. Discovering high-affinity ligands for proteins: SAR by NMR. *Science* **274**, 1531–1534 (1996).
103. Petros, A. M. *et al.* Discovery of a potent and selective Bcl-2 inhibitor using SAR by NMR. *Bioorg. Med. Chem. Lett.* **20**, 6587–6591 (2010).
104. Scott, D. E. *et al.* Using a fragment-based approach to target protein-protein interactions. *Chembiochem Eur. J. Chem. Biol.* **14**, 332–342 (2013).
105. Pomerantz, W. C. *et al.* Profiling the Dynamic Interfaces of Fluorinated Transcription Complexes for Ligand Discovery and Characterization. *ACS Chem. Biol.* **7**, 1345–1350 (2012).
106. Congreve, M., Carr, R., Murray, C. & Jhoti, H. A 'Rule of Three' for fragment-based lead discovery? *Drug Discov. Today* **8**, 876–877 (2003).
107. Köster, H. *et al.* A Small Nonrule of 3 Compatible Fragment Library Provides High Hit Rate of Endothiapepsin Crystal Structures with Various Fragment Chemotypes. *J. Med. Chem.* **54**, 7784–7796 (2011).
108. Jhoti, H., Williams, G., Rees, D. C. & Murray, C. W. The 'rule of three' for fragment-based drug discovery: where are we now? *Nat. Rev. Drug Discov.* **12**, 644–644 (2013).
109. Erlanson, D. A., McDowell, R. S. & O'Brien, T. Fragment-Based Drug Discovery. *J. Med. Chem.* **47**, 3463–3482 (2004).
110. Lodge, J. M., Rettenmaier, T. J., Wells, J. A., Pomerantz, W. C. & Mapp, A. K. FP Tethering: a screening technique to rapidly identify compounds that disrupt protein-protein interactions. *MedChemComm* **5**, 370–375 (2014).
111. Wang, N. *et al.* Ordering a Dynamic Protein Via a Small-Molecule Stabilizer. *J. Am. Chem. Soc.* **135**, 3363–3366 (2013).

112. Giannetti, A. M., Koch, B. D. & Browner, M. F. Surface plasmon resonance based assay for the detection and characterization of promiscuous inhibitors. *J. Med. Chem.* **51**, 574–580 (2008).
113. Erlanson, D. A., Wells, J. A. & Braisted, A. C. Tethering: fragment-based drug discovery. *Annu. Rev. Biophys. Biomol. Struct.* **33**, 199–223 (2004).
114. Dias, D. M. *et al.* Is NMR Fragment Screening Fine-Tuned to Assess Druggability of Protein–Protein Interactions? *ACS Med. Chem. Lett.* **5**, 23–28 (2013).
115. Braisted, A. C. *et al.* Discovery of a potent small molecule IL-2 inhibitor through fragment assembly. *J. Am. Chem. Soc.* **125**, 3714–3715 (2003).
116. Oltersdorf, T. *et al.* An inhibitor of Bcl-2 family proteins induces regression of solid tumours. *Nature* **435**, 677–681 (2005).
117. Urick, A. K. *et al.* Dual Screening of BPTF and Brd4 Using Protein-Observed Fluorine NMR Uncovers New Bromodomain Probe Molecules. *ACS Chem. Biol.* **10**, 2246–2256 (2015).
118. Van Molle, I. *et al.* Dissecting fragment-based lead discovery at the von Hippel-Lindau protein:hypoxia inducible factor 1 α protein-protein interface. *Chem. Biol.* **19**, 1300–1312 (2012).
119. Fielding, L. NMR Methods for the Determination of Protein- Ligand Dissociation Constants. *Curr. Top. Med. Chem.* **3**, 39–53 (2003).
120. Wiesner, S. & Sprangers, R. Methyl groups as NMR probes for biomolecular interactions. *Curr. Opin. Struct. Biol.* **35**, 60–67 (2015).
121. Ye, L., Larda, S. T., Frank Li, Y. F., Manglik, A. & Prosser, R. S. A comparison of chemical shift sensitivity of trifluoromethyl tags: optimizing resolution in ^{19}F NMR studies of proteins. *J. Biomol. NMR* **62**, 97–103 (2015).
122. Gee, C. T. *et al.* Protein-observed ^{19}F -NMR for fragment screening, affinity quantification and druggability assessment. *Nat. Protoc.* **11**, 1414–1427 (2016).
123. Urick, A. K., Calle, L. P., Espinosa, J. F., Hu, H. & Pomerantz, W. C. K. Protein-Observed Fluorine NMR Is a Complementary Ligand Discovery Method to $(1)\text{H}$ CPMG Ligand-Observed NMR. *ACS Chem. Biol.* **11**, 3154–3164 (2016).
124. Danielson, M. A. & Falke, J. J. Use of ^{19}F NMR to probe protein structure and conformational changes. *Annu. Rev. Biophys. Biomol. Struct.* **25**, 163–195 (1996).
125. Gee, C. T., Koleski, E. J. & Pomerantz, W. C. K. Fragment Screening and Druggability Assessment for the CBP/p300 KIX Domain through Protein-Observed ^{19}F NMR Spectroscopy. *Angew. Chem. Int. Ed.* **54**, 3735–3739 (2015).

126. Ge, X. *et al.* Ligand-induced conformational change of Plasmodium falciparum AMA1 detected using ¹⁹F NMR. *J. Med. Chem.* **57**, 6419–6427 (2014).
127. Leung, E. W. W. *et al.* ¹⁹F NMR as a Probe of Ligand Interactions with the iNOS Binding site of SPRY Domain-Containing SOCS Box Protein 2. *Chem. Biol. Drug Des.* **84**, 616–625 (2014).
128. Mittler, G. *et al.* A novel docking site on Mediator is critical for activation by VP16 in mammalian cells. *EMBO J.* **22**, 6494–6504 (2003).
129. Verger, A. *et al.* The Mediator complex subunit MED25 is targeted by the N-terminal transactivation domain of the PEA3 group members. *Nucleic Acids Res.* **41**, 4847–4859 (2013).
130. Sela, D. *et al.* Role for Human Mediator Subunit MED25 in Recruitment of Mediator to Promoters by Endoplasmic Reticulum Stress-responsive Transcription Factor ATF6. *J. Biol. Chem.* **288**, 26179–26187 (2013).

Chapter Two

Investigation of Med25 AcID and its protein-protein network

A. Abstract*

The activator interaction domain (AcID) of Med25 is a transcriptional coactivation motif that interacts with several transcriptional activators that are critical for normal cellular processes and certain disease states, including the ETV/PEA3 family transcription factors, the herpes simplex viral protein VP16, the oxidative stress response factor ATF6 α , and the master coactivator CBP.¹⁻⁴ However, Med25 AcID biochemistry and its modes of molecular recognition for individual binding targets had been poorly understood prior to this study. This chapter explores the binding modes for unique Med25 AcID-activator interactions to describe putative binding sites of the AcID domain. Additionally, this chapter describes the identification and biochemical characterization of the minimal interacting sequences of CBP and ATF6 α for Med25 AcID. These findings demonstrate that Med25 AcID contains two binding sites that are 180° apart, termed the H1 and H2 sites, and a putative third site flanked by H1 and H2. Data suggests that some activator ligands (VP16 H1 and VP16 H2, in particular) are capable of binding at multiple sites on Med25 AcID. Others, such as ERM and ATF6 α bind selectively at one site. This chapter builds a critical foundation for understanding the Med25 AcID-activator interactions further

*Several collaborators provided research assistance throughout Chapter Two. Dr. Felicia Gray (University of Michigan) collected HSQC NMR data of the Med25 AcID-ATF6 α and Med25 AcID-CBP interactions. Kevon Stanford (University of Michigan) assisted with the analysis of the minimal ATF6 α sequence and synthesized ATF6 α (53-75). Andy Henderson (University of Michigan) identified VP16 G450C as a peptide capable of efficiently Tethering to Med25 AcID and characterized its interactions with WT Med25 AcID. Collectively, Andy Henderson and I collected the data describing the effects of VP16 G450C on Med25 AcID mutants.

explored using protein-observed ^{19}F NMR in Chapter 3 and leveraged for small molecule discovery in Chapter 4.

B. Introduction

The protein-protein interactions (PPIs) between transcriptional coactivators and transcriptional activation domains (TADs) represent the molecular underpinnings of transcription and are therefore tightly regulated.^{5,6} Dysregulation of transcriptional PPI networks is common in disease states, and altered transcriptional networks are often either a cause or a direct effect of the disease.^{7,8} These PPIs are frequently transient, occur over large surface areas ($>1500 \text{ \AA}$) and demonstrate weak-to-moderate binding affinity.⁹⁻¹¹ The transcriptional coactivator involved in a particular PPI is typically capable of interacting with a wide array of TADs.¹² Likewise, transcriptional activators are also known to bind multiple proteins. This capability to bind multiple ligands often results from the ability of the coactivator to adopt multiple conformations dependent upon TAD binding.^{5,13} A better understanding of the subtle differences in binding mode and conformations of the coactivator would allow for further study of the impact of these PPIs on transcription and their implications for disease .

Mediator subunit Med25 and AcID motif

Med25, a subunit of the Mediator complex, is a transcriptional coactivator that has recently been implicated as a critical protein in the recruitment of the pre-initiation complex and subsequent gene transcription for a number of TADs.¹ Med25 consists of three unique motifs – a von Willebrand factor type A (VWA) domain that anchors Med25

to the multiprotein Mediator complex, a nuclear receptor (NR) box that is reported to interact with retinoic acid receptor α and the estrogen receptor α , and an activator interaction domain (AcID) that interacts with several TADs implicated in disease.^{1-4,14,15} Transcriptional activators reported to interact with Med25 AcID include VP16, a component of the herpes simplex virus responsible for lytic infections^{1,16}; ERM, a member of the Ets family of transcription factors that has been implicated in cancer progression and metastasis^{2,17,18}; and ATF6 α , an endoplasmic reticulum stress response transcription factor that is involved in the unfolded protein response.^{3,19,20} Additionally, the master coactivator CBP has been reported to interact with Med25 AcID; the biochemical rationale for this PPI is still relatively unknown.⁴

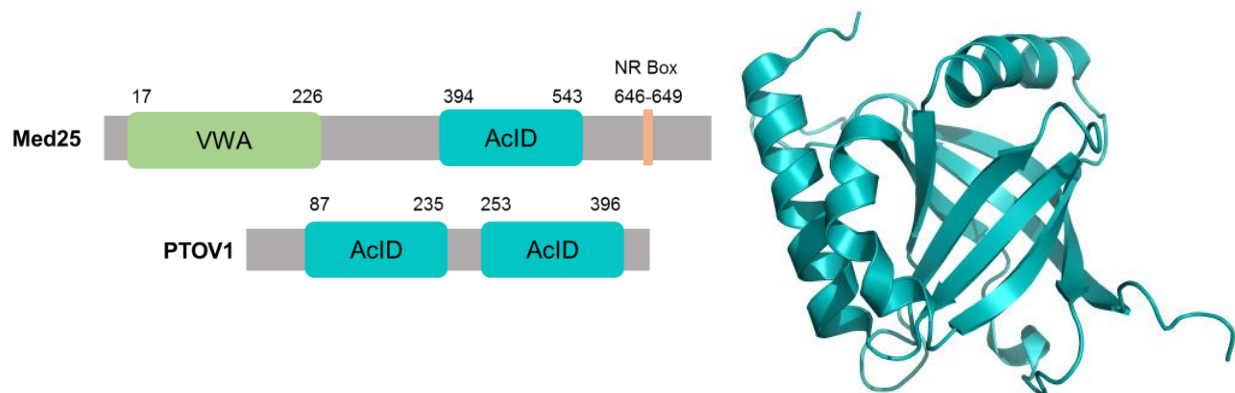


Figure 2.1. Domain architecture of Med25 and the structure of the AcID motif. At left, the domain architecture of Med25 (one AcID motif) and PTOV1 (two AcID motifs). At right, a cartoon image of Med25 AcID to demonstrate central β -barrel with three surrounding α -helices. (PDB 2XNF)

The AcID motif is an unprecedented structural fold among transcriptional coactivators, because it consists of a central β -barrel with three surrounding α -helices.²¹⁻²³ Typical transcriptional coactivator motifs, such as KIX and TAZ domains, consist primarily of α -helices.^{24,25} This motif is also unique in that it is only found in Med25 and Prostate Tumor Overexpressed 1 (PTOV1).²⁶ Interestingly, PTOV1, which contains two

AcID motifs, is overexpressed in a variety of cancers while not expressed at detectable levels in healthy tissues.²⁷⁻²⁹ Additionally, it has been shown to compete with Med25 for interaction with CBP.²⁶

Med25 AcID-activator protein-protein interactions

Previous NMR studies have reported on the interactions between Med25 AcID and the two canonical VP16 TADs, termed VP16 H1 and VP16 H2.^{21,23} These data demonstrated that Med25 AcID contained at least two presumed binding sites. Titration of VP16(413-451), the H1 TAD, into ¹⁵N-labeled Med25 AcID perturbed specific residues in the cleft of Med25 AcID formed by β 1- β 3- β 5 and α 2 (Figure 2.2.A).²³ This cleft of Med25 AcID is hereby referred to as the H1 site. Similarly, titration of VP16(452-490), the H2 TAD, into ¹⁵N-labeled Med25 AcID perturbed specific residues in the cleft of Med25 AcID formed by α 1 and β 6- β 7- β 4 (Figure 2.2.B).²¹ This region of Med25 AcID is hereby referred to as the H2 site. Additional reports of ¹H,¹⁵N-HSQC NMR studies of Med25 AcID in complex with ERM/ETV5 and ETV4 TADs¹ found that the TADs of both bound to the H1 site.^{17,3} A third putative site within Med25 AcID, formed at the junction of β 4- β 2 and α 2, was also recently reported to interact with the DNA-binding domain (DBD) of ETV4, as demonstrated by ¹H,¹⁵N-HSQC NMR (Figure 2.2.C).

However, even with these published reports, many questions regarding the selectivity of peptide ligands for unique binding sites and individual modes of molecular recognition remain. For example, the Med25-VP16 NMR publications disagree above the relative importance of the H1 versus H2 binding sites for interaction with VP16 TADs and subsequent VP16 transcriptional activation.^{21,23} This discrepancy requires a rigorous analysis of the binding determinants of each site and the selectivity of differing activator

ligands for one site over the others. Additionally, the minimal interacting regions of CBP and ATF6 α have not been reported. Identification of those sequences would allow for the biochemical characterization of these proteins with the AcID motif of Med25.

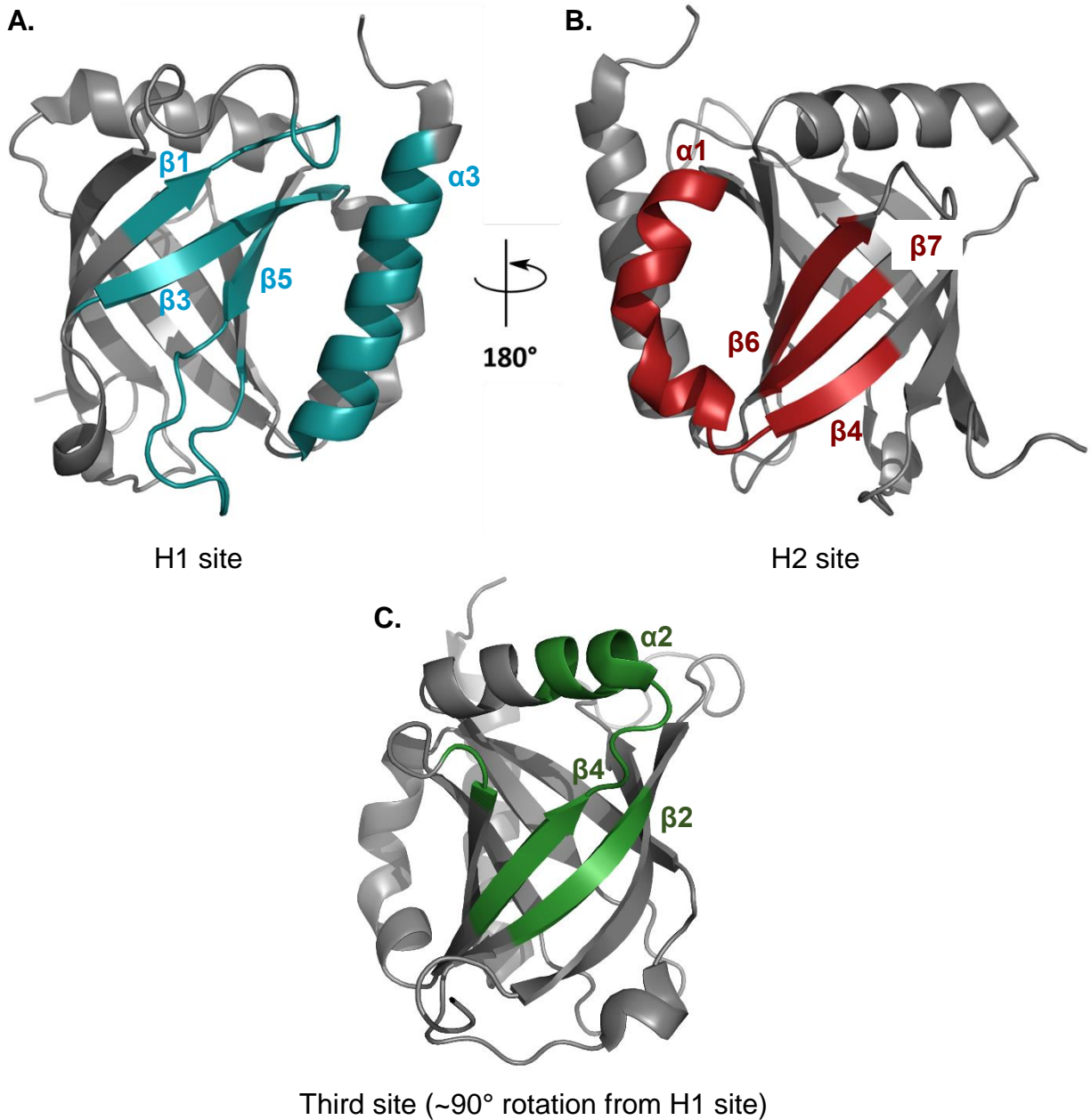


Figure 2.2. Med25 AcID contains multiple binding sites. (A) The H1 binding site (teal), as defined by Milbradt et al. (2011)²³, is formed by β 1– β 3– β 5 and α 2. (B) The H2 binding site (red), as defined by Vojnic et al. (2011)²¹, is formed by α 1 and β 6– β 7– β 4. (C) A proposed third binding site (green), as defined by Currie et al. (2017)³⁰, is formed by β 4– β 2 and α 2. (PDB 2XNF)

Role of electrostatic contacts in Med25 PPIs

Electrostatic contacts have been shown to play a significant role in activator-coactivator PPIs, consistent with the acidic nature of TAD sequences.³¹ Thus, it had been expected that Med25 AcID PPIs might also be dependent on electrostatic contacts to drive the binding of acidic TADs to the highly basic AcID motif. Experiments performed by Steve Sturlis (Mapp lab, University of Michigan) demonstrated that a 10 fold increase in the concentration of NaCl in fluorescence polarization (FP) experiments resulted in a >30 fold decrease in affinity of the VP16 peptides for Med25 AcID. This result is consistent with Med25 AcID being dependent upon electrostatic interactions. It was hypothesized that electrostatic interactions could be leveraged for the study of one Med25 binding site at a time, allowing for observation of activator interactions that might occur selectively within that binding site.

C. Results and discussion

Characterization of the Med25 AcID-CBP protein-protein interaction

Previous work had demonstrated that GST-tagged CBP(1-460) interacted specifically with the AcID domain of Med25 *in vitro*.⁴ While coactivator-coactivator PPIs are common (*e.g.* CBP iBiD interacts with steroid receptor coactivator 1³²), the Med25-CBP interaction is interesting because CBP was thought to be functioning as a TAD mimic. All other reported PPIs involving Med25 AcID represented more traditional activator-coactivator interactions. As such, more in-depth biochemical study of the CBP-Med25 PPI was intriguing but required the discovery of a minimal sequence of CBP necessary for the PPI than the N-terminal 460 residues.

CBP 20-**PGFSANDSTDFGSL**----**FDLENDLPDELI**-44
VP16 454-**PGFTPHDSAPYGALDMADFEFEQMFTDALG**-486

Figure 2.3. Sequence alignment of CBP(20-44) and VP16(454-486). A basic local alignment search of CBP(1-460) demonstrated that CBP(20-44) was homologous to the VP16 H2 transcriptional activation domain. CBP(20-44) shares numerous acidic and hydrophobic residues in common with the VP16 sequence.

An analysis using the Basic Local Alignment Search Tool (BLAST) of CBP(1-460) against the transcriptional activation domain of VP16, found that CBP(20-44) shared homology (38% identity, 52% similar) with a portion of the VP16 activation sequence (Figure 2.3).³³ Like the VP16 TAD, CBP(20-44) is very negatively charged (-7 charge) and contains a high percentage of aromatic and bulky hydrophobic residues.

Following the identification of the short sequence within CBP that shared homology with a VP16 TAD, a small panel of CBP-derived peptides extending from residue 20 through residue 76 of CBP were synthesized. This encompassed the entirety of the predicted TAD-like sequence from 20-44 as well as additional patches of hydrophobic residues and a predicted α -helical sequence C-terminal to that sequence. The CBP(20-44) sequence in particular had many of the critical characteristics of a canonical TAD, including a high number of negatively charged and aromatic amino acids as well as a region predicted to adopt an α -helical structure.^{31,34} Six peptides in total were designed and synthesized – CBP(20-44), CBP(20-55), CBP(30-44), CBP(33-55), CBP(50-64), and CBP(59-76). Each peptide was appended with a N-terminal fluorescein and an accompanying β -alanine linker for use in FP assays to detect direct binding with Med25 AcID.

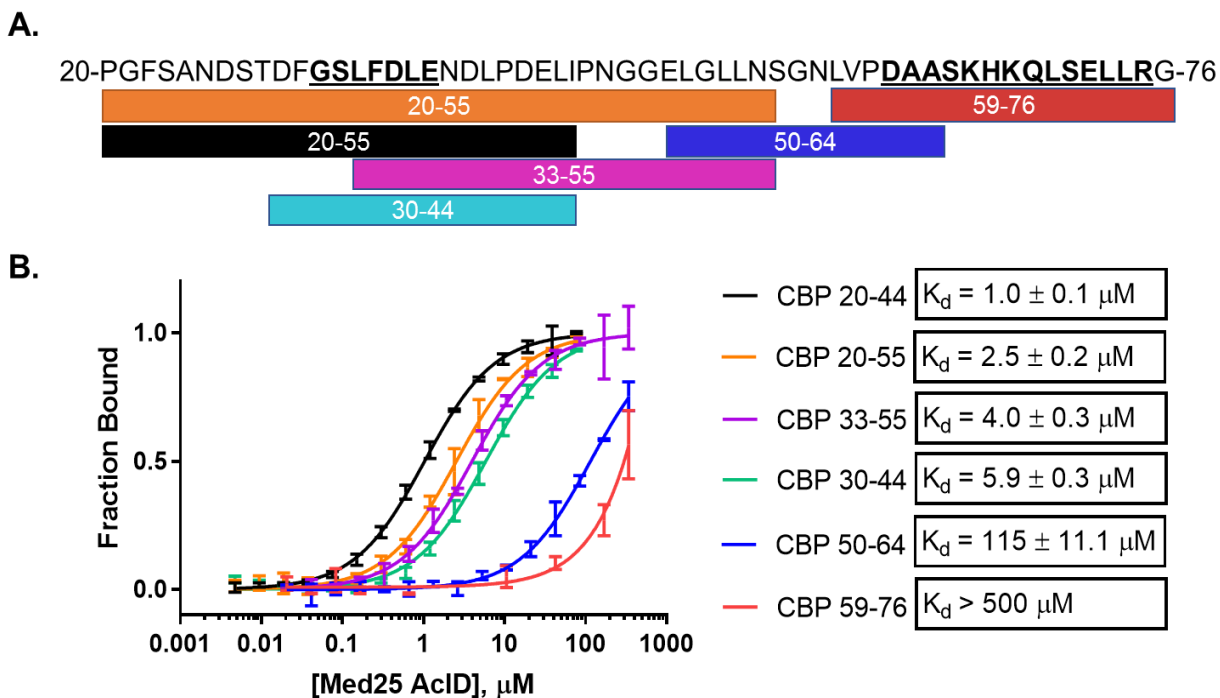


Figure 2.4. Minimal Med25 AcID-interacting sequences of CBP. (A) Sequence of CBP from 20-76. Predicted α -helical regions, from 32-38 and from 62-75, are bold and underlined. Synthesized peptides are shown, labeled and depicted as colored boxes, beneath their corresponding sequences. (B) Direct binding experiments between fluorescein-labeled CBP peptides and purified Med25 AcID. Binding curves are colored to match the sequences shown in (A). Data curves reported are average and standard deviations of triplicates of two independent experiments.

FP assays were consistent with a model in which residues 20-44 of CBP are the primary determinant for the interaction between Med25 AcID and the N-terminal region of CBP, as CBP(20-44) peptide bound Med25 AcID with a dissociation constant of $1.0 \pm 0.1 \mu\text{M}$. Binding affinity for Med25 AcID was not increased by shortening or extending this sequence, as evidenced by CBP(30-44) ($K_d = 5.9 \pm 0.3 \mu\text{M}$) and with CBP(20-55) ($K_d = 2.5 \pm 0.3 \mu\text{M}$) respectively. The most C-terminal peptides tested, CBP(50-64) and CBP(59-76), demonstrated very limited interaction with Med25 AcID with dissociation constants of $115 \pm 11.1 \mu\text{M}$ and $> 500 \mu\text{M}$ respectively. These results were unsurprising,

given the relative lack of negative charge present at the C-terminal region of the CBP(20-76) sequence.

A variant of the CBP(20-44) peptide replacing the N-terminal fluorescein with an acetyl group was synthesized to demonstrate that the observed PPI did not result from a specific interaction between Med25 AcID and fluorescein itself. In FP experiments with a 50% bound complex of Med25 AcID with fluorescein labeled CBP(20-44), acetylated CBP(20-44) was capable of disrupting this complex with a K_i of $9.4 \pm 0.8 \mu\text{M}$ (Figure 2.5). This level of inhibition, approximately 10x less than the binding affinity for FI-CBP(20-44), suggests that the fluorescein at the N-terminus of CBP(20-44) peptide does contribute slightly to the direct binding FP experiment. However, this degree of increased binding affinity can be explained by the hydrophobicity of fluorescein.

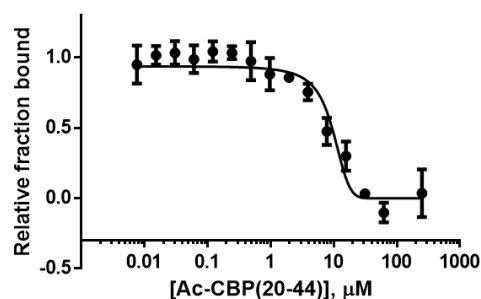


Figure 2.5. Acetylated CBP(20-44) inhibits Med25 AcID interaction with Fluorescein-CBP(20-44). At relative fraction bound of 1.0, Med25 AcID was 50% bound with FI-CBP(20-44). The data curve reported provides representative averages and standard deviations of triplicates.

Following confirmation that CBP(20-44) bound to Med25 AcID in FP experiments, ^1H - ^{15}N -HSQC experiments were performed to determine the binding site(s) of Med25 AcID responsible for this PPI. Acetylated CBP(20-44) peptide was titrated into ^{15}N -labeled Med25 AcID at 0, 1, 2, and 5 equivalents of peptide relative to protein. This titration demonstrated dose-dependent chemical shift perturbations of backbone amide bonds of

selected Med25 AcID residues (Figures 2.6, 2.7, 2.8). These dose-dependent chemical shifts demonstrated that Med25 AcID makes a specific PPI with CBP(20-44) and retention of most ^1H - ^{15}N resonances suggests that the overall structural fold of the protein remains intact.

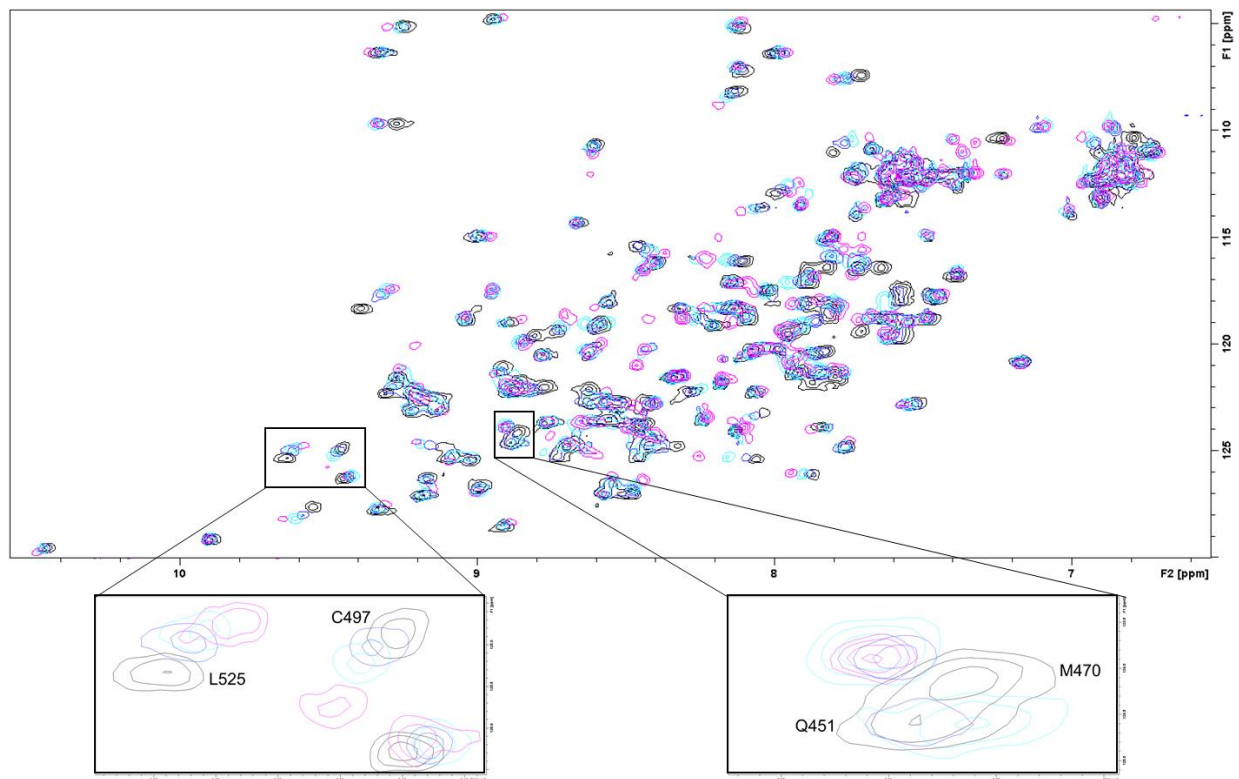


Figure 2.6. ^1H - ^{15}N -HSQC NMR spectra of Med25 AcID-CBP(20-44) complexes. An overlay of the HSQC spectra of ^{15}N -labeled Med25 AcID with DMSO (black), one equivalent of CBP(20-44) (light blue), two equivalents of CBP(20-44) (dark blue), and five equivalents of CBP(20-44) (pink) is shown.

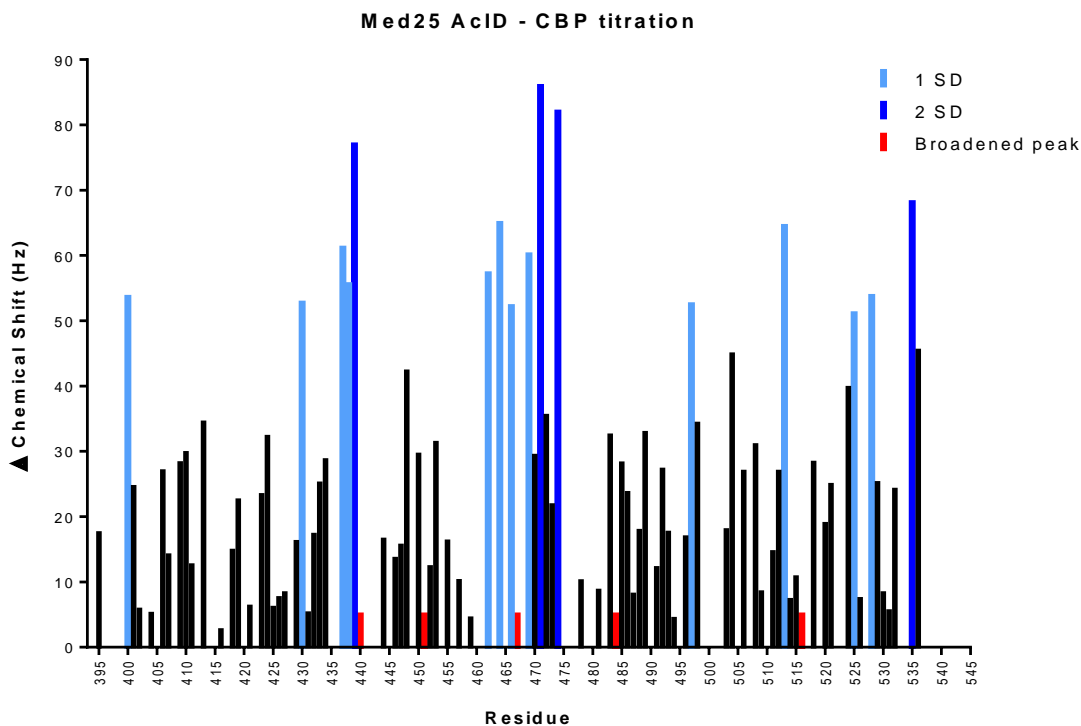


Figure 2.7. Chemical shift perturbations within Med25 AcID induced by saturating CBP(20-44) conditions. The magnitude of chemical shift perturbations, in Hz, are shown upon saturation of ^{15}N Med25 AcID with five equivalents CBP(20-44). Residues that shift 1-2 standard deviation (SD) above the mean (light blue), >2 standard deviations above the mean (dark blue), and that broaden into noise (red) are considered to be significantly affected by CBP(20-44).

Peaks in all of the collected HSQC spectra were assigned to specific residues using both a previously published NMR assignment²¹ and a *de novo* assignment performed by Andy Henderson (Mapp lab, University of Michigan). Notable residues of Med25 AcID that are most significantly affected by the addition of CBP(20-44) include residues located within the H1 face along $\beta 2/\beta 1/\beta 5$ and $\alpha 3$ (L406, Q409, E410, K413, M450, Q451, C497, V498, A504, C506, N535, and G536) in addition to the H2 face along $\beta 4/\beta 7/\beta 6$ and $\alpha 1$ (G462, L464, R466, N467, R469, V471, Q472, M512, L513, S516, G524, and L525). There were also several shifted peaks that correspond to residues that sit along $\beta 1/\beta 2$, the C-terminal

end of β_4 , α_2 , and on the loop between β_2 - β_3 (L400, L406, Q430, N434, E437, N438, L439, K440, F473, H474 L483, K484, G485, and L486).

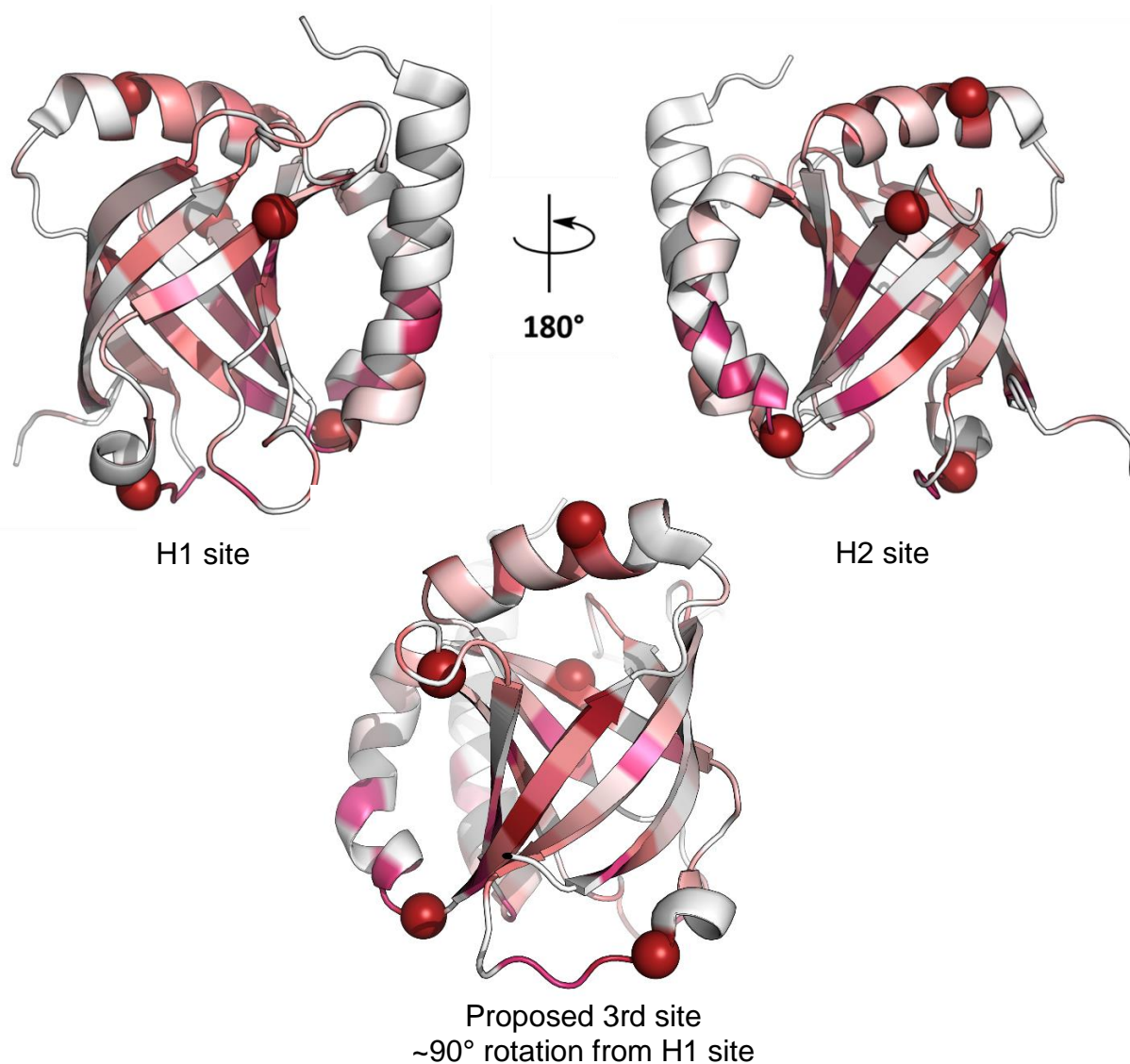


Figure 2.8. Chemical shift perturbations within Med25 AcID induced by saturating CBP(20-44) conditions. Mapped onto the structure of Med25 AcID are chemical shift perturbations upon binding to five equivalents CBP(20-44). Increasing shades of red indicate a gradient of increasing chemical shift perturbations. Red balls indicate residues that show near-complete peak broadening. (PDB 2XNF)

These data do not demonstrate that CBP(20-44) specifically interacts at the H1 or H2 sites of Med25 AcID. This indicates that CBP(20-44) binds to Med25 AcID with a

mechanism that is distinct from previously described activator partners. Instead, these data suggest that CBP(20-44) could interact at a newly reported third binding site located at $\beta 2/\beta 4/\alpha 2$, 90° away from the H2 site.³⁰ An interaction at this site would explain the high degree of significantly perturbed residues in that region of the protein. In the event that CBP(20-44) does interact at this third binding site, perturbation of residues in the H2 site would be explained by allosteric or through-molecule effects. Interestingly, this result is unexpected based on the BLAST analysis that demonstrated that CBP(20-44) was homologous to VP16 H1. Based on this homology experiment, it might be expected that CBP(20-44) would interact at the H1 site of Med25 AcID; That CBP(20-44) does not interact specifically at that site suggests that VP16 H1 itself might not be specific for the H1 site. Additional experiments described in Chapter 2 (mutagenesis at H1 and H2 binding sites) and in Chapter 3 (protein-observed ^{19}F NMR) provide additional evidence that CBP(20-44) interacts in a manner distinct from activators that directly bind at the H1 and H2 sites (such as VP16 H1, VP16 H2, ERM) and that it likely binds at the putative third site formed by $\beta 2/\beta 4/\alpha 2$.

Characterization of the Med25 AcID-ATF6 α protein-protein interaction

Similar to the N-terminus of CBP, previous reports demonstrated that the N-terminal 150-residue activation domain of ATF6 α interacted with Med25 AcID *in vitro*.³ However, the minimal binding region of ATF6 α for Med25 AcID was unknown. An analysis using BLAST was performed to discover that residues 42-67 of ATF6 α shared homology (38% identity, 48% similarity) with the VP16 H1 TAD, an interacting partner for Med25 AcID^{21–23,33}. Critically, this sequence of ATF6 α , similarly to VP16 H1, bears a net negative

charge (-9 charge for ATF6 α compared to -10 charge for the homologous region of VP16 H1) and is relatively hydrophobic (Figure 2.9).

ATF6 α 42-**DELQL**--**EAANET****YENNFDNLD****DFDL****DLM**-67
VP16 423-**DELRLDGE****EVDMT****PADALD**--**DFDL****EML**-448

Figure 2.9. Sequence alignment of ATF6 α (42-67) and VP16(423-448). A basic local alignment search of ATF6 α (1-150) demonstrated that ATF6 α (42-67) was homologous to the VP16 H1 transcriptional activation domain. ATF6 α (42-67) shares numerous acidic and hydrophobic residues in common with the VP16 sequence.

Again, in similar manner as was performed after discovery of CBP(20-44), a small panel of ATF6 α -derived peptides surrounding the region homologous to the VP16 H1 TAD were synthesized. This panel of peptides focused on synthesis of short sequences that were richest in negatively charged amino acids (Glu/Asp) and aromatic amino acids (Phe/Tyr/Trp) as well as predicted α -helical regions (D28-T39 and E43-A49). Recall that high proportion of negatively charged residues, amphipathic character, and a propensity to form α -helices are all common characteristics of TADs.³⁴ Seven peptides in total were synthesized – ATF6 α (13-33), ATF6 α (28-49), ATF6 α (40-66), ATF6 α (52-75), ATF6 α (63-75), and ATF6 α (66-80). The peptides of greatest interest at the time of synthesis were ATF6 α (40-66), designed to capture the entirety of the region homologous to VP16 H1; and ATF6 α (28-49), designed to encompass each of the predicted α -helices. Each peptide was appended with a N-terminal fluorescein and an accompanying β -alanine linker for use in FP assays to detect direct binding with Med25 AcID.

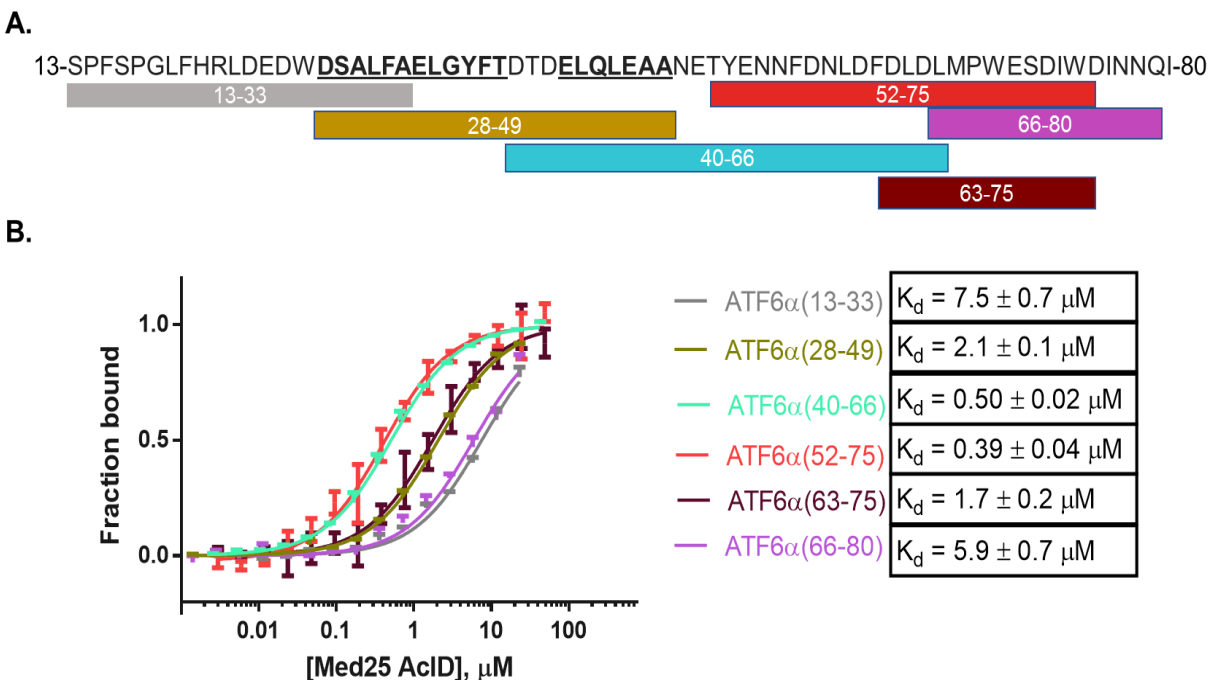


Figure 2.10. Minimal Med25 AcID-interacting sequences of ATF6α. (A) Sequence of ATF6α from 13-80. Predicted α -helical regions, from 28-39 and from 43-49, are bold and underlined. Synthesized peptides are shown, labeled and depicted as colored boxes, beneath their corresponding sequences. (B) Direct binding experiments between fluorescein-labeled ATF6α peptides and purified Med25 AcID. Binding curves are colored to match the sequences shown in (A). Data curves reported are average and standard deviations of triplicates of two independent experiments. Key

Each of the peptides synthesized demonstrated single-digit micromolar binding affinities towards Med25 AcID. Further, two peptides - ATF6α(40-66) and ATF6α(63-75) – exhibited binding affinities in submicromolar range. Collectively, this suggests that the ATF6α TAD is quite lengthy, spanning the majority of the 13-80 amino acid region that was explored. Since negatively charged and aromatic residues are dispersed throughout this ATF6α sequence, this observation is perhaps not unlikely. For future study of the Med25-ATF6α PPI, the ATF6α(40-66) peptide was chosen because of its homology with VP16 H1 and its tight binding affinity ($K_D = 0.50 \pm 0.02 \mu\text{M}$).

Next, ^1H - ^{15}N -HSQC experiments were performed to determine the binding site(s) of Med25 AcID responsible for its interaction with ATF6 α . Acetylated ATF6 α (40-66) peptide was titrated into ^{15}N -labeled Med25 AcID at 0, 0.25, 0.5, 1 and 3 equivalents of peptide relative to protein (Figures 2.11, 2.12, 2.13). Dose-responsive chemical shift perturbations of selected residues demonstrated that Med25 AcID specifically interacts with ATF6 α (40-66) and that the peptide does not destabilize the overall structural fold of Med25 AcID.

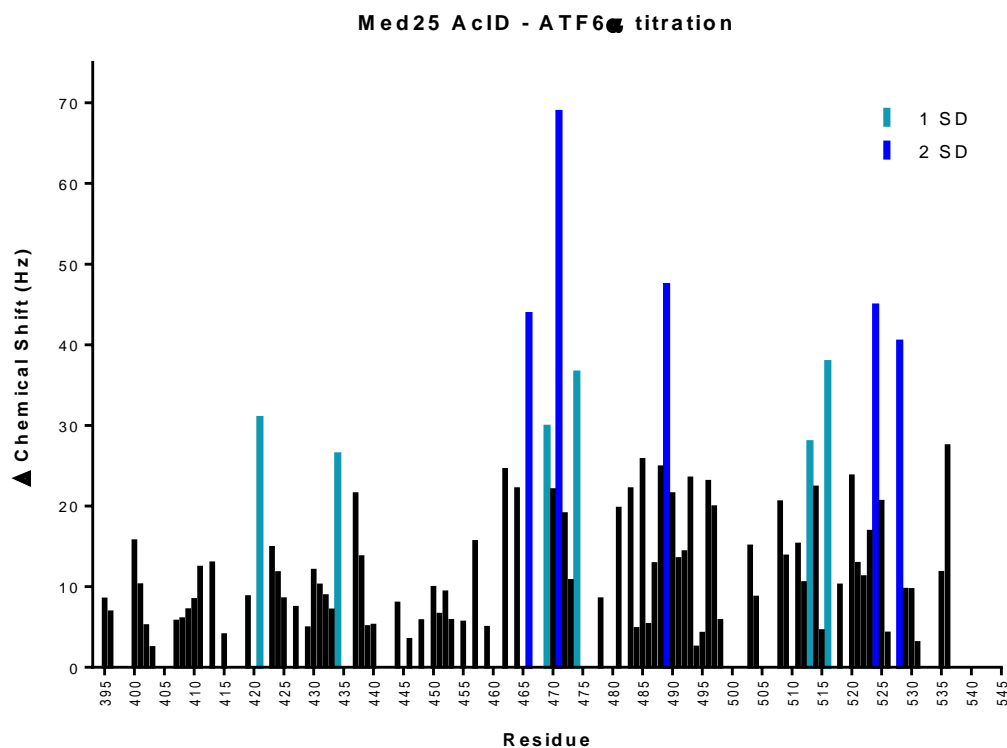


Figure 2.12. Chemical shift perturbations within Med25 AcID induced by saturating ATF6 α conditions. The magnitude of chemical shift perturbations, in Hz, are shown upon saturation of ^{15}N Med25 AcID with three equivalents ATF6 α (40-66). Residues that shift 1-2 standard deviation (SD) above the mean (light blue) and >2 standard deviations above the mean (dark blue) are considered to be significantly affected by ATF6 α (40-66).

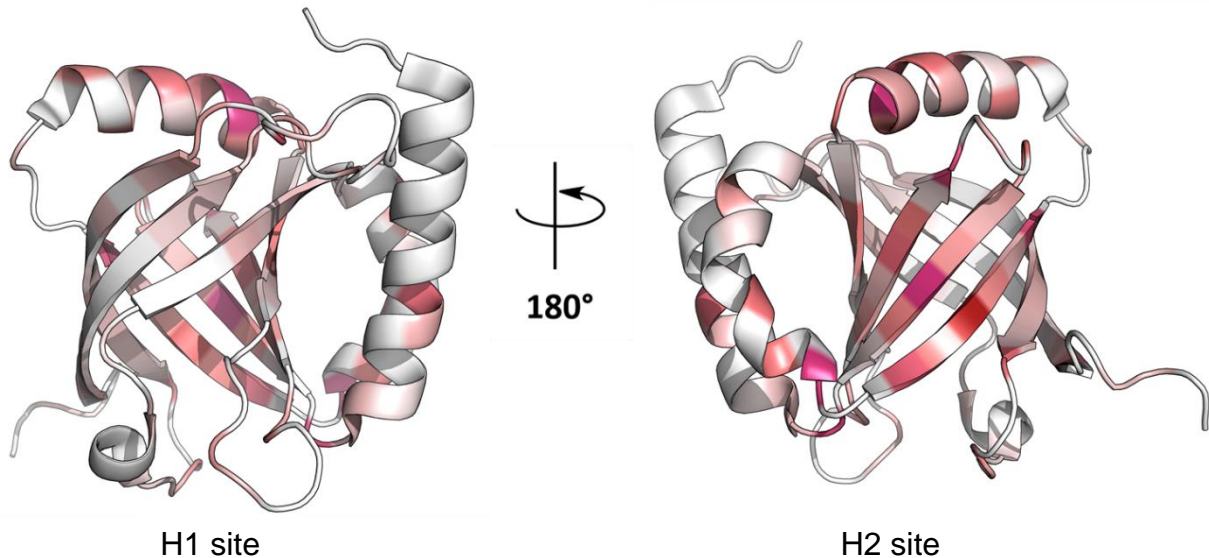


Figure 2.13. Chemical shift perturbations within Med25 AcID induced by saturating ATF6 α conditions. Mapped onto the structure of Med25 AcID are chemical shift perturbations upon binding to three equivalents ATF6 α (40-66). Increasing shades of red indicate increasing magnitude of chemical shift; Note that most of the significantly perturbed residues cluster around the H2 site. (PDB 2XNF)

As with CBP(20-44) titration, peaks in all of the collected HSQC spectra were assigned to specific residues using both a previously published NMR assignment²¹ and a *de novo* assignment performed by Andy Henderson (Mapp lab, University of Michigan). Notably, only residues of Med25 AcID located on the H2 face are significantly affected by the addition of ATF6 α (40-66). These affected residues located within the cleft of Med25 formed by β 4/ β 7/ β 6, α 1, and α 2 include G462, L464, R466, V471, H474, G485, R487, I488, M489, G490, G492, L513, L514, S516, M523, G524, and L525. The majority of these perturbed residues cluster within the H2 site of Med25 AcID in stark contrast to the similar experiment performed with CBP(20-44). There are minor, but not significant (>1 SD chemical shift), perturbations at the H1 face. These minor perturbations are likely a result of either a slight conformational change within Med25 AcID or through-molecule

effects. These data are consistent with ATF6 α (40-66) binding specifically to the H2 site of Med25 AcID.

Mutational analysis of Med25 to define binding models

Previous studies suggested that the two TADs of VP16 bind opposing faces of Med25 AcID. VP16 H1 binds to Med25 AcID at the surface formed by β 1– β 3– β 5 and α 2²³ and that VP16 H2 binds at the surface formed by α 1 and β 6– β 7– β 4²¹. However, the specificity of peptides for one site over the other remained an open and unanswered question. To better understand the specificity of individual binding partners towards each of the two binding sites, it was hypothesized that mutagenesis of specific Med25 AcID residues at each binding site could provide a more in-depth picture of these PPIs. Due to the observation made by others in the Mapp lab that charge-charge interactions between the positively charged Med25 AcID protein and negatively charged peptide ligands is a primary driver of these PPIs, most residues were mutated to introduce a negatively charged side chain (Glu or Asp). The introduction of negative charge at a single site was hypothesized to function as a mechanism to functionally block one site of Med25 while leaving the opposite site unaffected. This would allow for a determination of the selectivity of each discrete peptide ligands for unique binding sites on Med25 AcID. For example, it was anticipated that a Met-to-Glu mutation at residue 523, located in the center of the H2 face and perturbed by ATF6 α in HSQC NMR titrations, would cause a dramatic loss in binding affinity for ATF6 α (40-66) but have marginal effect on ERM(38-68), a ligand predicted to bind at the H1 face.

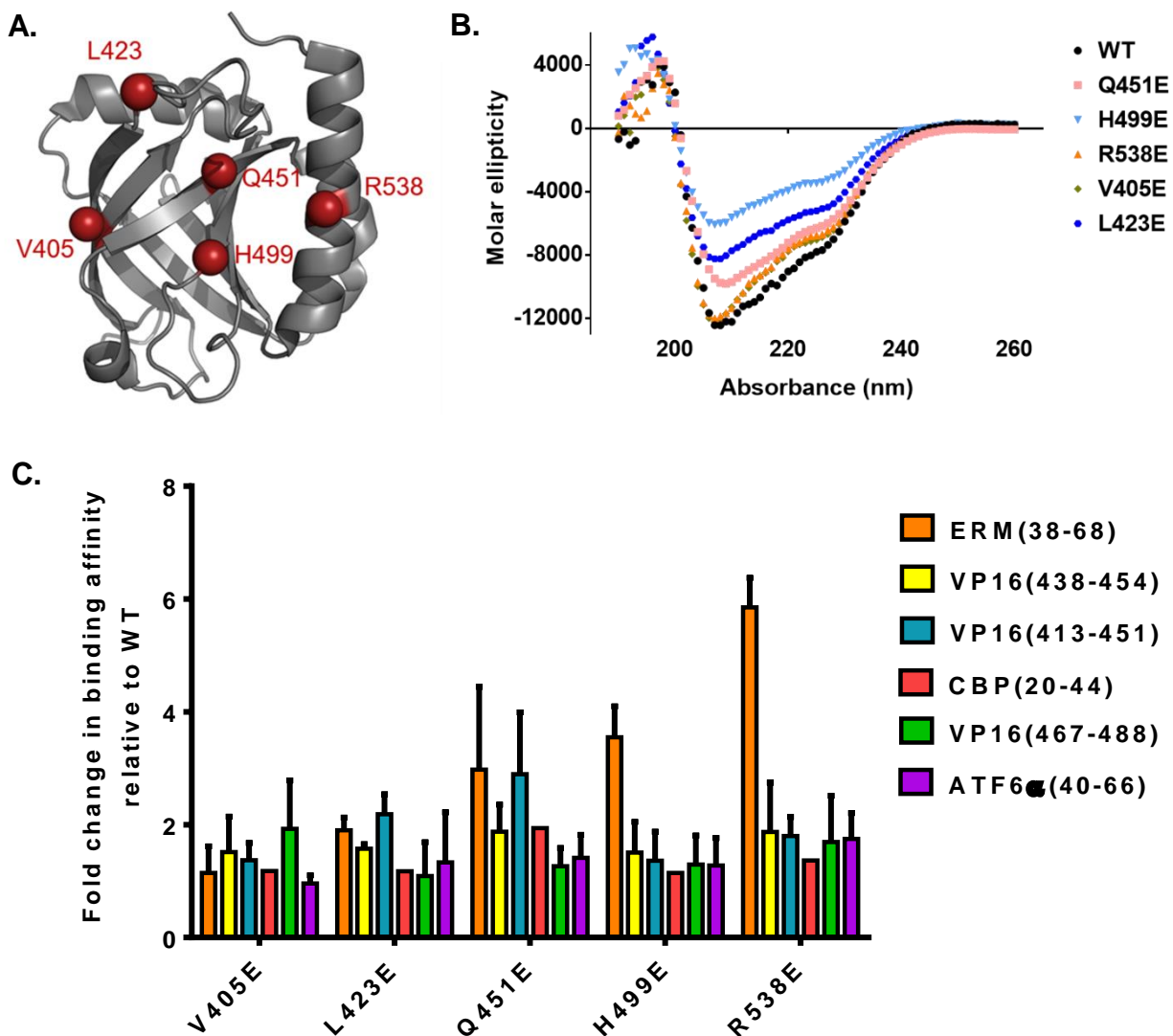


Figure 2.14. Mutagenesis at H1 site of Med25 AcID. (A) Residues selected for mutagenesis based on HSQC NMR titrations with ERM peptides. (B) Circular dichroism spectra of WT Med25 AcID and H1 site mutants. (C) Binding affinities of Med25-interacting peptides for H1 site mutants relative to WT Med25 AcID, as measured by FP. Bar graphs represent the average and standard deviations of the fold change of three independent experiments performed in triplicate.

$$Fold\ change = \frac{(K_D\ for\ Mutant\ Med25\ AcID-peptide\ interaction)}{(K_D\ for\ WT\ Med25\ AcID-peptide\ interaction)}$$

Initial residues selected for mutagenesis to introduce a negatively charged residue at the H1 binding face - V405, L423, Q451, H499, and R538 - were chosen based on analysis of published HSQC NMR data of the Med25-ERM PPI.¹⁷ All mutants, following

site-directed mutagenesis of a plasmid containing WT Med25 AcID, were expressed and purified following standard conditions defined for WT Med25 AcID. Mutant proteins were then subjected to a battery of biochemical experiments - FP assays against Med25-interacting peptide ligands, circular dichroism, and CD-monitored thermal denaturation – to determine the functional impact of the mutation (Figure 2.14). Circular dichroism, which measures protein secondary structure, suggested that most mutant proteins retained WT-like secondary structure. L423E and H499E both demonstrated minima at 208 and 228 nm that were of lesser magnitude than WT Med25 AcID. This suggests that these mutations had a slight effect on the helicity of the protein fold. This is not unexpected as L423E introduces a negative charge in the proximity of $\alpha 2$ while H499E places a negative charge in the proximity of $\alpha 3$. Interestingly, all single-point mutants tested behaved similarly in CD-monitored thermal denaturation experiments with 12-15% losses in melting temperature (58-60 °C compared to 71 °C for WT Med25 AcID). Taken together, these experiments demonstrate that mutations at the H1 face of Med25 AcID could result in minor losses in stability but have little effect on the overall structural integrity of Med25 AcID.

It had been anticipated that the introduction of glutamic acid within the H1 binding face would result in large losses in apparent binding affinity relative to WT Med25 AcID for peptides predicted to preferentially bind at the H1 face such as ERM(38-68), VP16 (438-454) – the helical region of VP16 H1 – and VP16(413-451) – the entirety of the VP16 H1 TAD. However, FP experiments utilizing these mutants demonstrated that they conferred only a modest effect on the binding affinities for Med25-interacting ligands. V405E and L423E demonstrated a less than two-fold loss in binding affinity for all peptides

tested relative to WT Med25 AcID. This could indicate that these two residues are outside of the H1 site, as neither mutation provided significant effects (greater than 3-fold change). Q451E, H499E, and R538E all demonstrated a significant effect on the binding interaction with ERM(38-68) with 3.0-, 3.5-, and 5.9- fold losses in binding affinity relative to WT, respectively. These data are consistent with ERM(38-68) binding preferentially to the H1 site. However, they do suggest that either a single mutation is not sufficient to fully block the H1 site or that ERM is capable of compensatory interactions at the H2 site. Q451E, H499E, and R538E did not significantly affect any other peptide ligand. Collectively, these data suggest that the H1 binding site is less dependent on electrostatic interactions and hotspot residues than previously assumed, that a single mutation is not sufficient to block the H1 site, and/or that the H1 site could allow for multiple conformations of binding.

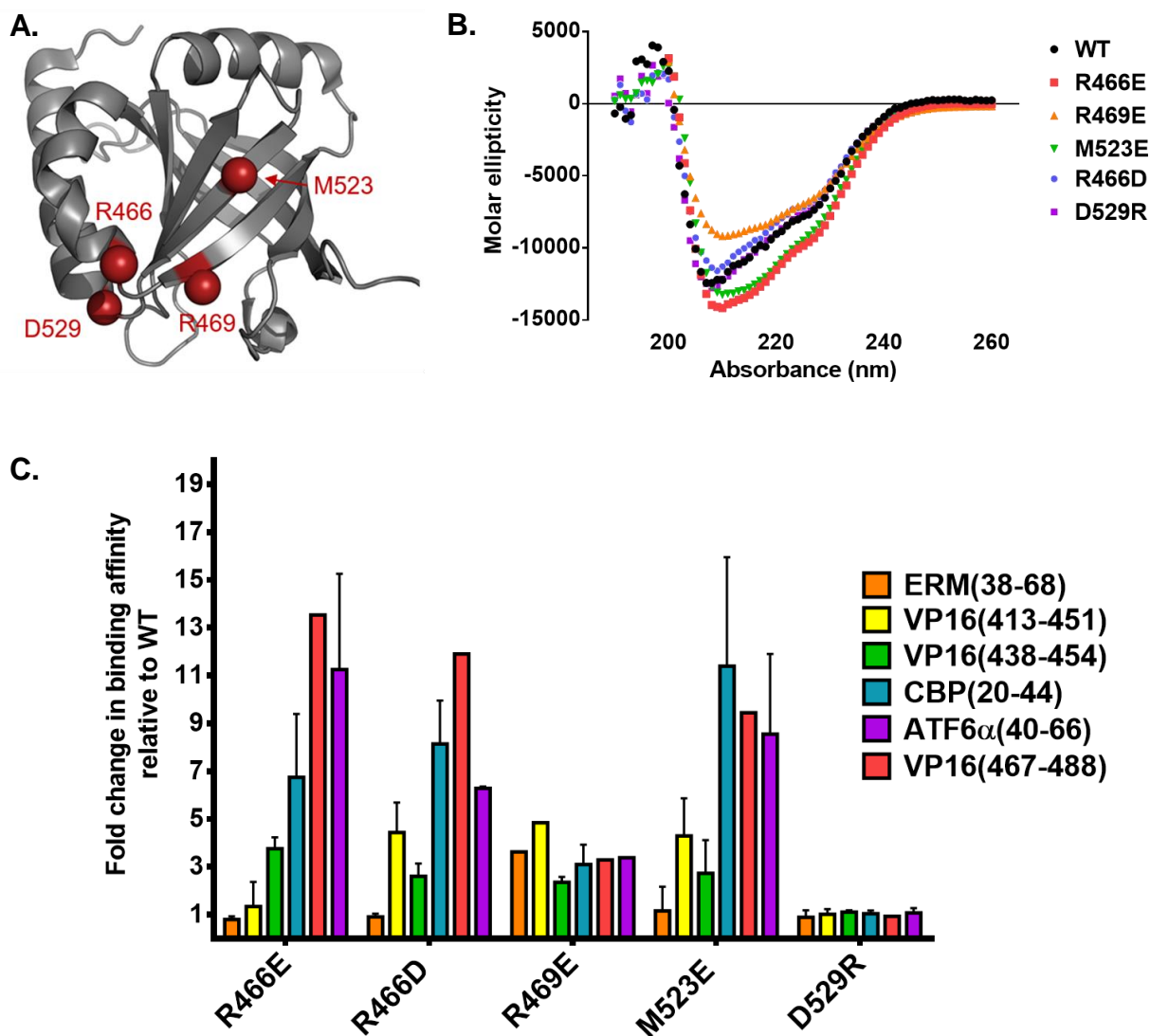


Figure 2.15. Mutagenesis at H2 site of Med25 AcID. (A) Residues selected for mutagenesis based on HSQC NMR titrations with ATF6 α (40-66). (B) Circular dichroism spectra of WT Med25 AcID and H2 site mutants. (C) Binding affinities of Med25-interacting peptides for H2 site mutants relative to WT Med25 AcID, as measured by FP. Bar graphs represent the average and standard deviations of the fold change of three independent experiments performed in triplicate.

$$\text{Fold change} = \frac{(K_D \text{ for Mutant Med25 AcID-peptide interaction})}{(K_D \text{ for WT Med25 AcID-peptide interaction})}$$

Initial residues selected for mutagenesis at the H2 binding face – R466, R469, and M523 – were chosen based on HSQC NMR data of the Med25-ATF6 α PPI (Figure 2.13). Negatively charged amino acids (Glu or Asp) were singly introduced at all three positions.

All mutants, following site-directed mutagenesis of parent Med25 plasmid, were expressed and purified following standard conditions defined for WT Med25 AcID. Circular dichroism demonstrated that single-point H2 mutant proteins (R466D, R466E, and M523E) retained the core secondary structure of WT Med25 AcID (Figure 2.15) with minor differences. CD spectra of R469E does have a minimum at 208 nm that is of meaningfully lesser magnitude than WT suggesting that this particular mutation affects the helical structure of Med25 AcID, potentially through disruption of α 1. Additionally, each single-point mutant brought minor losses in protein stability in CD-observed thermal denaturation experiments (15-19% decrease in melting temperatures relative to WT Med25 AcID).

Differing from the example of H1 mutations, FP experiments performed with R466D, R466E, and M523E demonstrated that introduction of negative charge within the predicted H2 binding face had dramatic effects on binding affinity for CBP(20-44), VP16(467-488) – the helical region of VP16 H2, and ATF6 α (40-66). Specifically, the binding affinities of R466E Med25 AcID to CBP(20-44), VP16(467-488), and ATF6 α (40-66) were, respectively 6.7-fold, 14-fold, and 11-fold weaker than the corresponding interactions with WT Med25 AcID. The binding affinities of R466D Med25 AcID to CBP(20-44), VP16(467-488), and ATF6 α (40-66) were, respectively, 8.1-fold, 11-fold, and 6.3-fold weaker than the corresponding interactions with WT Med25 AcID. Finally, the binding affinities of M523E Med25 AcID to CBP(20-44), VP16(467-488), and ATF6 α (40-66) were, respectively, 11-fold, 9.4-fold, and 8.5-fold weaker than the corresponding interactions with WT Med25 AcID. These experiments corroborate earlier experiments indicating that the H2 site is dependent on electrostatic contacts between positive charges

of Med25 AcID and negatively charged TADs. Additionally, these findings suggest that the peptides derived from ATF6 α , CBP, and VP16 H2 are specific interacting partners at the H2 face of Med25. If these peptide ligands could bind equally or nearly as well to the H1 face as to the H2 face, there would be a limited reduction in binding affinities to H2 mutants relative to WT. These three single-point mutants did not show decreases in binding affinities that were nearly as dramatic for ERM(38-68), VP16(413-451) or VP16(438-454). The lack of large reductions in binding affinity for these peptides, particularly ERM(38-68), suggests that the binding interaction of these peptide ligands for Med25 is not dependent on the H2 face.

The R469E mutation brought about a moderate but significant decrease in the binding affinity for all tested peptides. The minima observed at 208 nm and 228 nm, which represent α -helical character, in the CD spectrum of R469E were of lesser magnitude than that of WT Med25 AcID. Taken in concert, FP assays and CD analysis suggests that this mutation, with a side chain directed away from the center of the H2 binding face, could be affecting the structural integrity of Med25 AcID. It is possible that an introduction of negative charge at this position could result in the disruption of either α 1 or α 3. The D529R mutation was designed in part to function as a control mutation. D529 is positioned on α 3, away from both the H1 and H2 faces, and was not predicted to be involved in any PPIs. D529R Med25 AcID retained WT-like secondary structure and showed no effect (0.9-1.1 fold change) toward any Med25-interacting peptides.

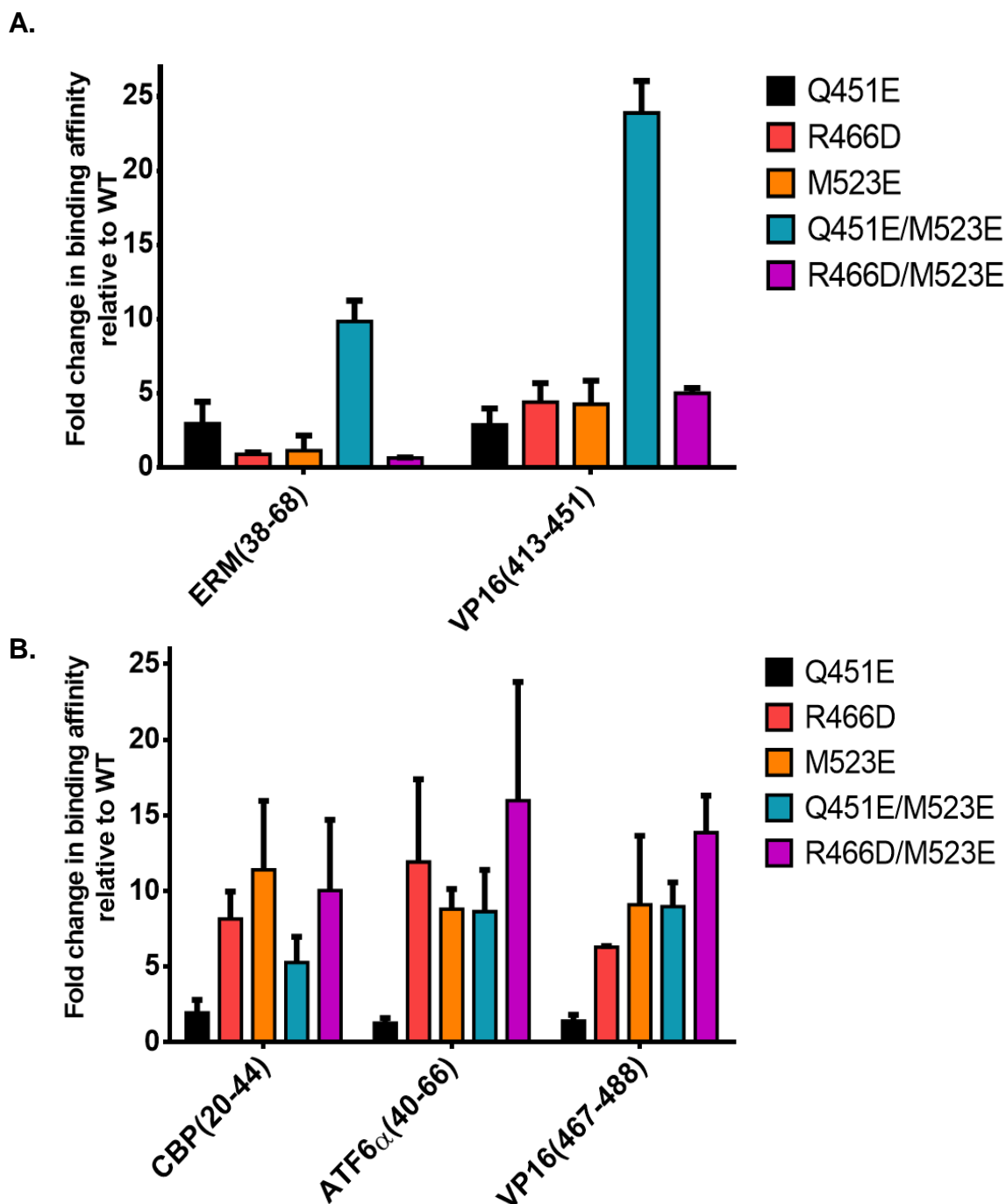


Figure 2.17 Mutagenesis to block H1 and H2 sites simultaneously. (A) Binding affinities of putative H1 site peptides for Med25 mutants relative to WT Med25 AcID, by FP. Bar graphs represent the average and standard deviations of the fold change of three independent experiments performed in triplicate. (B) Binding affinities of putative H2 site peptides for Med25 mutants relative to WT Med25 AcID.

$$\text{Fold change} = \frac{(K_D \text{ for Mutant Med25 AcID-peptide interaction})}{(K_D \text{ for WT Med25 AcID-peptide interaction})}$$

To continue the investigation into peptide selectivity between the putative H1 and H2 sites, methods to inhibit function at both sites were desired. Knowledge from the single mutagenesis experiments was leveraged to generate two doubly mutated Med25 AcID variants - Q451E/M523E and R466D/M523E.

An attempt to block the H1 and H2 faces simultaneously through the Q451E/M523E mutant was successful in corroborating that peptides believed to specifically target the H1 face – ERM(38-68) and VP16(413-451) – are capable of interacting at the H2 face (Figure 2.17.A). Q451E Med25 AcID bound ERM(38-68) 3.0-fold less tightly than WT Med25 AcID; Q451E/M523E bound ERM(38-68) 9.9 times less tightly than WT Med25 AcID. The single mutants R466D and M523E, as well as double mutant R466D/M523E, had no effect on the binding of ERM(38-68). This single mutant data suggests that ERM(38-68) has a preference for interaction at the H1 site, as evidenced by impact of negative charge at H1 face alone but not at H2 face alone. However, the large increase in the magnitude of the effect in the case of Q451E/M523E definitively demonstrates that ERM(38-68) must be capable of interacting at the H2 face when/if the H1 face is blocked. In the case of the other ligand predicted by NMR to bind the H1 face, each of the three single-point mutants (Q451E, R466D, M523E) inhibited VP16(413-451) equally well with 3.0- to 4.0- fold losses in binding affinity relative to WT Med25 AcID. This suggested that, contrary to published HSQC NMR experiments, VP16(413-451) could bind equally well at both the H1 and H2 faces of Med25 AcID. The double mutant Q451E/M523E validated this finding, since blocking both sites resulted in 24-fold loss in binding affinity.

The double mutagenesis was also effective at providing corroborating evidence that both ATF6 α (40-66) and VP16(467-488) are highly selective/specific for the H2 face of Med25 AcID (Figure 2.17.B). The double mutant Q451E/M523E had nearly identical effects on binding affinity towards ATF6 α (40-66) and VP16(467-488) as did M523E itself (9.4-fold loss in affinity vs. 8.6-fold loss against ATF6 α (40-66); 9.0-fold loss in affinity vs. 9.1-fold loss against VP16(467-488)). The inability of the H1 mutation to provide additional inhibitory benefit relative to a single H2 mutant demonstrates that neither peptide is affected by the blocking of the H1 face through the introduction of negative charge. Further, as anticipated, the double mutant R466D/M523E was more effective at inhibition of ATF6 α (40-66) and VP16(467-488) than either single mutant. The CBP(20-44) peptide, as in HSQC NMR experiments, behaved unlike all others. Neither double mutant was more effective at inhibition of CBP(20-44) than either R466D or M523E. In fact, Q451E/M523E bound CBP(20-44) more tightly (5.3-fold loss in binding affinity relative to WT) than M523E (11-fold loss in binding affinity). It is possible that this data suggests, in light of the HSQC NMR experiments, that CBP(20-44) is partially interacting at the putative third site of Med25 AcID. If this is the case, the inability of Q451E/M523E to replicate the effects of M523E alone could be explained by either a slight conformational change in Med25 AcID or an alteration in the orientation of the peptide interaction with the protein.

A secondary method to block both the H1 and H2 faces simultaneously was explored using a combination of mutagenesis and covalently tethered peptide ligands. It had been discovered that a unique derivative of VP16(438-454) that incorporated a cysteine at the G450 position can form a disulfide linkage with C506 of Med25 AcID. C506

of Med25 AcID is positioned on a loop nearby the H1 face site and nearly 100% labeling with the G450C peptide can be achieved using disulfide Tethering^{35,36}. HSQC NMR experiments of WT Med25 AcID tethered to G450C peptide demonstrate that the peptide does not destabilize the overall structure of the protein and that it likely interacts with the H1 face of Med25 AcID (Figure 2.18). Therefore, it was expected that the G450C peptide would function to block, or inhibit, the H1 face of Med25 AcID, likely more efficiently than does Q451E, R538E, or H499E.

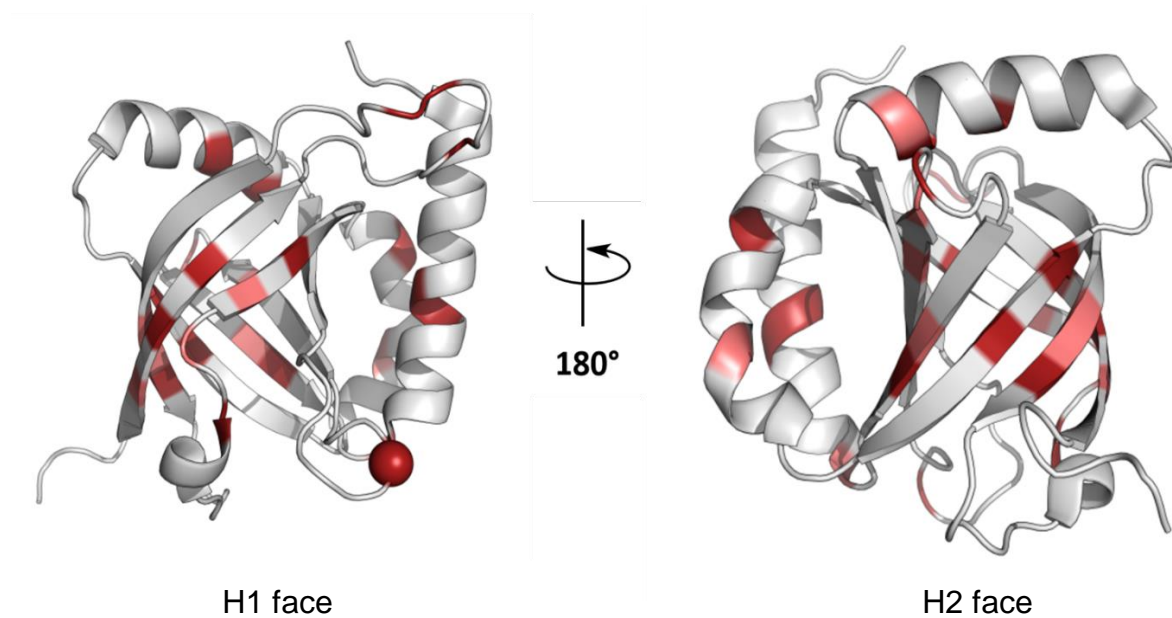


Figure 2.18. Chemical shift perturbations within Med25 AcID induced by tethered VP16 G450C peptide. Mapped onto the structure of Med25 AcID are chemical shift perturbations caused by formation of a covalent complex with VP16 G450C peptide. Significantly perturbed residues are depicted in pink (>1 standard deviation from mean) and red (>2 standard deviation). Cys506 is depicted with red sphere. (PDB 2XNF)

Modifications performed in tandem (G450C peptide at H1 site; mutagenesis at H2 site) designed to block both faces simultaneously performed similarly to the Q451E/M523E double mutation and corroborated the conclusions that were drawn from

that set of experiments for ERM(38-68), VP16(413-451), and VP16 H2 peptides (Figure 2.19).

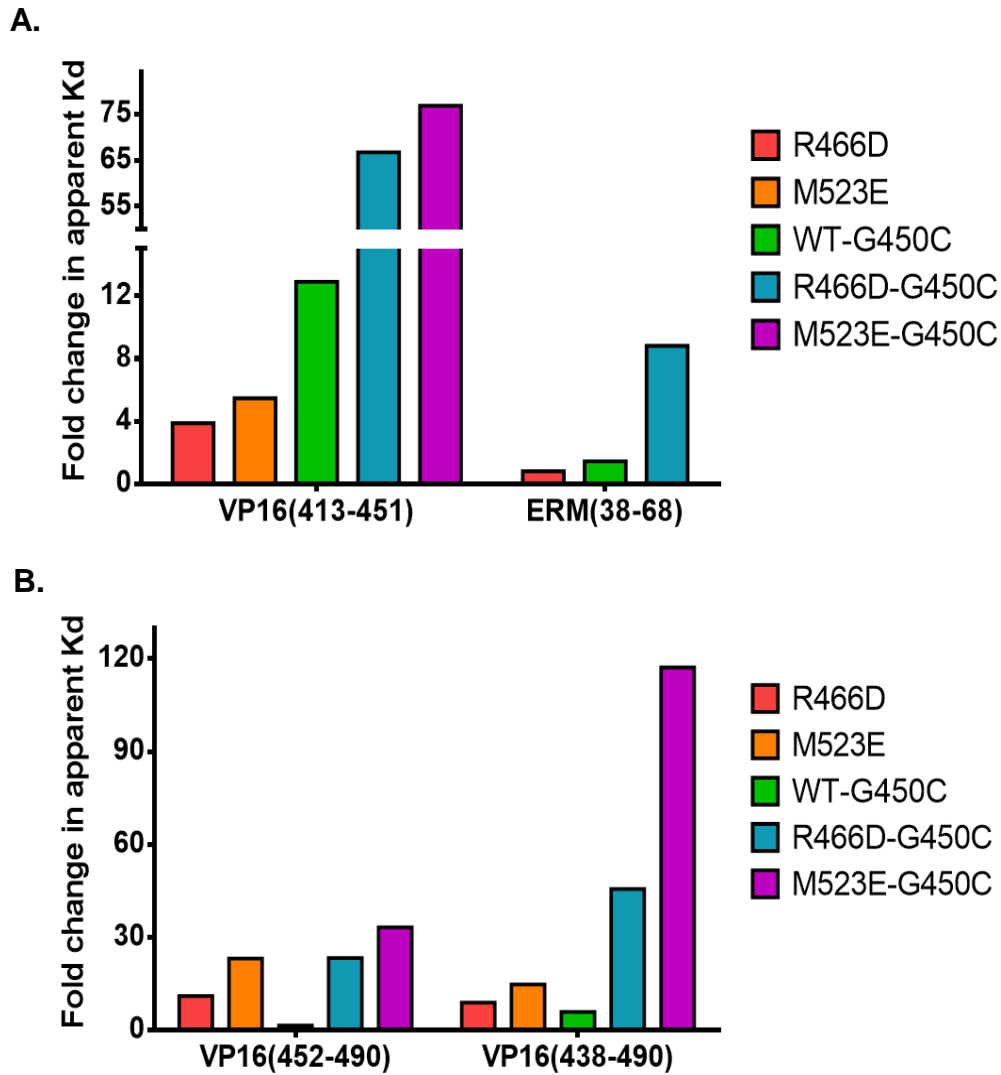


Figure 2.19 Mutant Med25-G450C peptide complexes to block H1 and H2 sites simultaneously.

(A) Binding affinities of putative H1 site peptides for Med25 mutants complexed to VP16 G450C relative to WT Med25 AcID, by FP. Bar graphs depict the average and standard deviations of the fold change of experiments performed in triplicate. (B) Binding affinities of putative H2 site peptides for Med25 mutants complexed to VP16 G450C relative to WT Med25 AcID, as measured by FP.

$$Fold\ change = \frac{(K_D\ for\ Mutant\ Med25\ AcID-peptide\ interaction)}{(K_D\ for\ WT\ Med25\ AcID-peptide\ interaction)}$$

Blocking either the H1 (G450C peptide complex) or H2 face (R466D) had negligible impact on the binding affinity of ERM(38-68) relative to WT Med25 AcID. However, a complex of R466D Med25 AcID tethered to G450C peptide bound ERM(38-68) with a 8.8-fold weaker binding affinity than WT Med25 AcID. Blocking the H1 face (G450C peptide complex) caused a 13-fold loss in binding affinity towards VP16(413-451); blocking the H2 face (R466D or M523E) caused a 4.0- to 5.5- fold loss in affinity. However, blocking both faces with mutant proteins, R466D and M523E, complexed to G450C peptide led to 67- and 77- fold losses in binding affinity, respectively. For each of these peptides, as had been shown in the Q451E/M523E set of experiments, these results add to the mountain of evidence suggesting that neither of ERM(38-68) nor VP16(413-451) binds exclusively to the H1 face.

Again, as had been shown in Q451E/M523E experiments, VP16 H2 is more specific for the H2 site than any of the presumed H1 peptides are for the H1 site. However, blocking the H1 site with G450C peptide proved to be more effective than the Q451E mutation. In the Q451E/M523E experiments, no additional inhibitory benefit against VP16(467-488) had been attributed to the Q451E mutation. However, the addition of G450C peptide to H2 mutant proteins did produce a more pronounced effect on the binding affinity of VP16(452-490) than R466D or M523E alone. R466D-G450C peptide complex bound VP16(452-490) with 23-fold decrease in binding affinity relative to WT Med25 AcID; R466D gave a 11-fold decrease. M523E-G450C peptide complex bound VP16(452-490) with 33-fold decrease in binding affinity relative to WT Med25 AcID; R466D gave a 23-fold decrease. This loss in specificity for the H2 site could be explained by a change in the peptide used during these experiments. VP16(452-490), the peptide

used in the mutant-G450C peptide experiments, is a larger VP16 H2-derived peptide than used in single and double mutagenesis work previously described. It is highly possible that the N-terminal portion of this construct is beginning to wrap around Med25 AcID and contacting the H1 site directly while the C-terminal portion is contacting the H2 site. The final peptide tested in this set of experiments, VP16(438-490), contains the helical region of VP16 H1 and the entirety of VP16 H2. It is known to interact with both the H1 and H2 sites²¹ simultaneously. Each of the three single-site inhibitory methods – R466D, M523E, and G450C peptide – cause a significant loss in binding affinity relative to WT Med25 AcID (8.9-, 15-, and 6.0- fold losses respectively). As anticipated, blocking both sites has a dramatic effect on binding to this particular peptide – R466D complexed with G450C peptide experienced a 46-fold loss in binding affinity relative to WT Med25 AcID and M523E complexed with G450C peptide experienced a 117-fold loss in binding affinity relative to WT Med25 AcID.

D. Conclusions and future directions

Through the work outlined in this chapter, I set out to expand the understanding of the molecular underpinnings of the interactions between Med25 AcID and its binding partners. Previous literature reports had demonstrated that Med25 AcID contains two binding sites that interact with VP16 TADs and ERM(38-68)^{17,21,23}. Additional data from the Mapp lab had determined that Med25 AcID-VP16 PPIs were dependent on electrostatic interactions between acidic TADs and basic amino acids on the surface of the AcID motif. However, the selectivity of unique activator ligands for single sites within Med25 AcID remained an open question at the beginning of this Chapter. In addition, the

minimal interacting regions of two Med25 AcID binding partners (CBP and ATF6 α) had not yet been identified and the PPIs had not been biochemically characterized.

Using basic local alignment searches coupled with peptide synthesis and FP assays, the minimal regions of CBP and ATF6 α that interact specifically with Med25 AcID were determined. Subsequent HSQC NMR suggested that CBP(20-44) bound Med25 AcID did not interact specifically at one of the two previously reported binding sites for VP16 and that ATF6 α (40-66) likely interacted at the H2 site of Med25 AcID.

The H1 and H2 sites of Med25 AcID were also investigated by selectively blocking each interface through the introduction of negative charges at the H1 and H2 sites using protein mutagenesis and the addition of a Tethered VP16 G450C peptide at the H1 site. Collectively, experiments to block the H2 site suggested that binding at the H2 site is more dependent on electrostatic interactions and 'hot spot' residues than the H1 site. Additionally, these data demonstrated that ATF6 α and VP16 H2 preferentially interact at the H2 site. However, peptides predicted to bind the H1 site by HSQC NMR^{17,23} – ERM and VP16 H1 – did not demonstrate similar selectivity for the H1 site. Instead, ERM and VP16 H1 were both capable of binding to the H2 site when the H1 site was blocked, as demonstrated by the double H1/H2 site inhibition experiments.

While the mutagenesis study and ¹H, ¹⁵N-HSQC NMR experiments within this chapter and in the literature, are consistent in loosely describing the multi-site binding model of Med25 AcID, there remained uncertainty regarding the specific differences between discrete Med25 AcID binding partners. Each of the described binding sites are very large (estimated at ~1800 Å²), as determined by HSQC NMR, which leads to several questions. Does every protein partner orient itself in the same direction within a binding

site? Do protein ligands associate with the entirety of a binding site or just a portion of it? Furthermore, it has been suggested in this chapter that some peptide ligands (e.g. VP16 H1) are capable of binding at the H1 and the H2 sites. What does this supposition mean for binding stoichiometry and the relative affinities that a ligand might have towards one binding site over another? Are some peptides capable of binding with >1:1 stoichiometry?

Many of these next-level mechanistic questions require higher levels of sensitivity than can be provided using either HSQC NMR or fluorescence polarization experiments. To overcome this sensitivity problem and to answer many of the questions posed above, protein-observed ^{19}F -NMR of Med25 AcID and its PPI network will be described in Chapter 3. This burgeoning technique involves the incorporation of site-selective ^{19}F nuclei into the side chains of Med25 AcID for the direct observation of individual protein-protein and protein-ligand interactions. These ^{19}F -incorporated residues are well-dispersed across the binding sites of Med25 and allow for precise determination of binding locations, relative affinities between differing binding sites, and binding stoichiometry of each Med25-peptide interaction.

E. Materials and methods

Reagents and Instrumentation

Unless otherwise noted, chemical and biological reagents were obtained from commercial sources and were used without additional modification. Protein, peptide, and DNA concentrations were determined using a NanoDrop ND-1000 UV-Vis Spectrophotometer and/or a Beckman Spectrophotometer.

Plasmids

pET21b-Med25(394-543)-His6 was provided by Patrick Cramer. Mutant Med25 AcID plasmids Point mutations of pET21b-Med25(394-543)-His6 were generated using standard molecular biology protocols.

Expression of Med25 AcID and Med25 AcID mutants

All WT Med25 AcID and Med25 AcID mutants were expressed as follows. pET21b-Med25(394-543)-His6 was transformed into chemically competent Rosetta pLysS cells (Novagen), plated onto LB/ampicillin/chloramphenicol agar, and incubated at 37 °C overnight. In the morning, agar plates were placed at 4 °C until further use. In the evening, a single colony from the transformed plate was placed into 25 mL Luria Broth with 0.1 mg/mL ampicillin and 0.034 mg/mL chloramphenicol and incubated at 37 °C overnight at ≥ 200 RPM. The following morning, 5-20 mL from the starter culture was added to 1 L Terrific Broth with 0.1 mg/mL ampicillin and bacteria were grown at 37 °C at ≥ 200 RPM to an OD₆₀₀ of 0.8-1.0. Temperature was reduced to 20 °C for a minimum of thirty minutes prior to induction of protein expression with 0.2-0.5 mM IPTG. Bacteria were shaken

overnight at 20 °C at ≥ 200 RPM. The following morning, bacterial cultures were centrifuged at 7000 x g for 20 mins at 4 °C. Cell pellets were then stored at -80 °C prior to protein purification.

Expression of ^{15}N -labeled Med25 AcID

pET21b-Med25(394-543)-His6 was transformed into chemically competent Rosetta pLysS cells (Novagen), plated onto LB/ampicillin/chloramphenicol agar, and incubated at 37 °C overnight. In the morning, agar plates were placed at 4 °C until further use. In the evening, a single colony from the transformed plate was placed into 25 mL Luria Broth with 0.1 mg/mL ampicillin and 0.034 mg/mL chloramphenicol and incubated at 37 °C overnight at ≥ 200 RPM. The following morning, 5-20 mL from the starter culture was added to 1 L Terrific Broth with 0.1 mg/mL ampicillin and bacteria were grown at 37 °C at ≥ 200 RPM to an OD_{600} of 0.8-1.0. Cells were centrifuged and washed with M9 minimal media. Cells were then resuspended in 1 L M9 minimal media with ampicillin and 2-3 mL BioXpress (Cambridge Isotope Laboratories) was added. Cultures were incubated at 37 °C overnight at ≥ 200 RPM for one hour reducing the temperature to 20 °C. After 30-45 minutes, 0.5 mM IPTG was added. Bacteria were shaken overnight at 20 °C at ≥ 200 RPM. The following morning, bacterial cultures were centrifuged at 7000 x g for 20 mins at 4 °C. Cell pellets were then stored at -80 °C prior to protein purification.

Purification of Med25 AcID and Med25 AcID mutants

The purification of Med25 AcID proteins was completed using two different protocols – one that used a Ni-NTA 5 mL HiTrap FPLC column and the other that used Ni-NTA resin (Qiagen). Both are described below.

1. Ni-NTA 5 mL HiTrap FPLC column

Cell pellets were thawed and resuspended with 30-35 ml Lysis Buffer (50 mM phosphate, 300 mM NaCl, 10 mM imidazole, pH 7.2). β -mercaptoethanol, at 1:1000 dilution, and one cComplete, Mini, EDTA-free Protease Inhibitor tablet (Sigma-Aldrich) were added to the resuspended cell pellet. To lyse, the cells were sonicated on ice for 4-6 min (Cycle - 3 seconds on, 7 seconds off) and/or until the cells had observable change in color (lighter brown) and viscosity. Following sonication, the lysed pellet in 50 mL conical tube(s) was centrifuged at 9,500 RPM for 30 min at 4 °C. The supernatant was decanted into fresh 50 mL conical tubes, the pellet was discarded, and the supernatant was centrifuged at 9,500 RPM for 10 min at 4 °C. After this second centrifugation step, the supernatant was filtered using a 0.2 μ m or 0.45 μ m syringe filter (Whatman). This filtered supernatant was then purified over a Ni-NTA 5 mL HiTrap column using an AKTA pure FPLC chromatography system. The gradient used for the purification is as follows: 1) Load protein onto the column (All flow rates during the purification at 2.5 mL/min); 2) Wash with 5 column volumes of Buffer A; 3) Wash with 5 column volumes at 10% Buffer B (90% Buffer A); 4) Wash with 5 column volumes at 15% Buffer B (85% Buffer A); 5) Gradient from 15-100% Buffer B relative to Buffer A over the

course of 10 column volumes; 6) Wash with 5 column volumes at 100% Buffer B. The composition of Buffer A is 50 mM phosphate, 300 mM NaCl, 30 mM imidazole, pH 7.2; Buffer B is 50 mM phosphate, 300 mM NaCl, 400 mM imidazole, pH 7.2. Fractions that contain Med25 AcID were combined and diluted by 4-fold with cold DI water or 50 mM phosphate buffer. 1 mM DTT was added to this protein solution. The protein was then purified over Source S 5 mL HiTrap column using an AKTA pure FPLC chromatography system. The gradient used for the purification is as follows: 1) Load protein onto the column (All flow rates during the purification at 2.5 mL/min); 2) Wash with 5 column volumes of Buffer A; 3) Gradient from 0-100% Buffer B relative to Buffer A over the course of 10 column volumes; The composition of Buffer A is 50 mM phosphate, 1 mM DTT, pH 7.2; Buffer B is 50 mM phosphate, 1 M NaCl, 1 mM DTT, pH 7.2. To check for purity after the purification, SDS-PAGE of eluted fractions was then performed (1X MES running buffer; 8-12% acrylamide gels). Fractions of pure protein (>95% pure by SDS-PAGE analysis) were combined and buffer exchanged into storage buffer (10 mM phosphate, 100 mM NaCl, 10% glycerol, 1 mM DTT, pH 6.8) using either overnight dialysis, a PD-10 column, or the concentrate-dilute-concentrate method. Protein concentration was determined by UV-Vis spectroscopy using an extinction coefficient, $\epsilon = 22,460 \text{ M}^{-1}\text{cm}^{-1}$ and samples were taken for mass spectroscopy analysis prior to storage of protein aliquots (300-400 μL at 100-150 μM concentration) at $-20 \text{ }^\circ\text{C}$.

2. Ni-NTA resin (Qiagen)

Cell pellets were thawed and resuspended with 30-35 ml Lysis Buffer (50 mM phosphate, 300 mM NaCl, 10 mM imidazole, pH 7.2). β -mercaptoethanol, at 1:1000

dilution, and one cOmplete, Mini, EDTA-free Protease Inhibitor tablet (Sigma-Aldrich) were added to the resuspended cell pellet. To lyse, the cells were sonicated on ice for 4-6 min (Cycle - 3 seconds on, 7 seconds off) and/or until the cells had observable change in color (lighter brown) and viscosity. Following sonication, the lysed pellet in 50 mL conical tube(s) was centrifuged at 9,500 RPM for 30 min at 4 °C. Concurrent with centrifugation of cells, 750 µl of Ni-NTA resin per 12 mL of cell lysate were washed three times with DI water. After centrifugation of the cell lysate, the supernatant was added to the washed Ni-NTA resin (Qiagen) and incubated for 1 hour at 4 °C. The resin was then centrifuged at 2500 RPM for 2 min at 4 °C before being washed five times with wash buffer (50 mM phosphate, 300 mM sodium chloride, 30 mM imidazole, pH 6.8). The resin was centrifuged at 2500 RPM for 1 min at 4 °C between washes. After the washing step, protein was incubated with 1 mL of elution buffer (50 mM phosphate, 300 mM sodium chloride, 400 mM imidazole, pH 6.8) per 750 µl of Ni-NTA resin for 30 min at 4 °C. The resin was centrifuged at 2500 RPM for 1 min at 4 °C and the protein supernatant containing Med25 AcID was saved. This elution step was repeated a total of three times. Fractions containing Med25 AcID were pooled and subjected to further purification using a Source S 5 mL HiTrap column using an AKTA pure FPLC chromatography system, as previously described.

Mass spectroscopy of proteins

Samples were not prepared. Protein was analyzed by mass spectrometry using an Agilent QTOF LC/MS following a partial separation with a Poroshell 300SB C8 reverse-phased HPLC column (5-100% acetonitrile with 0.1% formic acid over five minutes). Resultant

MS data was analyzed using Agilent software (Qualitative Analysis) with background subtraction and deconvolution settings for an intact protein of 10-30 KDa.

Solid-phase peptide synthesis and subsequent HPLC purification

Peptides were synthesized on CLEAR amide resin (Peptides International) using standard HBTU/HOBT/DIEA coupling conditions as previously described³⁷. TFA cleaved peptides were purified using reverse-phase HPLC (Agilent 1260) on a C18 Poroshell column (Agilent) using ammonium acetate/acetonitrile solvent systems. The concentration of fluorescein labeled peptides was then determined by UV-Vis spectroscopy following 1:500 dilution of DMSO stock solutions into 10 mM PBS, pH 7.4 using $\epsilon = 72,000 \text{ M}^{-1}\text{cm}^{-1}$, per the manufacturer (Pierce). Acetylated peptides, if they did not contain a native Tyr/Trp, were synthesized with a N-terminal Tyr residue next to a β -alanine linker prior to the start of desired sequence in order to allow for determination of the concentration of stock peptides by UV/VIS. Peptide identity was confirmed by electrospray mass spectrometry; peptide purity was determined by analytical HPLC.

Fluorescence polarization binding assays

Fluorescence polarization binding assays were performed in triplicate with a final sample volume of 16 μL in a low volume, non-binding, 384-well black plate (Corning). Peptides that were N-terminally labeled with fluorescein were diluted in assay buffer (5 mM HNa_2PO_4 , 5 mM NaH_2PO_4 , 100 mM NaCl, 10 % glycerol, pH 6.8) to 50 nM. Med25 AcID (16 μL per replicate) was serially diluted two-fold with assay buffer going down the columns of the 384-well plate (This allowed for eight total protein-peptide experiments on

a single plate). The final well, in Row P, was a negative control (no-protein, peptide-only). 8 μ L of the diluted fluorescent peptide stock was then added to each well of protein for a final peptide concentration of 25 nM. Plates were then incubated for 30 minutes at room temperature before fluorescence polarization was measured on either a Tecan Genios Pro or PHERAstar plate reader (polarized excitation at 485 nm and emission intensity measured through a parallel and perpendicularly polarized 535 nm filter). A binding isotherm that accounts for ligand depletion (assuming a 1:1 binding model of peptide to protein) was fit to the observed polarization values as a function of ACID to obtain the apparent equilibrium dissociation constant, K_D where 'a' and 'x' are the total concentrations of fluorescent peptide and protein, respectively; 'y' is the observed polarization at a given protein concentration; 'b' is the maximum observed polarization; 'c' is the minimum observed polarization value.

$$y = c + (b - c) \times \frac{[(K_D + a + x) - \sqrt{(K_D + a + x)^2 - 4ax}]}{2a}$$

Each K_D is the average and standard deviation of three technical replicates. For the mutagenesis study, the fold change in binding affinity for mutants relative to WT Med25 AcID is calculated using the following:

$$\text{Fold change} = \frac{(K_D \text{ for Mutant Med25 AcID-peptide interaction})}{(K_D \text{ for WT Med25 AcID-peptide interaction})}$$

Fluorescence polarization competition assays

Inhibition assays were performed in triplicate with a final sample volume of 20 μ L in a low volume, non-binding, 384-well black plate (Corning). A complex of the indicated

fluorescent peptide and protein was prepared at a two-fold the concentrations of protein and peptide to achieve 50% of the tracer bound during the assay. For peptide-based competition assays, an N-terminally acetylated variant of peptide was diluted in assay buffer (5 mM HNa_2PO_4 , 5 mM NaH_2PO_4 , 100 mM NaCl, 10 % glycerol, pH 6.8) to 100-1000 μM compound and serially diluted was serially diluted two-fold with assay buffer going down the columns of the 384-well plate (This allows for eight total protein-peptide experiments on a single plate). The final well, in Row P, was a negative control (protein-peptide, no inhibitor). 10 μL of the pre-formed fluorescent peptide-protein complex was then added to each well for a final volume of 20 μL . Samples were incubated for thirty minutes at room temperature before fluorescence polarization was measured a Tecan Genios Pro or PHERAstar plate reader (polarized excitation at 485 nm and emission intensity measured through a parallel and perpendicularly polarized 535 nm filter). Polarization values were converted to relative fraction bound and plotted against $\log[\text{inhibitor}]$. Inhibition curves were fit with a non-linear regression using Prism's 'log(inhibitor) vs response – variable slope' equation from which the IC_{50} value was calculated.

^1H , ^{15}N -HSQC NMR of Med25 AcID

Samples of purified ^{15}N -labeled Med25 AcID (50-100 μM) were complexed with molar equivalents of N-terminally acetylated peptides at 10% D_2O (final concentration) with NMR buffer (20 mM sodium phosphate buffer, pH 6.5, 150 mM NaCl, 3 mM DTT). HSQC experiments were completed by Felicia Gray (University of Michigan) using an Avance Bruker 600 MHz NMR spectrometer equipped with a 5 mm cryogenic probe. Data was

processed and analyzed by Matt Beyersdorf using TopSpin. Chemical shift analysis for individual peaks was quantified using the following:

$$\text{Chemical shift} = \text{SQRT}((\text{abs}(\Delta\delta^{15\text{N}})^2) + (\text{abs}(\Delta\delta^{1\text{H}})^2))$$

Circular dichroism of Med25 AcID

Circular dichroism spectra of Med25 AcID and mutants were acquired on a J-715 spectropolarimeter (Jasco Inc) using a 1 mM pathlength quartz cuvette. Protein was dialyzed into CD buffer (5 mM HNa_2PO_4 , 5 mM NaH_2PO_4 , 100 mM NaF, pH 6.8) overnight before analysis. Data was collected from 260-180 nm in 1 nm increments at a scanning speed of 100 nm/min. A background scan was performed using buffer only.

Data, after subtraction of the background scan, were converted to mean residue ellipticity according to the following equation where Ψ is the CD signal in degrees, n is the number of amides, l is the path length in centimeters, and c is the concentration in decimoles per cm^3 :

$$[\Theta] = \Psi / (1000 * n * l * c)$$

Each spectrum reported is the average of 8 scans.

Circular dichroism-observed thermal melt

CD-observed thermal melts were collected following collection of CD spectra; See above for instrument/buffer/etc. Using the 'Variable temperature' module, thermal melts were observed by CD. Protein was heated from 20-100 °C at a gradient of 1 °C/min; data was acquired by monitoring the molar ellipticity at 208 nm and 222 nm. Molar ellipticity was

collected at every third degree from 20-35 °C and at every degree from 35-100 °C. Molar ellipticity values were converted to Fraction Unfolded and T_m was determined by fitting data with Prism's 'log(inhibitor) vs response – variable slope' equation.

Tethering with VP16 G450C peptide

The cysteine of VP16 G450C peptide (sequence: ALDDFDLDMLGDCCDSPG) was capped with cysteamine by Andy Henderson. A two-fold molar excess of cysteamine-capped VP16 G450C in presence of 100 μM β-mercaptoethanol was incubated with WT or mutant Med25 overnight, shaking, at room temperature. During the following day, the protein-peptide complex was purified away from excess peptide using the FPLC IEX method described above, for purification of Med25 AcID.

F. References

1. Mittler, G. *et al.* A novel docking site on Mediator is critical for activation by VP16 in mammalian cells. *EMBO J.* **22**, 6494–6504 (2003).
2. Verger, A. *et al.* The Mediator complex subunit MED25 is targeted by the N-terminal transactivation domain of the PEA3 group members. *Nucleic Acids Res.* **41**, 4847–4859 (2013).
3. Sela, D. *et al.* Role for Human Mediator Subunit MED25 in Recruitment of Mediator to Promoters by Endoplasmic Reticulum Stress-responsive Transcription Factor ATF6. *J. Biol. Chem.* **288**, 26179–26187 (2013).
4. Lee, H.-K., Park, U.-H., Kim, E.-J. & Um, S.-J. MED25 is distinct from TRAP220/MED1 in cooperating with CBP for retinoid receptor activation. *EMBO J.* **26**, 3545–3557 (2007).
5. Dyson, H. J. & Wright, P. E. Role of Intrinsic Protein Disorder in the Function and Interactions of the Transcriptional Coactivators CREB-binding Protein (CBP) and p300. *J. Biol. Chem.* **291**, 6714–6722 (2016).
6. Ptashne, M. & Gann, A. *Genes and Signals (2002) Genes and Signals.* ((Cold Spring Harbor Lab Press, 2002).
7. Garner, A. L. & Janda, K. D. Protein-protein interactions and cancer: targeting the central dogma. *Curr. Top. Med. Chem.* **11**, 258–280 (2011).
8. Lee, T. I. & Young, R. A. Transcriptional regulation and its misregulation in disease. *Cell* **152**, 1237–1251 (2013).
9. Thompson, A. D., Dugan, A., Gestwicki, J. E. & Mapp, A. K. Fine-Tuning Multiprotein Complexes Using Small Molecules. *ACS Chem. Biol.* **7**, 1311–1320 (2012).
10. Cesa, L. C., Mapp, A. K. & Gestwicki, J. E. Direct and Propagated Effects of Small Molecules on Protein–Protein Interaction Networks. *Front. Bioeng. Biotechnol.* **3**, (2015).
11. Mapp, A. K., Pricer, R. & Sturlis, S. Targeting transcription is no longer a quixotic quest. *Nat. Chem. Biol.* **11**, 891–894 (2015).
12. Sigler, P. B. Acid blobs and negative noodles. *Nature* **333**, 210–212 (1988).
13. Arai, M., Sugase, K., Dyson, H. J. & Wright, P. E. Conformational propensities of intrinsically disordered proteins influence the mechanism of binding and folding. *Proc. Natl. Acad. Sci.* **112**, 9614–9619 (2015).
14. Shi, Z., Yang, W., Goldstein, J. A. & Zhang, S.-Y. Med25 is required for estrogen receptor alpha (ER α)-mediated regulation of human CYP2C9 expression. *Biochem. Pharmacol.* **90**, 425–431 (2014).
15. Xu, J.-Y. *et al.* Upregulation of human CYP2C9 expression by Bisphenol A via estrogen receptor alpha (ER α) and Med25. *Environ. Toxicol.* **32**, 970–978 (2017).
16. Wysocka, J. & Herr, W. The herpes simplex virus VP16-induced complex: the makings of a regulatory switch. *Trends Biochem. Sci.* **28**, 294–304 (2003).

17. Landrieu, I. *et al.* Characterization of ERM transactivation domain binding to the ACID/PTOV domain of the Mediator subunit MED25. *Nucleic Acids Res.* **43**, 7110–7121 (2015).
18. Aytes, A. *et al.* ETV4 promotes metastasis in response to activation of PI3-kinase and Ras signaling in a mouse model of advanced prostate cancer. *Proc. Natl. Acad. Sci.* **110**, E3506–E3515 (2013).
19. Haze, K., Yoshida, H., Yanagi, H., Yura, T. & Mori, K. Mammalian transcription factor ATF6 is synthesized as a transmembrane protein and activated by proteolysis in response to endoplasmic reticulum stress. *Mol. Biol. Cell* **10**, 3787–3799 (1999).
20. Yoshida, H. *et al.* ATF6 activated by proteolysis binds in the presence of NF-Y (CBF) directly to the cis-acting element responsible for the mammalian unfolded protein response. *Mol. Cell. Biol.* **20**, 6755–6767 (2000).
21. Vojnic, E. *et al.* Structure and VP16 binding of the Mediator Med25 activator interaction domain. *Nat. Struct. Mol. Biol.* **18**, 404–409 (2011).
22. Bontems, F. *et al.* NMR structure of the human Mediator MED25 ACID domain. *J. Struct. Biol.* **174**, 245–251 (2011).
23. Milbradt, A. G. *et al.* Structure of the VP16 transactivator target in the Mediator. *Nat. Struct. Mol. Biol.* **18**, 410–415 (2011).
24. Radhakrishnan, I. *et al.* Solution Structure of the KIX Domain of CBP Bound to the Transactivation Domain of CREB: A Model for Activator:Coactivator Interactions. *Cell* **91**, 741–752 (1997).
25. De Guzman, R. N., Liu, H. Y., Martinez-Yamout, M., Dyson, H. J. & Wright, P. E. Solution structure of the TAZ2 (CH3) domain of the transcriptional adaptor protein CBP. *J. Mol. Biol.* **303**, 243–253 (2000).
26. Youn, H.-S., Park, U.-H., Kim, E.-J. & Um, S.-J. PTOV1 antagonizes MED25 in RAR transcriptional activation. *Biochem. Biophys. Res. Commun.* **404**, 239–244 (2011).
27. Bénédit, P. *et al.* PTOV1, a novel protein overexpressed in prostate cancer containing a new class of protein homology blocks. *Oncogene* **20**, 1455 (2001).
28. Santamaría, A. *et al.* PTOV-1, a novel protein overexpressed in prostate cancer, shuttles between the cytoplasm and the nucleus and promotes entry into the S phase of the cell division cycle. *Am. J. Pathol.* **162**, 897–905 (2003).
29. Fernández, S. *et al.* PTOV1 is overexpressed in human high-grade malignant tumors. *Virchows Arch.* **458**, 323–330 (2011).
30. Currie, S. L. *et al.* ETV4 And AP1 Transcription Factors Form Multivalent Interactions With Three Sites On The MED25 Activator-Interacting Domain. *bioRxiv* 126458 (2017). doi:10.1101/126458
31. Jonker, H. R. A., Wechselberger, R. W., Boelens, R., Folkers, G. E. & Kaptein, R. Structural Properties of the Promiscuous VP16 Activation Domain †. *Biochemistry (Mosc.)* **44**, 827–839 (2005).

32. Livengood, J. A. *et al.* p53 Transcriptional activity is mediated through the SRC1-interacting domain of CBP/p300. *J. Biol. Chem.* **277**, 9054–9061 (2002).
33. Altschul, S. F., Gish, W., Miller, W., Myers, E. W. & Lipman, D. J. Basic local alignment search tool. *J. Mol. Biol.* **215**, 403–410 (1990).
34. Uesugi, M., Nyanguile, O., Lu, H., Levine, A. J. & Verdine, G. L. Induced alpha helix in the VP16 activation domain upon binding to a human TAF. *Science* **277**, 1310–1313 (1997).
35. Erlanson, D. A., Wells, J. A. & Braisted, A. C. Tethering: fragment-based drug discovery. *Annu. Rev. Biophys. Biomol. Struct.* **33**, 199–223 (2004).
36. Sadowsky, J. D. *et al.* Turning a protein kinase on or off from a single allosteric site via disulfide trapping. *Proc. Natl. Acad. Sci.* **108**, 6056–6061 (2011).
37. Majmudar, D. C. Y., Wang, B., Lum, D. J. K., Håkansson, P. D. K. & Mapp, P. D. A. K. A high resolution interaction map of three transcriptional activation domains with an essential co-activator from photocross-linking and multiplexed mass spectrometry. *Angew. Chem. Int. Ed Engl.* **48**, 7021 (2009).

Chapter Three

Defining binding mechanisms of Med25 AcID and its protein-protein interaction network using protein-observed ^{19}F -NMR

A. Abstract*

The structural study of coactivator-activator interactions has long been considered challenging due to the transient and dynamic natures of these interactions, weak-to-moderate binding affinities, and abilities of both coactivators and activators to bind multiple targets.¹⁻³ However, NMR techniques offer excellent methodologies to investigate protein dynamics due to their sensitivity and resolution.^{4,5} In particular, protein-observed fluorine (PrOF) NMR is desirable for the study of these interactions due to the short amount of time required for experimental and data analysis, the high sensitivity provided by the ^{19}F nucleus, and the lack of ^{19}F in naturally-occurring proteins.^{6,7} Previous work in the literature and in Chapter 2 of this thesis demonstrated the Med25 AcID contains multiple binding sites, each of which is suggested to be targeted by specific Med25-interacting proteins.⁸⁻¹² However, many questions regarding the mechanisms of recognition between Med25 AcID and its protein partners remained. This chapter set out to answer several of those mechanistic questions using PrOF NMR, an emerging technique to study protein-protein interactions. This chapter precisely describes the inherent differences between each unique Med25 AcID protein-protein interaction including differences in binding selectivity towards AcID binding sites, relative affinities,

*Several collaborators provided research assistance throughout Chapter Three. Prof. William Pomerantz and Clifford Gee (University of Minnesota) assisted with initial efforts to incorporate ^{19}F into Med25 AcID and resonance assignment of 3-fluorotyrosine Med25 AcID. Andy Henderson (University of Michigan) collected HSQC NMR of several Med25-activator complexes that were useful in describing binding models for discrete Med25 AcID protein-protein interactions. Drs. Paul Bruno and Steve Sturlis (University of Michigan) identified and characterized norstictic acid as an inhibitor of Med25 AcID. Andy Henderson identified fragment A6 in a Tethering screen against Med25 AcID; Dr. Clint Regan (University of Michigan) synthesized A6 and all A6 derivatives.

and binding stoichiometry. These observed differences in binding modes range from the subtle (ATF6 α and VP16 H2, both selectively for the H2 binding site, position themselves differently across this interface) to the highly dramatic (ERM, highly selective for the H1 site, appears capable of achieving a 2:1 binding stoichiometry). Finally, the mechanism of action for two recently identified small molecules (norstictic acid and the fragment A6) that target Med25 AcID is described, as determined using PrOF NMR of Med25 AcID.

B. Introduction

Limitations of ^1H , ^{15}N -HSQC NMR in study of protein-protein interactions

Protein-observed NMR has been extensively utilized to study protein-protein interactions (PPIs) and protein-ligand interactions for decades.⁴ ^1H , ^{15}N -HSQC NMR is the most commonly used technique and, as described in Chapters 2 and 4 of this thesis, has been effective in mapping the binding interactions between Med25 AcID and its native and small molecule ligand partners. However, this two-dimensional technique has several practical and experimental limitations. Long instrumental time (e.g. 90-100 minutes for a single ^1H , ^{15}N -HSQC NMR Med25 AcID experiment), the need for expensive isotopic reagents to produce ^{15}N -labeled protein, and time-intensive analysis of resulting 2-D NMR spectra complicate data collection and interpretation.¹³ Incomplete assignment of all resonances in ^1H , ^{15}N -HSQC NMR (e.g. Only 103 of the 151 residues of Med25 AcID can be definitively assigned) limits the depth of the analysis of the protein-of-interest, including difficulty in differentiation of orthosteric and allosteric effects.¹⁴ This lack of depth is especially problematic for the study of activator-coactivator interactions because these interactions are transient, weak affinity, and involve proteins that are highly dynamic and

often intrinsically disordered.^{2,3,15} Additionally, coactivator proteins often contain multiple binding sites with many protein partners; differentiation of these binding sites and binding partners is imperative for proper understanding of coactivator-activator function. Finally, this technique detects chemical shift perturbations of amide N-H bonds and thus offers little insight into side chain interactions.⁴

Protein-observed ¹⁹F-NMR for study of protein-protein interactions

Protein-observed ¹⁹F-NMR (PrOF NMR), a 1-D NMR experiment that complements ¹H, ¹⁵N-HSQC NMR, can overcome some of the inherent limitations of HSQC NMR. PrOF NMR is desirable for its short experimental time⁶, simple and quick analysis of 1-D spectra, and ability to observe side chain interactions of a select number of residues. Inherent advantages also offered by the ¹⁹F nucleus include its native isotopic abundance (100%), magnetic sensitivity (83% as sensitive as ¹H), and its low background signal in protein NMR (¹⁹F does not occur naturally in proteins)⁷. PrOF NMR has been effectively utilized to study several protein-protein and protein-ligand interactions including those involving the glucose- and galactose-binding protein¹⁶, avian lysozymes¹⁷, dihydrofolate reductase¹⁸, the aspartate receptor¹⁹, the coactivator domain CBP^{20,21}, and bromodomains^{22,23}.

Incorporation of ¹⁹F for PrOF NMR can be done using biosynthetic methodologies to integrate fluorinated amino acids into a protein-of-interest or through chemical modification to covalently label a residue onto the protein-of-interest with a fluorinated molecule.^{24,25} The most utilized amino acids for PrOF are fluorinated versions of tyrosine, tryptophan, and phenylalanine, all of which can be incorporated by auxotrophic bacterial

strains.²⁶ These aromatic amino acids are selected due to their range of native structural environments from conformationally dynamic loops to α -helical and β -sheet structures and at PPI interfaces.^{27–30} Additionally, aromatic amino acids are desirable due to their low abundance, which minimizes the total number of ^{19}F nuclei that are incorporated into protein, simplifying the subsequent PrOF spectrum.³¹ This also lessens the likelihood of significant effects of the fluorinated amino acids on protein structure and function. Common fluorinated variants of aromatic amino acids for direct incorporation into the primary structure of proteins include 3-fluorotyrosine, 2/3/4-fluorophenylalanine, and 4/5/6-fluorotryptophan. Alternatively, fluorine-containing small molecules can be incorporated into a protein after expression. This is typically accomplished through covalent modification of cysteine residues. Common molecules that have been successfully utilized for the methodology include 3-bromo-1,1,1-trifluoroacetone, 3-bromo-1,1,1-trifluoropropanone, and 2,2,2-trifluoroethanethiol, all of which are cysteine-reactive.^{32–35}

PrOF NMR for study of Med25 AcID and its protein-protein interaction network

PrOF NMR of Med25 AcID was pursued to complement ^1H , ^{15}N -HSQC NMR experiments and the mutagenesis study described in Chapter 2 to test the proposed binding models for each unique Med25 AcID PPI.

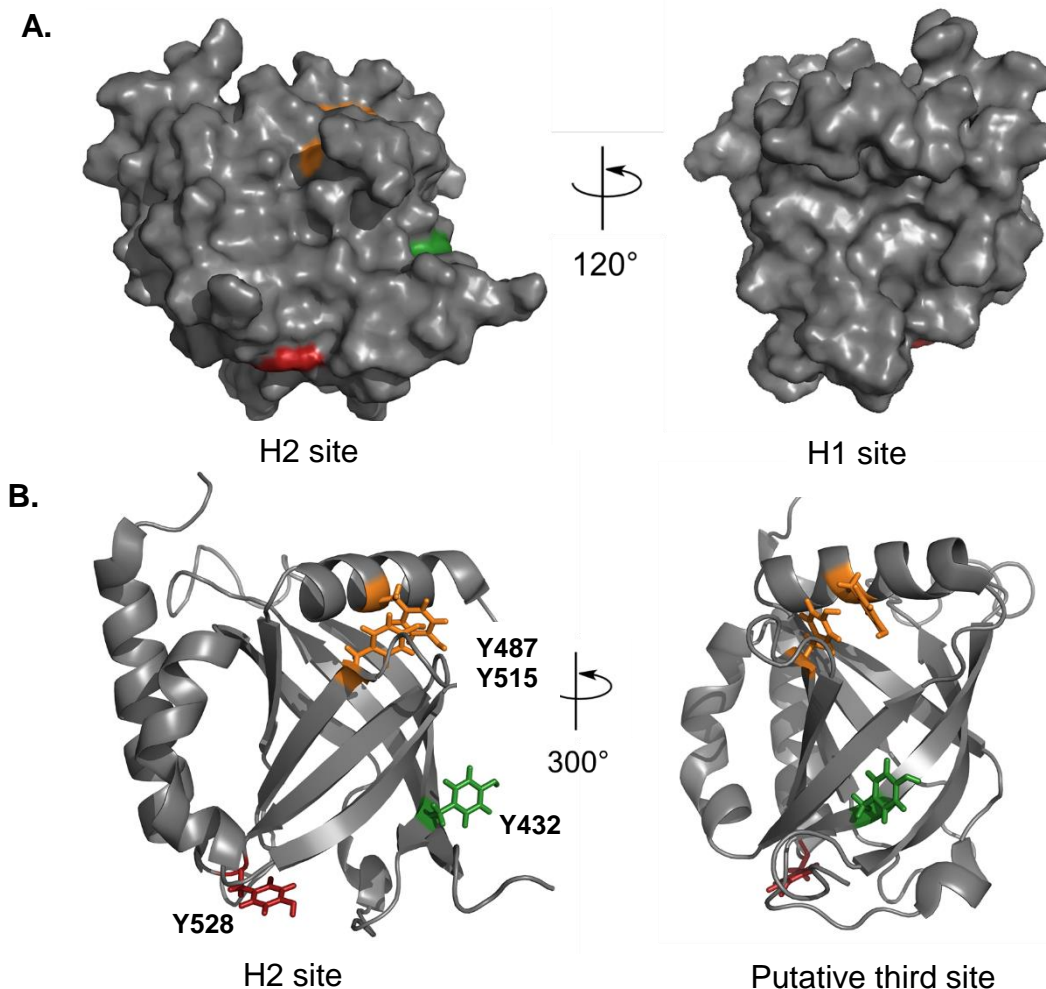


Figure 3.1. 3FY Med25 AcID structures. (A) Surface renderings of the H2 site (left) and H1 site (right) of Med25. Tyr residues are colored – Y528 (red), Y432 (green), Y487/Y515 (orange). (B) Cartoon images of the H2 site (left) and putative third site (right). (PDB 2XNF)

Incorporation of 3-fluorotyrosine (3FY) was proposed to provide NMR reporters of the H2 site of Med25 AcID due to the dispersed placement of Tyr residues across the H2 and third sites of Med25 (Figure 3.1). Y528 is located on the loop between $\beta 7$ and $\alpha 3$ with its side chain situated at the base of the H2 site. Y487 and Y515, thought to be a hydrogen-bonded pair, are situated at the opposite edge of the H2 site from Y528, on $\alpha 2$ and $\beta 5$ respectively. Finally, Y432 is situated within the putative third site and in proximity of the H2 site, near the C-terminal end of $\beta 2$. Notably, as shown in the image of the H1

site in Figure 3.1.A, none of the Tyr residues are situated proximal to the H1 site. It was hypothesized that PrOF NMR of 3FY Med25 AcID would provide corroborating evidence regarding the selectivity of VP16 H2 and ATF6 α for the H2 site of Med25 site, could definitively demonstrate the ability of ERM and VP16 H1 to bind at both the H1 and H2sites, and would provide additional evidence of the putative third site that CBP was proposed to bind in HSQC NMR experiments.

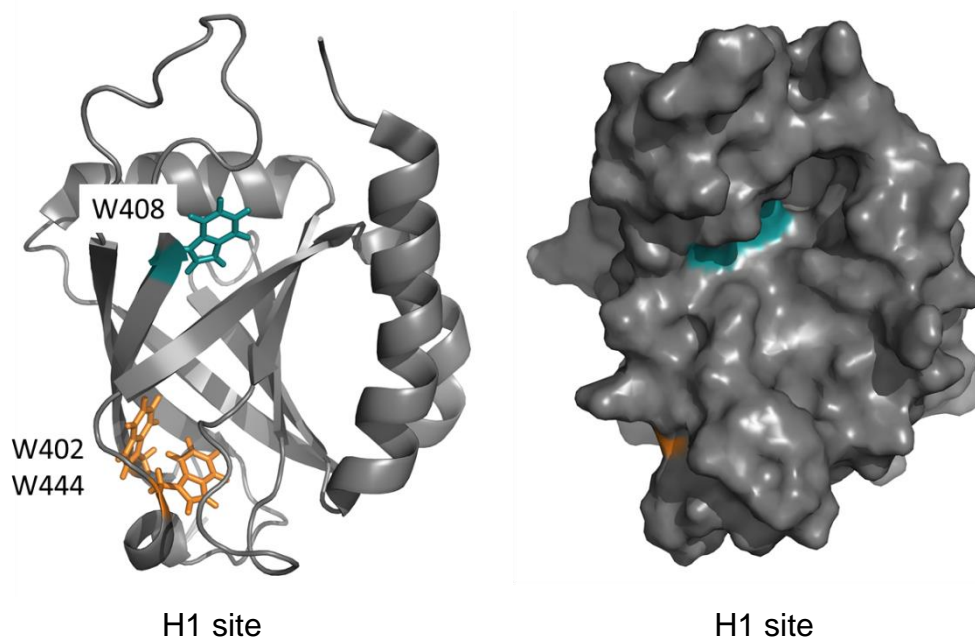


Figure 3.2. 5FW Med25 AcID structure. Cartoon (left) and surface (right) images of the H1 site of Med25 AcID. All three residues are near the H1 site and the side chains of W402/W444 are not solvent-exposed. (PDB 2XNF)

Incorporation of 5-fluorotryptophan (5FW) was proposed to function as a NMR reporter system to allow for observation of the H1 site of Med25 AcID. All three Trp residues of Med25 AcID are near to the H1 site on Med25 AcID (Figure 3.2). W402 and W444 are part of an aromatic triad (along with F500) within the core of the β -barrel and form an edge-to-face π - π stacking interaction with one another. W408 is located near the C-terminal end of β 1 and, with α 2, forms a cleft at the “top” of the β -barrel. This residue

is thought to be the most sensitive reporter of the three towards H1 ligands. It was hypothesized that PrOF NMR of 5FW would corroborate evidence that VP16 H2, ATF6 α (40-66), and CBP(20-44) do not interact with the H1 site, even at high concentrations of peptide. Furthermore, it was thought that PrOF NMR analysis would corroborate the working model that ERM, while capable of binding to the H2 site, interacts preferentially at the H1 site.

C. Results and discussion

Biochemical characterization of fluorinated Med25 variants

Fluorinated variants of Med25 were expressed using an auxotrophic bacterial strain, adapted from published expression conditions for other proteins.³⁶ 3-fluorotyrosine (3FY) expression resulted in high yields (35-40 mg protein per liter bacterial culture) with >99% ¹⁹F incorporation, as determined by mass spectrometry (Figure 3.3). Note that in all cases, the percentage of ¹⁹F incorporation was calculated by dividing the total peak areas of deconvoluted proteins in mass spectrometry by the sum of peak areas of all proteins that contain at least one ¹⁹F atom.³⁶ Furthermore, ~80% of 3FY Med25 AcID had 3FY incorporated at all four Tyr residues. 5-fluorotryptophan (5FW) expression resulted in lower yields (10-15 mg protein per liter bacterial culture) and lower incorporation of ¹⁹F (90% by mass spectrometry) than 3FY. However, protein quality and quantities were sufficiently high to perform subsequent experiments. The third amino acid, 4-fluorophenylalanine (4FF), provided poor results in terms of yield (<<5 mg protein per liter bacterial culture) and ¹⁹F incorporation (~70% labeled; however, most of the protein incorporated 4FF at fewer than four of the seven total Phe residues).

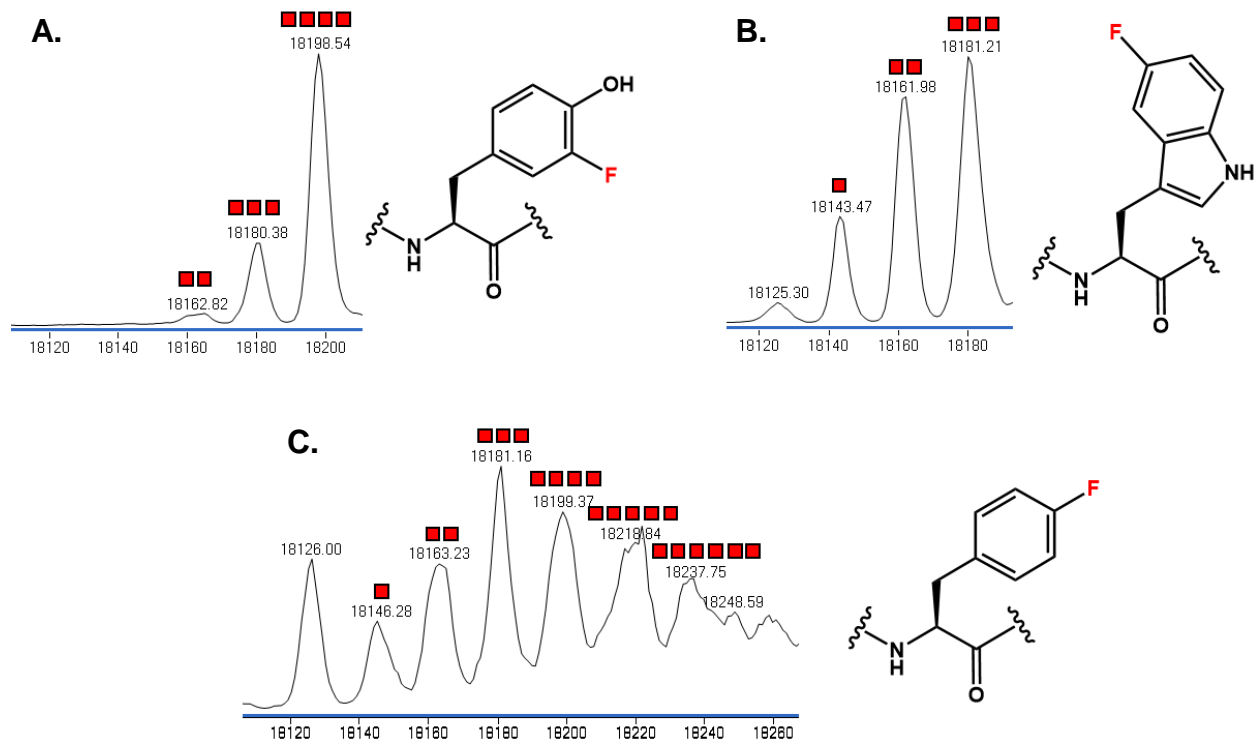


Figure 3.3. Mass spectrometry of fluorinated Med25 AcID variants. Deconvoluted mass spectra of A) 3-fluorotyrosine, (B) 5-fluorotryptophan, and (C) 4-fluorophenylalanine Med25 AcID with corresponding ^{19}F -containing amino acid structure. Red squares represent the number of incorporated ^{19}F -containing amino acids (+18 amu per ^{19}F). The percentage of ^{19}F incorporation was calculated by dividing the total peak areas of deconvoluted proteins in mass spectrometry by the sum of peak areas of all proteins that contain at least one ^{19}F atom.

Circular dichroism (CD) and fluorescence polarization (FP) were used to assess effects of the unnatural amino acids on Med25 AcID structure and function (Figure 3.4 and Table 3.1). CD spectra indicated that fluorine incorporation resulted in minimal perturbation of the secondary structure relative to WT. CD-observed thermal denaturation indicated that 3FY Med25 AcID was marginally *more* stable than WT Med25 AcID (67.0 ± 0.5 °C vs 64.8 ± 0.3 °C). Finally, FP assays demonstrated that 3FY Med25 AcID and 5FW Med25 AcID maintained similar function to WT. All tested peptides bound 3FY and 5FW Med25 with less than three-fold loss in binding affinity relative to WT.

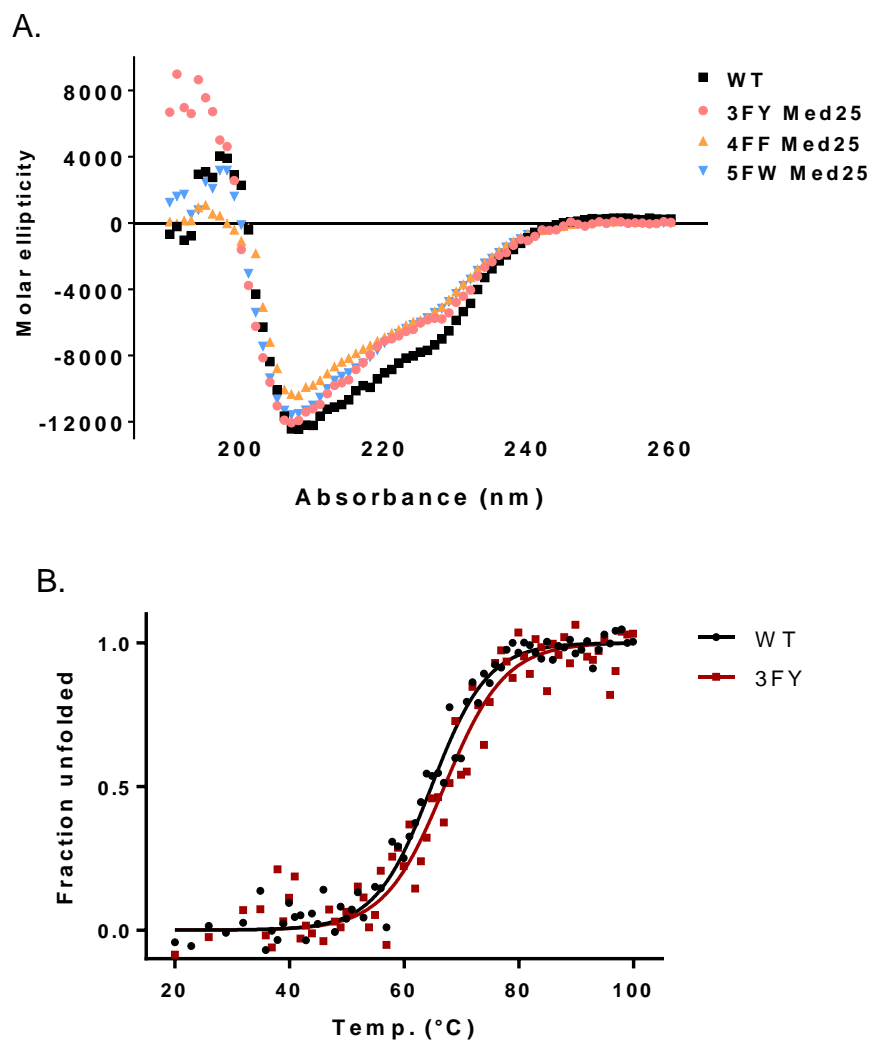


Figure 3.4 Structural stability of fluorinated Med25 Acid variants. (A) Circular dichroism spectra of 3FY, 4FF, and 5FW Med25. (B) CD-observed thermal denaturation of 3FY Med25 and WT Med25. Fraction unfolded was determined from circular dichroism measurements at 222 nm as protein samples were heated from 20-100 °C.

Table 3.1 Dissociation constants for Med25-interacting peptides to 3FY Med25 Acid. Each K_D was determined using FP assays performed in triplicate.

	VP16 α H2	CBP(20-44)	VP16 H1	ERM(38-68)
	(K_D)	(K_D)	(K_D)	(K_D)
WT Med25	$0.6 \pm 0.1 \mu\text{M}$	$2.5 \pm 0.1 \mu\text{M}$	$2.3 \pm 0.1 \mu\text{M}$	$0.7 \pm 0.1 \mu\text{M}$
3FY Med25	$1.3 \pm 0.1 \mu\text{M}$	$2.6 \pm 0.1 \mu\text{M}$	$6.8 \pm 0.4 \mu\text{M}$	$1.5 \pm 0.3 \mu\text{M}$

Following this initial suite of experiments to characterize the fluorinated Med25 AcID variants, each variant was independently subjected to PrOF analysis (Figure 3.5). The PrOF NMR spectrum of 3FY Med25, which contains four Tyr residues, provided four well-resolved resonances with excellent signal-to-noise in 1200-1600 total NMR scans (experimental time of 11-15 minutes). 5FW Med25 AcID provided two overlapped and broad resonances at -126.8 ppm with another resonance ~1.5 ppm upfield in 2400 scans (experimental time of ~20 minutes). The PrOF NMR spectrum of 4FF Med25 AcID was not well-resolved (up to five resonances overlapped from -116 to -118 ppm). Furthermore, 6000 scans (~1 hr of experimental time) were required to acquire a 4FF spectrum of the quality shown in Figure 3.5. 4FF Med25 AcID was not further pursued for PrOF NMR of Med25 due to its poor resonance dispersion, lengthy experimental time, and low protein yield.

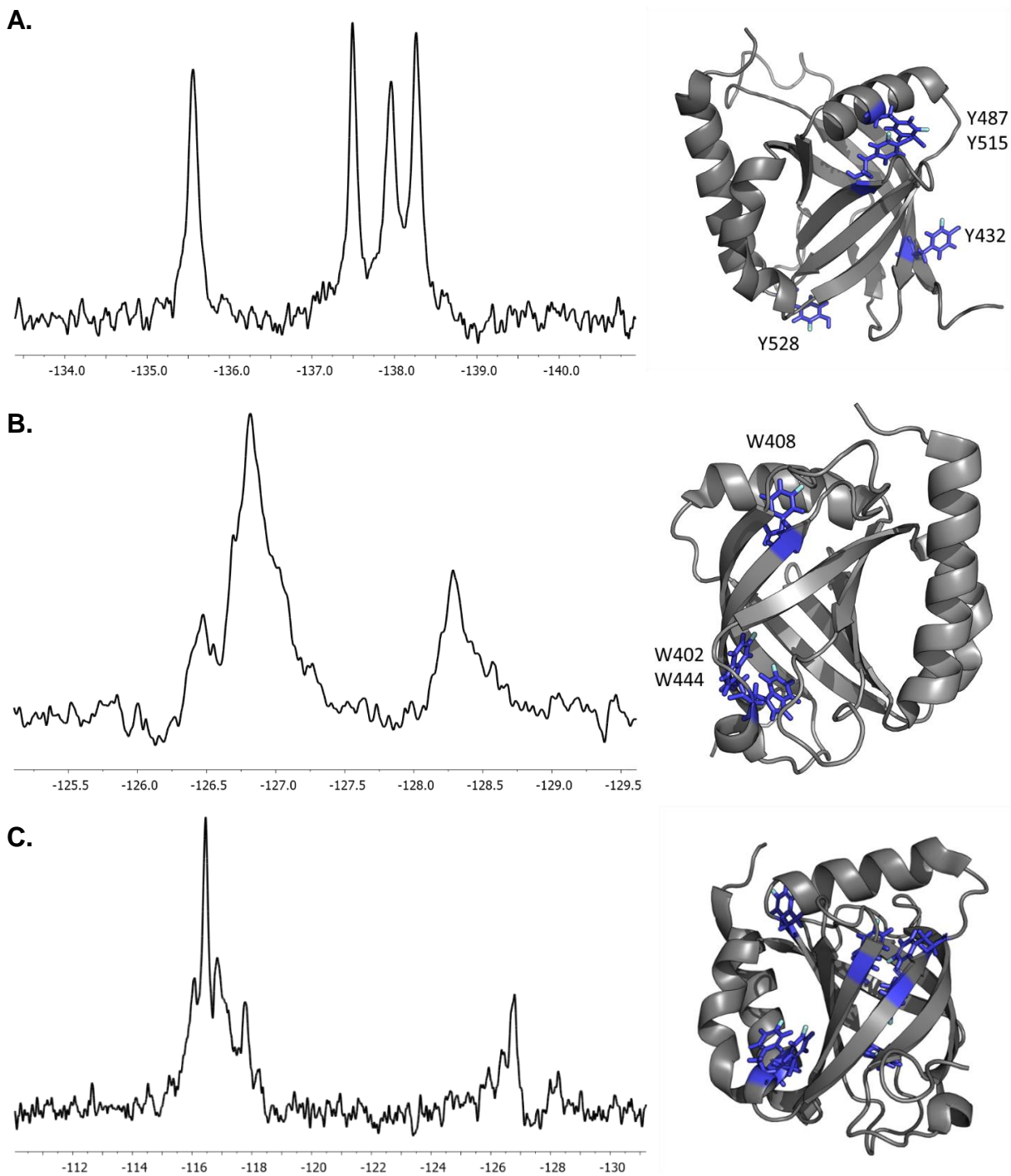


Figure 3.5. ^{19}F -NMR spectra of fluorinated Med25 Acid variants. (A) NMR spectra of 3-fluorotyrosine Med25 Acid; All four Tyr residues, shown in blue, are solvent exposed and located within or near the H2 site. (B) NMR spectra of 5-fluorotryptophan Med25 Acid; All three Trp residues, shown in blue, located in proximity of the H1 site. Only the side chain of W408 is solvent exposed. (C) NMR spectra of 4-fluorophenylalanine Med25 Acid; Only two of seven Phe residues, shown in blue, are solvent exposed. (PDB 2XNF)

Assignment of 3FY resonances

Prior to functional ligand studies, the ^{19}F -NMR resonances of 3FY Med25 needed to be independently assigned to specific residues of the protein. To accomplish this, four Tyr-to-Phe mutants were generated (Y432F, Y528F, Y487F, and Y515F Med25 AcID). Each mutant was successfully cloned, expressed and purified in low-to-moderate yield. Mass spectrometry of each mutant verified that a single mutation had been performed and that ^{19}F incorporation was sufficiently high for PrOF NMR analysis (Figure 3.6).

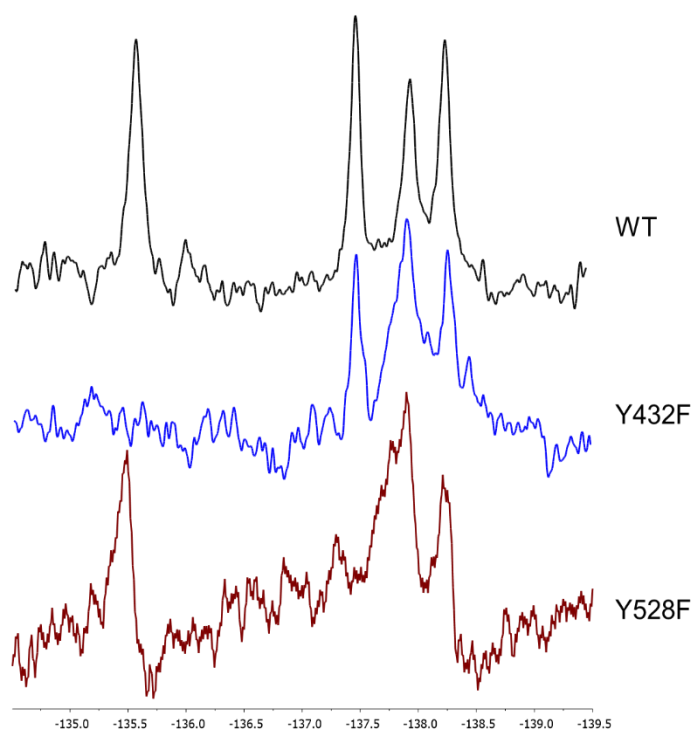


Figure 3.6. Assignment of Y432 and Y528 resonances of 3FY Med25. Tyr-to-Phe mutations at residues 432 and 528 allowed for the assignment of these ^{19}F -NMR resonances at -135.57 ppm and -137.48 ppm, respectively. Note that signal-to-noise of both Y432F and Y528F Med25 AcID spectra are low in part because each was expressed on small-scale (100 mL bacterial culture), resulting in low total protein.

Subsequent PrOF NMR spectra of Y432F Med25 AcID demonstrated that the resonance at -135.57 ppm was Y432 based on the absence of that peak from the collected spectra (Figure 3.6). Similarly, PrOF NMR spectra of Y528F Med25 AcID

demonstrated that the resonance at -137.48 ppm was Y528 based on the absence of that peak from the collected spectra. PrOF spectra of Y487F and Y515F Med25 AcID gave inconclusive results, possibly because these two Tyr residues might be engaged in a hydrogen bond interaction with one another. While the distances between the oxygen of one Tyr and the hydrogen of another are never closer than 3.5 Å in NMR structures (PDB 2XNF, 2KY6, 2L6U), these side chains are oriented such that they could be engaged in a transient hydrogen bond.

To assign the final two tyrosine residues, Y487 and Y515, which represent the most upfield resonances of the WT spectra, the “nudge” mutational method was utilized.³⁷ This methodology involves a soft mutation of a residue located in the physical proximity of a single target Tyr. This “nudge” mutation should then affect the local environment of only that target Tyr and perturb a single ¹⁹F-NMR resonance. The perturbed resonance can then be assigned to the Tyr residue near the nudge mutation. 3FY-containing K484R Med25 was generated in hopes of “nudging” Y487 and perturbing a single resonance (Figure 3.7). This residue was selected for mutation because it was near Y487 only and was solvent exposed, and therefore expected to have minimal effect on Med25 structure. PrOF spectrum of K484R Med25 allowed for the assignment of Y487 to be the resonance at -137.95 ppm in the WT spectra. The K484R mutation led to a 0.025 ppm shift in the resonance at -137.95 ppm while leaving the resonance at -138.26 ppm unperturbed. This final resonance at -138.26 ppm was assigned to Y515 by process of elimination.

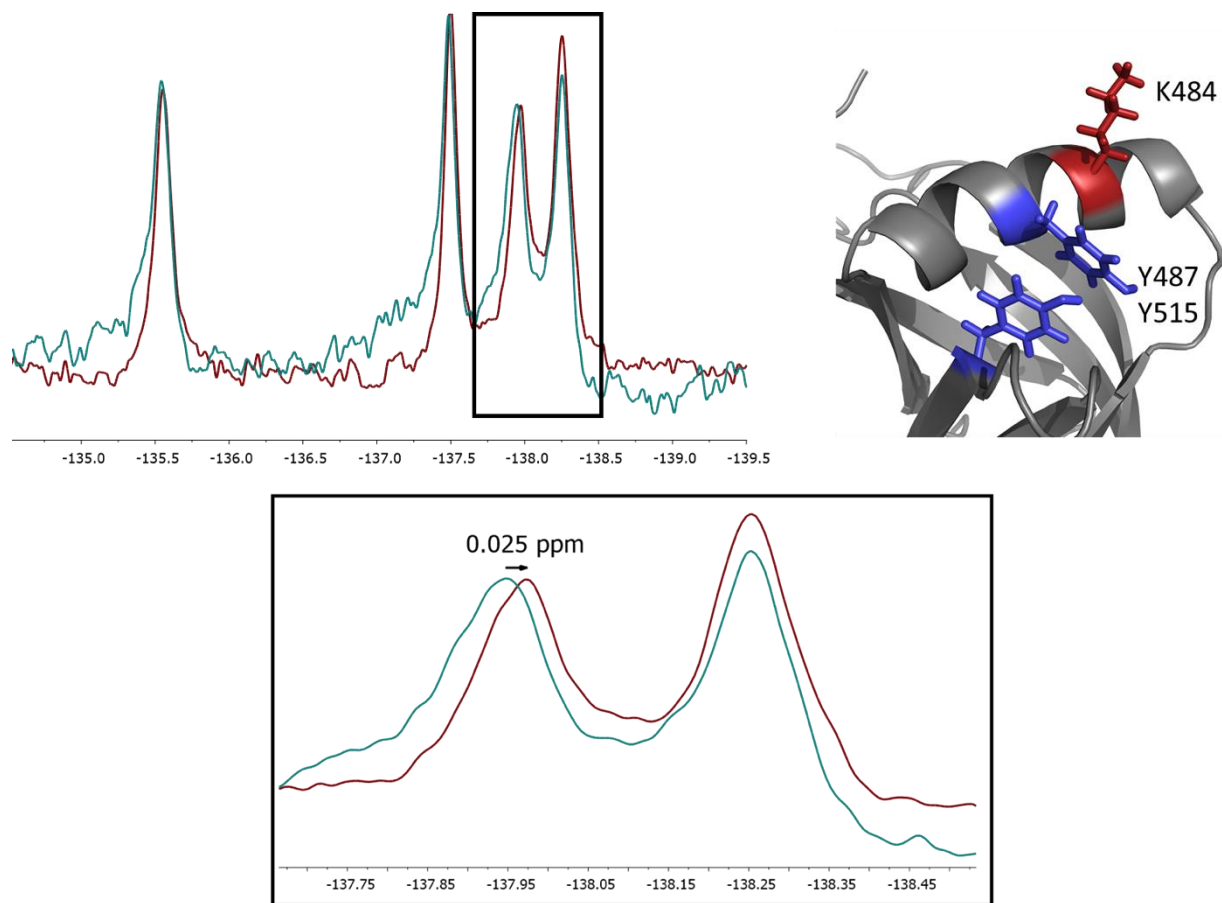


Figure 3.7. Assignment of Y487 and Y515 resonances of 3FY Med25. The nudge mutation method was used to assign these two Tyr residues. A K484R mutation perturbed the resonance at -137.95 ppm, indicating that it represents Y487. ^{19}F -NMR spectra of K484R 3FY Med25 shown in red; WT 3FY Med25 shown in light blue. (PDB 2XNF)

PrOF NMR titrations with Med25-interacting peptides against 3FY Med25 AcID

With assignments of 3FY Med25 AcID completed, PrOF NMR was used to define interactions between Med25 AcID and native peptide ligands. Titrations were performed with acetylated variants of the Med25-interacting peptides (the same peptide ligands used during previous mutagenesis and HSQC NMR work in Chapter 2).

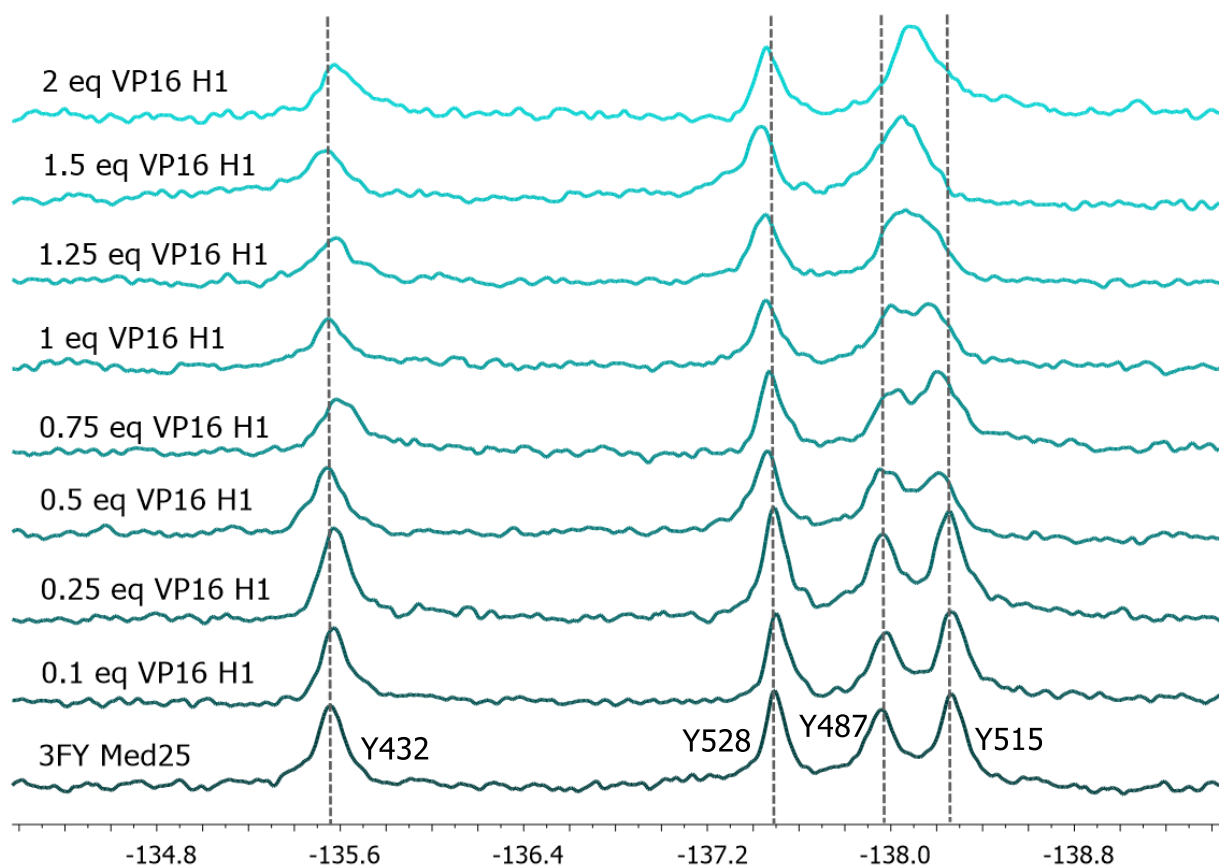


Figure 3.8. PrOF NMR of 3FY Med25 AcID-VP16 H1 complexes. Spectral analysis of 3FY Med25 AcID in the presence of increasing concentrations of VP16(413-451), the H1 TAD of VP16, demonstrated that VP16 H1 only perturbs the Y487/Y515 pair, in a dose-responsive manner. The resonance corresponding to Y528 is initially downshifted during the titration but reverts towards the WT chemical shift at 2 eq. VP16 H1.

An acetylated variant of VP16(413-451) (7.5 μ M, 18.75 μ M, 37.5 μ M, 56.25 μ M, 75 μ M, 93.75 μ M, 112.5 μ M and 150 μ M) was complexed with 3FY Med25 AcID (75 μ M) and subjected to PrOF NMR (Figure 3.8). The most significantly perturbed resonances corresponded to the Y487/Y515 pair, as these two peaks merged to form an overlapping resonance at -137.08 ppm in the spectra of 3FY Med25 with two equivalents of VP16(413-451), the H1 TAD of VP16. This new resonance represented an upfield shift of 0.12 ppm for Y487 and a downfield shift of 0.18 ppm for Y515. Additionally, starting at 0.5 and higher equivalents of VP16 H1, Y528 was perturbed (0.03 ppm downfield shift at 2 eq.

peptide). VP16 H1 had a much more significant impact on the Y487/Y515 than any of the H2/third site peptides - VP16 H2, ATF6 α , and CBP. This is consistent with an alternative mode of interaction. The effect on Y487/Y515 could be explained by an interaction between VP16 H1 and β 5, located at the center of the H1 cleft. A tight association with β 5 would likely cause a conformational change in α 2, the helix on which Y487 resides. The lack of perturbations at Y528 at 0.1 and 0.25 eq VP16 H1 along with the complete lack of perturbations at Y432 are consistent with the H2 site not being the primary target for VP16 H1 binding to Med25 AcID. However, the perturbation of Y528 at elevated concentration of VP16 H1 does corroborate mutagenesis data that suggests that VP16 H1 is capable of binding at the H2 site when the H1 face is blocked.

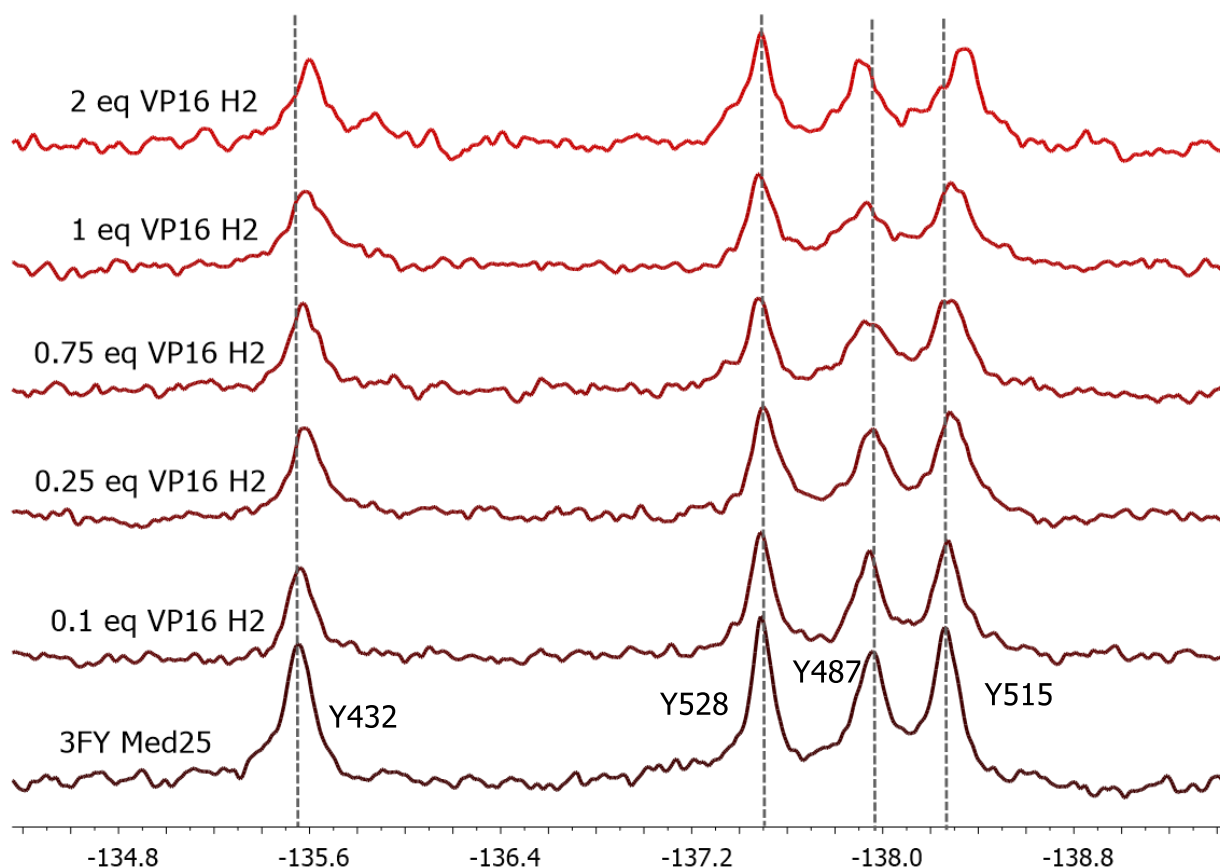


Figure 3.9. PrOF NMR of 3FY Med25 AcID-VP16 H2 complexes. Spectral analysis of 3FY Med25 AcID in the presence of increasing concentrations of VP16(452-490), the H2 TAD of VP16, demonstrated that VP16 H2 perturbs Y432 and the Y487/Y515 pair.

Increasing concentrations of VP16 H2 (residues 452-490 of VP16) (7.5 μM , 18.75 μM , 56.25 μM , 75 μM , and 150 μM) were then complexed with 3FY Med25 AcID (75 μM) and subjected to PrOF NMR (Figure 3.9). VP16(452-490), which comprises the entirety of the VP16 H2 TAD, significantly affected both Y432 (upfield shift of 0.05 ppm at 2 eq. peptide) and the Y487/Y515 pair (0.05 ppm downfield and 0.09 ppm upfield shifts at 2 eq. peptide). This result suggests that VP16 H2 binds at the H2 site, as expected by HSQC NMR⁸ and mutagenesis work. However, the difference in perturbed residues between VP16 H2 and ATF6 α (40-66) suggests that these two H2 site peptides interact

differentially with Med25 AcID. While PrOF and HSQC data suggest that ATF6 α binds perpendicular to the β -barrel and interacts with the C-terminal end of α 1, this PrOF result suggests that VP16 H2 likely extends towards the N-terminal end of the α 1 and proximal to α 2.

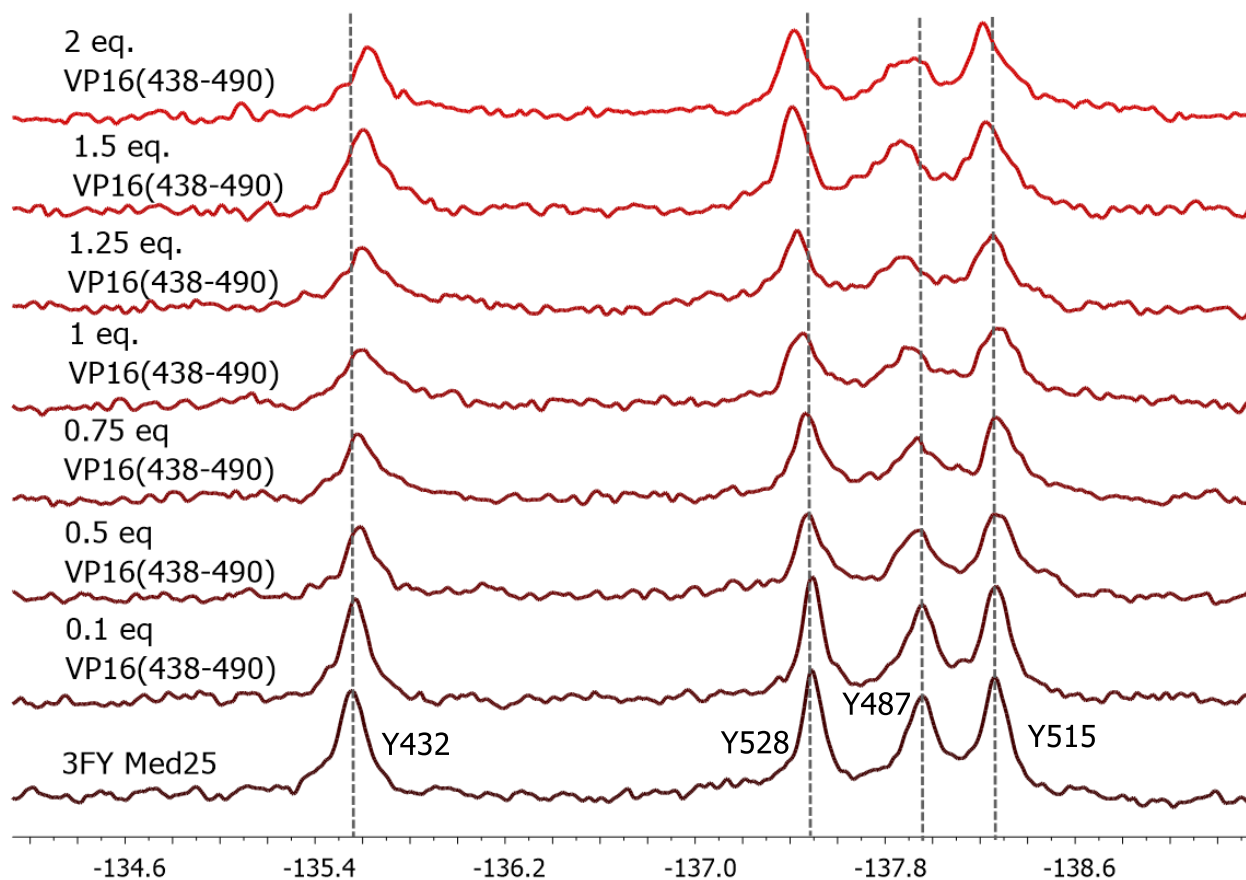


Figure 3.10. PrOF NMR of 3FY Med25 AcID-VP16(438-490) complexes. Spectral analysis of 3FY Med25 AcID in presence of increasing concentrations of VP16(438-490), the helical region of VP16 H1 and the entirety of VP16 H2, demonstrated perturbations of all four Tyr residues.

Acetylated VP16(438-490) (7.5 μ M, 37.5 μ M, 56.25 μ M, 75 μ M, 93.75 μ M, 112.5 μ M and 150 μ M) was complexed with 3FY Med25 AcID (75 μ M) and subjected to PrOF NMR (Figure 3.10). Based on the PrOF data for VP16(452-490), it is unsurprising that an extended VP16 construct, VP16(438-490), also perturbs Y432 (0.06 upfield shift

at 2 eq. peptide) and the Y487/Y515 pair (0.13 ppm downfield and 0.05 ppm upfield) in similar ways. However, an interesting difference between these two PrOF titrations is that VP16(438-490) also perturbs Y528 in a dose-responsive manner (0.07 ppm downfield shift at 2 eq. peptide). These data are consistent with a more complex binding mode for VP16(452-490) relative to VP16(438-490). For instance, VP16(438-490), which binds Med25 AcID much more tightly than VP16(452-490) (K_D of 82 nM for Med25-VP16(438-490) vs. 605 nM for Med25-VP16(452-490) in FP assays), could potentially bind twice to Med25, either at both the H1 and H2 sites simultaneously or twice at the H2 site itself. The N-terminal portion of VP16(438-490) which represents the helical region of the VP16 H1 TAD, could bind to the H1 face concurrent to the C-terminal portion's interaction with the H2 site. If this second scenario is true, the PrOF data, particularly the perturbation of Y528, would suggest that VP16(438-490) wraps around either $\alpha 1$ and $\alpha 3$ or "underneath" the β -barrel, 180° away from $\alpha 2$.

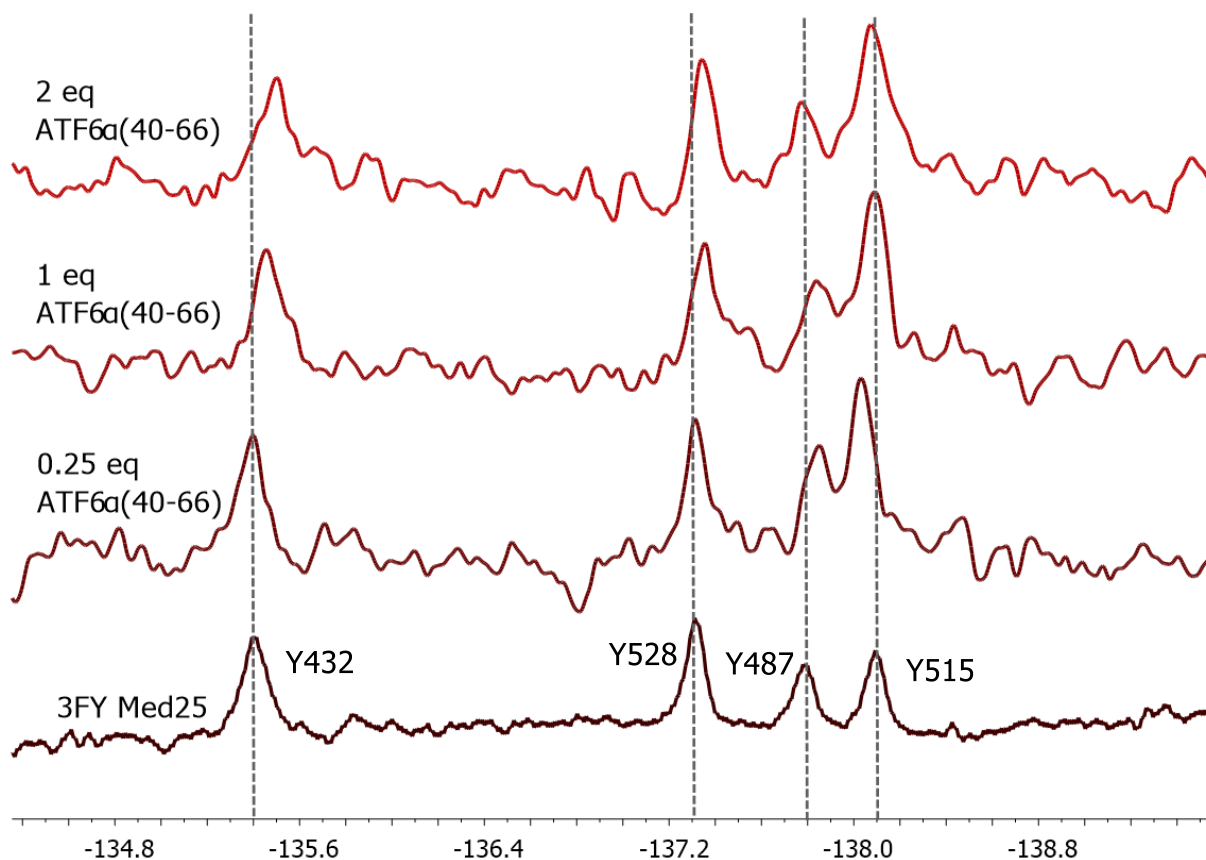


Figure 3.11. PrOF NMR of 3FY Med25 AcID-ATF6 α (40-66) complexes. Spectral analysis of 3FY Med25 AcID in presence of increasing concentrations of ATF6 α (40-66) demonstrated that ATF6 α (40-66) perturbs Y432 and Y528, each of which are located in proximity to the H2 site.

As performed with CBP(20-55), ATF6 α (40-66) peptide (8.75 μ M, 35 μ M, and 70 μ M) was complexed with 3FY Med25 AcID (35 μ M) and subjected to PrOF NMR (Figure 3.11). ATF6 α (40-66) caused dose-responsive shifts in both Y432 and Y528, with the highest concentration (2 eq peptide relative to 3FY Med25 AcID) providing upfield 0.12 ppm and 0.11 ppm shifts respectively. These data corroborate HSQC NMR evidence that ATF6 α (40-66) binds the H2 site at the cleft formed by β 6/ β 7/ β 4 and α 1 and suggests that the peptide does not directly bind to α 2, where Y487 is located.

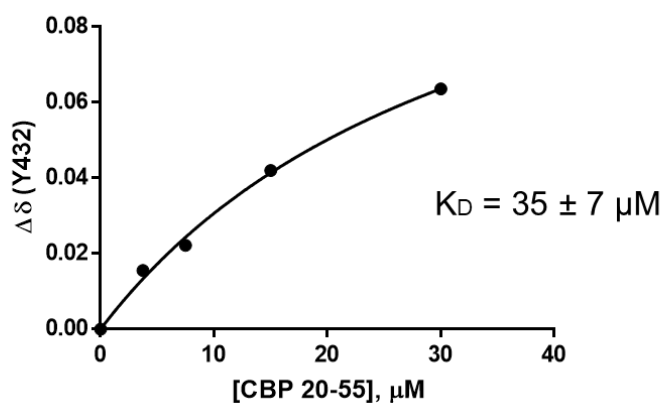
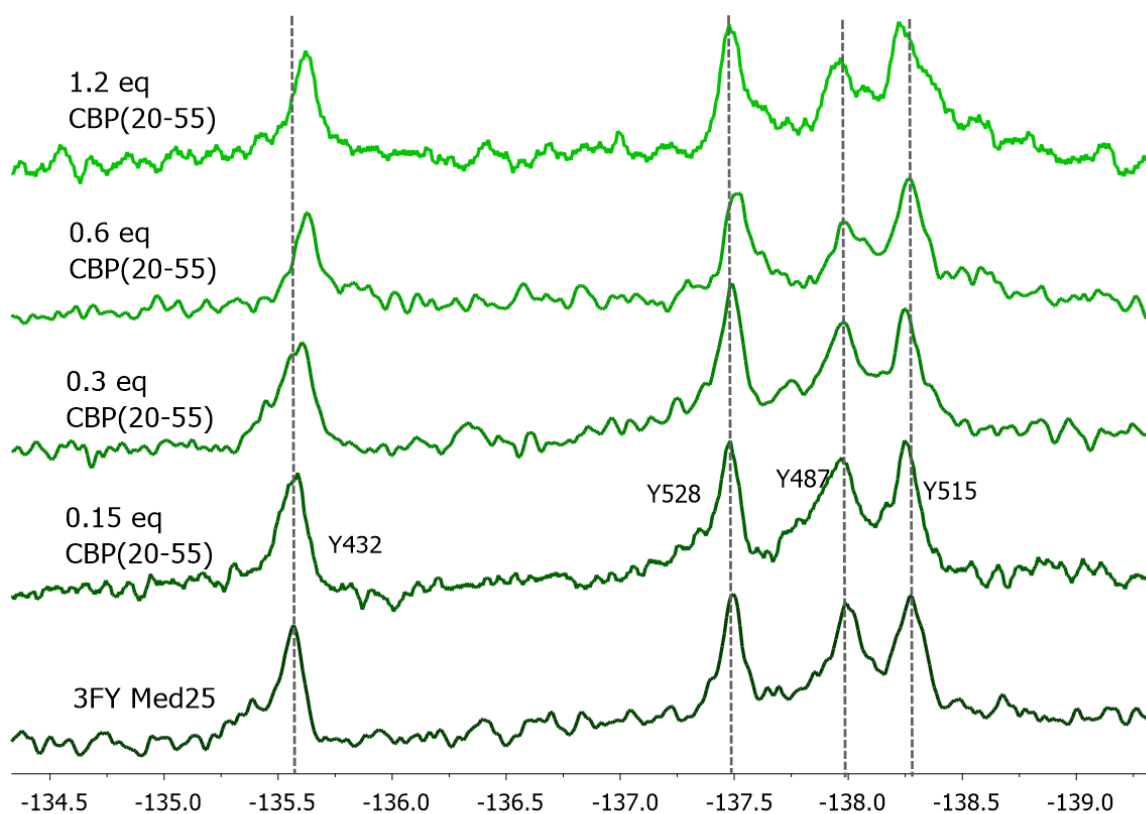


Figure 3.12. PrOF NMR of 3FY Med25 AcID-CBP(20-55) complexes. Spectral analysis of 3FY Med25 AcID in presence of increasing concentrations of CBP(20-55) demonstrated that CBP(20-55) specifically perturbs Y432. A binding isotherm for the Med25-CBP interaction can be determined using the chemical shift perturbation at Y432 with respect to [CBP(20-55)].

Increasing concentrations of acetylated CBP(20-55) peptide (7.5 μM , 15 μM , 30 μM , and 60 μM) were complexed with 3FY Med25 AcID (50 μM) and subjected to PrOF NMR (Figure 3.12). Only Y432 was significantly perturbed in a dose-responsive

manner. At the highest concentration (1.2 eq. CBP peptide relative to 3FY Med25 AcID), there was a 0.06 ppm upfield shift the Y432 resonance. The specific perturbation of this residue without affecting the other resonances suggests that CBP(20-55) does not bind directly to the H2 site. Instead, these data corroborate HSQC NMR evidence that suggested that CBP bound to Med25 by wrapping itself perpendicular to the β -barrel along $\beta 4/\beta 2/\beta 1$ in a binding mode that was unique compared to the Med25-interacting ligands.

A binding isotherm for the Med25-CBP PPI was determined using the dose-responsive chemical shift perturbation at Y432 to determine a binding affinity of $35 \pm 7 \mu\text{M}$. This result provided an additional validation that 3FY Med25 AcID functioned similarly to Med25 AcID, with a K_D approximately ten-fold higher than measured by FP. This loss in binding affinity can be explained by the lack of the hydrophobic N-terminal fluorescein in the acetylated CBP(20-55) peptide. A similar ten-fold loss in binding affinity was demonstrated in FP-based competition experiments (Figure 2.3). Notably, this PPI was the only interaction for which an appropriate K_D with minimal error could be measured. This could be explained if the Med25-CBP PPI occurs with different k_{on}/k_{off} values and/or exchange rates (k_{ex})³⁸. For interactions that occur on fast exchange regimes (high k_{ex}), titrations of one ligand into protein will provide NMR resonances that shift proportionally from the unbound state to the bound state.⁵ However, in the case of protein-ligand interactions that occur under intermediate exchange rates, the chemical shift is not necessarily proportional from the unbound state to the bound state. It is likely that the Med25-CBP PPI is operating in the fast exchange regime while the other Med25 PPIs occur on an intermediate timescale.

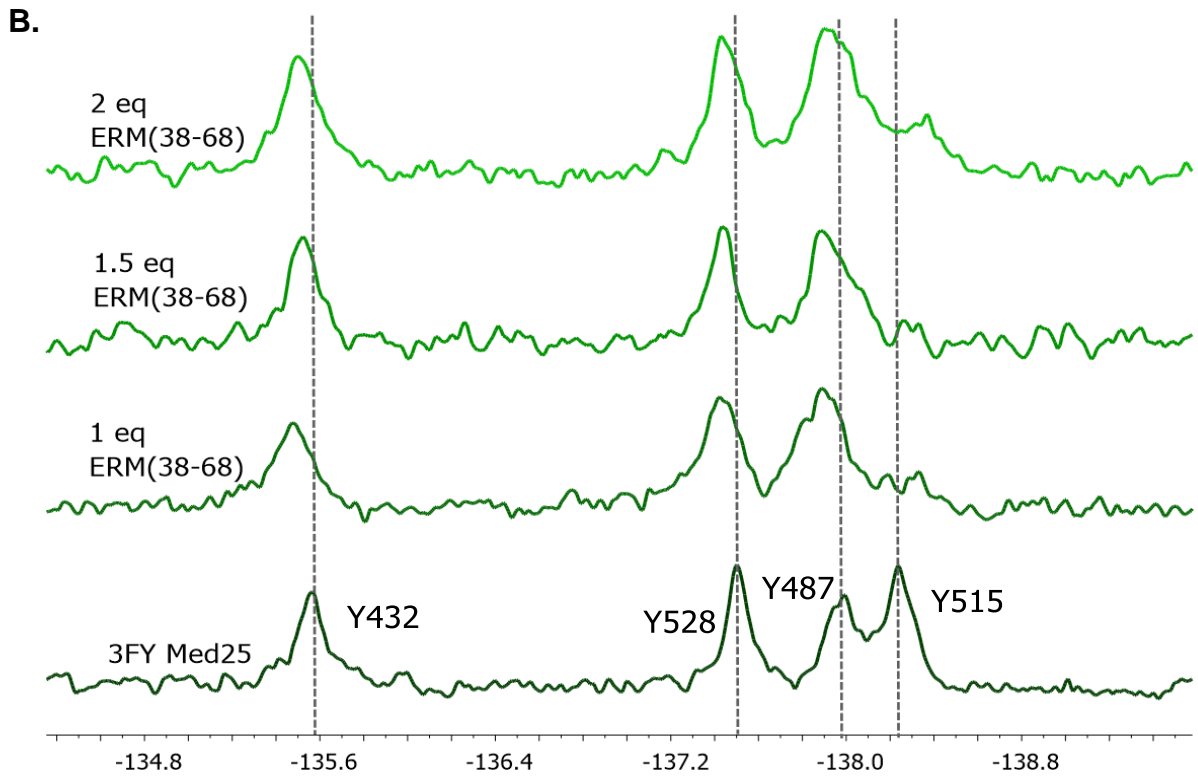
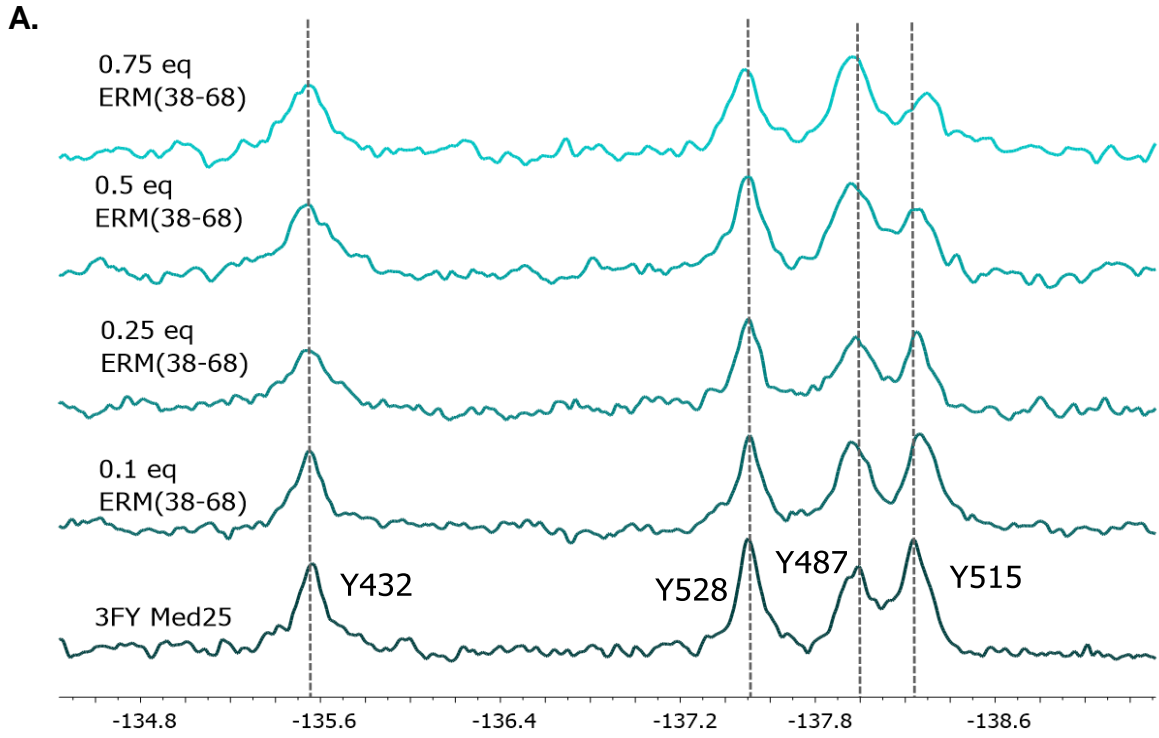


Figure 3.13. PrOF NMR of 3FY Med25 AcID-ERM(38-68) complexes. (Figure on previous page); Spectral analysis of 3FY Med25 AcID in the presence of increasing concentrations of ERM(38-68) demonstrates biphasic character. At substoichiometric concentrations (A), shown in blue, ERM(38-68) causes no significant chemical shifts but does broaden the Y515 resonance. At and above stoichiometric equivalents (B), shown in green, ERM(38-68) causes a downfield perturbation in all four Tyr residues.

Finally, ERM(38-68) peptide (7.5 μ M, 18.75 μ M, 37.5 μ M, 56.25 μ M, 75 μ M, 93.75 μ M, 112.5 μ M and 150 μ M) was titrated with 3FY Med25 AcID (75 μ M) and subjected to PrOF NMR in order to test the working hypothesis that ERM is the most selective peptide for the H1 site and also interacts at the H2 site with weaker affinity (Figure 3.13). Titration of 3FY Med25 AcID with ERM(38-68) demonstrated biphasic character. At substoichiometric concentrations of peptide (Figure 3.13.A), none of the 3FY resonances is shifted; The only effect that substoichiometric ERM(38-68) provides is a slight broadening of the resonance at Y515. Similar to VP16 H1, this difference could be explained by a slight conformational change in the protein that results from ERM(38-68) binding to the H1 site. The second phase of 3FY Med25 AcID induced by ERM(38-68) occurs at 1, 1.5, and 2 eq. of peptide relative to protein (Figure 3.13.B). These three spectra (1, 1.5, and 2 eq. ERM) overlap with each of the four resonances experiencing nearly identical downfield shifts relative to WT. These data suggest that either Med25 binds ERM peptide at two sites with measurably different affinities or that ERM binds at the H1 site and induces a significant conformational change in Med25 that causes uniform shifting in 3FY resonances after ERM saturation. Taken together with previous mutagenesis data demonstrating that ERM(38-68) is capable of binding Med25 even if the H1 site is inhibited, the first scenario is most consistent.

PrOF NMR titrations with Med25-interacting peptides against 5FW Med25 AcID

3-fluorotyrosine provided excellent reporters of ligand binding and conformational change at the H2 and third sites of Med25 AcID while also offering some nuance towards definition of the H1 site. However, for continued study of the H1 site using PrOF NMR, further development of a system that provided direct reporters within the H1 site was desired. Since 5-fluorotryptophan Med25 AcID was obtainable in high yields (10-15 mg protein per liter bacterial culture) at high ¹⁹F incorporation and provides direct reporters at the H1 site, this reagent was used in similar peptide titrations as performed with 3FY Med25 AcID.

Site-directed mutagenesis to assign the resonances in 5FW Med25 AcID were unsuccessful. None of the attempted mutants – W402F, W408F, and W444F – could be expressed. This inability to express W-to-F mutants likely results from the side chains of each of these Trp residues not being solvent exposed and thus potentially critical for protein folding and structure. However, for the scope of this work, independent assignment was thought to be unnecessary, in part because W402 and W444 are direct interaction partners. It is thought that the overlapped resonances from -126.3 to -127.3 ppm, which integrate for two fluorine atoms, likely represent the W402-W444 dyad. Furthermore, all three Trp residues are positioned near the H1 site, contain side chains that are not solvent exposed, and are presumed to be integral to Med25 structure. Therefore, it was hypothesized that 5FW resonances would be sensitive to only the most selective H1 site ligands.

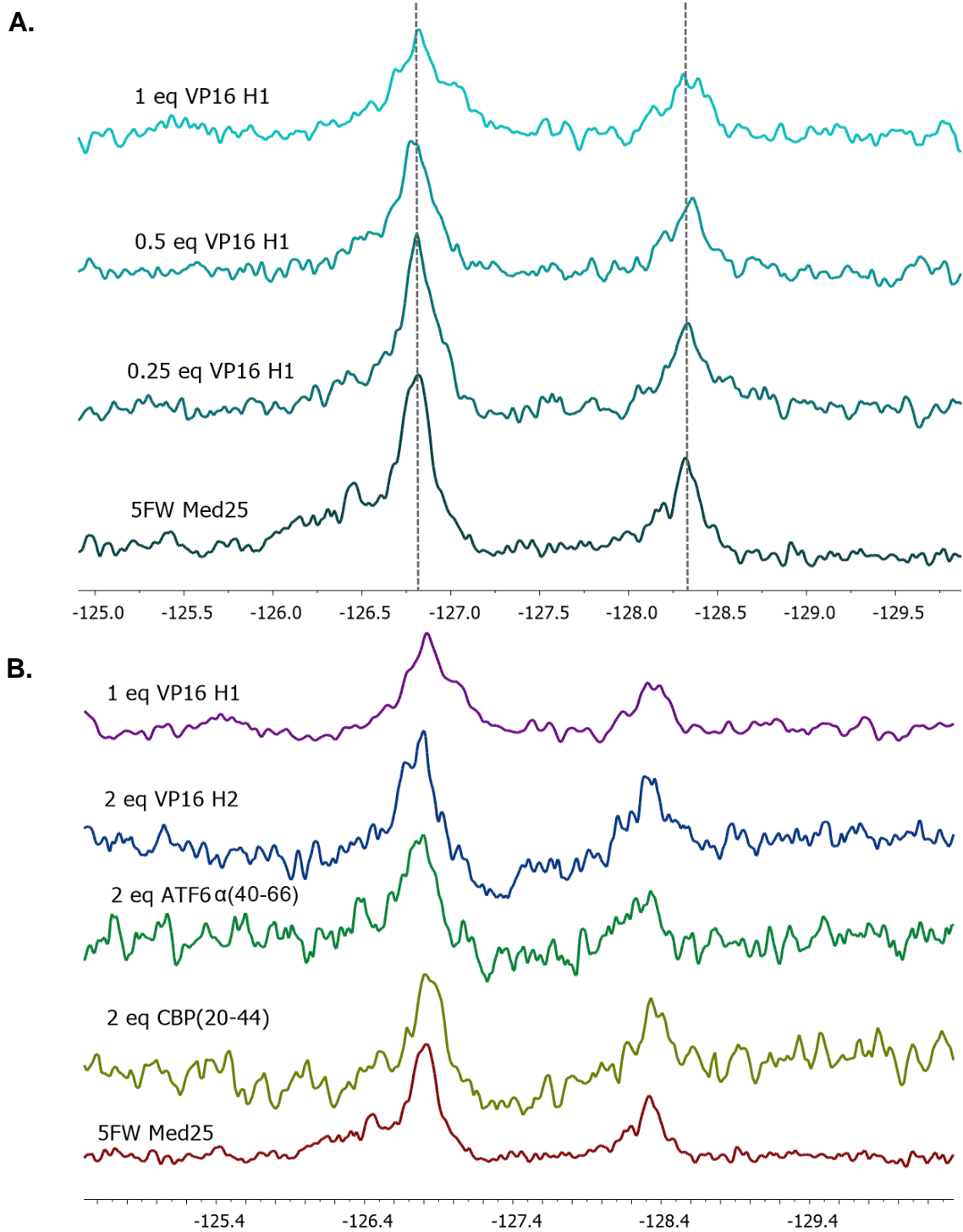


Figure 3.14. PrOF NMR of 5FW Med25 Acid complexes. (A) Spectral analysis of 5FW Med25 Acid in the presence of increasing concentrations of VP16(413-451), the H1 TAD of VP16. No Trp residue is significantly affected. This titration is representative of similar titrations of 5FW Med25 performed with VP16 H2, ATF6 α (40-66), and CBP(20-44), which also showed no effect. (B) Spectral analysis of 5FW Med25 in presence of highest concentrations of peptides tested,

Similar to the described experiments with 3FY Med25 AcID, peptide ligands that interact with Med25 AcID – CBP(20-44), ATF6 α (40-66), VP16 H1, and VP16 H2 – were incubated with 5FW Med25 AcID (Figure 3.14). 5FW Med25 was held constant at 75 μ M and peptide ligands were added at 18.75 μ M, 37.5 μ M, 75 μ M, and 150 μ M for PrOF NMR spectral analysis. Note that the VP16 H1 titration did not include the 150 μ M data point. None of these four peptide ligands had any effect on the 5FW Med25 spectra, indicating that none of them contacted, or caused a conformational change in, any of the three Trp residues. These results were expected for the CBP, ATF6 α , and VP16 H2 peptides, none of which appear to significantly interact at the H1 site. However, the lack of perturbation of W408 by VP16 H1 was puzzling as it was expected that VP16 H1 interacted with the loop between β 1 and β 2. This result suggests instead that VP16 H1 likely interacts with the H1 site parallel to, and up against α 3.

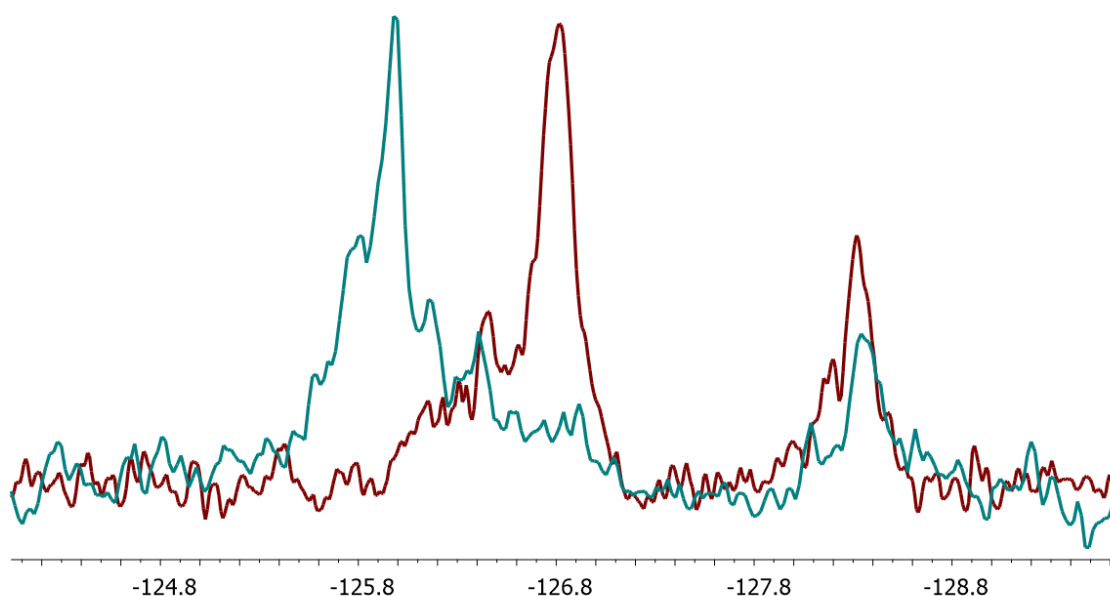


Figure 3.15. PrOF NMR of 5FW Med25 AcID in complex with 1 eq ERM(38-68). ERM(38-68) causes a significant perturbation (0.83 ppm shift) in the resonance centered around -126.7 ppm in spectra of 5FW Med25 AcID while not affecting the resonance at -128.3 ppm. 5FW Med25 complexed to ERM(38-68) shown in blue; 5FW Med25 only shown in red.

In contrast to the results of the H2/third site interacting peptides and the VP16 H1 experiments, the addition of 1 eq ERM(38-68) to 5FW Med25 AcID caused a dramatic perturbation of 5FW resonances (Figure 3.15). Specifically, ERM(38-68) caused a ~1 ppm downfield shift of the resonance at -126.7 ppm. As previously noted, this broad resonance integrates for two ^{19}F atoms and is proposed to represent the W402/W444 dyad. This result corroborates previous evidence that ERM(38-68) binds to the H1 site in a unique manner and quite differently than VP16 H1. In particular, when considering the lack of perturbations at $\alpha 2$ in 3FY PrOF experiments at substoichiometric ERM conditions, this result suggests that ERM(38-68) might bind perpendicular to the β -barrel at the H1 site.

Binding models for unique peptide interactions with Med25 AcID

At this stage, each discrete interaction between Med25 AcID and its protein interaction partners have been subjected to extensive analysis including ^1H , ^{15}N -HSQC NMR, the mutational study described in Chapter 2, and protein-observed ^{19}F NMR. Collectively, these data have informed proposed binding models to describe each of the known Med25 AcID PPI. Each methodology has its limitations (e.g. HSQC NMR cannot necessarily differentiate between allosteric and orthosteric effects) however, they are incredibly complementary, with each providing unique insights (e.g. PrOF NMR can provide selective differentiation of specific regions within a single binding site).

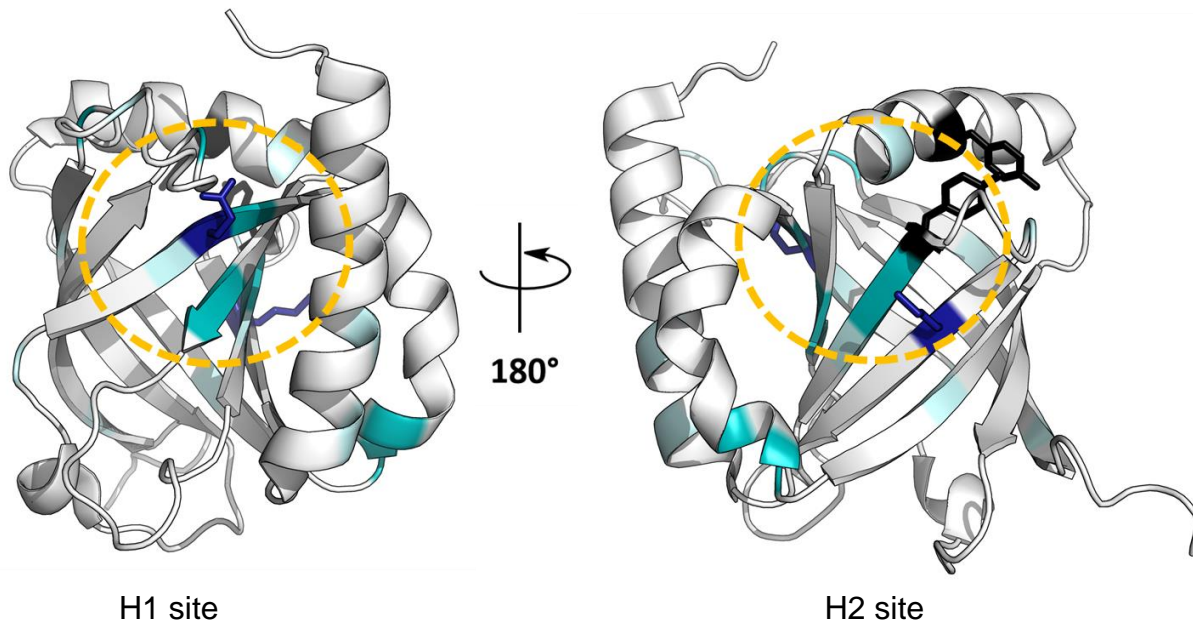


Figure 3.16. Model of the Med25 AcID-VP16 H1 PPI. Proposed binding locations of Med25 AcID for VP16(413-451) are highlighted by golden circles. Residues of Med25 AcID that are significantly perturbed by VP16 H1 peptide in HSQC NMR are colored in teal (2 standard deviations) and pale blue-green (1 standard deviation); Tyr residues that are affected in ProOF NMR experiments are shown as sticks in black; Residues where introduction of negative charge significantly inhibited the PPI are shown as sticks in dark blue. HSQC NMR performed by Andy Henderson. (PDB 2XNF)

In the mutagenesis study, blocking both the H1 and H2 sites with negative charge (Q451E/M523E mutant) resulted in a 24-fold loss in binding affinity for VP16 H1 relative to WT; Blocking either the H1 site (Q451E) or the H2 site (M523E) alone provided relatively minor losses in binding affinity (2.9-fold and 4.3-fold losses, respectively). This suggested that VP16 H1 could either bind at both the H1 and H2 sites or that VP16 H1 is an allosteric regulator of Med25 function; HSQC NMR data were consistent with these two possibilities. ProOF NMR of 3FY Med25 AcID suggested that VP16 H1 binding occurs “high” in the H2 site, near $\alpha 2$, as only the Y487/Y515 pair were significantly perturbed. The lack of perturbations in the ProOF NMR of 5FW Med25 (which provides NMR reporters at the H1 site only) indicated that the H1 site is *not* the sole target for binding to Med25

AcID, diminishing allosteric effects as the cause for H2 site perturbations in other experiments. Collectively, these data suggest that VP16 H1 binds at the H2 site with an affinity equivalent to that at the H1 site. It remains unknown however if multiple copies of the peptide are capable of binding to the protein simultaneously (Figure 3.16).

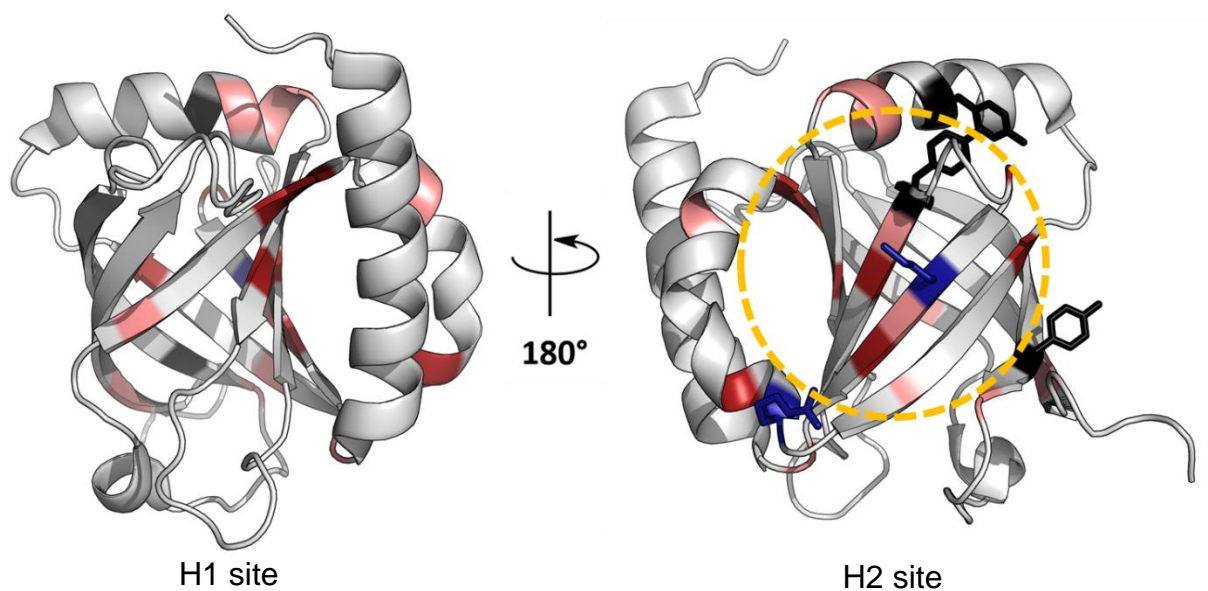


Figure 3.17. Model of the Med25 AcID-VP16 H2 PPI. The proposed binding location of Med25 AcID for VP16(452-490) is highlighted by the golden circle within the H2 site. Residues of Med25 AcID that are significantly perturbed by VP16 H2 in HSQC NMR are colored in red (2 standard deviations) and pink (1 standard deviation); ProOF NMR experiments of 3FY Med25 AcID caused perturbations in Y432 and the Y487/Y515 pair (sticks in black); Introduction of negative charge at R466 and M523 (sticks in blue) caused significant inhibition of the Med25 AcID-VP16 PPI. HSQC NMR performed by Andy Henderson. (PDB 2XNF)

HSQC NMR of the Med25 AcID-VP16 H2 demonstrated significant perturbations at the H1 and H2 sites, suggesting that the peptide might bind at both locations. However, the mutational and ProOF NMR studies were more definitive in demonstrating that VP16 H2 binds selectively to the H2 site. Mutagenesis to block the H2 site was incredibly effective at inhibiting VP16 H2 (R466D and M523E provided 11-fold and 23-fold losses in binding affinity relative to WT, respectively) while blocking the H1 site through

mutagenesis was ineffective at inhibiting VP16 H2. PrOF NMR studies of the Med25 AcID-VP16 H2 localized the VP16 H2 interaction to occur “high” in the H2 site, near $\alpha 2$, and likely extending perpendicular to the β -barrel towards Y432 (Figure 3.17).

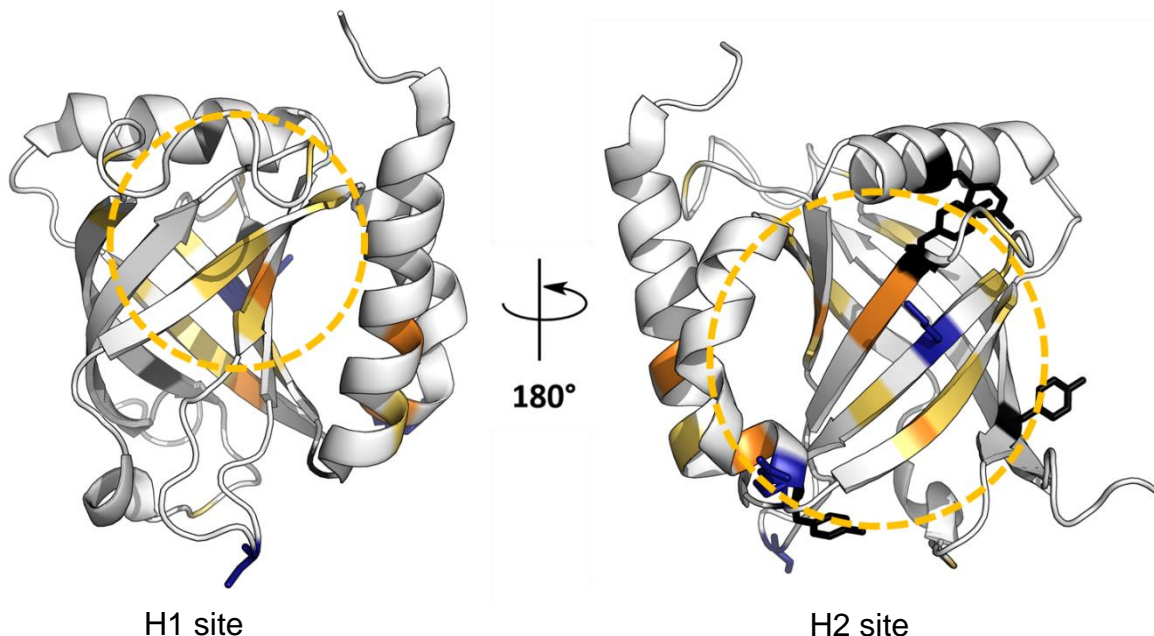


Figure 3.18. Model of the Med25 AcID-VP16(438-490) PPI. Proposed binding locations of Med25 AcID for VP16(438-490), which contains the α -helical region of VP16 H1 and the entirety of VP16 H2, are highlighted by golden circles. Residues of Med25 AcID that are significantly perturbed by VP16 H1 peptide in HSQC NMR are colored in orange (2 standard deviations) and yellow (1 standard deviation); Tyr residues that are affected in PrOF NMR experiments are shown as sticks in black; Shown as sticks in dark blue are residues at which introduction of negative charge to block the H2 site (R466 and M523) or tethering with a peptide to block the H1 site (C506) significantly inhibited the Med25-VP16(438-490) PPI. HSQC NMR performed by Andy Henderson. (PDB 2XNF)

Like VP16 H2, HSQC NMR of VP16(438-490), which contains the α -helical region of VP16 H1 and the entirety of VP16 H2, demonstrated significant chemical shift perturbations at both the H1 and H2 sites of Med25 AcID. However, the mutagenesis work and PrOF NMR could differentiate VP16 H2 from VP16(438-490), as VP16(438-490) had more dramatic impact within both studies. PrOF NMR of 3FY Med25 AcID perturbed all four Tyr residues dispersed among the H2 site. Individual inhibition of either

the H2 site through introduction of negative charge (R466D and M523E provided 8.9-fold and 15-fold losses in binding affinity relative to WT, respectively) or the H1 site through Tethering of VP16 G450C peptide (WT-VP16 G450C peptide provided a 6.0-fold loss in binding affinity relative to WT) significantly reduced binding affinity. Furthermore, blocking the H1 and H2 sites simultaneously had dramatic effects (R466D and M523E Tethered to VP16 G450C peptide provided 46-fold and 117-fold losses in binding affinity to WT, respectively). Collectively, these data suggest that VP16(438-490) likely binds to both the H1 and H2 faces simultaneously. It is likely that C-terminal portion, containing VP16 H2, interacts at the H2 site while the N-terminal binds at the H1 site (Figure 3.18). While the order in which these interactions occur is unknown, the first binding event would make the second binding event highly favorable, as the entropic cost of the second interaction would be lowered. This mechanism of action provides an explanation of why the VP16(438-490) peptide binds Med25 AcID with >7-fold higher affinity than VP16 H2 (K_D of 82 nM for Med25-VP16(438-490) vs. 605 nM for Med25VP16(452-490) in FP assays).

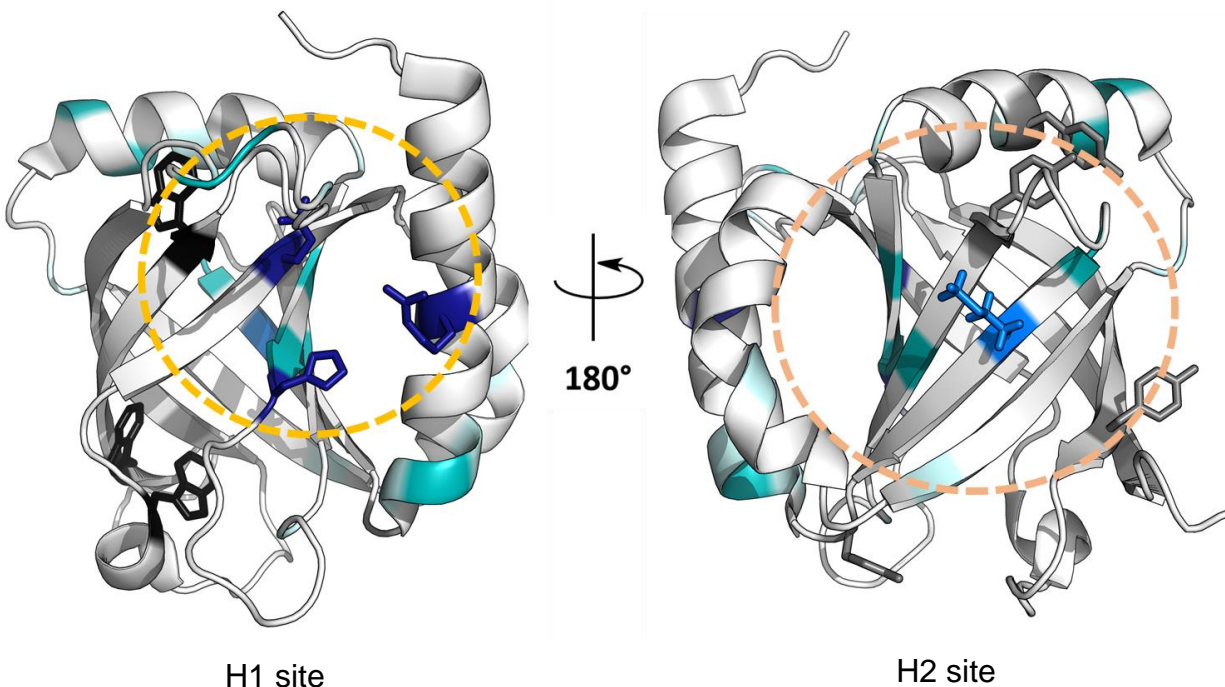


Figure 3.19. Model of the Med25 AcID-ERM PPI. The proposed primary binding location of Med25 AcID for ERM(38-68) is highlighted by the golden circle at the H1 site. A proposed secondary binding location, thought to represent a weaker affinity interaction, is highlighted by the tan circle at the H2 site. Residues of Med25 AcID that are significantly perturbed by saturation with ERM peptide in HSQC NMR are colored in teal (2 standard deviations) and pale blue-green (1 standard deviation). Shown as sticks in dark blue are residues (Q451, H499, and R538) at which introduction of negative charge to block the H1 site significantly inhibit ERM binding (These residues are also significantly perturbed in HSQC NMR experiments.). At the H1 site, Trp residues that are affected in ProOF NMR experiments are shown as sticks in black; At the H2 site, Tyr residues, shown as sticks in gray, are perturbed in ProOF NMR *only* at and above stoichiometric equivalents; Introduction of negative charge at M523, shown as sticks in light blue, inhibits ERM binding *only* if the H1 site is also blocked with Q451E (H1 site) mutation. HSQC NMR performed by Andy Henderson. (PDB 2XNF)

HSQC NMR of the Med25 AcID-ERM PPI, reported in the literature¹⁰ and performed in the Mapp lab, demonstrated significant chemical shift perturbations at the H1 site. Additional residues were significantly perturbed at the H2 site, opening the possibility that ERM(38-68) could behave like VP16 H1 and bind at both sites with similar affinities. However, both the mutagenesis study and ProOF NMR indicated that this is not the case. In the mutagenesis study, ERM was the only peptide that was significantly

affected by the introduction of negative charge at Q451, H499, and R538 (3.0-fold, 3.5-fold, and 5.9-fold losses in binding affinity to ERM(38-68) relative to WT, respectively). Furthermore, ERM(38-68) was the only interaction partner that perturbed 5FW Med25 resonances in PrOF NMR, all of which are located near the H1 site, and did *not* perturb any 3FY Med25 resonances at substoichiometric equivalencies. Collectively, these data demonstrated that ERM binds selectively at the H1 site when relative levels of ERM peptide are low (Figure 3.19).

Additional evidence suggested that ERM likely binds to the H2 site with a lesser relative affinity when the H1 site is already occupied with another copy of the peptide ligand. In PrOF NMR, 3FY Med25 resonances are unaffected by ERM until the concentration of ERM peptide is equal or, or greater than, the concentration of protein at which point all resonances become significantly perturbed. The mutational study provided additional evidence of a weak, second interaction between ERM and the H2 site. Inhibition of the H2 site through introduction of negative charge at M523 alone does not affect ERM binding (1.2-fold change relative to WT) however blocking both the H1 and H2 sites with the Q451E/M523E mutation provides 9.9-fold loss in binding affinity relative to WT (which is three-fold better inhibition than Q451E alone)

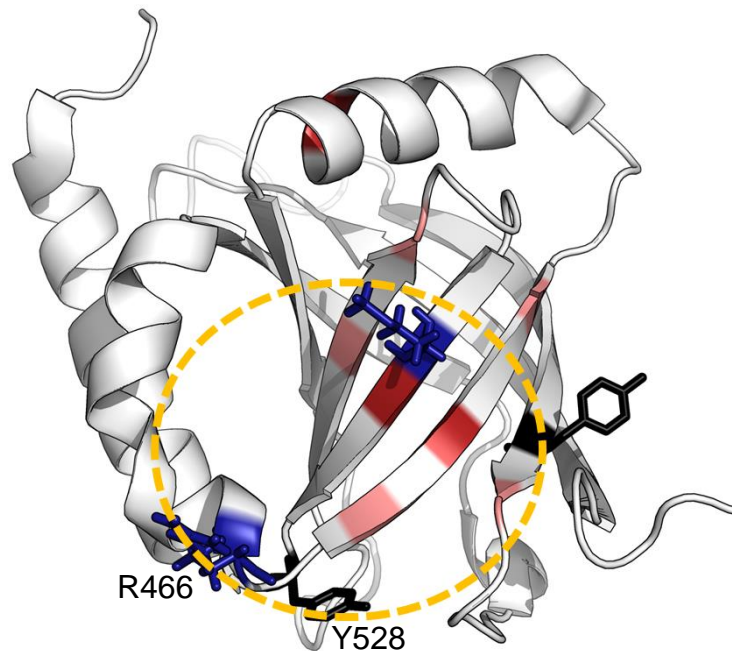


Figure 3.20. Model of the Med25 AcID-ATF6 α PPI. The proposed binding location of Med25 AcID for ATF6 α (40-66) is highlighted by the golden circle within the H2 site. Residues of Med25 AcID that are significantly perturbed by ATF6 α peptide in HSQC NMR are colored in red (2 standard deviations) and pink (1 standard deviation); R466 and Y528 (labeled) were also perturbed by >2 SD in HSQC NMR. PrOF NMR experiments of 3FY Med25 AcID caused perturbations in Y528 and Y432 (sticks in black). Finally, introduction of negative charge at R466 and M523 (sticks in blue) caused significant reduction in binding affinity of ATF6 α (40-66) for Med25 AcID. (PDB 2XNF)

Like VP16 H2, all experimental data suggest that ATF6 α binds selectively at the H2 site. HSQC NMR demonstrated that vast majority of significantly perturbed residues are within or near the H2 site; Inhibition at the H1 site through mutagenesis had no effect on the Med25-ATF α interaction however H2 site mutants provided large effects (M523E, R466D, and R466D/M523E provided 8.8-, 12-, and 16-fold losses in binding affinity relative to WT). PrOF NMR did however demonstrate that ATF6 α does interact differently with the H2 site than does VP16 H2. These data suggest that ATF6 α binds at the ‘bottom’ of the H2 site, away from α 2 and near the C-terminal end of α 1 (Figure 3.20).

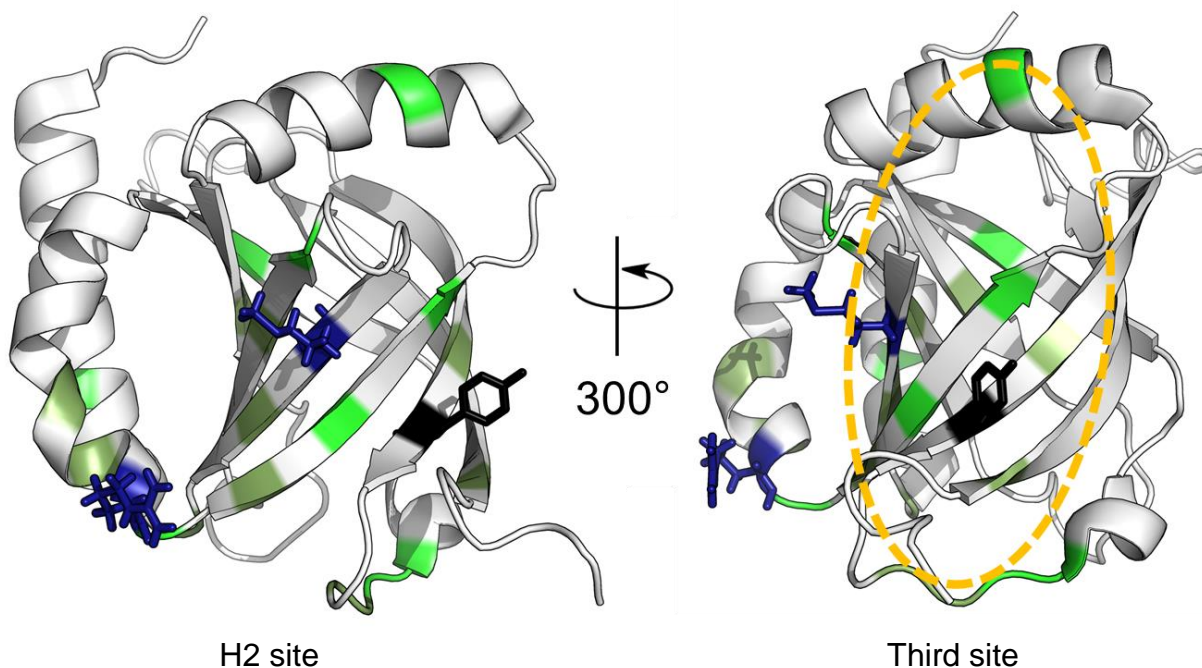


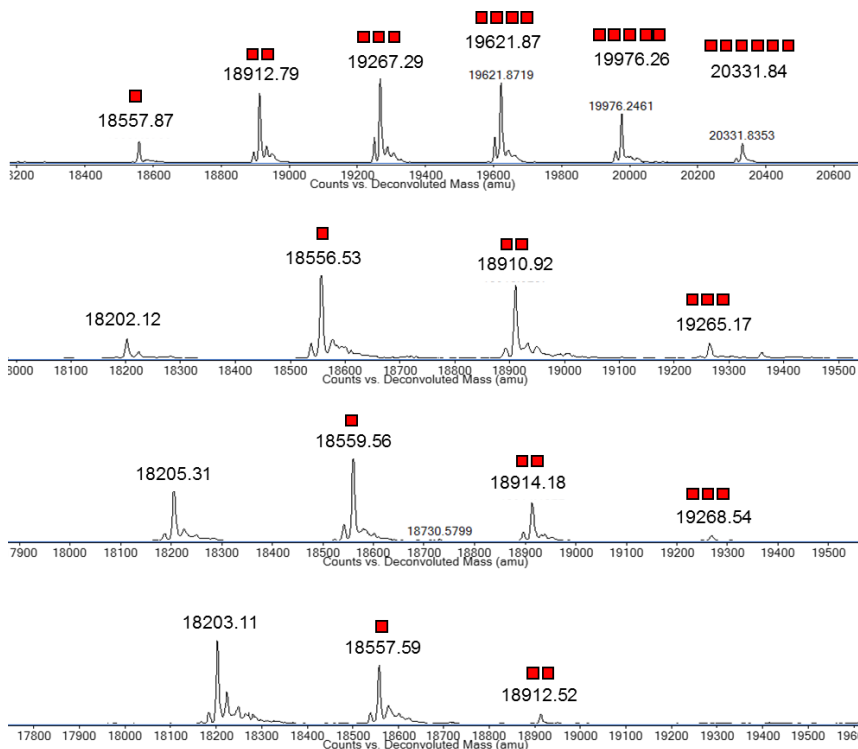
Figure 3.21. Model of the Med25 AcID-CBP PPI. The proposed binding location of Med25 AcID for CBP(20-44) is highlighted by the golden circle at the third site. Residues of Med25 AcID that are significantly perturbed by CBP peptide in HSQC NMR are colored in bright green (2 standard deviations) and dull green (1 standard deviation); Y432, the single Tyr residue that is perturbed in PrOF NMR experiments is shown as sticks in black; Residues where introduction of negative charge significantly inhibited the PPI are shown as sticks in dark blue. (PDB 2XNF)

The Med25 AcID-CBP PPI is unique from all Med25-activator PPIs, based on the data. HSQC perturbation patterns differ from all other peptides, providing significant chemical shift perturbations within the H2 site and at a cleft in the protein that could represent a third binding site formed by $\beta 2/\beta 4/\alpha 2$, 90° away from the H2 site. Notably, CBP(20-44) is the only tested peptide to perturb several residues in this region of the protein away from the H2 site. A recent report has suggested that the DNA-binding domain of ETV4 likely occupies this similar position on Med25 AcID.³⁹ Additional evidence that CBP(20-44) resides at this newly identified cleft of the protein and not at the H2 site comes from the PrOF NMR titration of 3FY with CBP. Only Y432, a residue that is situated between the H2 site and this putative third site, is perturbed by CBP. It should be noted

that it is unknown where the H2 site ends and this potential third site would begin (Figure 3.21). However, critically, the NMR binding signatures for the Med25-CBP(20-44) PPI are unique and unlike any other peptide ligand (as described) or small molecule ligand (to be described). This stark difference in binding signature could have important implications on Med25 AcID function. This newly identified site, if verified, could represent an interface that Med25 might exploit for allosteric purposes or to link activators to the master coactivator CBP/p300.

Protein-observed ¹⁹F-NMR experiments demonstrate model of Med25 AcID inhibition induced by norstictic acid

Norstictic acid is a single-digit micromolar inhibitor of Med25 AcID PPIs, and functions through formation of reversible covalent imine adducts with lysine residues of Med25 AcID. Site-specific mutations of lysine with arginine eliminated the possibility for covalent-adduct formation while maintaining positive charge. A single set of mutations – K518R/K519R/K520R, located on the H2 site – had negligible effects on native Med25-peptide interactions but strongly reduced inhibition by norstictic acid of Med25-VP16 H1 and Med25-VP16 H2 interactions. This suggested that norstictic acid covalently binds with these specific lysine residues within the H2 site however secondary evidence was desired. This Med25 AcID-ligand interaction offered an excellent opportunity to leverage the PrOF NMR system and knowledge gained during the PrOF analyses of Med25 PPIs towards the mechanistic understanding of a small molecule that targets Med25 AcID.



4 eq norstictic acid

6% single, 19% double, 24% triple, 32% quadruple, 14% 5x, 5% 6x

2 eq norstictic acid

10% unlabeled, 45% single, 37% double, 8% triple

1 eq norstictic acid

29% unlabeled, 47% single, 21% double, 3% triple

0.5 eq norstictic acid

55% unlabeled, 39% single, 6% double

Figure 3.22. Labeling of 3FY Med25 Acid with norstictic acid. 3FY Med25 (75 μ M) was incubated with 0.5, 1, 2, and 4 eq. of norstictic acid for four hours at room temperature before mass spectrometry and PrOF NMR analysis. Red squares indicate number of covalent norstictic acid; Each norstictic acid provided +354 mass units.

Norstictic acid was incubated with 3FY Med25 Acid, at four different concentrations relative to Med25, for four hours at room temperature prior to reduction of the resultant imine with sodium borohydride. Following a buffer exchange, these protein samples were then subjected to mass spectrometric analysis to demonstrate the formation of covalent Med25-norstictic acid adducts (Figure 3.22). Incubation of 3FY Med25 with 0.5 eq. norstictic acid provided 39% single-labeled protein (18557.59 Da) and 6% double-labeled protein (118912.52 Da). 3FY Med25 incubated with 1 eq. norstictic acid (47% single-, 21% double-, and 3% triple-labeled) and 2 eq. norstictic acid (45% single-, 37% double-, and 8% triple-labeled) both provided protein samples that were primarily labeled as a single adduct. Unsurprisingly, incubation with 4 eq. norstictic acid

gave the highest degree of labeling with > 50% of the total protein covalently bound with three or more norstictic acid molecules (6% single-, 19% double-, 24% triple-; 32% 4x-, 14% 5x-, 5% 6x-labeled).

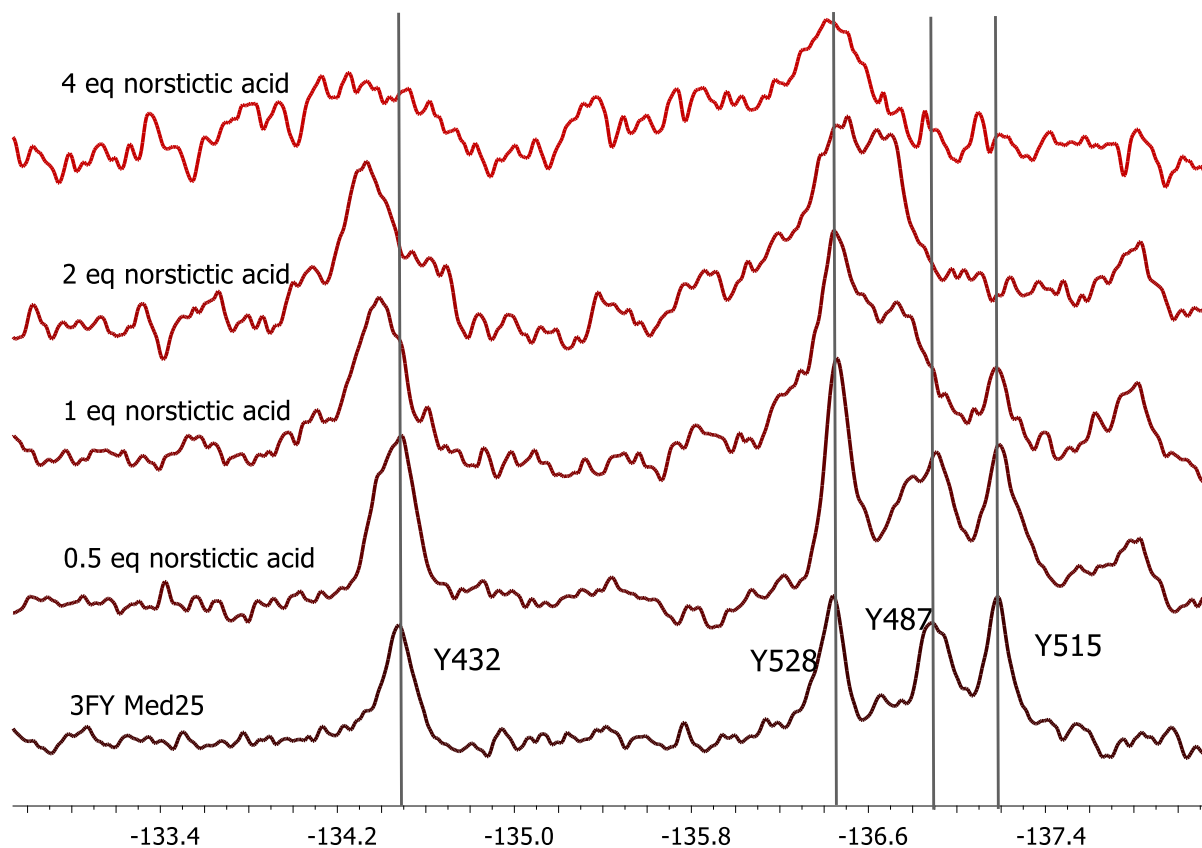


Figure 3.23. PrOF NMR of 3FY Med25 AcID labeled with norstictic acid. Spectral analysis of 3FY Med25 AcID incubated with 0.5, 1, 2, and 4 eq. of norstictic acid. Labeling with norstictic acid causes chemical shift perturbation at Y487 at 0.5 eq. and subsequent perturbations of Y432 and Y515 as [norstictic acid] increases.

After mass spectroscopy and a buffer exchange to remove excess norstictic acid, each sample was subjected to PrOF NMR analysis (Figure 3.23). The resultant spectra demonstrated that labeling with norstictic acid dramatically affects the tyrosine residues of 3FY Med25. The Med25 AcID sample incubated with 0.5 eq. norstictic acid was either unlabeled (55% by MS) or single-labeled (39% by MS). This single adduct caused a splitting of both the Y432 and Y487 resonances, as evidenced by the downfield shoulders

of the WT resonances at -134.5 and -136.9 ppm. These new peaks become more apparent in the 1 eq. norstictic acid sample, likely due to its lower % unlabeled by MS (29%). In the PrOF spectrum of the Med25 AcID sample incubated with 2 eq. norstictic acid sample, which contained significant amount of protein with two covalent adducts (37% double-labeled), both the Y487 and Y515 resonances were completely shifted downfield from their WT chemical shifts. The PrOF spectrum of the final sample, Med25 AcID incubated with 4 eq. norstictic acid, demonstrated significant broadening of all resonances in the noise, with peaks indistinguishable for Y432, Y487, and Y515. This could indicate that each of these tyrosine residues are near norstictic acid when Med25 AcID is labeled with more than one norstictic acid or that multiple-labeled adducts induce large conformational changes (Only 6% of this sample contained fewer than two adducts). The resonance for Y528, while broadened slightly, remained in its WT location.

Collectively, these PrOF experiments with Med25 AcID covalently labeled to increasing amounts of norstictic acid demonstrated that norstictic acid likely binds the protein in proximity of the Y487/Y515 pair and Y432 (Figure 3.24). Since it is known that the molecule forms a covalent adduct with the side chains of lysine, this PrOF data suggested that norstictic acid is likely to preferentially bind one of the lysine residues in the β 6- β 7 loop (K518/K519/K520) at least once, and potentially twice, before reacting with other residues. These are the only lysine residues in proximity of each of the Y487/Y515 and Y432 residues that are influenced by norstictic acid in PrOF experiments. This analysis is consistent with, and corroborates, previous Lys-to-Arg mutational work that demonstrated that K518/K519/K520 were critical for the inhibitory activity of norstictic acid⁴⁰. In addition to providing corroboration of the location of the Med25-norstictic acid

interaction, this result demonstrated that PrOF NMR of fluorinated Med25 variants offers a unique method of studying Med25-ligand interactions in addition to Med25 PPIs

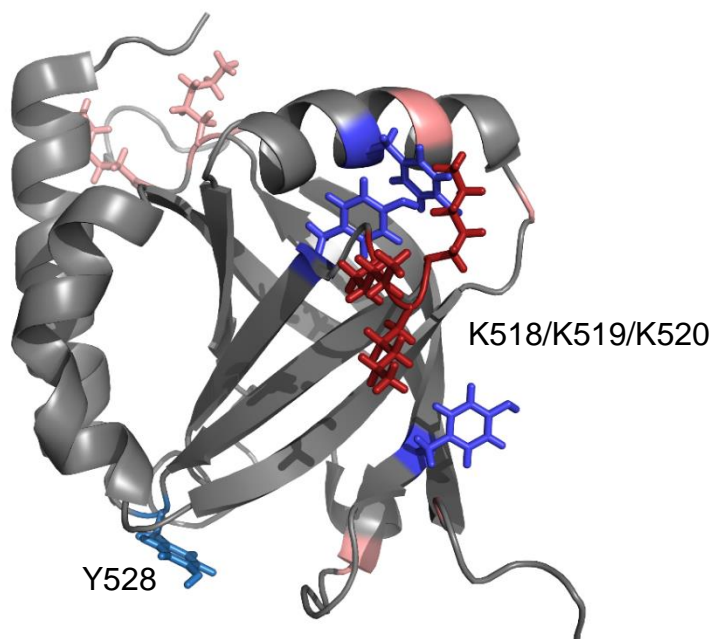


Figure 3.24. Model of norstictic acid labeling of Med25 AcID. PrOF NMR analysis corroborated that K518/K519/K520 (shown in red) on loop between β 6- β 7 is likely primary target for covalent labeling of norstictic acid for Med25 AcID. Dark blue residues indicate 3FY residues perturbed in PrOF experiments; pink represents additional Lys residues; Light blue represents Y528, which is not affected by norstictic acid labeling. (PDB 2XNF)

PrOF NMR allows for characterization and development of a small molecule fragment that targets Med25 AcID

The Med25 AcID-ERM PPI had been screened against a library of 1600 small molecule fragments maintained by the Wells lab at the University of California – San Francisco using the FP Tethering approach (Andy Henderson, University of Michigan and Zach Hills, UCSF).^{41,42} This methodology allows for the discovery of fragments that undergo disulfide exchange with solvent exposed cysteine residues of a protein-of-interest. Med25 AcID contains two such cysteines – C497, located in the center of the H1 site, and C506, located on a loop near the base of the H1 site. Thus, this methodology

was anticipated to discover molecules that inhibited Med25 AcID at the H1 site. Following screening of the Med25-ERM complex at three different stringencies (0.2 mM, 1 mM, and 5 mM β -mercaptoethanol) and removal of fluorescent artifacts, thirty-one unique compounds were discovered to significantly inhibit Med25-ERM. One of the most potent fragments discovered, termed A6, was independently synthesized (Clint Regan, University of Michigan) containing an irreversible iodoacetamide electrophile in place of the disulfide used during the Tethering screen (Figure 3.25). As with norstictic acid, it was hypothesized that PrOF NMR could be leveraged to provide mechanistic understanding of the interaction of this fragment small molecule with Med25 AcID.

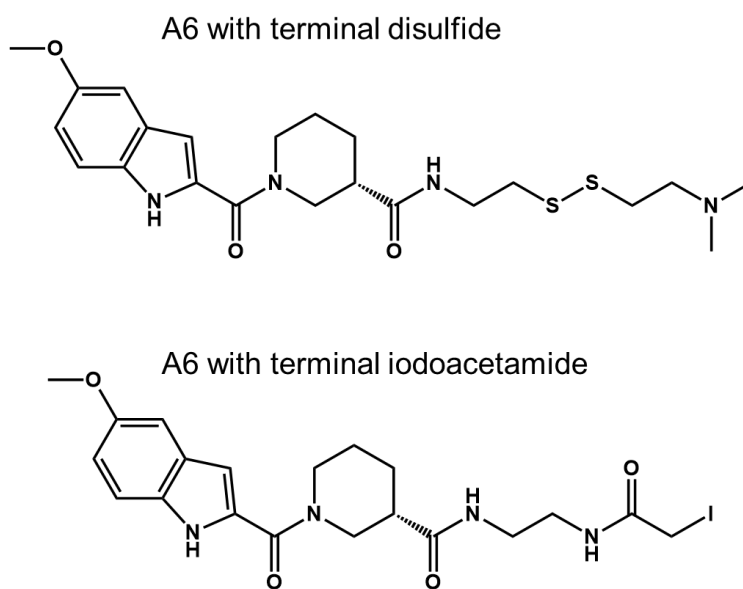


Figure 3.25. Structures of fragment A6. A6 is shown with a right-side terminal disulfide (structure of originally discovered molecule in Tethering screen; allows for reversible disulfide exchange with cysteine) and with a right-side terminal iodoacetamide (allows for covalent labeling at cysteine residues)

Med25 AcID was incubated with four equivalents of A6-iodoacetamide fragment for six hours, resulting in a protein sample that was singly labeled (>95% by mass spectroscopy). Longer incubation times and/or higher equivalencies of A6 did produce

Med25 AcID that was doubly labeled; however, this second labeling event was much slower than the first. Labeling studies with C506A and C497A mutants were used to determine which of the two solvent exposed cysteines was the preferred target for A6-iodoacetamide (Andy Henderson, University of Michigan). These experiments demonstrated that A6-iodoacetamide efficiently labels C497A Med25 AcID but does not label C506A Med25 AcID, a result indicating that the Cys at 506 is the likely target of A6-iodoacetamide.

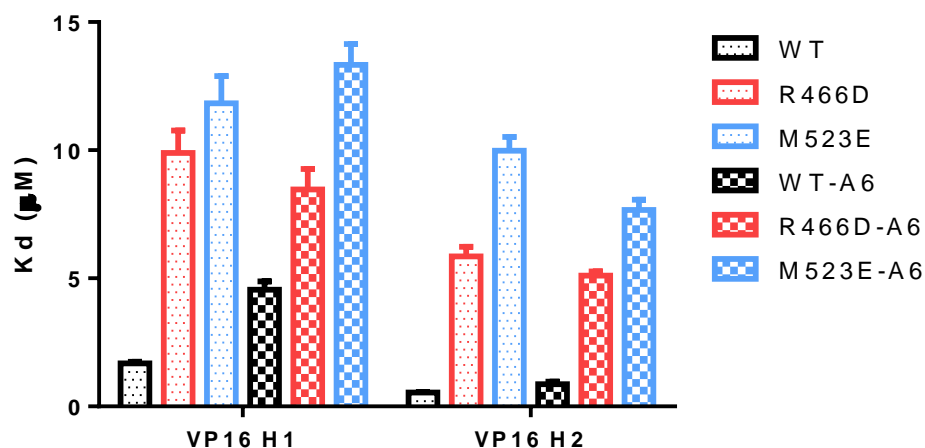


Figure 3.26. Mutant Med25-A6 complexes fail to block H1 and H2 sites simultaneously. Binding affinities of VP16 H1 and VP16 H2 peptides for Med25 mutants complexed to A6, as measured by FP.

The ability of A6 to inhibit binding of peptide ligands to the H1 site of Med25 was investigated using WT Med25 AcID and Med25 mutants that block the H2 site (R466D, and M523E), in similar manner as performed with VP16 G450C peptide (Figure 3.26). It was hypothesized that A6 would be capable of moderate and significant inhibition of the Med25-VP16 H1 PPI based on the effects of VP16 G450C peptide when tethered to C506 of Med25 AcID. Tethering of VP16 G450C peptide to WT Med25 AcID caused a 12.8-fold loss in VP16 H1 binding affinity while Tethering of VP16 G450C peptide to R466D had

caused a 67-fold loss in VP16 H1 binding affinity. These results had demonstrated that the combination of an H2 site mutant and VP16 G450C peptide appended to the H1 site was capable of successfully blocking the H1 and H2 sites simultaneously. Considering these large inhibitory effects provided by VP16 G450C, it was hypothesized that the small molecule fragment A6 Tethered to the same C506 residue of Med25 AcID would be capable of comparable inhibitory effects.

For all three Med25 AcID variants (WT, R466D, and M523E), excess A6-iodoacetamide was incubated with protein until >95% single labeling was achieved according to MS analysis. Binding affinities of labeled and unlabeled protein to VP16 H1 and VP16 H2 were then measured by FP. WT Med25 AcID bound VP16 H1 and VP16 H2 with a K_D of 1.7 ± 0.1 and 0.6 ± 0.1 μM , respectively; Tethering of A6 to WT Med25 AcID had a minimal effect on the affinity towards VP16 H1 (2.7-fold loss; $K_D = 4.6 \pm 0.3$ μM) and VP16 H2 (1.6-fold loss; $K_D = 0.9 \pm 0.1$ μM). Labeling of R466D and M523E, two mutants that block the H2 site, with A6-iodoacetamide did not improve the capability of parent proteins to block VP16 H1 or VP16 H2 interactions. In fact, R466D Med25 labeled with A6 bound VP16 H1 and VP16 H2 with slightly *tighter* affinities than WT Med25 AcID (e.g. R466D Med25 AcID bound VP16 with K_D of 9.9 ± 0.9 μM compared to a K_D of 8.5 ± 0.8 μM for WT Med25 AcID).

PrOF NMR of Med25 AcID, utilizing both VP16 G450C and A6 tethered to C506, was then pursued to determine why A6 was incapable of successfully blocking the H1 site even while being tethered to C506. It was hypothesized that differences in binding locations of VP16 G450C and A6 to Med25 AcID as determined using PrOF NMR could explain their differences in efficacy. 3FY Med25 was independently labeled with VP16

G450C peptide and fragment A6 before being subjected to PrOF NMR analysis (Figure 3.27)

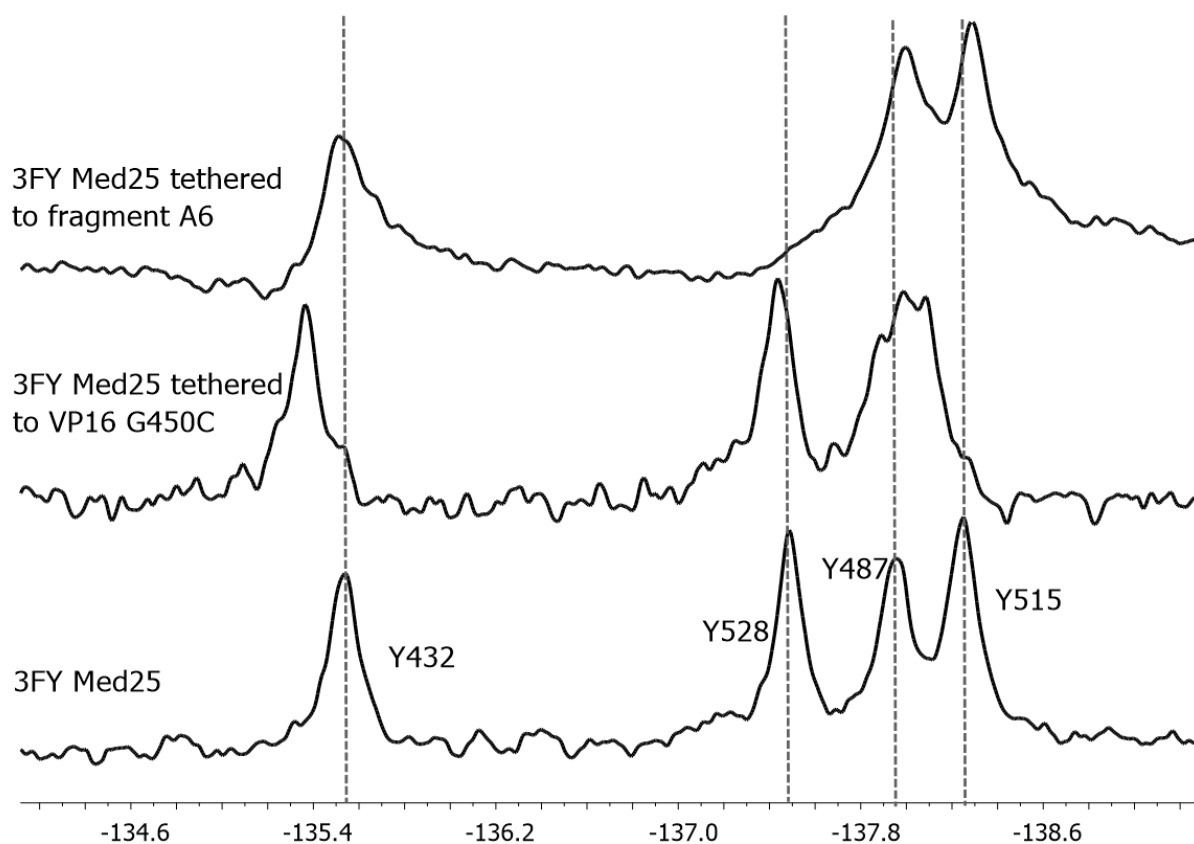


Figure 3.27. PrOF NMR of 3FY Med25 AcID labeled with VP16 G450C peptide or fragment A6. Spectral analysis of 3FY Med25 AcID covalently tethered to either VP16 G450C peptide or A6 at C506.

As expected, VP16 G450C caused chemical shift perturbations in each tyrosine residue in 3FY Med25 relative to unlabeled 3FY Med25. This result was consistent with VP16 G450C likely inducing a conformational change in Med25 AcID when 100% bound to the protein. The large effects on Y432 and the Y487/Y515 pair indicate that VP16 G450C is likely extending across the H1 site from C506 up to $\alpha 2$ of Med25 AcID. Finally, Y528 was the least perturbed resonance of the four tyrosines in 3FY Med25 AcID, further corroborating that VP16 G450C extends into the H1 site and thus away from Y528. Of

note for this discussion – The side chain of Y528 is only 12-18 Å away from the sulfur atom of C506 in every published NMR structure.

Differing from the PrOF NMR spectra of 3FY Med25-VP16 G450C, which demonstrated chemical shifts for all resonances, the PrOF NMR spectrum of 3FY Med25 AcID was dramatically perturbed at a single resonance by labeling with A6. The resonance attributed to Y528, at -137.5 ppm, was completely broadened into noise in the 3FY Med25-A6 PrOF spectra. The lack of major perturbations in the Y487/Y515 pair and Y432 suggests that, unlike VP16 G450C peptide, A6 does not extend into the H1 site towards $\alpha 2$ of Med25 AcID when tethered to C506. Instead, the broadening of the Y528 resonance suggested that A6 is likely interacting with the ‘bottom’ of the β -barrel, away from the H1 site, and could be making direct contact with Y528. Further, it was proposed that the 5-methoxy-indole of A6 could be forming a π - π interaction or hydrogen bond with the side chain of Y528 or a nearby residue. Based on molecular distances, this hypothesis is plausible. A6 is predicted to extend ~ 20 Å from end-to-end in its lowest energy structure, longer than the distance (12-18 Å) between C506 and Y528.

To investigate the hypothesis that the 5-methoxy-indole of A6 interacted with the base of the β -barrel and thus diminished its ability to inhibit Med25 PPIs similarly to VP16 G450C, A6 was chemically modified to remove hydrogen bonding and/or aromatic character (Figure 3.28). Syntheses of an A6 derivative that replaced the 5-methoxy-indole with benzene and another that replaced the 5-methoxy-indole with cyclohexane were completed by Clint Regan (University of Michigan).

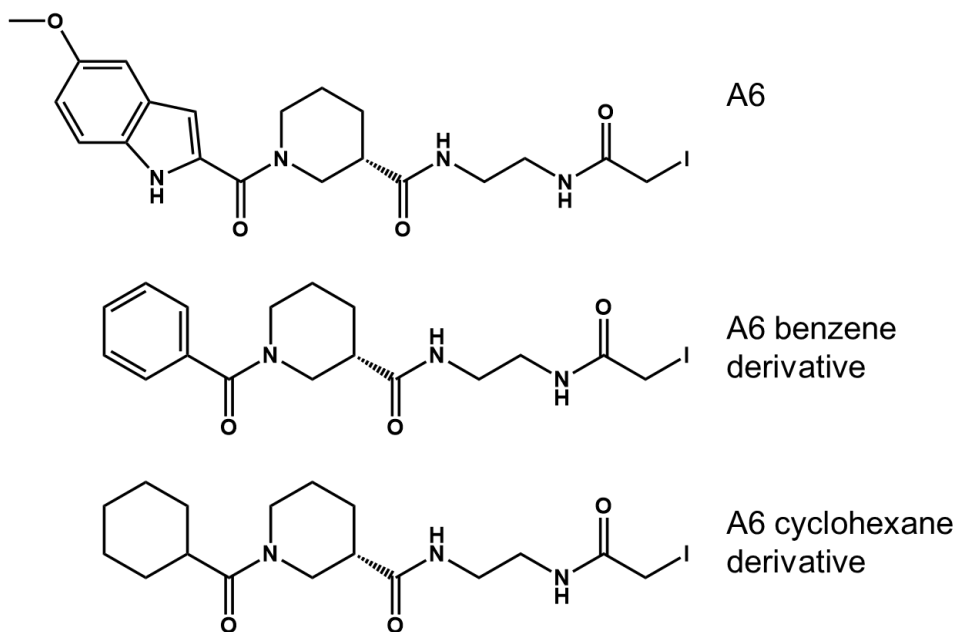


Figure 3.28. Structures of A6 derivatives. Two derivatives of A6 were designed to investigate the hypothesis that the 5-methoxy-indole of A6 interacts with the base of the β -barrel to significantly broaden the Y4528 resonance in PrOF NMR.

Following synthesis of the A6 derivatives, samples of 3FY Med25 AcID were independently labeled with each molecule to >95% singly labeled by MS and then subjected to PrOF NMR analysis (Figure 3.29). PrOF NMR spectrum of 3FY Med25 AcID tethered to the A6 benzene derivative demonstrated a partial recovery of the Y528 resonance relative to the 3FY Med25-A6 spectrum and a ‘new’ resonance at -136.8 ppm. This peak and the Y528 resonance at -136.5 ppm both integrate for ~ 0.6 ^{19}F relative to the Y432 resonance (the Y487/Y515 pair integrate for 2.05 ^{19}F) suggesting that these resonances represent two distinct conformers of Y528, a WT-like state and another in which Y528 is interacting with the A6 benzene derivative. Additionally, moderate perturbations in the Y487/Y515 pair suggest that $\alpha 2$, located on the opposite end of the β -barrel from C506, is affected by the A6 benzene derivative. Collectively, this result indicated that the A6 benzene derivative was likely interacting with the bottom of the β -

barrel about 50% as tightly or consistently as A6 and that the A6 benzene derivative was partially adopting VP16 G450C character.

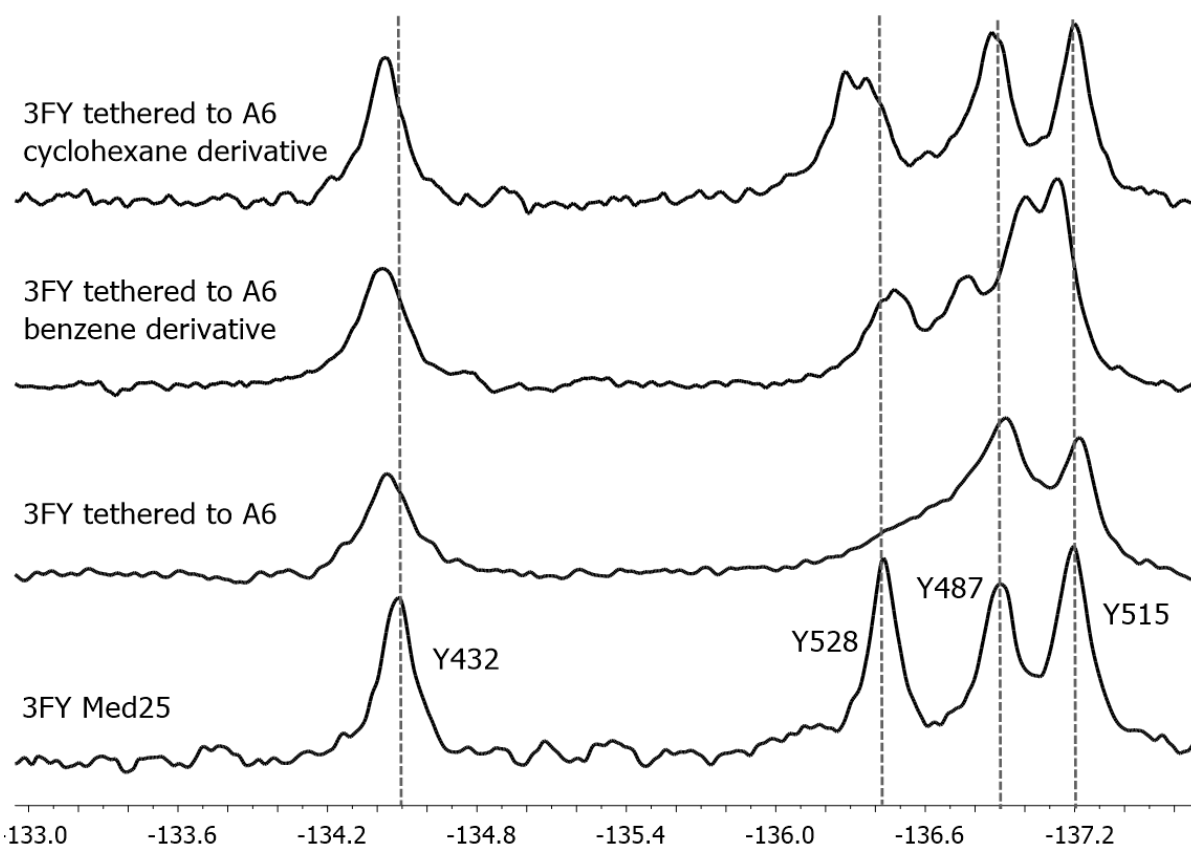


Figure 3.29. ProOF NMR of 3FY Med25 AcID labeled with A6 or A6 derivatives. Spectral analysis of 3FY Med25 AcID covalently tethered to A6 or A6 derivatives at C506. As proposed, chemical modification of the 5-methoxy-indole of A6 to remove aromaticity and/or ability for hydrogen bonding allowed for observation of the Y528 resonance.

ProOF NMR spectrum of the A6 cyclohexane derivative demonstrated nearly complete recovery of the resonance at Y528. The chemical shift of the doubled peak is significantly perturbed relative to WT, however the peak itself has recovered signal-to-noise and integrates for 1.1 ^{19}F relative to Y432. This result suggests that the A6 cyclohexane derivative no longer significantly interacts with Y528 and the bottom of the β -barrel, likely due to the replacement of the 5-methoxy-indole functionality of A6 with a saturated cyclohexane ring incapable of π - π stacking or hydrogen bond formation. It is

possible that the molecule could now be occupying the H1 site instead even though the A6 cyclohexane derivative does not perturb the Y487/Y515 pair, which are affected by VP16 G450C peptide.

This chemical modification and subsequent PrOF NMR strategy was successful in demonstrating that the inability of the parent fragment A6 to significantly inhibit Med25 PPIs when fully bound at C506 likely results from its binding location on Med25 AcID. This strategy demonstrated that by removing the aromatic and hydrogen bond donors/acceptors at the end of this molecule, the fragment started to bind at the H1 site in a manner similar to VP16 G450C, a highly effective inhibitor of Med25 PPI at the H1 site, as opposed to associating with the bottom of the β -barrel and apart from any of the putative Med25 AcID binding sites. While it is yet unknown if these modified fragments will be useful Med25 inhibitors, this study should provide future guidance in the rational development of Med25 fragments that target the H1 site. Additionally, this study demonstrated the power and utility of PrOF NMR in the development and characterization of small molecule modulators of Med25 AcID.

D. Conclusions and future directions

In this chapter, I hypothesized that protein-observed ^{19}F -NMR of Med25 AcID would be a useful methodology for the study of Med25 and its protein-protein interaction network that would complement previously performed ^1H , ^{15}N -HSQC NMR from the literature and Chapter 2 of this thesis.^{8-10,39} Previous data demonstrated that Med25 AcID contained two or three discrete binding interfaces. Additionally, the H1 site was determined to be less dependent on hotspot residues and electrostatic interactions than

the H2 site and that several Med25-interacting partners that bound at the H1 site were proposed to be capable of compensatory interactions at the H2 site.

Two unique PrOF NMR strategies were developed to specifically differentiate between the H1 and H2/third sites of Med25 AcID. The incorporation of 3-fluorotyrosine into Med25 AcID was hypothesized to allow for precise study of the H2 and 'third' sites due to the dispersion of four solvent-exposed Tyr residues surrounding the putative bounds of the H2 site. The incorporation of 5-fluorotryptophan into Med25 AcID was hypothesized to allow for direct observation of the H1 site. 3FY Med25 and 5FW Med25 AcID were biosynthesized in high yields and subjected to PrOF NMR analysis. 3FY Med25 AcID provided four well-resolved resonances that were independently assigned to each of the four Tyr residues using Y-to-F and 'nudge' mutagenesis strategies. 5FW Med25 AcID provided an interpretable spectrum in a reasonable timeframe (~20 minutes of experimental time) however resonances were assigned to specific Trp residues.

Subsequent titrations of each Med25-interacting peptide ligand with 3FY Med25 AcID and 5FW Med25 AcID were analyzed by PrOF NMR. The titration of peptide ligands previously proposed to bind specifically at the H2 site (ATF6 α and VP16 H2) caused significant chemical shift perturbations in multiple 3FY Med25 resonances while not affecting any resonances of 5FW Med25 AcID. PrOF NMR of CBP(20-55) in complex with 3FY Med25 AcID demonstrated a significant chemical shift in a single residue (Y432) located along the nebulous barrier between the H2 site and the third site. This demonstrated that CBP binds Med25 AcID in a manner unlike other Med25-interacting ligands and likely associates directly at the third site located along β 4/ β 2/ β 1 and the N-termini of α 2. PrOF NMR demonstrated significant differences in the binding modes of

the two previously proposed peptides (ERM and VP16 H1) that were thought to be somewhat selective for the H1 site. Increasing concentrations of VP16 H1 were found to cause significant chemical shift perturbations in the Y487/Y515 pair of residues in 3FY Med25 AcID while having no impact on resonances of 5FW Med25 AcID. However, increasing concentrations of ERM(38-68) had no impact on 3FY Med25 AcID at substochiometric equivalencies while causing a significant shift in 5FW Med25 AcID. This suggested that while VP16 H1 might be equally capable of binding to the H1 or H2 sites, ERM is highly selective for the H1 site at substochiometric concentrations. Collectively, these analyses of Med25 PPIs by PrOF NMR coupled with experiments performed in Chapter 2 and by another member of the Mapp lab (Andy Henderson) allowed for the generation of hypothesized models to describe each of the binding interactions for Med25 AcID and its discrete protein partners.

In addition to the study of Med25 and its PPI network, PrOF NMR was successfully applied to the characterization of two small molecules discovered by other members of the Mapp lab. PrOF NMR spectra of 3FY Med25 AcID samples labeled with norstictic acid provided decisive evidence regarding norstictic acid's mode of inhibition. This primary binding of this molecule, previously known to function through covalent adduct formation with lysine residues of Med25 AcID, was localized to the β 6- β 7 loop of H2 site. PrOF NMR was also successfully utilized to suggest the reason for the inability of a molecule that binds Med25 AcID to significantly inhibit Med25 AcID function. This molecule, a fragment termed 'A6' was discovered by a Tethering screen against Med25 AcID. However, even when fully bound to the protein, A6 offered minimal inhibitory effects. PrOF NMR of 3FY Med25 labeled with A6-iodoacetamide demonstrated that the 5-methoxyindole

functionality of this fragment was likely forming a π - π interaction or hydrogen bond with a region of Med25 AcID that directed the molecule away from the H1 binding site. Removal of that 5-methoxyindole functionality provided A6-derivatives that are thought to bind into the H1 site in a manner similar to a known peptide-based inhibitor of the H1 site, VP16 G450C. This study could provide future guidance in the rational development of Med25 inhibitors that target the H1 site.

Future work to develop additional fluorinated variants of Med25 AcID for the study of the H1 site could be beneficial. Only a single peptide, ERM(38-68) was capable of perturbing any of the resonances of 5FW Med25 AcID. However, while this result was incredibly useful in demonstrating the unique binding mode of ERM towards Med25 AcID, recall that at least two of the Trp residues within Med25 AcID are *not* solvent-exposed. It is thought that more environmentally sensitive ^{19}F reporters could be useful in detecting weak interactions of other peptide ligands with the H1 site. To this end, future PrOF NMR experiments could be pursued using Med25 AcID labeled with trifluoroacetone. Preliminary work has demonstrated that the solvent-exposed cysteines (C497 and C506) of Med25, both of which reside within the H1 site, can both be reacted with 3-bromo-1,1,1-trifluoroacetone to generate a Med25 AcID covalently linked to two trifluoroacetone molecules (Figure 3.30). A subsequent PrOF NMR spectrum provided three distinct resonances, indicating that the trifluoroacetone bound to each Cys residue are resolved. Three NMR resonances, as opposed to the anticipated two, suggests that one of the two cysteine-trifluoroacetone species likely exists in multiple conformations. Assignment of these resonances should be possible by labeling C497A and C506A Med25 mutants with trifluoroacetone to provide singly labeled protein species.

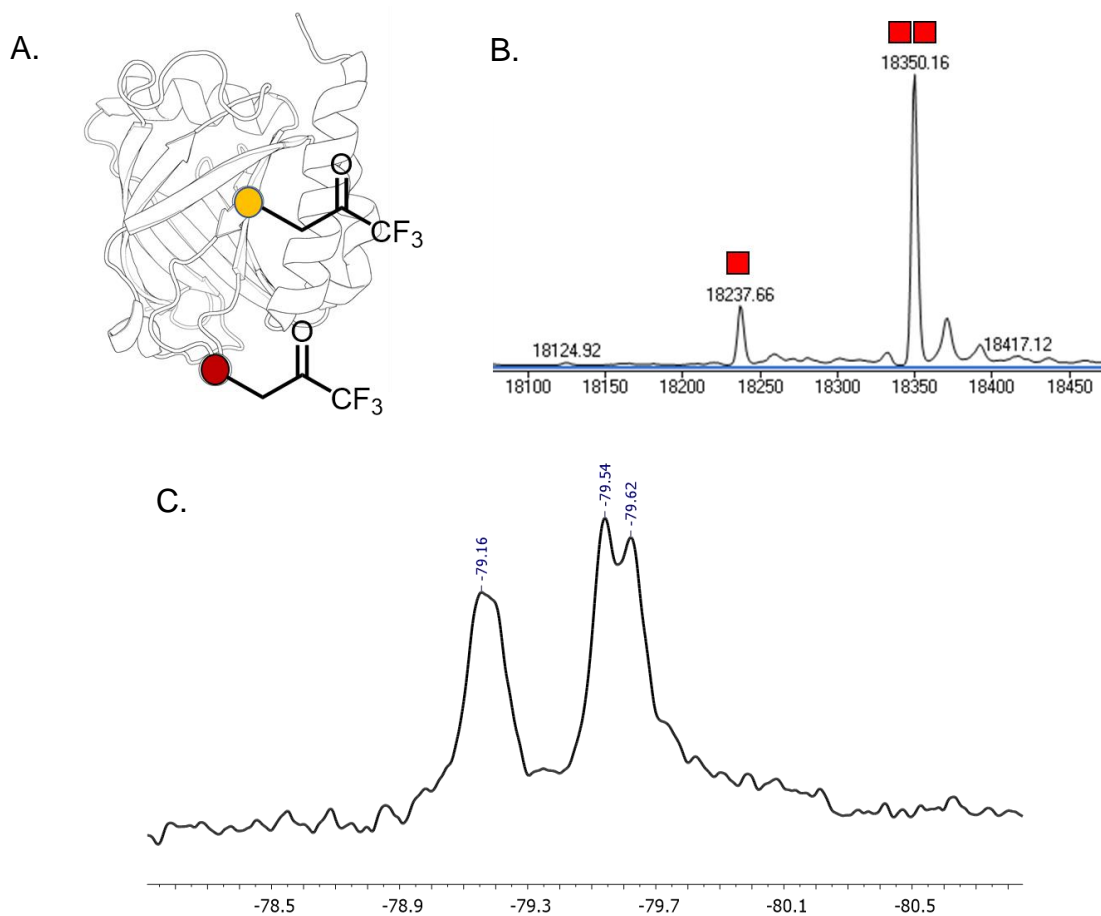


Figure 3.30. ProOF NMR of Med25 Acid labeled with trifluoroacetone. (A) Med25 was reacted with 3-bromo-1,1,1-trifluoroacetone to covalently label C497 (orange) and C506 (red) with trifluoroacetone. (B) Mass spectroscopy of Med25-trifluoroacetone sample demonstrated that Med25 Acid was 16% singly labeled and 83% double labeled. (C) ProOF NMR spectra of Med25-trifluoroacetone sample provided three resonances (-79.16, -79.54, -79.62 ppm).

E. Materials and methods

Plasmids

pET21b-Med25(394-543)-His6 was provided by Patrick Cramer. Mutant Med25 AcID plasmids. Point mutants of pET21b-Med25(394-543)-His6 were generated using standard molecular biology protocols.

Previously described methods

Relevant methods that were previously described in Chapter Two include Med25 AcID purification, mass spectroscopy of proteins, FP binding experiments, circular dichroism, thermal melts, and solid-phase peptide synthesis.

Expression of ¹⁹F-labeled Med25 AcID

pET21b-Med25(394-543)-His6 was transformed into chemically competent DL39(DE3), plated onto LB/ampicillin agar, and incubated at 37 °C overnight. In the morning, agar plates were placed at 4 °C until further use. In the evening, a single colony from the transformed plate was placed into 25 mL Luria Broth with 0.1 mg/mL ampicillin and incubated at 37 °C overnight at ≥ 200 RPM. The following morning, 5-20 mL from the starter culture was added to 1 L Luria Broth with 0.1 mg/mL ampicillin and bacteria were grown at 37 °C at ≥ 200 RPM to an OD₆₀₀ of ~ 0.8 . Cells were centrifuged and supernatant was decanted. Cells were then resuspended in 0.5-1 L of the minimally defined media, as described³⁶ with minor changes as noted. For the expression of 3FY Med25, media was supplemented with either 48 mg/L L-3-fluorotyrosine (Alfa Aesar) or 96 mg/mL DL-3-fluorotyrosine (Sigma Aldrich). For the expression of 5FW Med25, media

was supplemented with either 60 mg/L L-5-fluoroindole (Alfa Aesar) or 120 mg/mL DL-5-fluoroindole (Sigma Aldrich). For the expression of 4FF Med25, media was supplemented with either 29 mg/L L-4-fluorophenylalanine (Alfa Aesar) or 58 mg/mL DL-4-fluorophenylalanine (Sigma Aldrich). Cultures were incubated at 37 °C overnight at ≥ 200 RPM for 90 minutes before reducing the temperature to 20 °C. After 30 minutes, 0.5 mM IPTG was added. Bacteria were shaken overnight at 20 °C at ≥ 200 RPM. The following morning, bacterial cultures were centrifuged at 7000 x g for 20 mins at 4 °C. Cell pellets were then stored at -80 °C prior to protein purification (performed as done with unlabeled Med25 AcID, described in Chapter Two)

1-D ^{19}F -NMR of ^{19}F -labeled Med25 AcID

To prepare for PrOF NMR, ^{19}F -labeled Med25 AcID was dialyzed into PrOF buffer (50 mM HEPES, 100 mM NaCl, 1 mM DTT, pH 7.2). All PrOF experiments were performed with 10% D₂O and 0.01% trifluoroacetic acid (TFA) as an internal ^{19}F reference. PrOF NMR data were acquired on a Varian 500 MHz NMR spectrometer with a Varian 5 mm PFG OneNMR Probe. Spectra were obtained without proton decoupling. NMR pulse parameters - D1 relaxation time of 1 sec and an acquisition time of 0.6 sec with a 10 ppm sweep width (centered on -136 ppm for 3FY Med25, -125 ppm for 5FW Med25, and -117 ppm for 4FF Med25). 1200-1600 total scans were collected for experiments with 3FY Med25 AcID; 2400 scans for 5FW Med25 AcID; 6000 scans for 4FF Med25 AcID. For each protein sample, a second TFA reference experiment was also performed (32 scans, D1 – 1 sec, Ac. time – 0.6 sec; centered on -76.55 ppm).

Labeling of 3FY Med25 AcID with norstictic acid

Varying molar equivalents of norstictic acid were added to 3FY Med25 AcID, in PrOF buffer. The protein-small molecule mixture was incubated for 4 hours at room temperature with gentle shaking using an orbital shaker. The protein was then reduced with excess sodium borohydride for 1 hour at room temperature with gentle shaking using an orbital shaker. After reduction, the protein was buffer exchanged in PrOF buffer and prepared for PrOF NMR analysis.

Labeling of Med25 AcID with A6 and its derivatives

A four-fold molar excess of compound was incubated with WT, mutant, or ¹⁹F-labeled Med25 for four hours, or until >95% single-labeled protein was obtained by mass spectroscopy. The protein-small molecule complex was incubated at room temperature with gentle shaking using an orbital shaker. After labeling, the protein was centrifuged and buffer exchanged into either FP assay or PrOF buffer.

Labeling of Med25 with 3-bromo-1,1,1-trifluoroacetone

A five-fold molar excess of compound was incubated with WT Med25 overnight. The protein-small molecule complex was incubated at room temperature with gentle shaking using an orbital shaker. After labeling, the protein was centrifuged and buffer exchanged into PrOF buffer.

F. References

1. Wright, P. E. & Dyson, H. J. Intrinsically unstructured proteins: re-assessing the protein structure-function paradigm. *J. Mol. Biol.* **293**, 321–331 (1999).
2. Thompson, A. D., Dugan, A., Gestwicki, J. E. & Mapp, A. K. Fine-Tuning Multiprotein Complexes Using Small Molecules. *ACS Chem. Biol.* **7**, 1311–1320 (2012).
3. Smith, M. C. & Gestwicki, J. E. Features of protein–protein interactions that translate into potent inhibitors: topology, surface area and affinity. *Expert Rev. Mol. Med.* **14**, (2012).
4. Cavanagh, J., Fairbrother, W. J., III, A. G. P. & Skelton, N. J. *Protein NMR Spectroscopy: Principles and Practice*. (Academic Press, 1995).
5. Kleckner, I. R. & Foster, M. P. An introduction to NMR-based approaches for measuring protein dynamics. *Biochim. Biophys. Acta* **1814**, 942–968 (2011).
6. Urick, A. K., Calle, L. P., Espinosa, J. F., Hu, H. & Pomerantz, W. C. K. Protein-Observed Fluorine NMR Is a Complementary Ligand Discovery Method to (1)H CPMG Ligand-Observed NMR. *ACS Chem. Biol.* **11**, 3154–3164 (2016).
7. Danielson, M. A. & Falke, J. J. Use of 19F NMR to probe protein structure and conformational changes. *Annu. Rev. Biophys. Biomol. Struct.* **25**, 163–195 (1996).
8. Vojnic, E. *et al.* Structure and VP16 binding of the Mediator Med25 activator interaction domain. *Nat. Struct. Mol. Biol.* **18**, 404–409 (2011).
9. Milbradt, A. G. *et al.* Structure of the VP16 transactivator target in the Mediator. *Nat. Struct. Mol. Biol.* **18**, 410–415 (2011).
10. Landrieu, I. *et al.* Characterization of ERM transactivation domain binding to the ACID/PTOV domain of the Mediator subunit MED25. *Nucleic Acids Res.* **43**, 7110–7121 (2015).
11. Verger, A. *et al.* The Mediator complex subunit MED25 is targeted by the N-terminal transactivation domain of the PEA3 group members. *Nucleic Acids Res.* **41**, 4847–4859 (2013).
12. Sela, D. *et al.* Role for Human Mediator Subunit MED25 in Recruitment of Mediator to Promoters by Endoplasmic Reticulum Stress-responsive Transcription Factor ATF6. *J. Biol. Chem.* **288**, 26179–26187 (2013).
13. Harner, M. J., Frank, A. O. & Fesik, S. W. Fragment-Based Drug Discovery Using NMR Spectroscopy. *J. Biomol. NMR* **56**, 65–75 (2013).
14. Dias, D. M. *et al.* Is NMR Fragment Screening Fine-Tuned to Assess Druggability of Protein–Protein Interactions? *ACS Med. Chem. Lett.* **5**, 23–28 (2013).
15. Cesa, L. C., Mapp, A. K. & Gestwicki, J. E. Direct and Propagated Effects of Small Molecules on Protein–Protein Interaction Networks. *Front. Bioeng. Biotechnol.* **3**, (2015).

16. Luck, L. A. & Falke, J. J. ^{19}F NMR studies of the D-galactose chemosensory receptor. 1. Sugar binding yields a global structural change. *Biochemistry (Mosc.)* **30**, 4248–4256 (1991).
17. Lian, C. *et al.* Fluorine-19 Nuclear Magnetic Resonance Spectroscopic Study of Fluorophenylalanine- and Fluorotryptophan-Labeled Avian Egg White Lysozymes. *Biochemistry (Mosc.)* **33**, 5238–5245 (1994).
18. Hoeltzli, S. D. & Frieden, C. ^{19}F NMR spectroscopy of [6- ^{19}F]tryptophan-labeled *Escherichia coli* dihydrofolate reductase: equilibrium folding and ligand binding studies. *Biochemistry (Mosc.)* **33**, 5502–5509 (1994).
19. Danielson, M. A., Biemann, H. P., Koshland, D. E. & Falke, J. J. Attractant- and disulfide-induced conformational changes in the ligand binding domain of the chemotaxis aspartate receptor: a ^{19}F NMR study. *Biochemistry (Mosc.)* **33**, 6100–6109 (1994).
20. Pomerantz, W. C. *et al.* Profiling the Dynamic Interfaces of Fluorinated Transcription Complexes for Ligand Discovery and Characterization. *ACS Chem. Biol.* **7**, 1345–1350 (2012).
21. Gee, C. T., Koleski, E. J. & Pomerantz, W. C. K. Fragment Screening and Druggability Assessment for the CBP/p300 KIX Domain through Protein-Observed ^{19}F NMR Spectroscopy. *Angew. Chem. Int. Ed.* **54**, 3735–3739 (2015).
22. Mishra, N. K., Urick, A. K., Ember, S. W. J., Schönbrunn, E. & Pomerantz, W. C. Fluorinated aromatic amino acids are sensitive ^{19}F NMR probes for bromodomain-ligand interactions. *ACS Chem. Biol.* **9**, 2755–2760 (2014).
23. Urick, A. K. *et al.* Dual Screening of BPTF and Brd4 Using Protein-Observed Fluorine NMR Uncovers New Bromodomain Probe Molecules. *ACS Chem. Biol.* **10**, 2246–2256 (2015).
24. Gee, C. T. *et al.* Protein-observed ^{19}F -NMR for fragment screening, affinity quantification and druggability assessment. *Nat. Protoc.* **11**, 1414–1427 (2016).
25. Ye, L., Larda, S. T., Frank Li, Y. F., Manglik, A. & Prosser, R. S. A comparison of chemical shift sensitivity of trifluoromethyl tags: optimizing resolution in ^{19}F NMR studies of proteins. *J. Biomol. NMR* **62**, 97–103 (2015).
26. Sykes, B. D. & Hull, W. E. Fluorine nuclear magnetic resonance studies of proteins. *Methods Enzymol.* **49**, 270–295 (1978).
27. Gavenonis, J., Sheneman, B. A., Siegert, T. R., Eshelman, M. R. & Kritzer, J. A. Comprehensive analysis of loops at protein-protein interfaces for macrocycle design. *Nat. Chem. Biol.* **10**, 716–722 (2014).
28. Bullock, B. N., Jochim, A. L. & Arora, P. S. Assessing Helical Protein Interfaces for Inhibitor Design. *J. Am. Chem. Soc.* **133**, 14220–14223 (2011).
29. Jones, S. & Thornton, J. M. Principles of protein-protein interactions. *Proc. Natl. Acad. Sci. U. S. A.* **93**, 13–20 (1996).

30. Arntson, K. E. & Pomerantz, W. C. K. Protein-Observed Fluorine NMR: A Bioorthogonal Approach for Small Molecule Discovery: Miniperspective. *J. Med. Chem.* **59**, 5158–5171 (2016).
31. UniProtKB/Swiss-Prot Release 2017_06 statistics. Available at: <http://web.expasy.org/docs/relnotes/relstat.html>. (Accessed: 22nd June 2017)
32. Thomas, M. R. & Boxer, S. G. ¹⁹F NMR of trifluoroacetyl-labeled cysteine mutants of myoglobin: structural probes of nitric oxide bound to the H93G cavity mutant. *Biochemistry (Mosc.)* **40**, 8588–8596 (2001).
33. Didenko, T., Liu, J. J., Horst, R., Stevens, R. C. & Wüthrich, K. Fluorine-19 NMR of integral membrane proteins illustrated with studies of GPCRs. *Curr. Opin. Struct. Biol.* **23**, 740–747 (2013).
34. Bouchard, M. *et al.* Interaction between G-Actin and Various Types of Liposomes: A ¹⁹F, ³¹P, and ²H Nuclear Magnetic Resonance Study. *Biochemistry (Mosc.)* **37**, 3149–3155 (1998).
35. Loewen, M. C. *et al.* Solution ¹⁹F nuclear Overhauser effects in structural studies of the cytoplasmic domain of mammalian rhodopsin. *Proc. Natl. Acad. Sci. U. S. A.* **98**, 4888–4892 (2001).
36. Gee, C. T. *et al.* Protein-observed ¹⁹F-NMR for fragment screening, affinity quantification and druggability assessment. *Nat. Protoc.* **11**, 1414–1427 (2016).
37. Drake, S. K., Bourret, R. B., Luck, L. A., Simon, M. I. & Falke, J. J. Activation of the Phosphosignaling Protein CheY. *J. Biol. Chem.* **268**, 13081–13088 (1993).
38. Williamson, M. P. Using chemical shift perturbation to characterise ligand binding. *Prog. Nucl. Magn. Reson. Spectrosc.* **73**, 1–16 (2013).
39. Currie, S. L. *et al.* ETV4 And AP1 Transcription Factors Form Multivalent Interactions With Three Sites On The MED25 Activator-Interacting Domain. *bioRxiv* 126458 (2017). doi:10.1101/126458
40. Sturlis, S. M. *et al.* Identifying Depsidone Inhibitors of Med25-AcID Mediated Transcription. *Manuscr. Prep.*
41. Erlanson, D. A., Wells, J. A. & Braisted, A. C. Tethering: fragment-based drug discovery. *Annu. Rev. Biophys. Biomol. Struct.* **33**, 199–223 (2004).
42. Lodge, J. M., Rettenmaier, T. J., Wells, J. A., Pomerantz, W. C. & Mapp, A. K. FP Tethering: a screening technique to rapidly identify compounds that disrupt protein-protein interactions. *MedChemComm* **5**, 370–375 (2014).

Chapter Four

Small molecule inhibition of Med25-activator interactions

A. Abstract*

Med25 AcID, a structurally unique and dynamic transcriptional coactivator, makes critical contacts with several transcriptional activators that are critical for normal cellular processes and certain disease states, including the oxidative stress response factor ATF6 α and the ETV/PEA3 family of transcription factors.^{1,2} Previous work had demonstrated that Med25 contains two discrete binding sites, one of which demonstrates high selectivity for interaction with ATF6 α while the other is moderately selective for the ETV5/ERM activator. It is proposed that small molecule inhibition of Med25 AcID and its protein-protein interaction (PPI) network would be beneficial in studying the function of Med25 in a cellular context and could be beneficial in the study of cancer progression and metastasis through inhibition of ETV- and ATF6 α -mediated transcriptional activation. Two distinct strategies to develop and characterize small molecules that selectively target Med25 AcID *in vitro* and *in cellulo* are described herein. A pilot fragment screening effort that utilized PrOF NMR of Med25 identified nine preliminary compounds that target the AcID motif. Additionally, a novel natural product compound, termed 34913 lipopeptide, has been identified as a potent and selective inhibitor of Med25 AcID. This molecule, thought to mimic the structure of a transcriptional activation domain, interacts with the H2 site of Med25 AcID in a binding mode that is nearly identical to that of the ATF6 α activation

*Several collaborators provided research assistance throughout Chapter Four. Andy Henderson (University of Michigan) identified EN300-51104 in a HSQC fragment screening effort; Julie Garlick (University of Michigan) collected the inhibition data presented in Figure 4.2. Dr. Ashootosh Tripathi and Pam Schultz (University of Michigan) purified 34913 lipopeptide; Dr. Tripathi elucidated the structure of 34913 lipopeptide. Brian Linhares (University of Michigan) collected HSQC NMR data of the Med25 AcID-34913 lipopeptide interaction.

domain. Furthermore, the 34913 lipopeptide exhibited dose-dependent inhibition of a critical ATF6 α gene product, GRP78, in a cellular environment. Collectively, this chapter represents a key advance in the discovery of small molecules that modulate Med25 AcID function and should allow for future determination of the role of Med25 and its PPI network in several disease contexts.

B. Introduction

Difficulties in targeting protein-protein interactions

Protein-protein interactions (PPIs), particularly those in the transcriptional activator-coactivator class, have long been characterized as “undruggable”.^{3,4} The contact interfaces of PPIs are generally large (1500 – 3000 Å²) and shallow, lacking a traditional binding pocket present in protein-ligand interactions.^{4,5} Activator-coactivator interactions bring an additional set of difficulties. These PPIs are transient, moderate-affinity interactions (binding affinities range from 500 nM to 100 μ M) and each protein involved is structurally dynamic, often intrinsically disordered, and uses the same binding surface to interface with a large number of interaction partners.^{6–8}

Natural products for the inhibition of protein-protein interactions

As a result of the inherent character of activator-coactivator interactions described above, traditional screening, medicinal chemistry efforts and rational design methodologies have led to limited success towards targeting this class of PPIs.⁹ Natural products, however, offer promise towards targeting this class of PPIs, and several natural products have recently been developed as tool compounds to target PPIs.^{10–14} These

natural product compounds derive great utility from their inherent structural complexity, ability to maintain high degrees of rigidity and chirality, and their vast diversity of molecular structure and scaffolds.¹⁵ In fact, nearly 40% of compounds represented in the Dictionary of Natural Products contain unique structural elements that are not otherwise represented in purely synthetic compounds.^{16,17} Furthermore, it is thought that the scientific community has discovered small fractions of the total chemical matter that nature has designed, particularly from the marine environment.^{18,19} Resulting from recent advances in fermentation, sample collection techniques, and structural elucidation technologies, natural product exploration into the marine environment (and other underutilized biological sources) has become more accessible.^{20,21}

An excellent example of natural product inhibition of a PPI was demonstrated by Majmudar and coworkers in their discovery of depsides and depsidones that inhibited the KIX transcriptional coactivation domain of CBP and its transcriptional activation network.⁸ Two unique compounds, sekikaic acid (depside) and lobaric acid (depsidone), were capable of inhibition of CBP KIX and were highly selective for this coactivator motif relative to transcription factor-DNA interactions and related coactivator-activator PPIs (Figure 4.1). Molecular dynamics simulations of sekikaic acid demonstrated that this molecule adopts an amphipathic structure that mimics an α -helix, suggesting that depsides and depsidones might be privileged scaffolds for the inhibition of PPIs.

Molecular inhibition of Med25 AcID for study of disease

The ETV/PEA3 family of transcriptional activators and the oxidative stress response activator ATF6 α represent emerging targets for disease, particularly metastatic

cancers.^{22,23} The Mediator subunit Med25, a common transcriptional interaction partner of these two TADs, represents a potential target for small molecule intervention of these activators and their downstream gene products.^{1,2}

Under normal cellular conditions, the transcriptional activator ATF6 α is a transmembrane protein found in the endoplasmic reticulum (ER). However, conditions of oxidative stress cause cleavage of ATF6 α and subsequent translocation to the nucleus.²⁴ Once in the nucleus, ATF6 α interacts with promoters that contain endoplasmic reticulum stress response elements and activates pro-survival and anti-apoptotic genes associated with the unfolded protein response (UPR), most notably the chaperone protein GRP78.^{25,26} As a critical component of the UPR, induction of GRP78 acts to suppress oxidative stress and misfolding of proteins to protect the cell from apoptosis during times of external stress, particularly in cancerous tumors.^{27,28} It is hypothesized that selective disruption of ATF6 α activity through inhibition of the Med25-ATF6 α PPI could be therapeutically beneficial in downregulating GRP78 and related gene targets. Additionally, small molecule inhibition of the Med25-ATF6 α PPI would be incredibly beneficial in determining the role of Med25 in the ATF6 α pathway, the UPR, and the role of the UPR in cancer progression.²⁹

The ETV family of transcriptional activators (ETV1/ER81, ETV4/PEA3, and ETV5/ERM) are involved in the transition into a metastatic phenotype across several cancer types.^{22,30-32} Overexpression of the ETV activators has been correlated with an invasive cancer phenotype and shRNA knockdown of all three ETV activators has been shown to decrease the transcription of genes associated with cancer metastasis.^{33,34} It is hypothesized that targeting Med25 AcID with small molecules would function similarly to

shRNA knockdown of the ETVs and downregulate cancer metastasis genes (e.g. Matrix metalloprotease I).

Initial success in demonstrating that Med25 can be targeted with small molecules

Similar to CBP KIX, depsidone scaffolds have been discovered that selectively inhibit Med25 AcID PPIs (relative to other coactivator-activators interactions).³⁵ Two compounds, norstictic acid and psoromic acid, are capable of targeting Med25 AcID *in cellulo* with specific inhibition of the Med25-ATF6 α PPI having been demonstrated through downregulation of GRP78. Additionally, these compounds decreased the migratory ability of breast cancer cells, presumably by downregulating the expression of Matrix metalloprotease I, an ETV gene product.

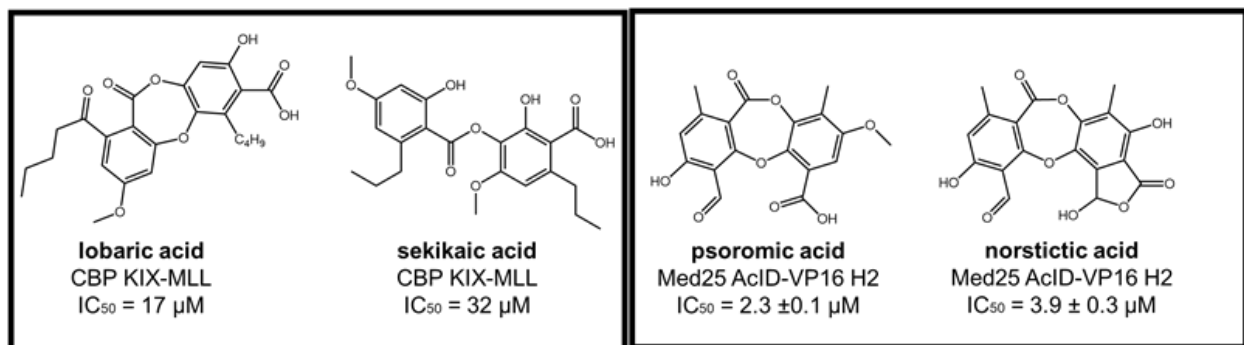


Figure 4.1. Despide and depsidones that target CBP KIX and Med25 AcID. These classes of molecules are part of a class of molecules that mimic α -helical structure and are amphipathic, thought to make a privileged scaffold for inhibition of transcriptional PPIs.

However, these small molecules bring inherent issues that could hamper their usefulness as molecular probes to study Med25 function in more complicated cellular experiments. First, each molecule contains an aldehyde functionality that has been shown to efficiently and covalently label Med25 AcID *in vitro*. Second, each molecule is highly oxygenated and presumed to be highly redox active. Each of these two characteristics

(covalent mode of action and redox activity) lessen their likely utility as molecular probes *in cellulo*.

Additional tools will be required for a more complete understanding of Med25 function both *in cellulo* and *in vivo*. This chapter will highlight the methodologies (fragment discovery, natural product discovery) that have been pursued to discover novel small molecules that target Med25 AcID and lack one or both undesirable qualities of norstictic and psoromic acids. Additionally, through biochemical and biophysical techniques, we sought to find small molecule ligands that could function to selectively target a single binding site within Med25 AcID. This would allow for future work in dissecting the relevant roles that each individual binding site plays within the context of the cell.

C. Results and discussion

NMR fragment screening allows for rapid discovery of weak-to-moderate affinity ligands

NMR screening has been successfully used to identify fragments that interact with a protein-of-interest with weak-to-moderate binding affinity in a medium-throughput manner.^{36–38} NMR as a screening methodology for fragments provides two essential benefits – differentiation of multiple binding sites and preliminary characterization of binding mechanism during the screening process and a high degree of sensitivity for molecules that interact weakly with the protein-of-interest.^{37,39} These discovered fragments have been successfully used to study underlying biochemical mechanisms of their target proteins and, in several cases, have ultimately led to the generation of lead clinical target molecules.^{40–42} PrOF NMR strategies were pursued for the discovery of novel fragments that bind Med25 AcID.

A previous ^1H ^{15}N -HSQC NMR screen of ^{15}N -labeled Med25 AcID against a medium-sized fragment library (532 total compounds) maintained by the Cierpicki lab at the University of Michigan discovered a single hit fragment (Andy Henderson, University of Michigan). This hit rate of 0.2% was incredibly low and unfortunately provided few lead fragments for molecule discovery, indicating that chemical shift perturbations induced in HSQC NMR of Med25 AcID are not sensitive enough to detect weak binding fragment molecules. Subsequent FP inhibition assays with this fragment, EN300-51104, demonstrated that this fragment inhibited Med25 AcID-VP16 H1 with an IC_{50} value of $139 \pm 10 \mu\text{M}$ and Med25 AcID-VP16 H2 with an IC_{50} value of $79 \pm 7 \mu\text{M}$ (Figure 4.2).

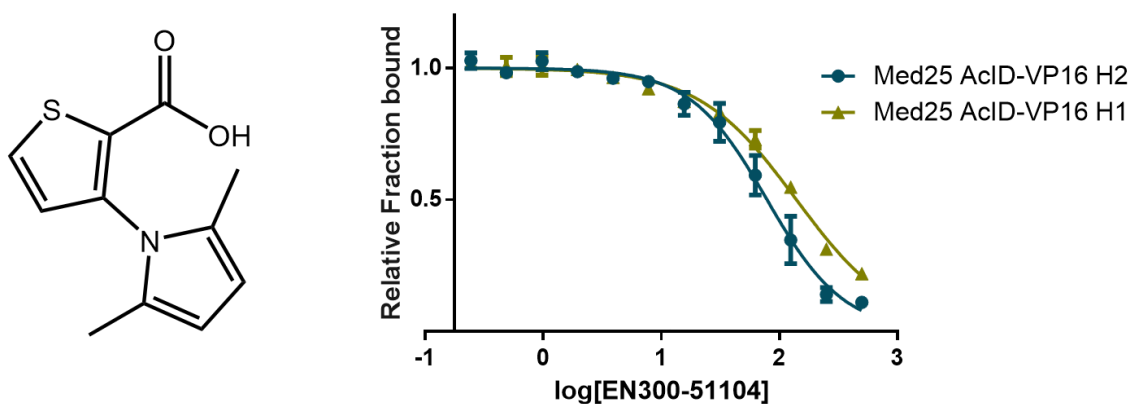


Figure 4.2. Fragment EN300-51104 is a weak inhibitor of Med25 AcID. This fragment, identified in a HSQC NMR screen against Med25 AcID inhibits the Med25 AcID-VP16 H1 PPI with an IC_{50} value of $139 \pm 10 \mu\text{M}$ and the Med25 AcID-VP16 H2 PPI with an IC_{50} value of $79 \pm 7 \mu\text{M}$ by FP. Inhibition data collected by Julie Garlick.

PrOF NMR presents a sensitive screening methodology for the discovery of small molecule fragments that target Med25 AcID

The weak inhibitor EN300-51104 provided an excellent positive control for determining the sensitivity of 3FY Med25 AcID in PrOF NMR experiments for weak fragments (Figure 4.3). All PrOF experiments performed with 3FY Med25 AcID had

previously been performed with peptide and small molecule ligands that bound WT Med25 AcID with single-digit micromolar binding affinities. It should be noted that the HSQC NMR screen was run at 1 mM fragment. It was thus hypothesized that if EN300-51104 caused a significant chemical shift perturbation in 3FY Med25 AcID at ≤ 1 mM concentration that PrOF NMR would represent a potentially successful screening strategy.

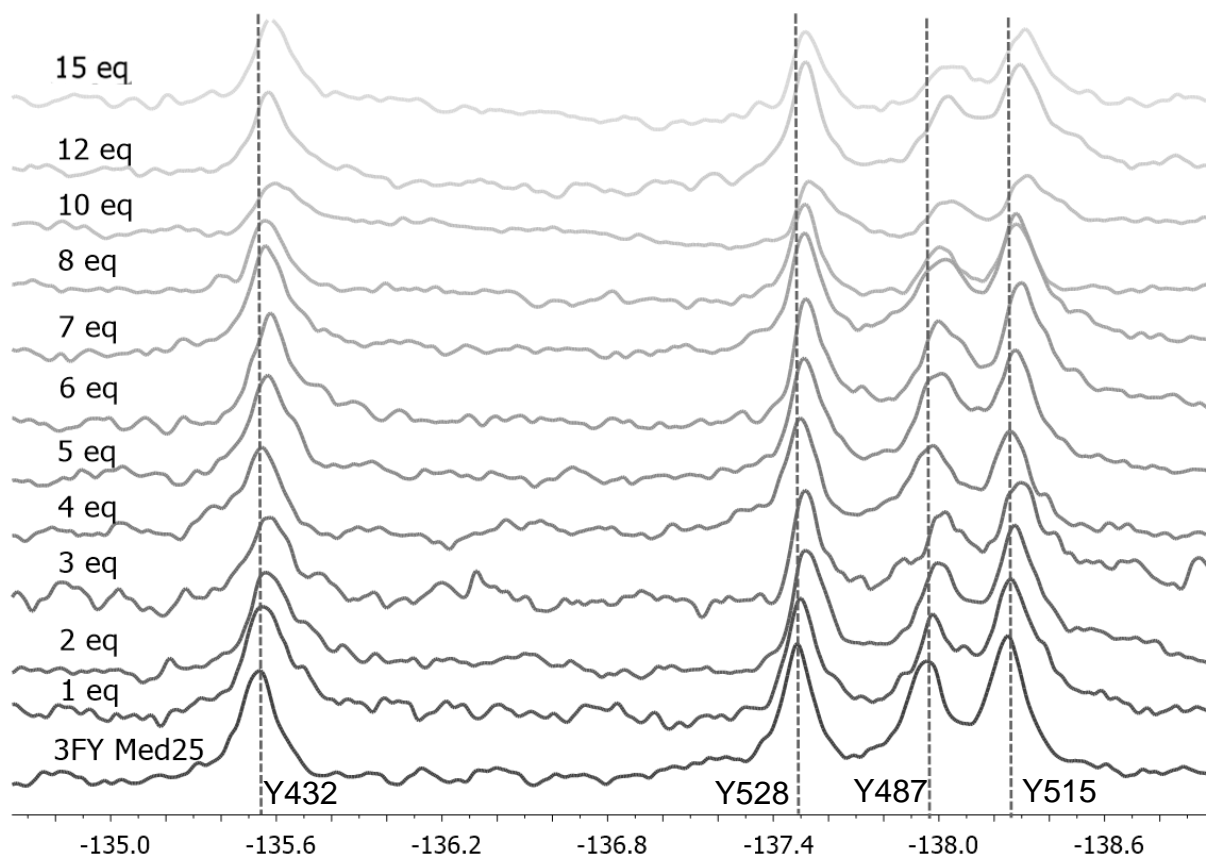


Figure 4.3. PrOF NMR of 3FY Med25 AcID in presence of EN300-51104. These data, demonstrating a dose-dependent shift in 3FY resonances and significant (>0.03 ppm) chemical shifts below 1 mM (10 eq.), suggested that PrOF NMR of 3FY Med25 AcID represented a viable screening strategy.

PrOF NMR of 3FY Med25 with increasing concentrations of EN300-51104 demonstrated dose-dependent chemical shift perturbations of Y487/Y515 resonances. Additionally, at higher equivalencies of the fragment, perturbations at both Y432 and Y528

are observed; It would not be surprising if, at high concentrations, that the fragment would be capable of binding multiple times to the protein. Critically, the fragment did demonstrate a chemical shift perturbation well below the concentration of molecule relative to protein that was screened in the HSQC NMR screen (1 mM fragment; which in these experiments is closest to 12 eq relative to Med25 AcID). Furthermore, a significant chemical shift perturbation (>0.03 ppm shift) in the Y487/Y515 pair was detected at an even lower concentration (3 eq. relative to protein) than the HSQC NMR screen was performed. This suggests that a PrOF NMR screen with 3FY Med25 AcID would be as sensitive, if not more sensitive, than an HSQC NMR screen with ^{15}N Med25 AcID.

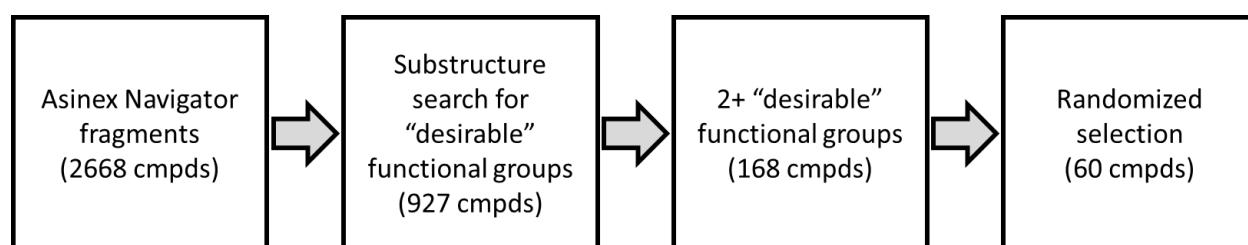


Figure 4.4. Generation of fragment library for PrOF NMR screening. Flowchart to describe methodology behind the generation of a selected number of fragments to test for Med25 binding in PrOF NMR screening

A pilot, small-scale fragment screening effort using PrOF NMR against 3FY Med25 was performed (Figure 4.4). To maximize the potential for the discovery of Med25-interacting fragments, we leveraged knowledge of functional groups that had either previously been found in Med25-interacting ligands (peptides, norstictic acid, fragment A6, EN300-51104) or are known to be commonly found in PPI inhibitors.^{8,43–45} A commercially available fragment library (Asinex Navigator) maintained by the Center for Chemical Genomics was mined for all fragments that contained functional groups contained within Med25 AcID inhibitors (carboxylic acid, amide, indole, highly oxygenated

groups) in addition to other common functional groups (e.g. piperazine, nipecotic acid, morpholine, sulfonamide) to provide 927 unique compounds. A second filtering step, a requirement that all fragments contain at least two of these “desirable” functional groups for PPI inhibition, trimmed the potential list to 168 total fragments. Finally, sixty unique fragments to be screened by PrOF NMR were randomly selected from this shortlist of 168 fragments with two or more “desirable” functional groups.

The sixty fragments selected for screening were combined into fifteen unique mixtures (termed Mix 1 through Mix 15) at a stock concentration of 25 mM per compound in DMSO. All mixtures were subsequently screened at 750 μ M compound and 3% DMSO (9 μ L fragment mixture into 300 μ L final sample volume) in the presence of 75 μ M 3FY Med25 AcID. All experiments were performed using 1600 scans and required less than 15 min of instrumental time (240 min total instrument time to screen all 15 mixtures and run a 3% DMSO negative control) (Figures 4.5 and 4.6).

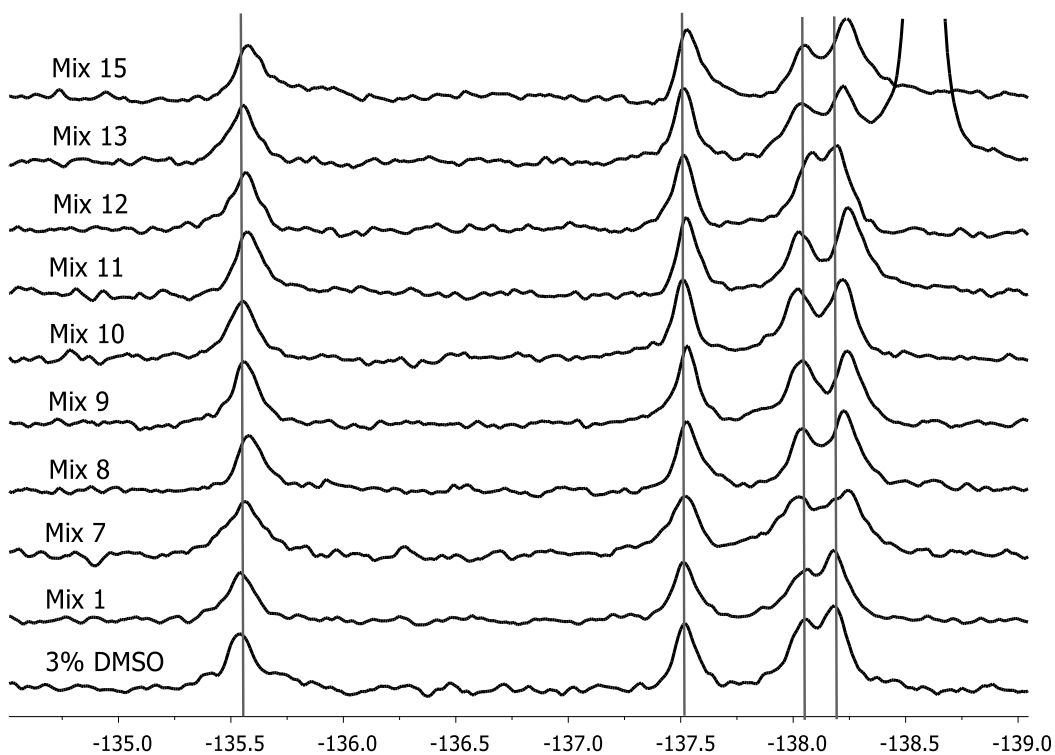


Figure 4.5. ProOF NMR of fragment mixtures not classified as hits. Overlay of 3FY Med25 AcID in presence of fragment mixtures that did not significantly perturb any 3FY resonances relative to average chemical shift of all fragment mixtures. Note that Mixt 13 contained a fluorine-containing small molecule that is presumed to give the large resonance at -138.7 ppm.

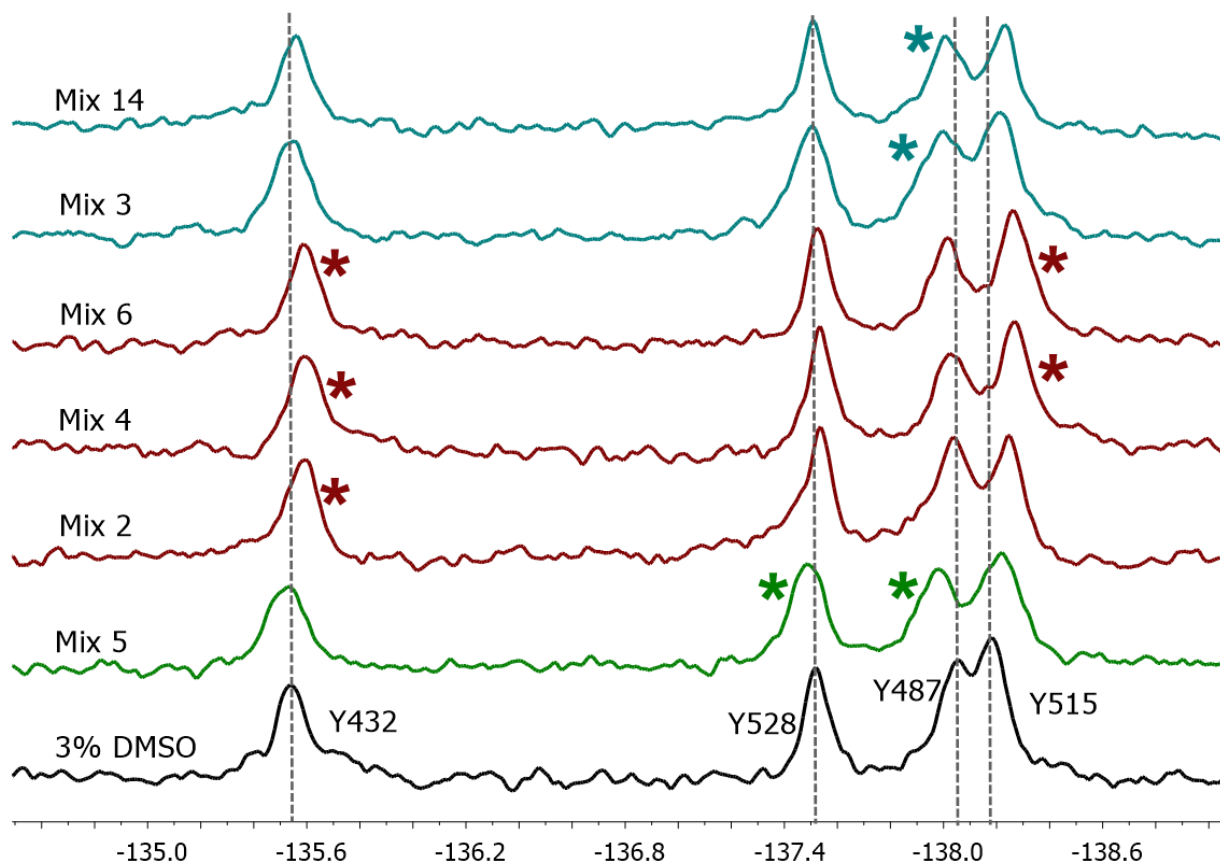


Figure 4.6. ProOF NMR of fragment mixtures classified as hits. Overlay of 3FY Med25 AcID in presence of fragment mixtures 5, 2, 4, 6, 3, and 14 with 3% DMSO control. Mix 5 was classified as a hit based on significant (>1 standard deviation in magnitude relative to average chemical shift of screened fragment mixtures) perturbation of Y528 and Y487 (green asterisks); Mixes 2, 4, and 6 were classified as hits based on significant perturbation of Y432 (red asterisk). Mixes 3 and 14 were classified as hits based on perturbation of Y487 (blue asterisk)

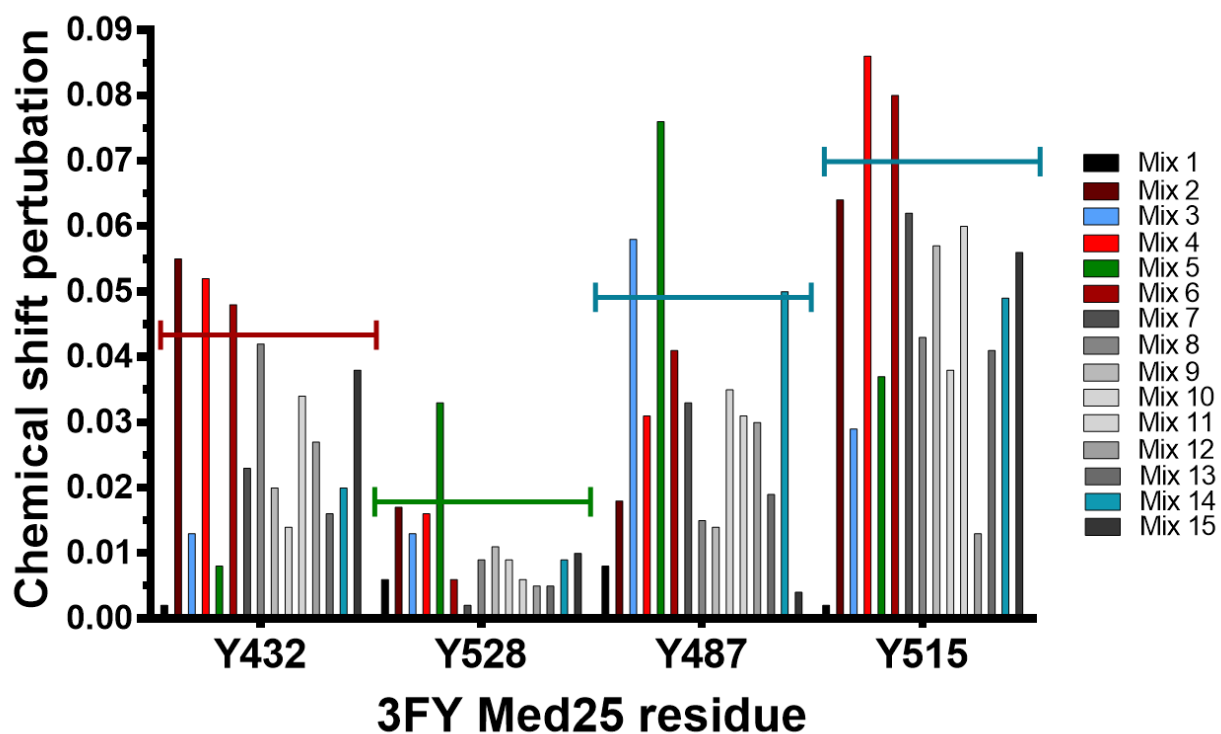


Figure 4.7. Chemical shift perturbations of 3FY Med25 AcID residues in PrOF NMR fragment screening. The chemical shift perturbations induced by each fragment mixture are shown. Mixtures that were classified as hits are depicted in colors that correspond to the residue that is significantly perturbed. The statistical cutoff to designate a significant chemical shift (1 standard deviation above average chemical shift perturbation of all mixtures) for each 3FY residue is shown with a colored line. (e.g. Mixture 2, shown in dark red, was classified as a hit as a result of significant perturbation of Y432)

Following the initial screening of the fragment mixtures using PrOF NMR, the chemical shifts of resonances for each spectrum was determined to calculate the absolute magnitude of the chemical shift perturbation relative to the 3% DMSO. From there, mixtures were scored as hits if the chemical shift of one of their resonances was perturbed by more than one standard deviation greater than the mean perturbation for that residue (Figure 4.7). This strategy found six fragment mixtures to contain at least one statistically significant chemical shift perturbation – Mix 2, Mix 3, Mix 4, Mix 5, Mix 6, and Mix 14 (Figure 4.6). Mixes 3 and 14 were classified as hits based on the downfield perturbation

of Y487, indicating that these mixtures contain at least one fragment capable of binding to Med25 AcID near $\alpha 2$ at either the H1 or H2 sites. Mixes 2, 4, and 6 were classified as hits based on perturbation at Y432 and, in the case of mixes 4 and 6, at Y515. This result would indicate that these mixtures contain at least one fragment that binds either high in the H2 site, near $\alpha 2$, or at the putative third site. Finally, Mix 5 was classified as a hit due to perturbation at Y528 and Y487, indicating that this mixture likely contains at least one fragment that binds at the H2 site and would likely be an orthosteric inhibitor of H2 site peptides such as ATF6 α (40-66). Most fragment mixtures were not classified as hits because none of their resonances were significantly perturbed (Figure 4.5).

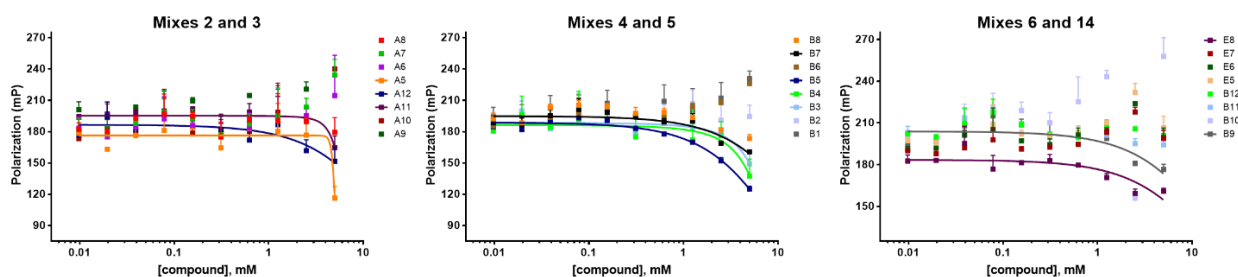
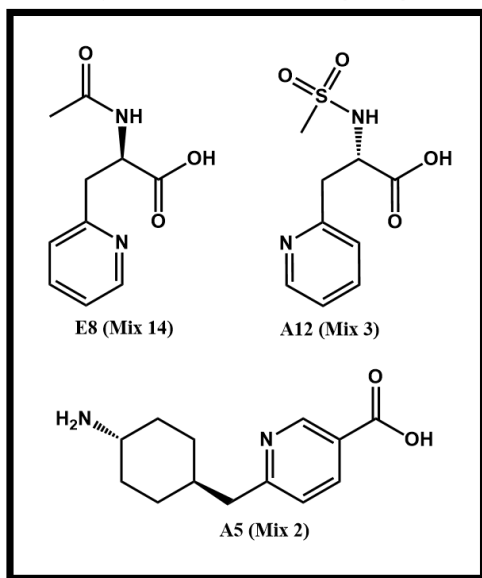


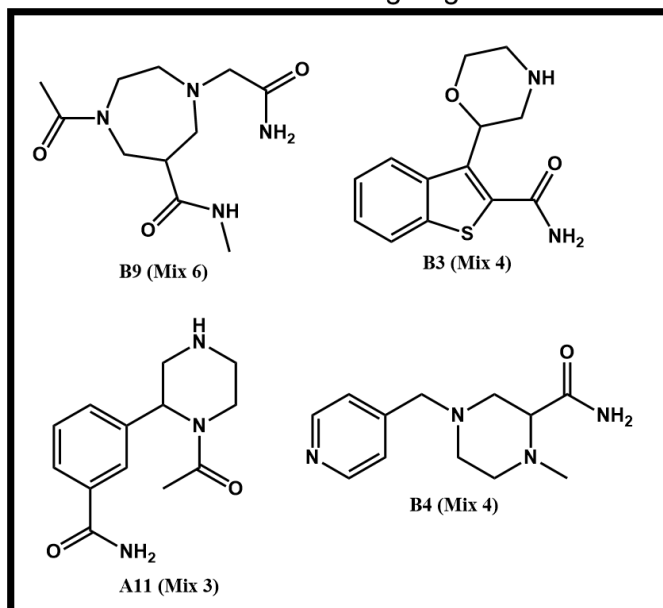
Figure 4.8. Secondary screening of ProOF NMR fragment mixtures. The individual fragments that comprised the six hit fragment mixtures were all tested for inhibition of Med25 AcID-VP16 H2 in FP assays. Weak inhibition of nine fragments was demonstrated; These fragments represent potential Med25 inhibitors and require additional characterization in ProOF NMR experiments.

This initial screening of this sixty-compound library narrowed potential Med25-interacting fragments to 24 unique compounds. To rapidly perform a secondary screening/filtering step, these 24 compounds were tested for inhibition of Med25 PPIs in an FP assay (Figure 4.8) This yielded nine potential inhibitors of Med25 AcID for further investigation in ProOF NMR titrations with 3 FY Med25 AcID (Figure 4.9).

Carboxylic acid-containing fragments



Acetamide-containing fragments



Mix 5 fragments

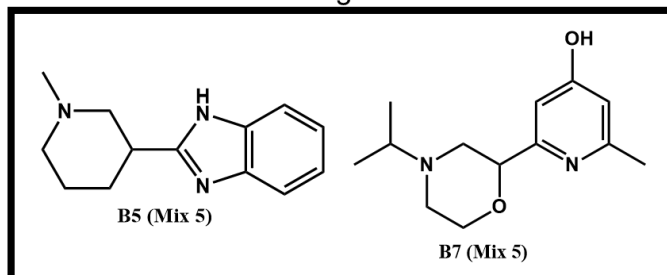


Figure 4.9. Structures of discovered fragments in ProOF NMR screen of Med25 Acid. Nine fragment molecules have been classified as preliminary hit molecules in a ProOF NMR screen of 3FY Med25. This set includes three carboxylic acid-containing and four acetamide-containing fragments. All molecules require additional characterization to verify potential for Med25 inhibition.

As anticipated, preliminary fragments from the ProOF NMR screen include a couple of carboxylic acid-containing molecules. Interestingly, two of these fragments – A12 and E8 – are highly similar molecules. Both fragments the same pyridylalanine core; this could represent an excellent starting point for rational design of downstream Med25 ligands. Four of the nine potential Med25 fragments contain an acetamide functionality and a saturated ring system with two heteroatoms. Each of these nine potential Med25 fragment

molecules, while apparent weak inhibitors of Med25 AcID, represent an opportunity to pursue rational design of novel Med25 PPI inhibitors pending independent verification of binding to Med25 AcID in PrOF and ^1H ^{15}N -HSQC NMR experiments.

A naturally occurring lipopeptide demonstrates selective inhibition of Med25 AcID

As discussed, the binding sites of Med25 are large (1500 – 3000 Å²) and shallow with moderate-affinity interactions with several TADs. Additionally, Med25 AcID has been demonstrated to be structurally dynamic and many of its interacting partners are intrinsically disordered. Collectively, these features make targeting Med25 AcID with high-affinity small molecules difficult. However, as has been shown with norstictic acid and garcinolic acid, natural product compounds present great utility for Med25 AcID inhibition. Natural products possess high degrees of structural complexity that offer high rotational and conformational plasticity that are thought to be beneficial in inhibition of transcriptional PPIs. It was hypothesized that natural products discovery towards Med25 AcID inhibition could be beneficial in targeting Med25 without some of the challenges presented by previously identified molecules (e.g. Norstictic acid functions through covalent adduct formation and has redox reactivity, both impediments for study of Med25 function in cellular context).

Concurrent with the follow-up and deconvolution of a high-throughput screen (HTS) of a natural product extracts library (described in the Appendix), a previously unidentified lipopeptide was isolated from a cyanobacterial strain. This cyanobacterial strain, hereby referred to using its internal identification number 34913, had demonstrated ~20% inhibition of the Med25-ERM PPI in the aforementioned HTS, below the arbitrary

cutoff (30% inhibition) for a hit extract. The novel lipopeptide from strain 34913 consists of a D-amino acid-containing heptapeptide (Glu-Asp-Leu-Leu-Leu-Leu-Val) connected to a lipophilic alkyl chain via an amide bond (Figure 4.10). This structure was determined using high-resolution mass spectrometry, to provide an exact mass of 1054.6982 Da, and rigorous 1-D and 2-D NMR analysis (Ashu Tripathi, University of Michigan). I noted that the lipopeptide appeared to mimic the structural elements of a transcriptional activator and decided to test the novel molecule for activity against Med25 AcID and its PPI network.

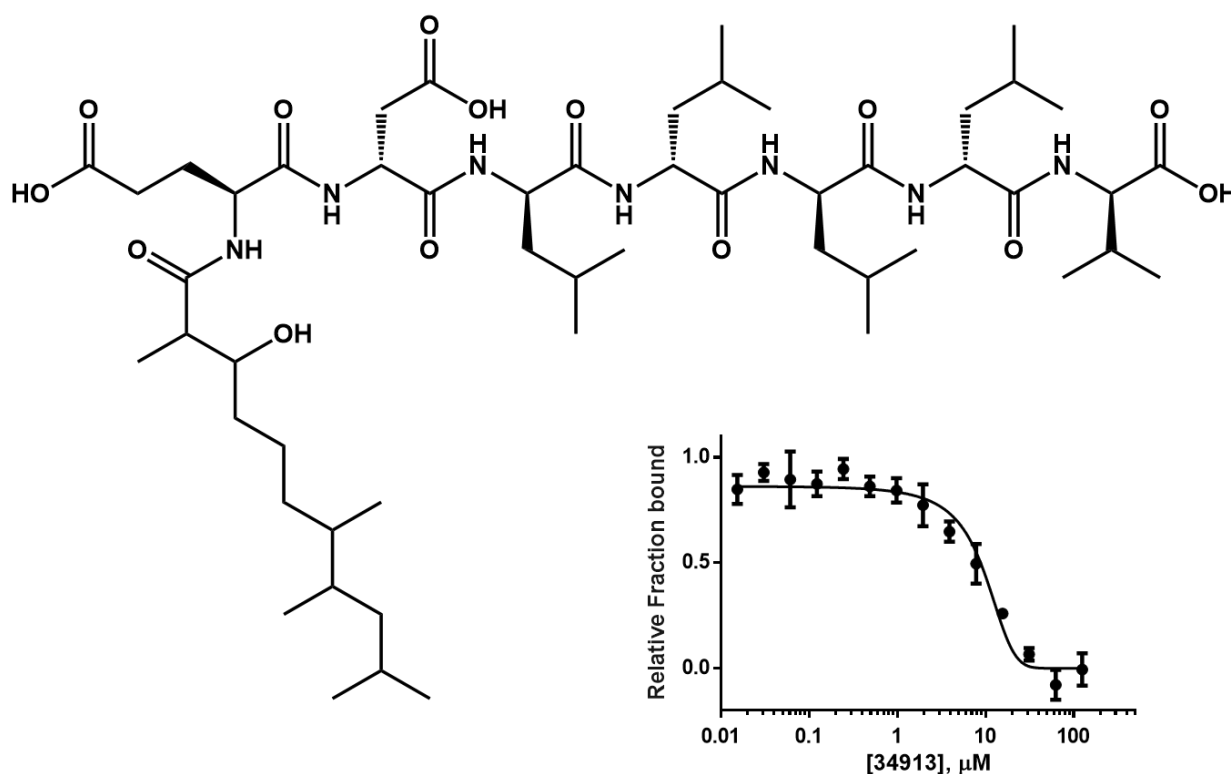


Figure 4.10. 34913 lipopeptide is a potent inhibitor of the Med25-ATF6 α PPI. The 34913 lipopeptide, consisting of an acidic, D-amino acid heptapeptide connected through an amide linkage to a branched lipophilic alkyl chain, is thought to function as a TAD mimetic. It demonstrates single-digit micromolar inhibition of the Med25-ATF6 α PPI (K_i of $8.8 \pm 0.6 \mu\text{M}$)

FP-based inhibition experiments demonstrated that the 34913 lipopeptide is a potent inhibitor of Med25 AcID with a K_i of $8.8 \pm 0.6 \mu\text{M}$ against the Med25-ATF6 α PPI

and a K_i of $11 \pm 2 \mu\text{M}$ against the Med25-ERM PPI. Each of the amino acids in the peptide portion of this small molecule are D-amino acids, a potentially beneficial structural aspect for *in cellulo* and *in vivo* studies as D-amino acids are less prone to proteolysis than L-amino acids⁴⁶. Taking the free carboxy terminus of the peptide portion into account, this molecule has a net -3 charge. A net negative charge would be expected for a potent inhibitor of Med25 Acid PPIs. The alkyl moiety consists of an eleven-carbon chain with four methyl branches and a single hydroxyl group gamma to the carbon of the amide bond that connects the alkyl chain to the peptide portion of the molecule.

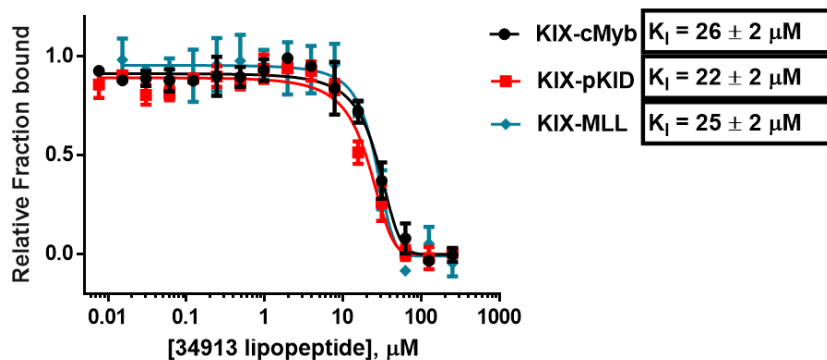


Figure 4.11. Inhibitory effects of 34913 lipopeptide against CBP KIX. The 34913 lipopeptide demonstrates inhibition of Med25 Acid that is approximately 3-fold stronger than CBP KIX (K_i of $9 \mu\text{M}$ for Med25 Acid versus $25 \mu\text{M}$ for CBP KIX), as measured by FP.

Following the discovery of this novel natural product and its potent single-digit micromolar inhibition of Med25 Acid PPIs, FP-based inhibition assays against CBP KIX were performed to test for selectivity of the molecule towards Med25 Acid (Figure 4.11). The lipopeptide did successfully inhibit CBP KIX function (K_i values of $\sim 25 \mu\text{M}$ for all three canonical CBP KIX-TAD PPIs tested). Critically, this indicates that the 34913 lipopeptide is three times more active against the Med25 Acid-ATF6 α PPI than against CBP KIX,

providing a window of selectivity that is necessary and beneficial to study Med25 AcID function *in cellulo* and *in vivo*.

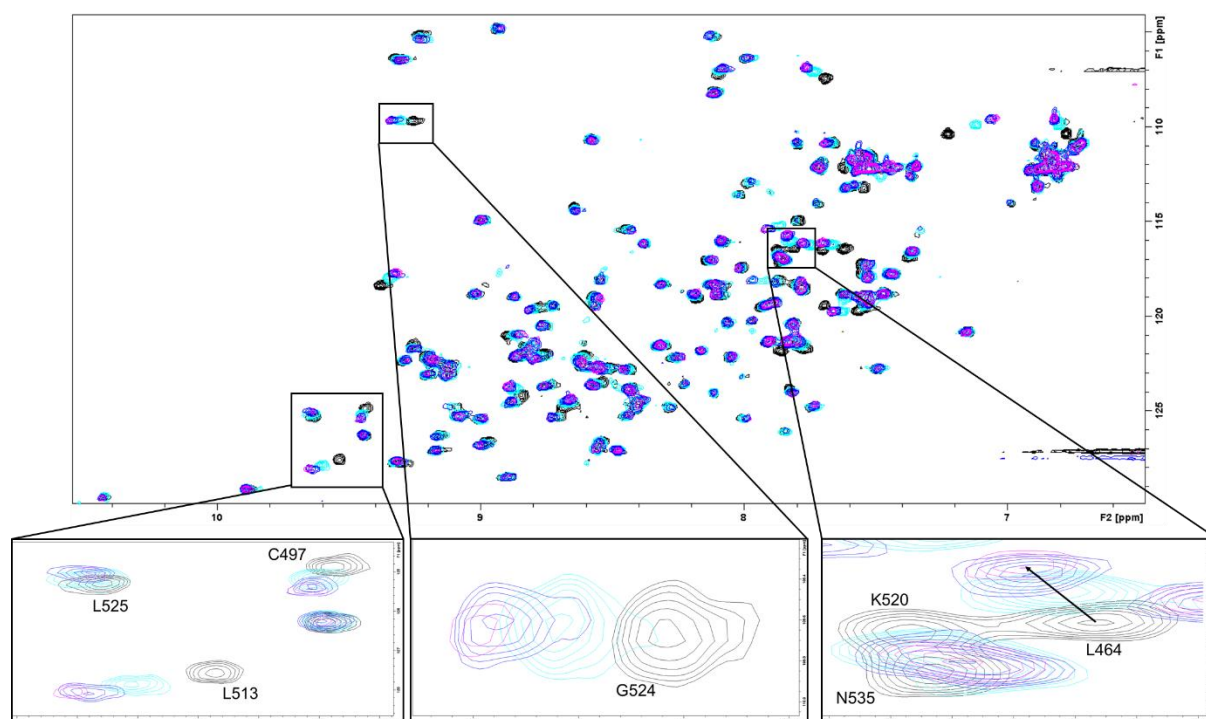


Figure 4.12. ^1H - ^{15}N -HSQC NMR spectra of Med25 AcID in complex with 34913 lipopeptide. Overlay of the HSQC spectra of ^{15}N -labeled Med25 AcID with DMSO (black), 1 eq. molecule (light blue), 2 eq. (dark blue), and 5 eq. (pink) is shown. Inserts show selected resonances have been significantly perturbed including H2 site residues (L513, G524, and L464) and H1 site residues (C497).

With a selective molecule in hand, biophysical experiments – ^1H ^{15}N -HSQC and PrOF NMR experiments – were performed to map the binding location of the 34913 lipopeptide onto Med25 AcID. Based on the slight increase in potency towards the Med25-ATF6 α PPI (specific for the H2 site) compared to the Med25-ERM PPI (the most specific H1 site peptide ligand), it was proposed that the 34913 lipopeptide would be a H2 site binding ligand and thus an orthosteric inhibitor of the ATF6 α TAD.

^1H - ^{15}N -HSQC experiments were performed in which 34913 was complexed with ^{15}N -labeled Med25 AcID at 0, 1, 2, and 4 equivalents of small molecule relative to protein.

These data demonstrated that the molecule bound to Med25 AcID in a specific orientation and did not cause significant protein unfolding or aggregation as several resonances corresponding to specific residues were perturbed in a dose-dependent manner (Figures 4.12 4.13, 4.14). Peaks in each of the collected spectra were assigned to specific residues using a previously published NMR assignment⁴⁷ and a recent assignment performed in the Mapp lab (Andy Henderson, University of Michigan).

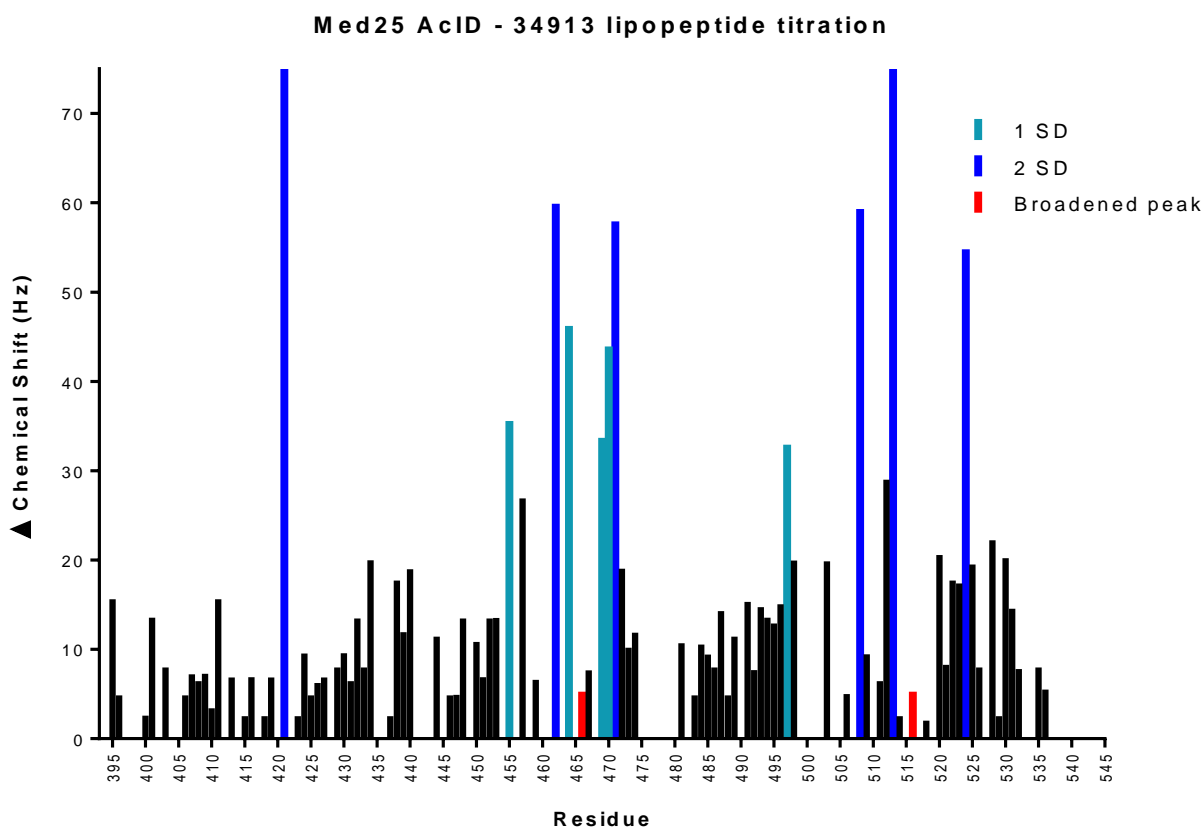


Figure 4.13. Chemical shift perturbations within Med25 AcID induced by saturating 34913 lipopeptide. The magnitude of chemical shift perturbations, in Hz, are shown upon saturation of ¹⁵N Med25 AcID with 4 eq. 34913 lipopeptide. Residues that shift 1-2 standard deviation (SD) above the mean (light blue), >2 SD (dark blue), and broadened into noise level (red) are significantly perturbed.

Saturation of the 34913 lipopeptide onto Med25 AcID caused significant chemical shift perturbations (>2 standard deviations above the mean) in selected

residues located in the H2 site of the protein along $\alpha 1$ and $\beta 6/\beta 7/\beta 4$. All perturbed shifts reside at the 'bottom' of the H2 site, away from $\alpha 2$. These statistically significant chemical shift perturbations specifically correspond to Q455, G462, L464, R469, M470, V471, L513, and G524. Additionally, the residue R466, located at the C-terminus of $\alpha 1$ and known to be critical for H2 site peptide ligand binding based on mutagenesis work performed in Chapter 2, was broadened into the noise level at all concentrations of 34913 lipopeptide tested. This suggested that this residue is likely in direct contact with the molecule when the lipopeptide is bound to Med25 AcID. These data are consistent with the 34913 lipopeptide functioning as an orthosteric inhibitor of ATF6 α (40-66) at the base of the H2 site. Furthermore, the residues that are significantly perturbed by binding of 34913 lipopeptide represent many of the same residues that are significantly perturbed by ATF6 α (40-66) (Figure 4.15). In addition to H2 site perturbations, the HSQC data also demonstrates that a small number of residues at the H1 site are significantly perturbed (T421, C497, V508). The C497 residue, in particular, is located in the center of the H1 site and is among those residues significantly perturbed by ERM peptide ligands in HSQC NMR experiments⁴⁸. This could suggest that the 34913 lipopeptide is capable of allosteric inhibition of H1 site mutants, explaining its inhibitory effects towards the Med25 AcID-ERM(38-68) PPI.

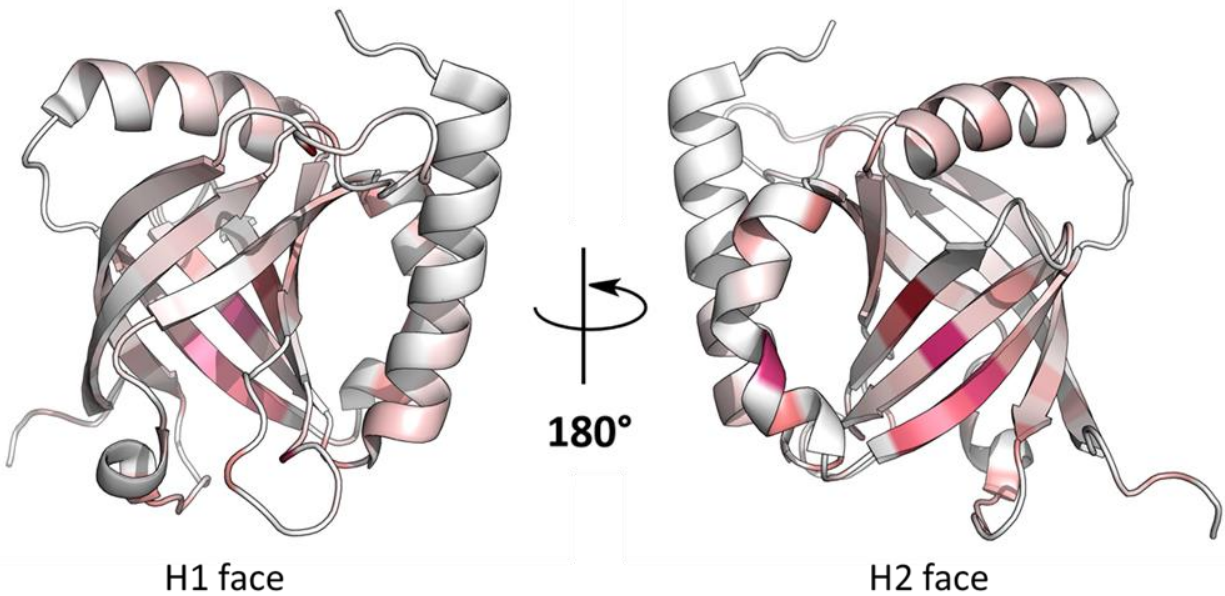


Figure 4.14. Chemical shift perturbations induced by 34913 lipopeptide mapped on Med25 AcID. Residues are colored with increasing shades of red to indicate a gradient of increasing chemical shift perturbations. These data suggest that 34913 lipopeptide interacts specifically with the H2 face of Med25 AcID.

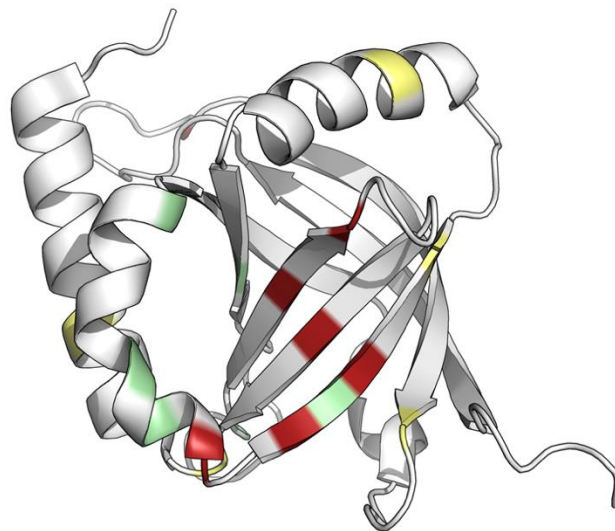


Figure 4.15. Overlay of ATF6 α (40-66)-induced and 34913 lipopeptide-induced Med25 AcID chemical shifts in HSQC NMR. Residues of Med25 AcID that are significantly affected by both ATF6 α and 34913 lipopeptide are shown in red. These data demonstrate that 34913 lipopeptide binds to the H2 site in a binding mode very similar to that of ATF6 α , suggesting that the lipopeptide is an orthosteric inhibitor of the Med25-ATF6 α PPI. Residues significantly affected by 34913 lipopeptide only are shown in green; residues affected by ATF6 α (40-66) only are shown in yellow.

Concurrent with HSQC analysis, PrOF NMR experiments were also performed to characterize the Med25 AcID interaction with the 34913 lipopeptide. Increasing concentrations of 34913 lipopeptide (0, 0.25 eq., 0.5 eq., 1 eq. relative to protein) were complexed with 3FY Med25 AcID and subjected to PrOF NMR analysis (Figure 4.16).

The HSQC data also demonstrates that the 34913 lipopeptide affects the Tyr residues of 3FY Med AcID in a similar manner as does ATF6 α (40-66) peptide. All four residues are perturbed in a dose-dependent manner; however the intensity of the observed chemical shift perturbations is less than with ATF6 α peptide. This could be explained by the large difference in size between the 34913 lipopeptide and the 25-residue ATF6 α peptide particularly if the lipopeptide binds specifically at the 'bottom' of the H2 site and away from α 2 (on which Y487 is located), as predicted by HSQC NMR.

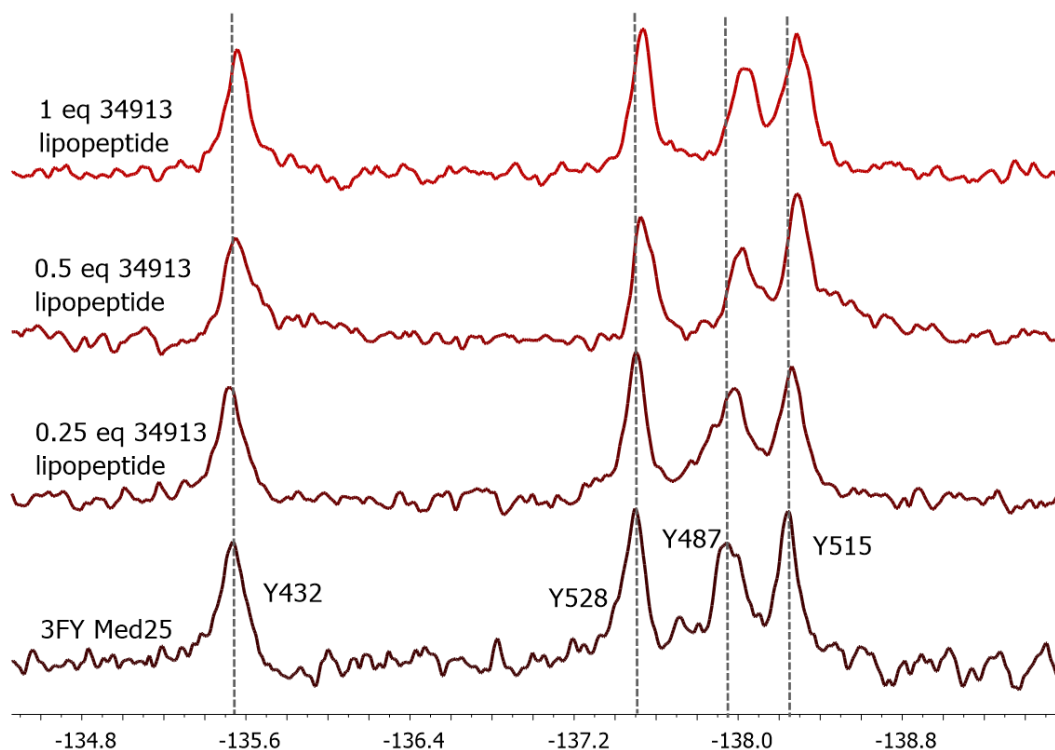


Figure 4.16. PrOF NMR of 3FY Med25 AcID in complex with 34913 lipopeptide. Spectral analysis of 3FY Med25 AcID in presence of increasing concentrations of 34913 lipopeptide corroborated HSQC NMR evidence that 34913 binds Med25 AcID in similar mode as ATF6 α (40-66).

The 34913 lipopeptide is an effective inhibitor of Med25 function in a cellular context

With structural characterization of the molecule and biochemical assessment of its interaction with Med25 AcID completed, experiments were pursued to demonstrate inhibition of Med25 function *in cellulo*. It was hypothesized that the 34913 lipopeptide could traverse the cellular membrane based on its amphipathic nature (lipophilic portion attached to linear peptide chain) and, once inside the cell, interact specifically with Med25 AcID (based on observed 3-fold selectivity against CBP KIX).

Previous literature on Med25 function reported an interaction between the retinoic acid receptor and the nuclear receptor box of Med25 in order to recruit Med25 and the Mediator complex to retinoic acid receptor promoter elements.⁴⁹ A subsequent interaction, as has been described in Chapter 2, between Med25 AcID and CBP(20-44), results in the recruitment of CBP to the same retinoic acid promoter. This set of interactions was then leveraged to design a luciferase reporter to observe the Med25 – CBP – retinoic acid receptor interactions *in cellulo*.⁴⁹ HEK293T cells were transfected with a luciferase reporter driven by a retinoic acid receptor element promoter in addition to a constitutively expressed β -galactosidase (for normalization purposes). Concurrent with stimulation of the luciferase reporter gene using retinoic acid, cells were co-dosed with increasing concentrations of the 34913 lipopeptide (Figure 4.17). It was hypothesized that the 34913 lipopeptide would be capable of inhibition of the luciferase output by direct inhibition of the Med25 AcID-CBP PPI. Disruption of this interaction should disrupt formation of the pre-initiation complex and binding of RNA polymerase II to the retinoic acid receptor promoter.

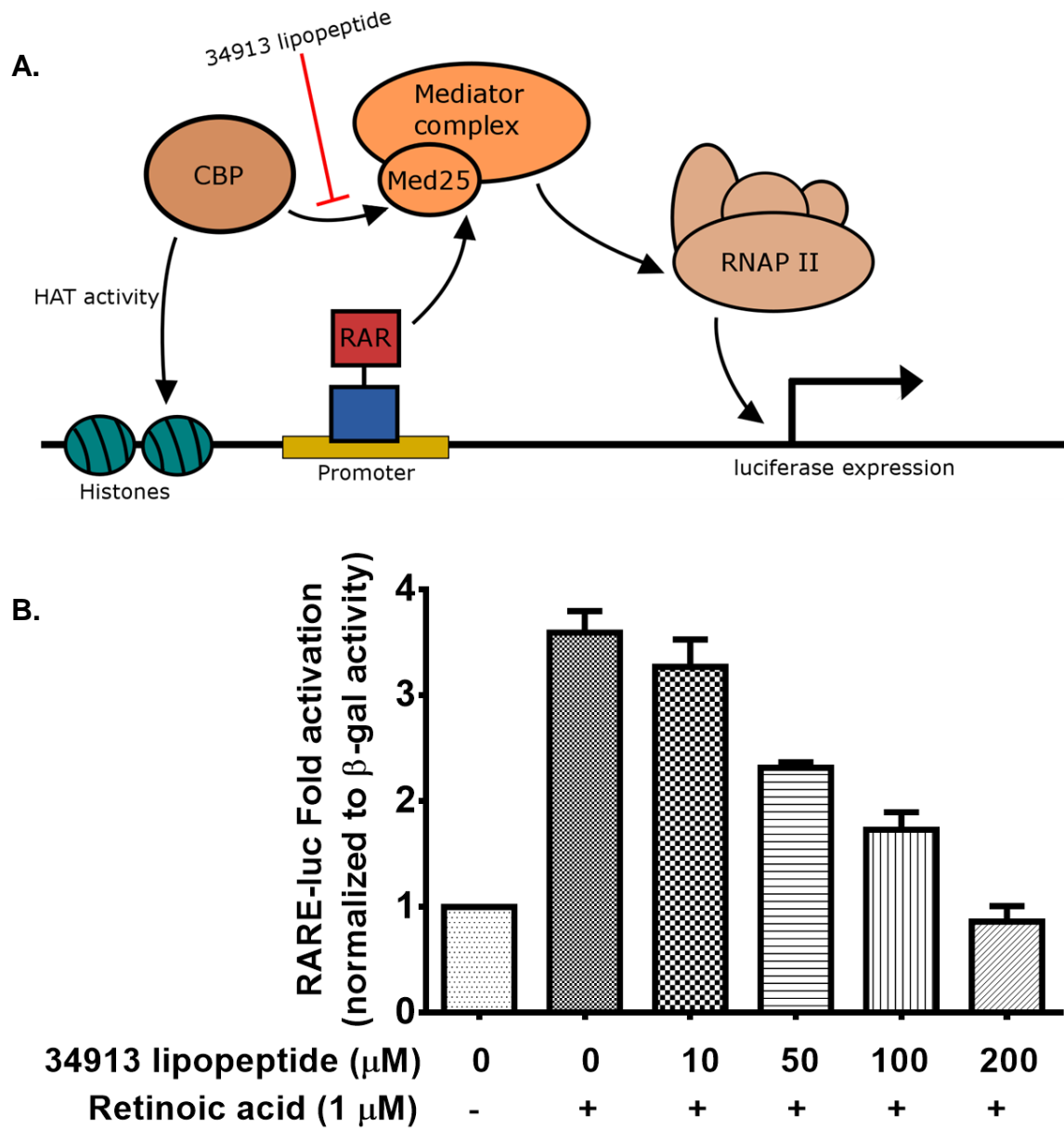


Figure 4.17. Inhibition of a Med25-dependent luciferase reporter by the 34913 lipopeptide. (A) Schematic of the RAR α -luciferase reporter assay. RAR α binds to a RARE promoter on the luciferase reporter plasmid following stimulation with retinoic acid and recruits the Mediator complex through an interaction with the NR region of Med25. The AcID domain of Med25 then recruits CBP to the promoter, which can then modify upstream histones using its histone acetyltransferase domain, resulting in elevated expression of luciferase. (B) The 34913 lipopeptide demonstrated a dose-dependent reduction in the transcriptional activation of a luciferase reporter driven by the retinoic acid receptor. This luciferase inhibition is presumed to occur through direct inhibition of the Med25 AcID-CBP PPI, which leads to a lowered recruitment of the master coactivator CBP to the promoter elements of the retinoic acid receptor. All luciferase signals were normalized to β -gal activity and represent the mean and standard deviation of three biological replicates

The 34913 lipopeptide was capable of dose-dependent inhibition in this Med25-dependent luciferase reporter assay. These data demonstrated that this molecule can cross the cell membrane and target Med25 AcID in the cellular milieu. Excitingly, the molecule provided complete inhibition of normalized luciferase output at 200 μ M with nearly 50% inhibition at 50 μ M.

Following these successful preliminary cellular experiments, we were interested in the potential for 34913 lipopeptide to inhibit the Med25-ATF6 α PPI, an interaction thought to be important in the unfolded protein response and hypoxia.^{1,50} This PPI leads to the activation of pro-survival and anti-apoptotic genes associated with the UPR under hypoxic conditions.^{25,26} The most notable of these ATF6 α -regulated genes is GRP78 (also known as HSPA5), a chaperone protein that suppresses oxidative stress, prevents misfolding of proteins, and stabilizes intracellular calcium levels during periods of hypoxia.^{51,52} To test for inhibition of the Med25-ATF6 α PPI, we measured the effects of increasing doses of 34913 lipopeptide on GRP78 expression levels after thapsigargin-induced hypoxic stress, as previously described for inhibition of Med25-ATF6 α , using qPCR for analysis¹. HeLa cells were dosed with 34913 lipopeptide for three hours prior to induction of hypoxic stress with thapsigargin dosing for another three hours (Figure 4.18). It was hypothesized that the lipopeptide would be capable of downregulating GRP78 expression levels through the inhibition of the Med25 AcID-ATF6 α PPI.

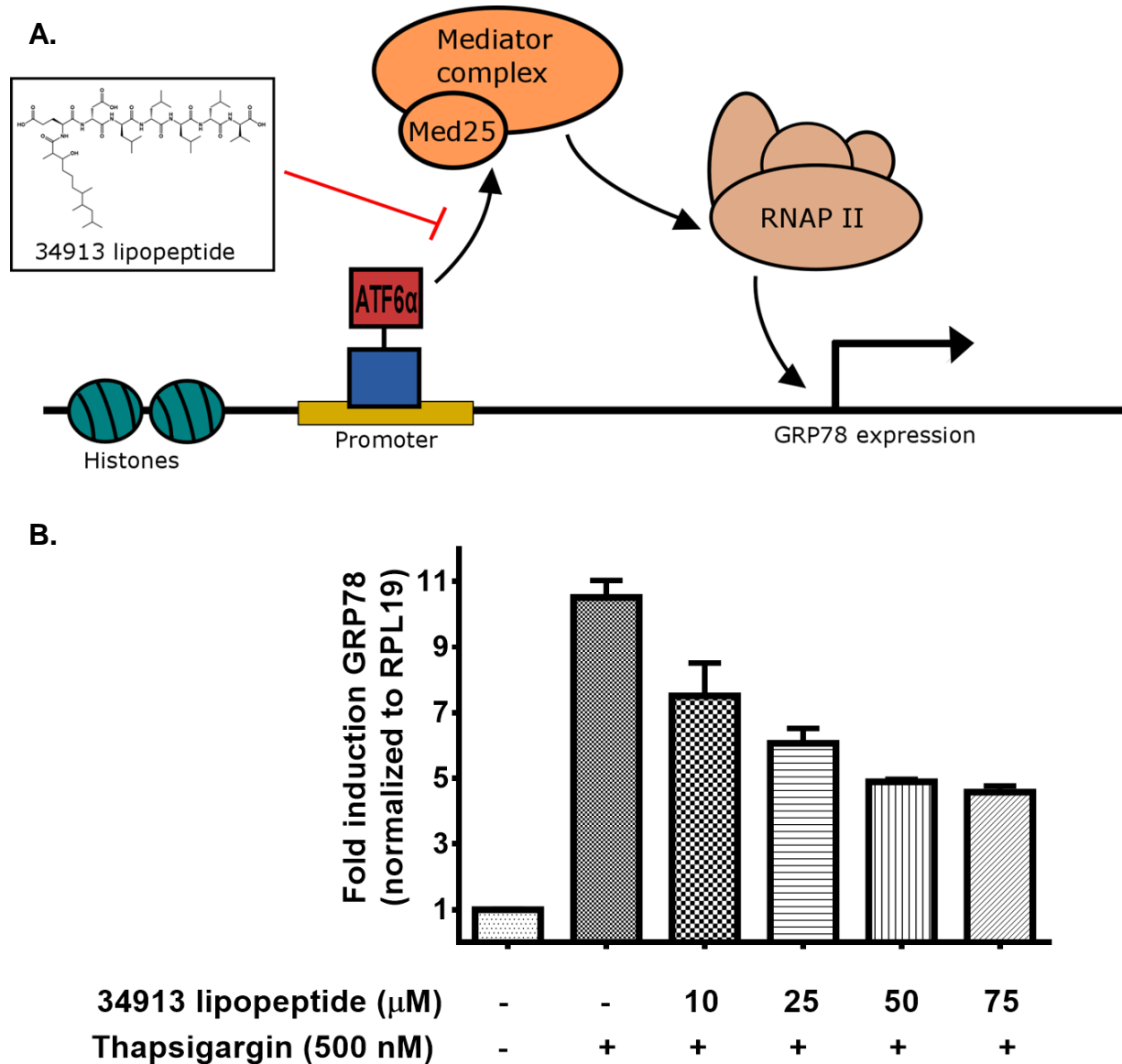


Figure 4.18. Inhibition of the Med25 AcID-ATF6 α PPI in a cellular context by the 34913 lipopeptide. (A) Schematic of the activation of GRP78. The transcriptional activation domain of ATF6 α recruits the Mediator complex through a specific protein-protein interaction with Med25 AcID to activate expression of GRP78. (B) The 34913 lipopeptide downregulated the production of GRP78, an ATF6 α gene product, in a dose-dependent manner, as assessed by qPCR. This downregulation is presumed to occur through orthosteric inhibition of the Med25 AcID-ATF6 α PPI. Expression levels of GRP78 were normalized to expression levels of RPL19. All signals represent the mean and standard deviation of two technical replicates.

GRP78 gene output, as assessed by qPCR, was inhibited by 34913 lipopeptide in a dose-dependent manner with ~50% inhibition achieved at 50 μ M molecule. Interestingly, 34913 lipopeptide at 75 μ M did not inhibit GRP78 more efficiently than the 50 μ M dosage. This could indicate that the lipopeptide is at saturating levels in the cell at 50 μ M or, that GRP78 is being produced in compensatory mechanisms that are not Med25-dependent. If the latter is true, the 34913 lipopeptide could be a useful as a synergistic inhibitor of molecules known to target other proteins involved in hypoxia and the unfolded protein response. Collectively, these data demonstrate that this novel 34913 lipopeptide is capable of on-target inhibition of a potential therapeutic gene target. Based on biochemical evidence that the 34913 lipopeptide interacts with the H2 site of Med25 AcID in a similar fashion to ATF6 α (40-66), this inhibition of GRP78 is presumably a result of direct inhibition of Med25 AcID *in cellulo*.

D. Conclusions and future directions

The overarching hypothesis of this work is that the discovery and characterization of small molecules that inhibit Med25 AcID function could provide molecular probes for the study of disease through inhibition of the Med25-ERM and Med25-ATF6 α PPIs. Specifically, with respect to ERM/ETV5, these molecules could be useful towards a better understanding of ETV5 and related ETV activators and their role in cellular processes related to cancer progression and metastasis. With respect to ATF6 α , molecules that inhibit Med25 PPIs could be therapeutically beneficial in downregulating ATF6 α gene products, such as GRP78, and could useful in determining the role of Med25 in the ATF6 α pathway, the unfolded protein response, and the role of the unfolded protein response in

cancer progression.²⁹ In this chapter, we developed and characterized several small molecules that inhibit Med25 AcID function. These molecules were discovered using multiple screening strategies, from fragment identification by Tethering and NMR methodologies to natural products isolation following competition-based fluorescence polarization assays.

PrOF NMR of Med25 AcID was developed to allow for a pilot screening effort of a small fragment library. This technique is uniquely sensitive for the detection of weakly binding fragment molecules as NMR allows for screening of high [compound] in a multiplexed format. Furthermore, PrOF NMR, a 1-D methodology, specifically offers short experimental and analysis timeframes as well as high native abundance of the ¹⁹F isotope, high magnetic sensitivity (83% as sensitive as ¹H), low background signal and low background signal. Using a PrOF NMR screen of 3FY Med25 AcID, nine compounds were discovered as preliminary hits against Med25 AcID. These fragments represent excellent compounds for future biochemical and NMR characterization with Med25 AcID and could demonstrate novel scaffolds for rationally designed fragment inhibitors.

A novel lipopeptide isolated from cyanobacteria has been discovered as a potent single-digit micromolar inhibitor of the Med25-ATF6 α PPI in FP assays that demonstrates three-fold selectivity for Med25 AcID relative to CBP/p300 KIX. HSQC and PrOF NMR demonstrated that this lipopeptide binds at the H2 site of Med25 AcID in a binding mode nearly identical to that of the ATF6 α transcriptional activator. In cellular experiments, GRP78 gene output, as assessed by qPCR, was downregulated by the novel lipopeptide in a dose-dependent manner with ~50% inhibition achieved at 50 μ M compound. Critically, this novel natural product represents the first highly selective, potent, and non-

covalent small molecule that targets Med25 AcID function both *in vitro* and *in cellulo*. It demonstrates tremendous promise as a lead candidate for future study of the roles that Med25 AcID plays in disease contexts, particularly cancer metastasis and tumor progression.

Going forward, we are developing two strategies for future production of this novel lipopeptide and related compounds. The cyanobacterial strain, 34913, that produces this compound will be engineered to produce the compound in higher yields using ribosomal and/or metabolic strategies.^{53,54} Concurrently, synthetic derivatives of this lipopeptide are being generated that incorporate aromaticity into the peptide portion and vary the alkyl chain (Figure 4.19). If a similar compound with similar inhibitory properties can be readily synthesized, this would represent the route with highest potential throughput for cellular studies of Med25 AcID function.

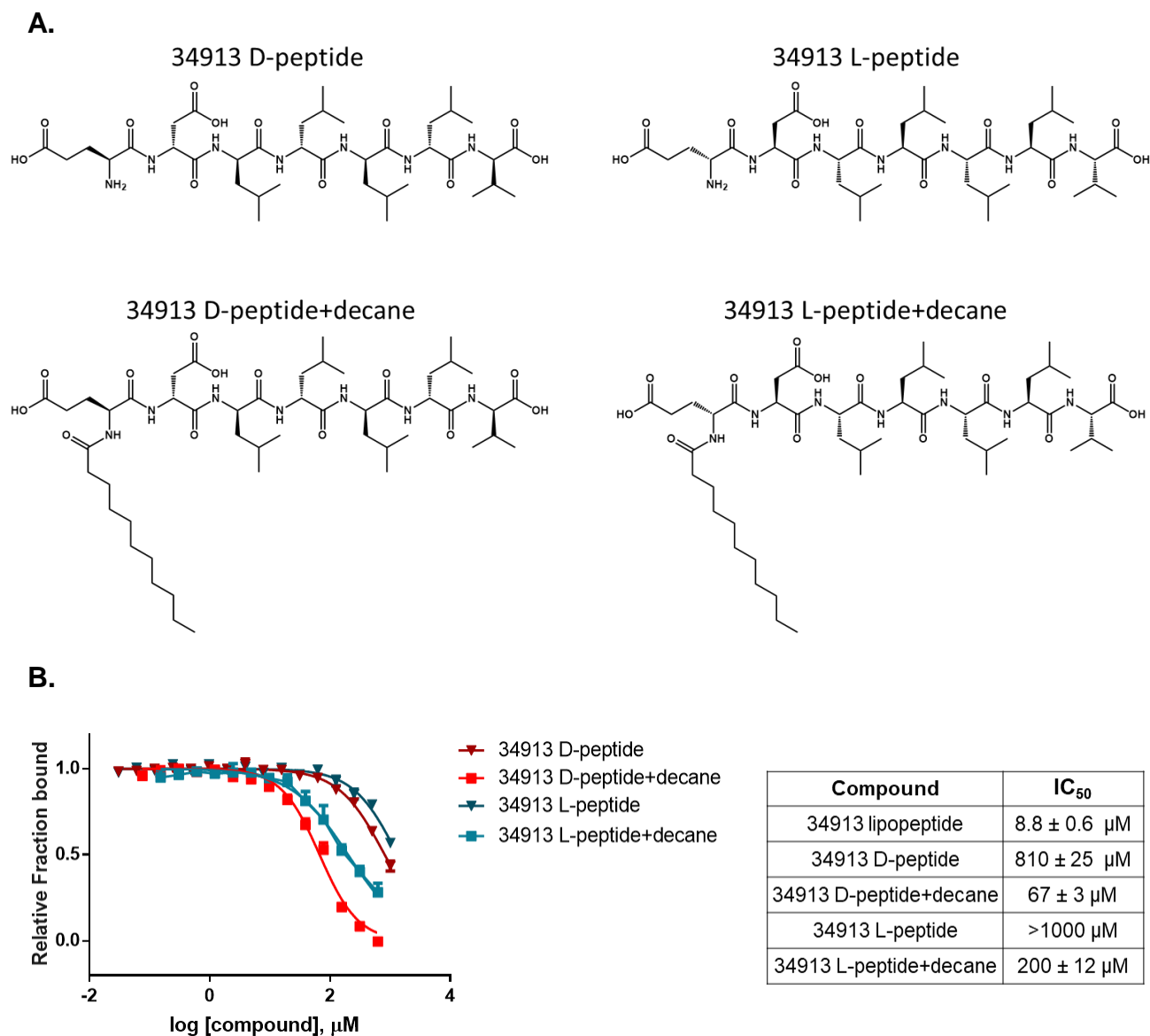


Figure 4.19. Structures and activity of 34913 lipopeptide derivatives. (A) Four 34913 lipopeptide derivatives are provided. The peptide portion has been synthesized with all D-amino acids and with all L-amino acids; Both peptides has been derivatized with a ten-carbon chain appended to its N-terminus. (B) Inhibition of the Med25-ATF6α PPI by 34913 derivatives.

E. Materials and methods

Previously described methods

Relevant methods that were previously described in Chapter Two include Med25 AcID purification, mass spectroscopy of proteins, FP binding experiments, FP competition experiments, production of ¹⁵N-labeled protein, HSQC NMR and solid-phase peptide synthesis.

Relevant methods that were previously described in Chapter Three include the production of ¹⁹F-labeled protein and PrOF NMR.

PrOF NMR screening

The sixty fragments selected for screening were combined into fifteen unique mixtures (termed Mix 1 through Mix 15) at a stock concentration of 25 mM per compound in DMSO. All mixtures were subsequently screened at 750 μM compound and 3% DMSO (9 μL fragment mixture into 300 μL final sample volume) in the presence of 75 μM 3FY Med25 AcID. All experiments were performed using 1600 scans.

Expression and purification of CBP KIX

CBP KIX was expressed and purified according to previously published protocols⁵⁵.

Med25-CBP-RARα luciferase reporter assay

The RARα luciferase reporter plasmid containing 3 tandem RARα promoter elements (termed 'pRARE-luc') was obtained from Addgene. A constitutively active β-galactosidase coding plasmid driven by a CMV promoter (termed 'CMV β-Gal') was provided by Dr.

Jorge Iñiguez-Lluhí (University of Michigan). pCDNA3, a non-coding vector, used for transfection controls was provided by Dr. Jorge Iñiguez-Lluhí. All cells were maintained in 5% CO₂ at 37°C. HeLa cells were grown in Dulbecco's modified Eagle's medium (DMEM, Invitrogen) supplemented with 10% FBS. For luciferase assays, 4x10⁵ cells were plated in a 6-well dish and allowed to adhere overnight. The media was removed and cells were transfected in OptiMEM (Invitrogen) with 1 µg RAR α :luc, 200 ng CMV: β :Gal, and 800 ng pCDNA using Lipofectamine 2000 (Life Technologies) according to manufacturer's instructions. After 4.5 hours, transfection solution was removed and replaced with DMEM containing 10% FBS. At 24 h after transfection, cells were trypsinized and resuspended in DMEM supplemented with 10% FBS before plating into a 96-well plate at a density of 15x10³ cells per well. After an additional 16 hours, media was removed and replaced with OptiMEM containing DMSO control or 34913 lipopeptide and 1 µM retinoic acid. After cells 16 hours, media was removed and cells were lysed with 60 µL of passive lysis buffer. Luciferase and β :Galactosidase activities were determined as previously described⁵⁶. RAR α luciferase activity and response curve analysis was performed using GraphPad software.

RT-qPCR analysis of GRP78 gene expression

For endogenous gene expression analysis, 1x10⁵ HeLa cells were plated into a 24-well plate and allowed to adhere overnight. Media was removed and replaced with OptiMEM containing DMSO control or 34913 lipopeptide. After incubating for 2 hours, cells were treated with 500 nM thapsigargin. After 2 h, the media was removed and total RNA was isolated using RNeasy Plus RNA isolation kits (Qiagen) according to manufacturer's

instructions. Each RNA sample was used to synthesize cDNA using iScript cDNA synthesis kits (Bio-Rad). RT-qPCR reactions were carried out in duplicate in an Applied Biosystems StepPlusOne instrument using SYBR green master mix and primers for: human RPL19 F pr. 5':ATGTATCACAGCCTGTACCTG:3'; R Pr., 5':TTCTTGGTCTCTCTTCCTCCTTG:3') and GRP78 (F Pr., 5':CTGGGTACATTTGATCTGACTGG:3'; R Pr., 5':CTTACCGACCTTTCGGTGGTCCTACG:3'). RT-qPCR analysis was carried out using the comparative CT Method ($\Delta\Delta$ CT Method) to estimate GRP78 mRNA levels relative to the reference RPL19 mRNA levels.

Synthesis of 34913 derivatives

34913-derived peptide were synthesized using solid-phase peptide synthesis, as described in Chapter Two. '34913_D-peptide+decane' and '34913_L-peptide+decane' were synthesized using standard peptide coupling, on solid phase resin, between the N-terminus of the 34913 peptide sequence and undecanoic acid.

F. References

1. Sela, D. *et al.* Role for Human Mediator Subunit MED25 in Recruitment of Mediator to Promoters by Endoplasmic Reticulum Stress-responsive Transcription Factor ATF6. *J. Biol. Chem.* **288**, 26179–26187 (2013).
2. Verger, A. *et al.* The Mediator complex subunit MED25 is targeted by the N-terminal transactivation domain of the PEA3 group members. *Nucleic Acids Res.* **41**, 4847–4859 (2013).
3. Nero, T. L., Morton, C. J., Holien, J. K., Wielens, J. & Parker, M. W. Oncogenic protein interfaces: small molecules, big challenges. *Nat. Rev. Cancer* **14**, 248–262 (2014).
4. Wells, J. A. & McClendon, C. L. Reaching for high-hanging fruit in drug discovery at protein–protein interfaces. *Nature* **450**, 1001–1009 (2007).
5. Lo Conte, L., Chothia, C. & Janin, J. The atomic structure of protein-protein recognition sites. *J. Mol. Biol.* **285**, 2177–2198 (1999).
6. Thompson, A. D., Dugan, A., Gestwicki, J. E. & Mapp, A. K. Fine-Tuning Multiprotein Complexes Using Small Molecules. *ACS Chem. Biol.* **7**, 1311–1320 (2012).
7. Smith, M. C. & Gestwicki, J. E. Features of protein–protein interactions that translate into potent inhibitors: topology, surface area and affinity. *Expert Rev. Mol. Med.* **14**, (2012).
8. Cesa, L. C., Mapp, A. K. & Gestwicki, J. E. Direct and Propagated Effects of Small Molecules on Protein–Protein Interaction Networks. *Front. Bioeng. Biotechnol.* **3**, (2015).
9. Spencer, R. W. High-throughput screening of historic collections: observations on file size, biological targets, and file diversity. *Biotechnol. Bioeng.* **61**, 61–67 (1998).
10. Majmudar, C. Y. *et al.* Sekikaic Acid and Lobaric Acid Target a Dynamic Interface of the Coactivator CBP/p300. *Angew. Chem. Int. Ed.* **51**, 11258–11262 (2012).
11. Sperl, B., Seifert, M. H. J. & Berg, T. Natural product inhibitors of protein–protein interactions mediated by Src-family SH2 domains. *Bioorg. Med. Chem. Lett.* **19**, 3305–3309 (2009).
12. Hollis, A., Sperl, B., Gräber, M. & Berg, T. The Natural Product Betulinic Acid Inhibits C/EBP Family Transcription Factors. *ChemBioChem* **13**, 302–307 (2012).
13. Ardi, V. C., Alexander, L. D., Johnson, V. A. & McAlpine, S. R. Macrocycles That Inhibit the Binding between Heat Shock Protein 90 and TPR-Containing Proteins. *ACS Chem. Biol.* **6**, 1357–1366 (2011).
14. Lepourcelet, M. *et al.* Small-molecule antagonists of the oncogenic Tcf/β-catenin protein complex. *Cancer Cell* **5**, 91–102 (2004).
15. Dias, D. A., Urban, S. & Roessner, U. A historical overview of natural products in drug discovery. *Metabolites* **2**, 303–336 (2012).

16. Ertl, P., Roggo, S. & Schuffenhauer, A. Natural Product-likeness Score and Its Application for Prioritization of Compound Libraries. *J. Chem. Inf. Model.* **48**, 68–74 (2008).
17. Rodrigues, T., Reker, D., Schneider, P. & Schneider, G. Counting on natural products for drug design. *Nat. Chem.* **8**, 531–541 (2016).
18. Cragg, G. M., Grothaus, P. G. & Newman, D. J. Impact of Natural Products on Developing New Anti-Cancer Agents †. *Chem. Rev.* **109**, 3012–3043 (2009).
19. Newman, D. J. & Cragg, G. M. Natural Products As Sources of New Drugs over the 30 Years from 1981 to 2010. *J. Nat. Prod.* **75**, 311–335 (2012).
20. Fenical, W. & Jensen, P. R. Developing a new resource for drug discovery: marine actinomycete bacteria. *Nat. Chem. Biol.* **2**, 666–673 (2006).
21. Molinski, T. F. Microscale methodology for structure elucidation of natural products. *Curr. Opin. Biotechnol.* **21**, 819–826 (2010).
22. Aytes, A. *et al.* ETV4 promotes metastasis in response to activation of PI3-kinase and Ras signaling in a mouse model of advanced prostate cancer. *Proc. Natl. Acad. Sci.* **110**, E3506–E3515 (2013).
23. Backer, M. V., Backer, J. M. & Chinnaiyan, P. Targeting the Unfolded Protein Response in Cancer Therapy. in *Methods in Enzymology* **491**, 37–56 (Elsevier, 2011).
24. Haze, K., Yoshida, H., Yanagi, H., Yura, T. & Mori, K. Mammalian transcription factor ATF6 is synthesized as a transmembrane protein and activated by proteolysis in response to endoplasmic reticulum stress. *Mol. Biol. Cell* **10**, 3787–3799 (1999).
25. Yoshida, H. *et al.* ATF6 activated by proteolysis binds in the presence of NF-Y (CBF) directly to the cis-acting element responsible for the mammalian unfolded protein response. *Mol. Cell. Biol.* **20**, 6755–6767 (2000).
26. Wang, Y. *et al.* Activation of ATF6 and an ATF6 DNA binding site by the endoplasmic reticulum stress response. *J. Biol. Chem.* **275**, 27013–27020 (2000).
27. Fernandez, P. M. *et al.* Overexpression of the glucose-regulated stress gene GRP78 in malignant but not benign human breast lesions. *Breast Cancer Res. Treat.* **59**, 15–26 (2000).
28. Xia, F. *et al.* Glucose-regulated protein 78 and heparanase expression in oral squamous cell carcinoma: correlations and prognostic significance. *World J. Surg. Oncol.* **12**, 121 (2014).
29. Ma, Y. & Hendershot, L. M. The role of the unfolded protein response in tumour development: friend or foe? *Nat. Rev. Cancer* **4**, 966–977 (2004).
30. Benz, C. C. *et al.* HER2/Neu and the Ets transcription activator PEA3 are coordinately upregulated in human breast cancer. *Oncogene* **15**, 1513–1525 (1997).
31. de Launoit, Y. *et al.* The PEA3 group of ETS-related transcription factors. Role in breast cancer metastasis. *Adv. Exp. Med. Biol.* **480**, 107–116 (2000).

32. Pellecchia, A. *et al.* Overexpression of ETV4 is oncogenic in prostate cells through promotion of both cell proliferation and epithelial to mesenchymal transition. *Oncogenesis* **1**, e20 (2012).
33. Myers, E. *et al.* A positive role for PEA3 in HER2-mediated breast tumour progression. *Br. J. Cancer* **95**, 1404–1409 (2006).
34. Fauquette, V. *et al.* The antagonistic regulation of human MUC4 and ErbB-2 genes by the Ets protein PEA3 in pancreatic cancer cells: implications for the proliferation/differentiation balance in the cells. *Biochem. J.* **386**, 35–45 (2005).
35. Sturlis, S. M. *et al.* Identifying Depsidone Inhibitors of Med25-AcID Mediated Transcription. *Manuscr. Prep.*
36. Shuker, S. B., Hajduk, P. J., Meadows, R. P. & Fesik, S. W. Discovering high-affinity ligands for proteins: SAR by NMR. *Science* **274**, 1531–1534 (1996).
37. Harner, M. J., Frank, A. O. & Fesik, S. W. Fragment-Based Drug Discovery Using NMR Spectroscopy. *J. Biomol. NMR* **56**, 65–75 (2013).
38. Gee, C. T., Koleski, E. J. & Pomerantz, W. C. K. Fragment Screening and Druggability Assessment for the CBP/p300 KIX Domain through Protein-Observed ¹⁹F NMR Spectroscopy. *Angew. Chem. Int. Ed.* **54**, 3735–3739 (2015).
39. Arntson, K. E. & Pomerantz, W. C. K. Protein-Observed Fluorine NMR: A Bioorthogonal Approach for Small Molecule Discovery: Miniperspective. *J. Med. Chem.* **59**, 5158–5171 (2016).
40. Liebeschuetz, J. W. *et al.* PRO_SELECT: Combining Structure-Based Drug Design and Array-Based Chemistry for Rapid Lead Discovery. 2. The Development of a Series of Highly Potent and Selective Factor Xa Inhibitors. *J. Med. Chem.* **45**, 1221–1232 (2002).
41. Park, C.-M. *et al.* Discovery of an Orally Bioavailable Small Molecule Inhibitor of Prosurvival B-Cell Lymphoma 2 Proteins. *J. Med. Chem.* **51**, 6902–6915 (2008).
42. Wyatt, P. G. *et al.* Identification of N-(4-Piperidinyl)-4-(2,6-dichlorobenzoylamino)-1H-pyrazole-3-carboxamide (AT7519), a Novel Cyclin Dependent Kinase Inhibitor Using Fragment-Based X-Ray Crystallography and Structure Based Drug Design. *J. Med. Chem.* **51**, 4986–4999 (2008).
43. Morelli, X., Bourgeas, R. & Roche, P. Chemical and structural lessons from recent successes in protein–protein interaction inhibition (2P2I). *Curr. Opin. Chem. Biol.* **15**, 475–481 (2011).
44. Arkin, M. Protein–protein interactions and cancer: small molecules going in for the kill. *Curr. Opin. Chem. Biol.* **9**, 317–324 (2005).
45. Sammak, S. & Zinzalla, G. Targeting protein-protein interactions (PPIs) of transcription factors: Challenges of intrinsically disordered proteins (IDPs) and regions (IDRs). *Prog. Biophys. Mol. Biol.* **119**, 41–46 (2015).
46. Nelson, D. & Cox, M. *Principles of Biochemistry.* (W.H. Freeman).

47. Vojnic, E. *et al.* Structure and VP16 binding of the Mediator Med25 activator interaction domain. *Nat. Struct. Mol. Biol.* **18**, 404–409 (2011).
48. Landrieu, I. *et al.* Characterization of ERM transactivation domain binding to the ACID/PTOV domain of the Mediator subunit MED25. *Nucleic Acids Res.* **43**, 7110–7121 (2015).
49. Lee, H.-K., Park, U.-H., Kim, E.-J. & Um, S.-J. MED25 is distinct from TRAP220/MED1 in cooperating with CBP for retinoid receptor activation. *EMBO J.* **26**, 3545–3557 (2007).
50. Lee, J. & Ozcan, U. Unfolded Protein Response Signaling and Metabolic Diseases. *J. Biol. Chem.* **289**, 1203–1211 (2014).
51. Li, J. & Lee, A. S. Stress induction of GRP78/BiP and its role in cancer. *Curr. Mol. Med.* **6**, 45–54 (2006).
52. Pyrko, P., Schonthal, A. H., Hofman, F. M., Chen, T. C. & Lee, A. S. The Unfolded Protein Response Regulator GRP78/BiP as a Novel Target for Increasing Chemosensitivity in Malignant Gliomas. *Cancer Res.* **67**, 9809–9816 (2007).
53. Park, S. R. *et al.* Discovery of cahuitamycins as biofilm inhibitors derived from a convergent biosynthetic pathway. *Nat. Commun.* **7**, ncomms10710 (2016).
54. Pickens, L. B., Tang, Y. & Chooi, Y.-H. Metabolic Engineering for the Production of Natural Products. *Annu. Rev. Chem. Biomol. Eng.* **2**, 211–236 (2011).
55. Buhrlage, S. J. *et al.* Amphipathic small molecules mimic the binding mode and function of endogenous transcription factors. *ACS Chem. Biol.* **4**, 335–344 (2009).
56. Bates, C. A., Pomerantz, W. C. & Mapp, A. K. Transcriptional tools: Small molecules for modulating CBP KIX-dependent transcriptional activators. *Biopolymers* **95**, 17–23 (2011).

CHAPTER FIVE

Conclusions and future directions

A. Summary

Historically, targeting protein-protein interactions (PPIs) with small molecule modulators has been a significant challenge.^{1,2} This difficulty has been especially true with regards to transcriptional PPIs which are transient, weak-to-moderate affinity, and for which structural studies have been limited. However, there have been recent successes born from the field of natural products and from screening strategies that utilize protein-observed ¹⁹F-NMR (PrOF NMR) towards the identification of small molecule modulators that target transcriptional PPIs.³⁻⁶

This dissertation sought to leverage natural products and PrOF NMR for the identification and characterization of selective small molecule inhibitors that target the activator interaction domain (AcID) of Med25 and its PPI network. Molecular inhibition of Med25 AcID is desired as a potential avenue for the investigation of the ETV/PEA3 family of transcriptional activators and the oxidative stress response activator ATF6 α in disease, such as metastatic cancer.^{7,8} Towards this end, we first sought to better understand the mechanistic details between Med25 and its binding partners. This was accomplished using a mutagenesis strategy designed to selectively inhibit a single Med25 binding, PrOF and HSQC NMR methodologies. Through this process, we demonstrated that discrete protein partners of Med25 AcID interact with unique binding profiles and signatures that could be exploited during the small molecule discovery process. Following these analyses, several small molecules that target Med25 AcID were characterized and developed as inhibitors of this coactivator motif. These identified molecules will enable

for future study of the role of Med25 AcID in cellular contexts, including in model systems of cancer and disease.

B. Conclusions

The bulk of this thesis, as described in Chapters Two and Three, has focused on the investigation of Med25 AcID and its underlying mechanistic biochemistry. Prior to this dissertation, structural data of Med25 AcID in complex with the two canonical VP16 TADs, termed VP16 H1 and VP16 H2, had been reported.^{9,10} These data demonstrated that Med25 AcID contained two putative binding sites, termed the H1 and H2 sites. Chapter Two identified the minimal regions of ATF6 α and CBP that bind Med25 AcID and subsequent HSQC NMR suggested that ATF6 α (40-66) likely bound at the H2 site of Med25 AcID while CBP(20-44) did not interact specifically at either one of these two previously reported H1 or H2 binding sites. Chapter Two then described a strategy to selectively inhibit the H1 and H2 sites of Med25 AcID. Inhibition at the H1 site was accomplished through the introduction of negative charge using protein mutagenesis and peptide Tethering at a solvent-exposed cysteine near the H1 site; The H2 site was inhibited using protein mutagenesis to introduce negative charge. Collectively, experiments to block the H2 site suggested that binding at the H2 site is more dependent on electrostatic interactions and 'hot spot' residues than the H1 site. This suggests that the H2 is likely to be a more druggable interface than the H1 site.

Chapter Three described a strategy for studying Med25 AcID and its protein-protein and protein-ligand interactions using PrOF NMR. 3-fluorotyrosine (3FY) and 5-fluorotryptophan (5FW) were successfully incorporated into Med25 AcID, providing

two model systems for study. The precise refinement of binding locations, relative affinities between differing binding sites, and binding stoichiometry for each Med25 AcID interaction were described using PrOF NMR, HSQC NMR, and analyses from the mutagenesis study to block the H1/H2 sites. These data demonstrated that Med25 AcID interacts with discrete activators using multiple mechanisms. As demonstrated in Figure 5.1, ERM binds selectively at the H1 site of Med25 AcID at substoichiometric concentrations; ATF6 α binds selectively at the H2 site of Med25 AcID; VP16 binds at both sites simultaneously. The observed level of selectivity between the two sites demands logical questions to be answered in the future. Are the two sites differentially regulated in normal tissues? In disease states? Can multiple activators bind to the protein simultaneously in the cell?

Chapters Three and Four described the identification and biochemical characterization of several small molecules that target Med25 AcID and its PPI network. PrOF NMR was leveraged to gain mechanistic insight into the Med25-related function of the small molecule fragment, A6, and a natural product compound, norstictic acid. Additionally, PrOF NMR of 3FY Med25 AcID was utilized for the screening of a small molecule fragment library that identified nine lead compounds for future study. Finally, a novel natural product, termed 34913 lipopeptide, was identified as a potent and selective inhibitor of Med25 AcID. This molecule, thought to mimic the structure of a transcriptional activation domain (TAD), interacts with Med25 AcID in a binding mode that is nearly identical to that of the ATF6 α activation domain. Furthermore, it demonstrates effective inhibition of the Med25-ATF6 α PPI in a cellular context, indicating that it could be exploited in future experiments to investigate Med25 and its PPI network in disease.

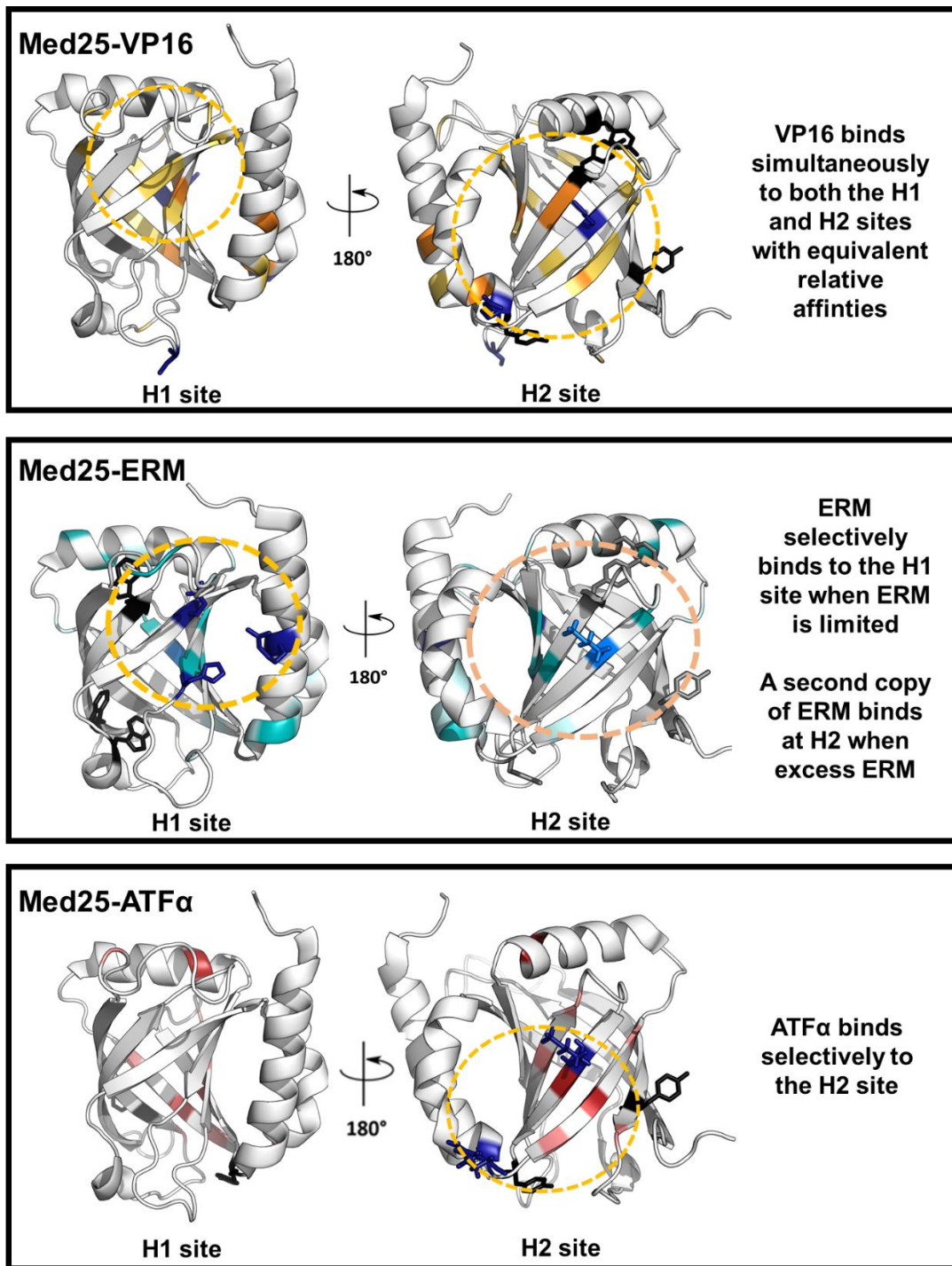


Figure 5.1. Three critical activators bind Med25 AcID in three unique binding modes. For each Med25-activator interaction shown, proposed binding locations are shown by golden circles. Data that informs the conclusions presented are indicated as Med25 residues that are significantly perturbed in HSQC NMR (VP16 – shades of orange; ERM – shades of teal; ATF6α – shades of pink), ProOF NMR (black, as sticks), and in the mutagenesis study (dark blue, as sticks) are shown. Detailed figure captions and discussions can be found in Chapter Three (Fig 3.18, 3.19, 3.20) (PDB 2XNF)

C. Future Directions

34913 lipopeptide will be used to study the role of Med25 in ATF6 α transcriptional processes the unfolded protein response

Under normal cellular conditions, the transcriptional activator ATF6 α is a transmembrane protein found in the endoplasmic reticulum (ER). However, conditions of oxidative stress cause cleavage of ATF6 α and subsequent translocation to the nucleus.¹¹ Once in the nucleus, ATF6 α activates pro-survival and anti-apoptotic genes associated with the unfolded protein response (UPR), most notably GRP78.^{12,13} As a key player in the UPR, induction of GRP78 acts to suppress oxidative stress and misfolding of proteins while stabilizing intracellular calcium levels.¹⁴ Collectively, these actions lead to protection of the cell from apoptosis during times of external stress. It is thus unsurprising that expression of GRP78 is held at low levels under normal cellular conditions while being strongly overexpressed in many disease states, such as in cancerous tumors.^{15,16} This overexpression represents an inherent mechanism through which cancer cells can resist apoptosis; indeed, GRP78 overexpression resulting from increased ATF6 α activity protects cancer cells from apoptosis in model systems.¹⁷ Additionally, increased activity of ATF6 α and expression of GRP78 has been indicated in both metastasis and disease relapse in Hodgkin's lymphoma, breast, and liver cancers.¹⁸⁻²¹ Thus, disruption of ATF6 α activity and the anti-apoptotic pathways of the UPR through small molecule inhibition of the Med25-ATF6 α could be therapeutically beneficial in sensitizing cancer cells towards apoptosis (Figure 5.2).

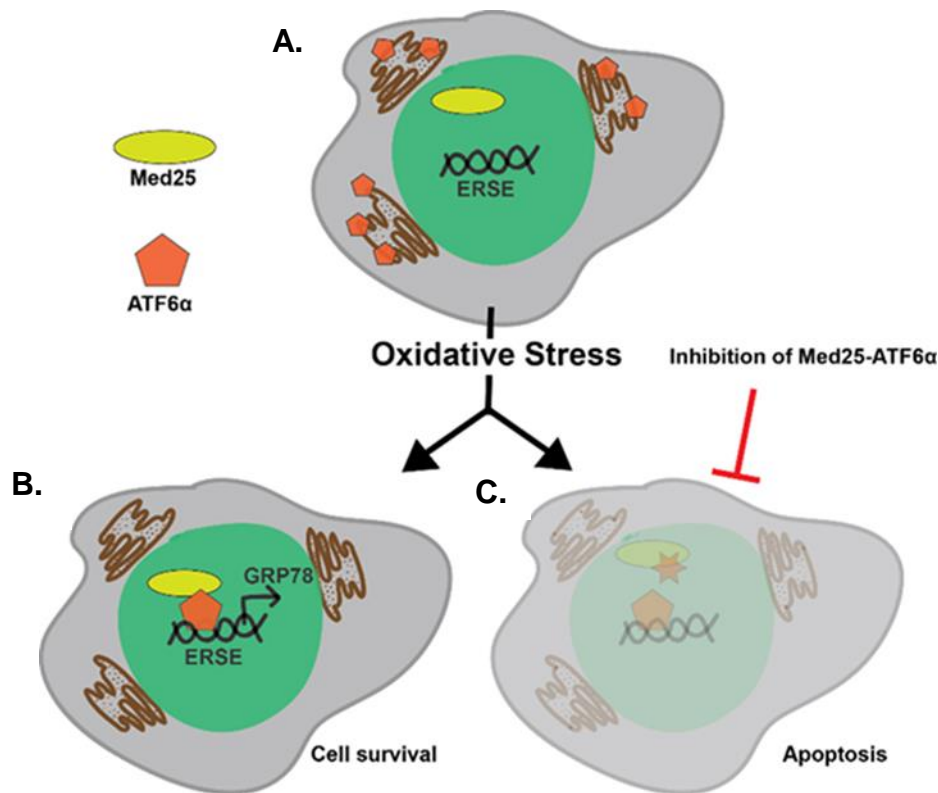


Figure 5.2. Activation of ATF6 α and GRP78 (A) Under normal cellular conditions, ATF6 α is a transmembrane protein found in the endoplasmic reticulum (ER). (B) Oxidative stress, such as hypoxia in cancer cells, causes ATF6 α to translocate to the nucleus where it binds to ERSE promoters. An interaction between ATF6 α and Med25 leads to activation of anti-apoptotic genes associated with the UPR, notably GRP78. (c) It is hypothesized that molecular inhibition of the Med25-ATF6 α PPI represents a viable target for the inhibition of ATF6 α -related, anti-apoptotic pathways of the UPR in hypoxic cancers and would sensitize cancer cells to apoptosis.

As described in Chapter 4, we have identified a novel natural product, termed the 34913 lipopeptide, as a potent and selective inhibitor of Med25 AcID *in vitro* that binds to the AcID domain with a binding signature that is nearly identical to that of the ATF6 α TAD. Additionally, we have demonstrated that this molecule inhibits the expression of the ATF6 α target gene GRP78 under hypoxic conditions. To test the hypothesis that the 34913 lipopeptide is functioning by specifically targeting the Med25-ATF6 α PPI (as opposed to causing downregulation of GRP78 through some other avenue), we plan to test the inhibitory capability of 34913 lipopeptide towards additional ATF6 α gene products

that are involved in the unfolded protein response (e.g. p58, HYOU1, CRT-1, and GRP9449)⁸. Selectivity for targeting the Med25-ATF6 α PPI in the context of the unfolded protein response (UPR) will then be assessed by determining the effects of the 34913 lipopeptide towards gene targets that are upstream of IRE1 and PERK, the other primary transcriptional activators involved in the UPR²². It is expected that the lipopeptide will show no effect on these pathways, indicating that it functions to selectively target the Med25 AcID-ATF6 α PPI.

We also plan to assess the ability of 34913 lipopeptide to decrease cancer cell viability and proliferation as determined using WST-1 assays, cellular migration as determined using a wound healing assay, and cancer invasion as determined using a Matrigel invasion assay. Since the UPR is ubiquitous in cancer cells and its role in differing cell types is not well understood, it would be useful to perform these phenotypic assays in multiple cancer cell types (e.g. breast, liver, Hodgkin's lymphoma, and head and neck). Additionally, 34913 lipopeptide could be tested for its ability to sensitize hypoxic cancer cells towards apoptosis through combination treatments with common cytotoxic agents (e.g. cisplatin, doxorubicin) in common cancer cell lines as well as drug-resistant cell lines (e.g. cisplatin-resistant A2780 cells²³).

The role of PTOV1 will be determined through the biochemical study of its AcID domains

The AcID motif is highly unique to Med25; Based on primary structure, only one other protein, Prostate Tumor Overexpressed factor 1 (PTOV1), has been proposed to contain an AcID domain. However, unlike Med25, PTOV1 contains *two* AcID domains in tandem (Figure 5.3). PTOV1 was originally reported as a protein that was overexpressed

in primary tumors of advanced and early prostate cancer patients^{24,25}. It has been since been discovered that PTOV1, while undetectable in most normal cell tissues, is overexpressed in a wide variety of early- and late-stage cancer types²⁶. Reports suggest that PTOV1 functions as a negative regulator of Med25 AcID function by competing for interaction with the N-terminal region of CBP²⁷. These publications demonstrate that a chemical biology-focused study of the AcID motifs of PTOV1 could provide excellent insight into Med25 function and its mechanisms of regulation within normal and disease contexts. Additionally, the PTOV1 AcID domains could represent an excellent model system against which to study selectivity within this unique structural class of coactivation domains. However, prior to this dissertation, the excised AcID domains of PTOV1 had not been biochemically characterized.

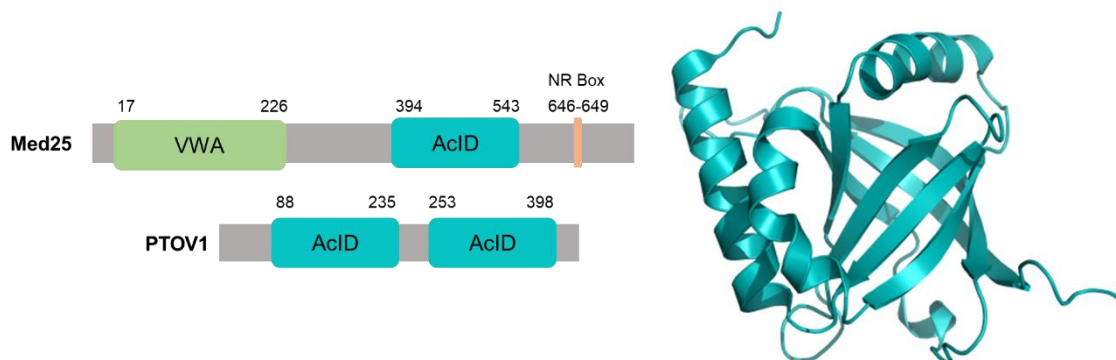


Figure 5.3. Domain architecture of PTOV1 and structure of the AcID motif. At left, domain architecture of Med25 (one AcID motif) and PTOV1 (two AcID motifs). At right, cartoon image of Med25 AcID to demonstrate central β -barrel with three surrounding α -helices. (PDB 2XNF)

The AcID motifs of PTOV1, termed AcID-A (residues 88-235) and AcID-B (residues 253-398) share homology with the AcID motif of Med25 (81% identity to AcID-A and 72% to AcID-B). However, many of the differences between the primary sequences of Med25 AcID and the PTOV1 AcID domains lie within the H1 and H2 binding sites. We

plan to investigate the role of PTOV1 and its interplay with Med25, biochemical characterization of each of the two AcID motifs, AcID-A and AcID-B, was desired. Neither domain had been previously expressed as a standalone protein construct.

Multiple attempts to express and purify PTOV1 AcID-A and AcID-B were unsuccessful. A variety of gene constructs of differing lengths and with a variety of solubility tags (*e.g.* Glutathione S-transferase) were attempted. In the end, codon-optimized genes for each PTOV1 AcID motif were designed into pET21-b plasmids and purchased (Genscript). As demonstrated in Figure 5.4, this strategy provided purified PTOV1 AcID-A and PTOV1 AcID-B that was well-folded according to circular dichroism. Additionally, both PTOV1 AcID motifs demonstrated equivalent stability relative to Med25 AcID in thermal melting experiments (T_m of 63 ± 1 °C and 66 ± 1 °C for AcID-A and AcID-B, respectively, compared to 65 ± 1 °C for Med25 AcID). Preliminary FP assays with both PTOV1 AcID domains suggest that both bind each of the Med25 AcID-interacting peptide ligands with similar affinities to Med25 AcID.

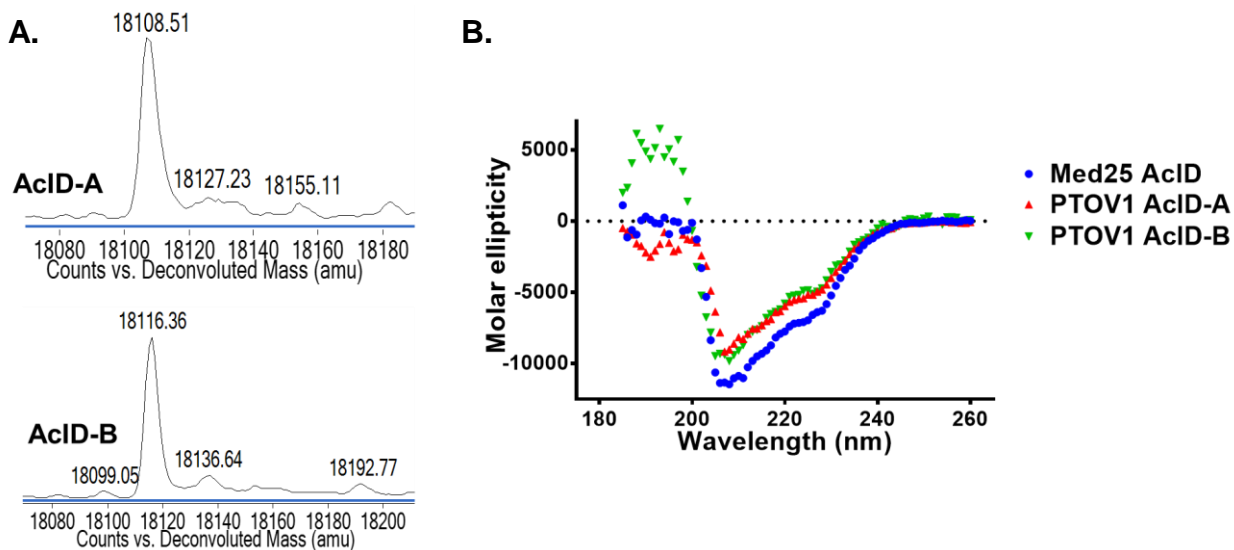


Figure 5.4. Production of PTOV1 AcID-A and AcID-B. (A) Deconvoluted mass spectra of PTOV1 AcID-A and AcID-B. (B) Circular dichroism spectra of all three AcID domains. Data were collected with Julie Garlick and Olivia Pattelli (University of Michigan).

These data demonstrating the production of functional AcID domains from PTOV1 offer a new avenue for future investigation into the AcID domain. While it currently unknown whether these excised domains can recapitulate the function of full-length PTOV1 either alone or in trans, this represents a critical first step towards answering this question. Future work will be performed to study the excised PTOV1 AcID domains using HSQC and PrOF NMR to assess any minor differences from the Med25 AcID structure. In addition, these AcID motifs will be valuable in small molecule inhibition studies to determine if the three AcID motifs can be selectively targeted.

D. Materials and Methods

Plasmids

pET21b plasmids that encoded for PTOV1(88-235), termed 'PTOV1 AcID-A', and PTOV1(253-398), termed 'PTOV1 AcID-B', were purchased from Genscript.

Previously described methods

Relevant methods that were previously described in Chapter Two include mass spectroscopy of proteins, FP binding experiments, circular dichroism, thermal melts, and solid-phase peptide synthesis.

Expression and purification of PTOV1 AcID domains

Protein expression was completed as described for Med25 AcID.

Cell pellets were thawed and resuspended with 30-35 ml Lysis Buffer (50 mM phosphate, 300 mM NaCl, 10 mM imidazole, pH 7.2). β -mercaptoethanol, at 1:1000 dilution, and one cComplete, Mini, EDTA-free Protease Inhibitor tablet (Sigma-Aldrich) were added to the resuspended cell pellet. To lyse, the cells were sonicated on ice for 4-6 min (Cycle - 3 seconds on, 7 seconds off) and/or until the cells had observable change in color (lighter brown) and viscosity. Following sonication, the lysed pellet in 50 mL conical tube(s) was centrifuged at 9,500 RPM for 30 min at 4 °C. Concurrent with centrifugation of cells, 500 μ l of TALON Cobalt resin per 12 mL of cell lysate were washed three times with DI water. After centrifugation of the cell lysate, the supernatant was added to the washed TALON Cobalt resin and incubated for 1 hour at 4 °C. The resin was then centrifuged at 2500 RPM for 2 min at 4 °C before being washed five times with wash

buffer (50 mM phosphate, 300 mM sodium chloride, 30 mM imidazole, pH 6.8). The resin was centrifuged at 2500 RPM for 1 min at 4 °C between washes. After the washing step, protein was incubated with 1 mL of elution buffer (50 mM phosphate, 300 mM sodium chloride, 400 mM imidazole, pH 6.8) per 500 µl of TALON Cobalt resin for 30 min at 4 °C. The resin was centrifuged at 2500 RPM for 1 min at 4 °C and the protein supernatant containing PTOV1 AcID was saved. This elution step was repeated a total of three times. Fractions containing PTOV1 AcID were pooled and subjected to further purification using a Source S 5 mL HiTrap column using an AKTA pure FPLC chromatography system, as previously described.

E. References

1. Thompson, A. D., Dugan, A., Gestwicki, J. E. & Mapp, A. K. Fine-Tuning Multiprotein Complexes Using Small Molecules. *ACS Chem. Biol.* **7**, 1311–1320 (2012).
2. Cesa, L. C., Mapp, A. K. & Gestwicki, J. E. Direct and Propagated Effects of Small Molecules on Protein–Protein Interaction Networks. *Front. Bioeng. Biotechnol.* **3**, (2015).
3. Majmudar, C. Y. *et al.* Sekikaic Acid and Lobaric Acid Target a Dynamic Interface of the Coactivator CBP/p300. *Angew. Chem. Int. Ed.* **51**, 11258–11262 (2012).
4. Hollis, A., Sperl, B., Gräber, M. & Berg, T. The Natural Product Betulinic Acid Inhibits C/EBP Family Transcription Factors. *ChemBioChem* **13**, 302–307 (2012).
5. Gee, C. T., Koleski, E. J. & Pomerantz, W. C. K. Fragment Screening and Druggability Assessment for the CBP/p300 KIX Domain through Protein-Observed ¹⁹F NMR Spectroscopy. *Angew. Chem. Int. Ed.* **54**, 3735–3739 (2015).
6. Urick, A. K. *et al.* Dual Screening of BPTF and Brd4 Using Protein-Observed Fluorine NMR Uncovers New Bromodomain Probe Molecules. *ACS Chem. Biol.* **10**, 2246–2256 (2015).
7. Aytes, A. *et al.* ETV4 promotes metastasis in response to activation of PI3-kinase and Ras signaling in a mouse model of advanced prostate cancer. *Proc. Natl. Acad. Sci.* **110**, E3506–E3515 (2013).
8. Backer, M. V., Backer, J. M. & Chinnaiyan, P. Targeting the Unfolded Protein Response in Cancer Therapy. in *Methods in Enzymology* **491**, 37–56 (Elsevier, 2011).
9. Vojnic, E. *et al.* Structure and VP16 binding of the Mediator Med25 activator interaction domain. *Nat. Struct. Mol. Biol.* **18**, 404–409 (2011).
10. Milbradt, A. G. *et al.* Structure of the VP16 transactivator target in the Mediator. *Nat. Struct. Mol. Biol.* **18**, 410–415 (2011).
11. Haze, K., Yoshida, H., Yanagi, H., Yura, T. & Mori, K. Mammalian transcription factor ATF6 is synthesized as a transmembrane protein and activated by proteolysis in response to endoplasmic reticulum stress. *Mol. Biol. Cell* **10**, 3787–3799 (1999).
12. Yoshida, H. *et al.* ATF6 activated by proteolysis binds in the presence of NF-Y (CBF) directly to the cis-acting element responsible for the mammalian unfolded protein response. *Mol. Cell. Biol.* **20**, 6755–6767 (2000).
13. Wang, Y. *et al.* Activation of ATF6 and an ATF6 DNA binding site by the endoplasmic reticulum stress response. *J. Biol. Chem.* **275**, 27013–27020 (2000).
14. Chen, J. J. *et al.* ATF6 Activation Reduces the Secretion and Extracellular Aggregation of Destabilized Variants of an Amyloidogenic Protein. *Chem. Biol.* **21**, 1564–1574 (2014).
15. Fernandez, P. M. *et al.* Overexpression of the glucose-regulated stress gene GRP78 in malignant but not benign human breast lesions. *Breast Cancer Res. Treat.* **59**, 15–26 (2000).

16. Xia, F. *et al.* Glucose-regulated protein 78 and heparanase expression in oral squamous cell carcinoma: correlations and prognostic significance. *World J. Surg. Oncol.* **12**, 121 (2014).
17. Jamora, C., Dennert, G. & Lee, A. S. Inhibition of tumor progression by suppression of stress protein GRP78/BiP induction in fibrosarcoma B/C10ME. *Proc. Natl. Acad. Sci. U. S. A.* **93**, 7690–7694 (1996).
18. Schewe, D. M. & Aguirre-Ghiso, J. A. ATF6alpha-Rheb-mTOR signaling promotes survival of dormant tumor cells in vivo. *Proc. Natl. Acad. Sci. U. S. A.* **105**, 10519–10524 (2008).
19. Dong, D. *et al.* A critical role for GRP78/BiP in the tumor microenvironment for neovascularization during tumor growth and metastasis. *Cancer Res.* **71**, 2848–2857 (2011).
20. Chang, K.-C., Chen, P. C.-H., Chen, Y.-P., Chang, Y. & Su, I.-J. Dominant expression of survival signals of endoplasmic reticulum stress response in Hodgkin lymphoma. *Cancer Sci.* **102**, 275–281 (2011).
21. Ac, R., L, Z., Ap, A. & Ja, A.-G. Functional coupling of p38-induced up-regulation of BiP and activation of RNA-dependent protein kinase-like endoplasmic reticulum kinase to drug resistance of dormant carcinoma cells., Functional Coupling of p38-Induced Up-regulation of BiP and Activation of RNA-Dependent Protein Kinase-Like Endoplasmic Reticulum Kinase to Drug Resistance of Dormant Carcinoma Cells. *Cancer Res.* **66**, 1702, 1702–1711 (2006).
22. Lee, J. & Ozcan, U. Unfolded Protein Response Signaling and Metabolic Diseases. *J. Biol. Chem.* **289**, 1203–1211 (2014).
23. Rixe, O. *et al.* Oxaliplatin, tetraplatin, cisplatin, and carboplatin: spectrum of activity in drug-resistant cell lines and in the cell lines of the National Cancer Institute's Anticancer Drug Screen panel. *Biochem. Pharmacol.* **52**, 1855–1865 (1996).
24. Bénédict, P. *et al.* PTOV1, a novel protein overexpressed in prostate cancer containing a new class of protein homology blocks. *Oncogene* **20**, 1455 (2001).
25. Santamaría, A. *et al.* PTOV-1, a novel protein overexpressed in prostate cancer, shuttles between the cytoplasm and the nucleus and promotes entry into the S phase of the cell division cycle. *Am. J. Pathol.* **162**, 897–905 (2003).
26. Fernández, S. *et al.* PTOV1 is overexpressed in human high-grade malignant tumors. *Virchows Arch.* **458**, 323–330 (2011).
27. Youn, H.-S., Park, U.-H., Kim, E.-J. & Um, S.-J. PTOV1 antagonizes MED25 in RAR transcriptional activation. *Biochem. Biophys. Res. Commun.* **404**, 239–244 (2011).

Appendix

A. The identification of a CBP-CBP protein-protein interaction presents a potential mechanism for the regulation of CBP function

In Chapter Two of this dissertation, the identification of an N-terminal sequence of CBP that interacts specifically with Med25 AcID was described. This sequence of CBP shares high homology with the transcriptional activation domain (TAD) of VP16 and, as a result, was suspected to function as a TAD mimic (Figure A.1).

```
CBP      20-PGFSANDSTDFGSL----FDLENDLPDELI-44
VP16    454-PGFTPHDSAPYGALDMADEFEFEQMFTDALG-486
```

Figure A.1. Sequence alignment of CBP(20-44) and VP16(454-486). A basic local alignment search of CBP(1-460) demonstrated that CBP(20-44) was homologous to the VP16 H2 transcriptional activation domain. CBP(20-44) shares numerous acidic and hydrophobic residues in common with the VP16 sequence.

Following the investigation of the CBP(20-44) and its proximal downstream residues and its interaction with Med25 AcID, it was hypothesized that this TAD-like sequence of CBP could also function to interact specifically with other coactivation domains. A panel of CBP-derived peptides, labeled with N-terminal fluorescein, were synthesized and tested for binding to CBP KIX, as had been performed with Med25 AcID (Figure A.2). The supposition that CBP(20-44) could interact specifically with CBP KIX was demonstrated to be correct, as CBP(20-44) and CBP(20-55) bound to the CBP KIX domain with dissociation constants of $37 \pm 2 \mu\text{M}$ and $49 \pm 6 \mu\text{M}$, respectively, by fluorescence polarization (FP).

CBP sequence

20 55

| |

PGFSAN DSTDFGSLFDLENDLPDELIPNGGELGLLN

<u>CBP peptide</u>	<u>Binding affinity (K_D)</u>
20-44	37 ± 2 μM
20-55	49 ± 6 μM
33-55	75 ± 9 μM
50-64	>250 μM
59-76	>250 μM

Figure A.2. CBP-derived peptides bind to the KIX domain of CBP. The sequence of CBP from residues 20-55 is shown; Acidic (red) and hydrophobic (green) residues are indicated. CBP(20-44) and CBP(20-55) bind to the CBP KIX domain with dissociation constants of $37 \pm 2 \mu\text{M}$ and $49 \pm 6 \mu\text{M}$, respectively, by fluorescence polarization. Data reported are average and standard deviations of triplicates.

Several TADs have been shown to interact with CBP KIX through a phosphorylation-dependent mechanism, including the KID domain of CREB, p53, and FOXO3a.¹⁻⁴ Each of these proteins interact with CBP with relevant affinities after their TAD sequences have become phosphorylated. Noting that the CBP(20-44) sequence contained two Ser residues that are part of predicted recognition sites for casein kinase II, we synthesized a variant of CBP(20-44) peptide to contain phosphoserine at the 23 and 32 positions.^{5,6} Subsequent FP assays determined that this phosphorylated variant bound to CBP KIX with a nearly 2-fold increase in binding affinity (K_D of $19 \pm 2 \mu\text{M}$ for the doubly phosphorylated variant compared to $35 \pm 2 \mu\text{M}$), suggesting that phosphorylation may play a role in regulating this interaction. Interestingly, this doubly phosphorylated

CBP(20-44) also bound Med25 with an affinity that was 4-fold tighter than the non-phosphorylated variant (K_D of $0.25 \pm 0.01 \mu\text{M}$ compared to $1.1 \pm 0.1 \mu\text{M}$).

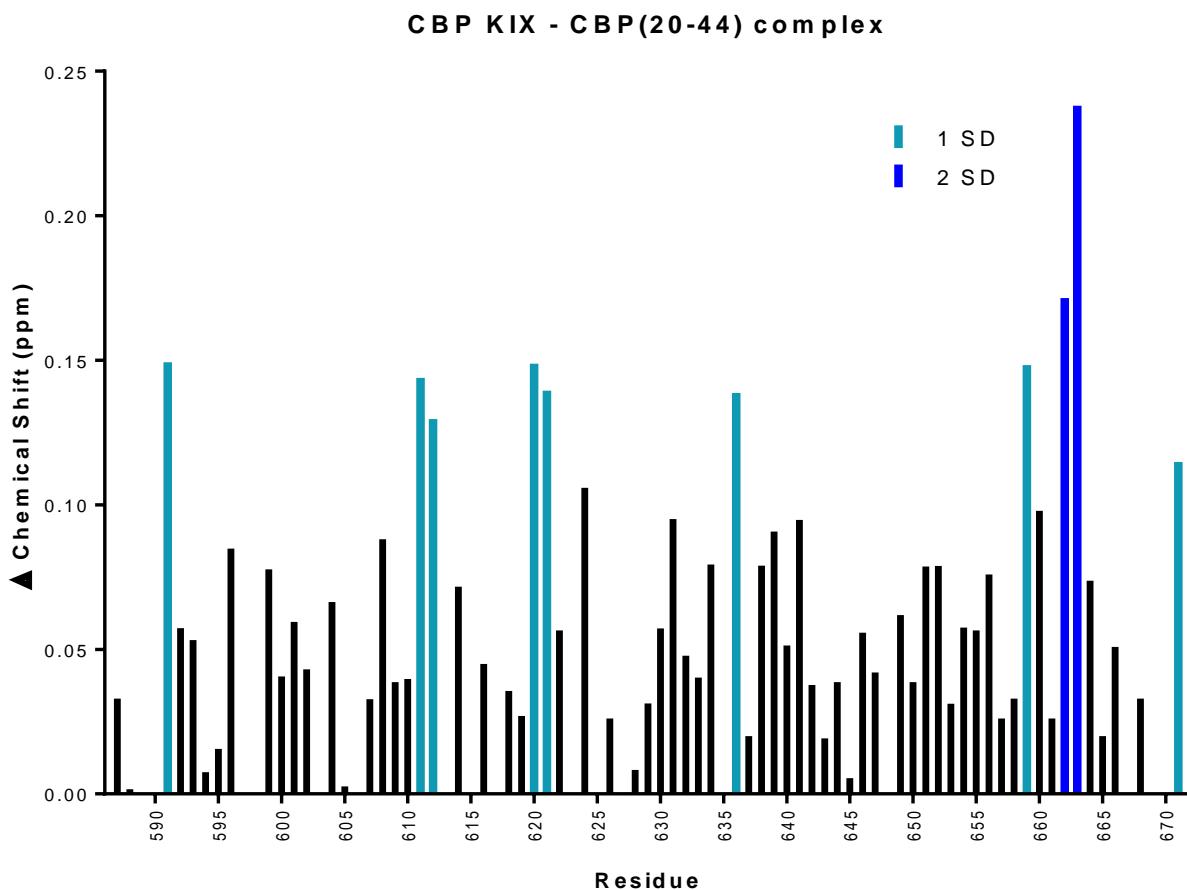


Figure A.3. Chemical shift perturbations within CBP KIX induced by complexation with CBP(20-44). The magnitude of chemical shift perturbations, in ppm, are shown upon complexation of ^{15}N CBP KIX with two equivalents CBP(20-44). Residues that shift 1-2 standard deviation (SD) above the mean (light blue) and >2 SD above the mean (dark blue) are considered to be significantly affected by CBP(20-44).

Following confirmation that CBP(20-44) bound to CBP KIX in FP experiments, ^1H - ^{15}N -HSQC experiments were performed to determine the binding location of the peptide ligand towards CBP KIX. Acetylated CBP(20-44) peptide was titrated into ^{15}N -labeled CBP KIX at 0, 1, and 2 equivalents of peptide relative to protein. This titration demonstrated dose-dependent chemical shift perturbations of backbone amide bonds of

selected CBP KIX residues (Figures A.3). These dose-dependent chemical shifts demonstrated that CBP(20-44) binds specifically to CBP KIX; additionally, these experiments demonstrated that CBP(20-44) does not affect the structural integrity and fold of the protein. Furthermore, these data demonstrated that CBP(20-44) binds selectively to the MLL site of CBP KIX, evidenced by the significant chemical shift perturbation of several residues (I611, F612, E636, K659, K662, E663) known to be important for the KIX-MLL interaction(Figure A.4).⁷

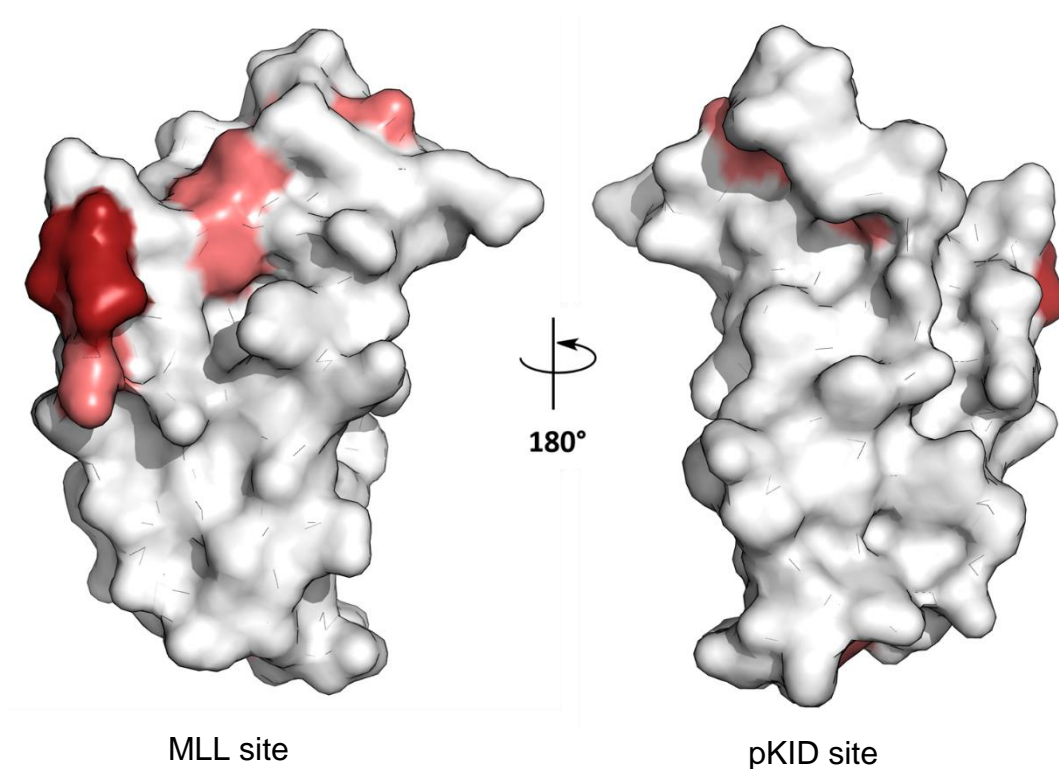


Figure A.4. Chemical shift perturbations induced by CBP(20-44) mapped on CBP KIX. Mapped onto the structure of CBP KIX (4I9O) are chemical shift perturbations upon binding to 2 eq. CBP(20-44) peptide. Residues that are perturbed by 1-2 standard deviations (SD) (pink) and >2 SD (red) are considered to be significantly affected by CBP(20-44).

As demonstrated, the minimally defined sequence of CBP that interacts with Med25 AcID mimics a canonical TAD (high concentration of acidic and hydrophobic amino acids across a predicted α -helix) and makes a specific contact with the MLL site of

CBP KIX. It is possible this interaction between CBP(20-44) and the KIX domain represents a novel mechanism through which CBP could be regulated. As described, phosphorylation of the CBP(20-44) peptide sequence at Ser23 and Ser32 caused a 2-fold increase in its affinity for the KIX domain. Both Ser23 and Ser32 are predicted to be phosphorylation sites for casein kinase II, a protein that is activated by Wnt signaling, a common dysregulated signaling pathway in cancer.^{8,9} It is hypothesized that phosphorylation of Ser23 and/or Ser32 by casein kinase II would increase the affinity of the N-terminus of CBP for the MLL site of the KIX domain (Figure A.5). This intra- or inter-molecular PPI and subsequent inhibition of the MLL site of the KIX domain would decrease the transcriptional output of MLL and other activators that target this site of the KIX domain.

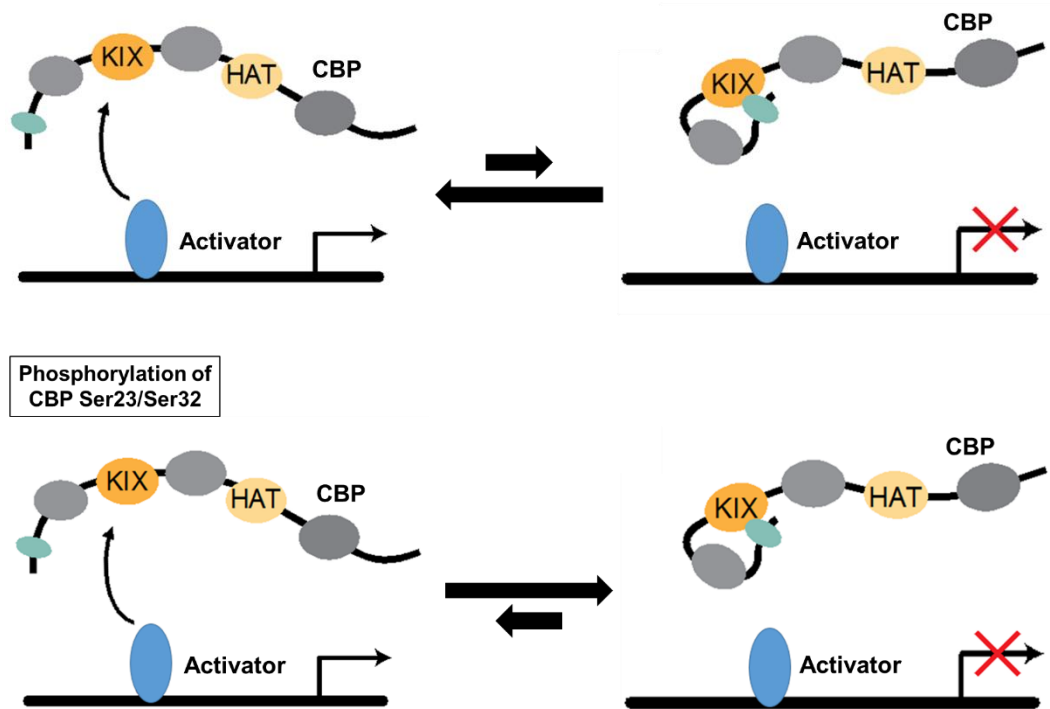


Figure A.5. Model for the CBP-CBP interaction. It is proposed that the KIX domain of CBP is in a binding equilibrium with the N-terminus of CBP and activators. (A) Under normal conditions, the higher relative affinities of KIX-activator interactions cause the equilibrium to reside in favor of KIX-activator interactions. (B) Phosphorylation of Ser23/Ser32 is proposed to shift the equilibrium towards the KIX-CBP interaction. Note that the indicated ratios between KIX-activator and KIX-CBP are arbitrary; Their purpose is to demonstrate the relative difference between the two scenarios.

B. An identified intramolecular salt bridge within Med25 AcID is likely important for Med25 function and stability

As is the case with many activator-coactivator interactions, electrostatic interactions have been demonstrated as a primary binding determinant for Med25 AcID and its protein-protein interactions (PPIs).¹⁰ It has been demonstrated that ten-fold increase the salt concentration of buffers used in fluorescence polarization (FP) experiments results in > 30-fold decreases in the binding affinity of VP16 peptides for Med25 AcID. Additionally, in Chapter 2, the introduction of negative charge within the H1 and H2 binding sites of Med25 disrupted the formation of Med25-peptide complexes. These data are consistent with Med25 AcID being dependent upon electrostatic interactions.

With this dependence on electrostatic contacts, it is likely that the protein itself would contain electrostatic salt bridges to assist with structural stability. Indeed, published NMR structures indicated that D529 and R466 are oriented such that they might form a salt bridge.¹¹⁻¹³ It should be noted that the distance between these two residues is beyond that of a traditional salt bridge interaction however, this region of Med25 AcID is dynamic and flexible and a crystal structure of Med25 has not been determined. It was hypothesized that the addition of a second mutation, D529R to R466D Med25 AcID, could partially recover WT Med25 AcID function. This would invert the proposed salt bridge interaction between residues 466 and 529.

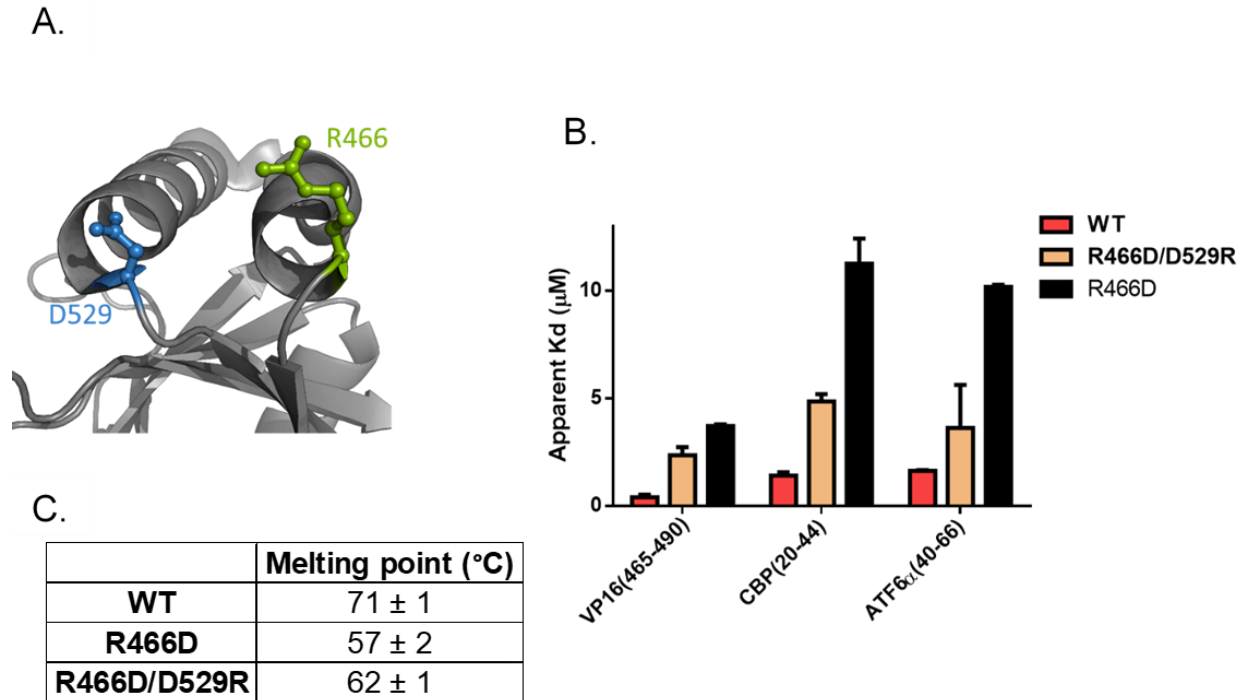


Figure A.6. Intramolecular salt bridge within Med25 Acid. (A) D529 and R466 are oriented to potentially form a stabilizing salt bridge between $\alpha 1$ and $\alpha 3$. (B) Binding affinities of Med25 variants against H2 site-interacting peptides, as measured by FP. Two sets of experiments were performed in triplicate. (C) Melting temperatures of Med25 variants determined by CD-observed thermal denaturation.

Following expression and purification of R466D/D529R Med25 Acid, FP assays and CD-observed thermal denaturation experiments were performed (Figure 2.16). R466D/D529R bound H2-interacting peptides VP16(467-488), CBP(20-44), and to ATF6 α (40-66) with binding affinities of 2.3 μ M, 4.8 μ M, and 3.6 μ M, respectively. These binding affinities are all >40% tighter than corresponding affinities towards R466D (VP16(467-488) - 3.7 μ M, CBP(20-44) - 11.3 μ M, ATF6 α (40-66) - 10.2 μ M) and likely represent a partial recovery of WT binding function. Completely regained WT function would have been unlikely, as the double mutant R466D/D529R does still place a negative charge in the middle of the presumed H2 binding site. CD-observed thermal denaturation experiments also supported the presence of a 466-529 salt bridge interaction. The single-

point R466D mutation caused a 19% decrease in melting temperature compared to WT Med25 AcID (57.0 ± 2.0 °C vs. 70.8 ± 1.3 °C); Restoration of the putative salt bridge with the R466D/D529R mutation restored 39% ($+5.4$ °C compared to R466D) of the lost thermal stability.

C. Garcinolic acid is an effective but non-selective inhibitor of Med25 AcID

Identification and initial selectivity screening of garcinolic acid

Garcinolic acid was discovered as a hit molecule in a competition-based FP high-throughput screening effort against the Med15 KIX-Pdr1 PPI performed using a small molecule library maintained by the Center for Chemical Genomics at the University of Michigan (Meg Breen, University of Michigan). During selectivity screening of this molecule, it was found to be a pan-inhibitor of several disparate coactivator motifs including, most notably for this thesis, Med25 AcID (Figure A.7 and Table A.1).

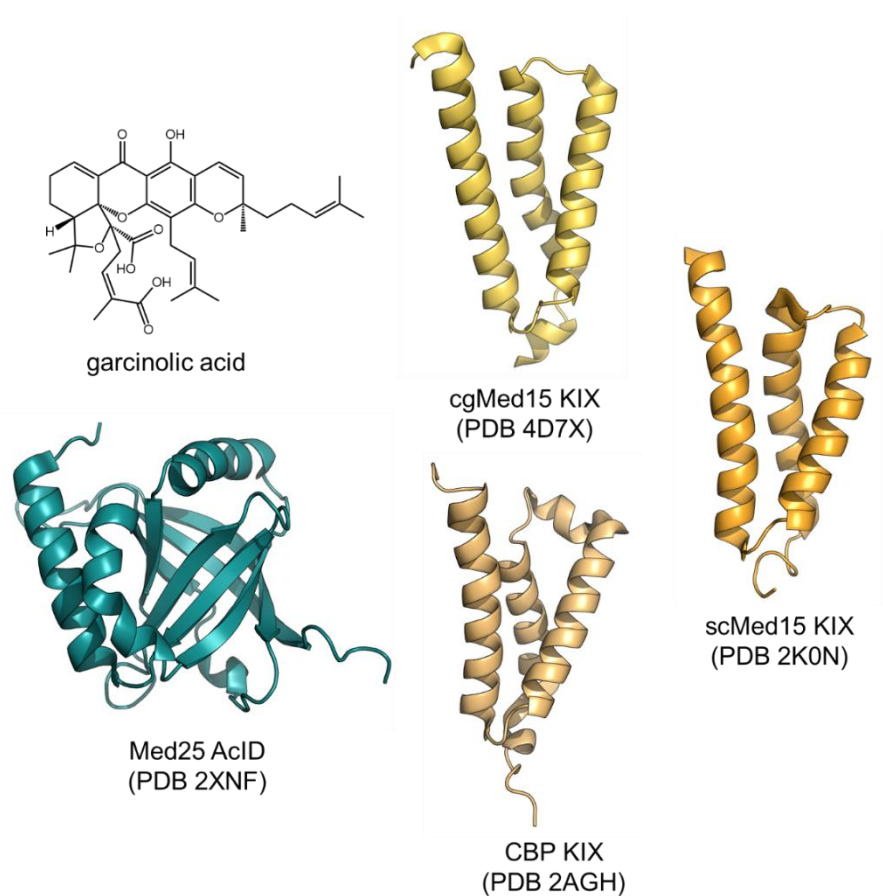


Figure A.7. Garcinolic acid targets several transcriptional coactivation domains. Structures of related – cgMed15 KIX (PDB 4D7X), scMed15 KIX (PDB 2K0N), CBP KIX (PDB 2AGH) – and unrelated – Med25 AcID (PDB 2XNF) – proteins whose function are inhibited by garcinolic acid.

Table A.1. Summary of the inhibitory effects of garcinolic acid. Half maximal inhibitory constants of garcinolic acid for tested coactivator-activator PPIs in FP assays. (Performed with Meg Breen and Sam DeSalle)

Coactivator domain	TAD peptide	IC ₅₀
scMed15 KIX	Pdr1	27 μM
cgMed15 KIX	Pdr1	59 μM
CBP KIX	MLL	3.3 ± 0.9 μM
CBP KIX	c-Myb	4.5 ± 1.0 μM
p300 KIX	MLL	4.6 ± 1.4 μM
p300 KIX	c-Myb	7.2 ± 1.8 μM
Med25 AcID	ATF6α	3.4 ± 0.6 μM
Med25 AcID	VP16 H1	4.9 ± 1.0 μM

While garcinolic acid was discovered using a HTS of *Saccharomyces cerevisiae* (sc) Med15 KIX and *Candida galbrata* (cg) Med15 KIX, it is more potent against Med25 AcID and the KIX motifs of CBP and p300. Garcinolic inhibited the Med25 AcID and CBP/p300 KIX domains with single-digit micromolar IC₅₀ values in FP assays. While this molecule does not offer selectivity between CBP/p300 KIX and Med25 AcID, it did provide a non-covalent and potent inhibitor of AcID function *in vitro* that could be leveraged for use in downstream cellular experiments to study AcID function *in cellulo* and *in vivo*. However, prior to cellular study, we wanted to establish whether garcinolic acid could selectively target a single site of either Med25 AcID and CBP/p300 KIX, as potential selectivity differences between unique *activators* of either coactivator domain would be beneficial during *in cellulo* experimental design and interpretation.

As described previously, both the CBP/p300 KIX and Med25 AcID motifs contain multiple binding sites responsible for interactions with unique transcriptional activators.

Additionally, both the CBP KIX and Med25 AcID domains share at least one common *in vitro* interacting partner, MLL (Data not shown). To provide secondary confirmation of these protein-ligand interactions and to determine the binding mode of garcinolic acid for each protein, ^1H ^{15}N -HSQC and PrOF NMR of the Med25 AcID-garcinolic acid and CBP KIX-garcinolic acid interactions were pursued. It was thought that these methodologies could test the hypothesis that garcinolic acid functions to potentially inhibit two structurally distinct coactivator motifs by mimicking a transcriptional activator and whether garcinolic acid selectively targets singular sites of both proteins.

Biochemical characterization of the Med25 AcID-garcinolic acid interaction

^1H - ^{15}N -HSQC experiments were performed in which garcinolic acid was complexed with ^{15}N -labeled Med25 AcID at 0, 1, 2, and 4 equivalents of small molecule relative to protein. This set of experiments demonstrated dose-dependent chemical shift perturbations and significant broadening of resonances that represented many Med25 AcID residues (Figures A.8, A.9, A.10). As with previous HSQC experiments with Med25 AcID, peaks in all of the collected spectra were assigned to specific residues using both a previously published NMR assignment¹¹ and a *de novo* assignment performed by Andy Henderson (University of Michigan). Residues that demonstrated a dose-dependent and statistically significant (>1 standard deviation above the mean) chemical shift perturbation were almost exclusively located within the H2 site of Med25, indicating that garcinolic acid likely bound within this region of the protein. Specifically, significantly perturbed residues were located across the lengths of β 5, β 4, β 7, and β 6, along α 1, and near the C-terminal end of α 2 (L457, G462, L464, R466, M470, F473, H474, M490, G496, M512, L514, K520,

F522, M523, N535). In addition to resonances that were significantly perturbed, several residues were completely broadened into noise at all tested concentrations of garcinolic acid. These residues – 471, 472, 513, 516, 524, and 529 – were within the ‘bottom’ of the H2 site (away from $\alpha 2$) except for D529, located on the loop between $\beta 7$ and $\alpha 3$. Collectively, these experiments demonstrated that garcinolic acid is likely making direct contact with Med25 AcID at the portion of H2 face away from $\alpha 2$. The large number of resonances that are broadened into noise, even at the lowest concentration of garcinolic acid, suggested a highly specific and tight affinity interaction.

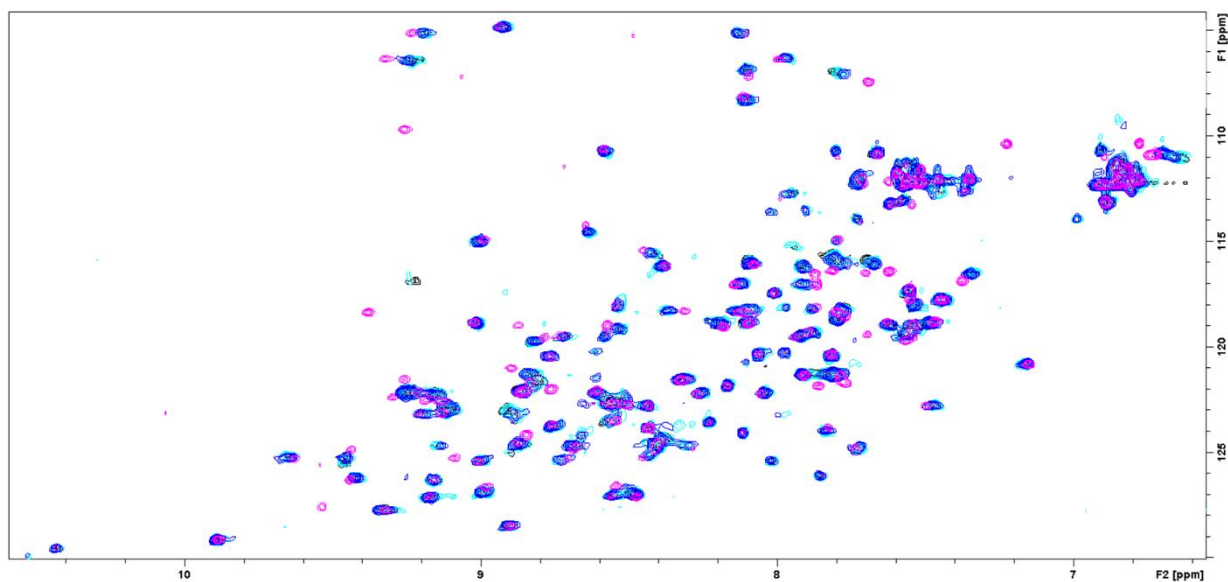


Figure A.8. ¹H-¹⁵N-HSQC NMR spectra of Med25 AcID-garcinolic acid complexes. Overlay of the HSQC spectra of ¹⁵N-labeled Med25 AcID with DMSO (pink), one equivalent of garcinolic acid (dark blue), two equivalents (light blue), and four equivalents (black) is shown.

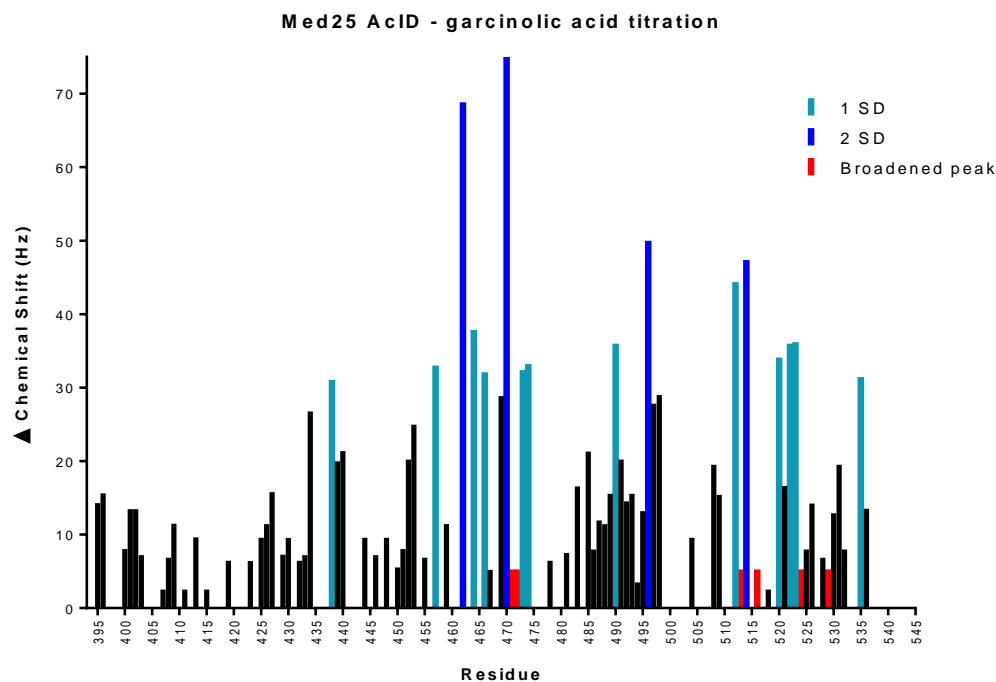


Figure A.9. Chemical shift perturbations within Med25 AcID induced by saturating garcinolic acid conditions. The magnitude of chemical shift perturbations, in Hz, are shown upon saturation of ^{15}N Med25 AcID with four eq garcinolic acid. Residues that shift 1-2 standard deviation (SD) above the mean (light blue), >2 SD (dark blue), and that broaden into noise (red) are significantly perturbed.

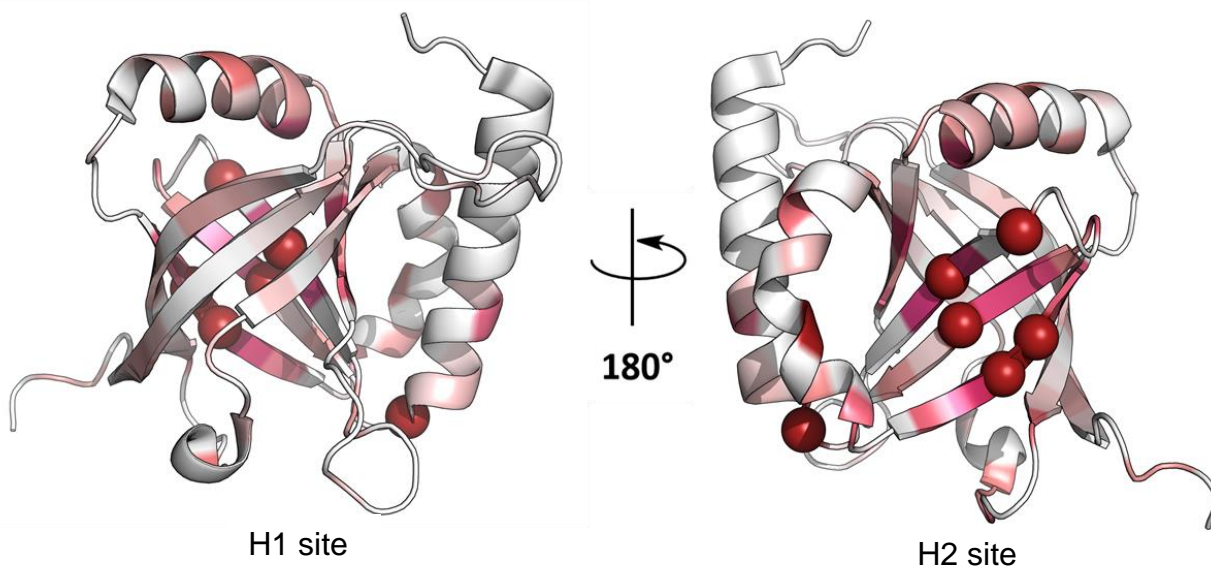


Figure A.10. Chemical shift perturbations induced by garcinolic acid mapped on Med25 AcID. Mapped onto the structure of Med25 AcID are chemical shift perturbations upon binding to four eq. garcinolic acid. Increasing shades of red indicate a gradient of increasing chemical shift perturbations. Red balls indicate residues that show complete peak broadening.

PrOF NMR spectra of 3FY Med25 AcID in complex with increasing concentrations of garcinolic acid (0, 0.1, 0.5, 1 and 2 equivalents of small molecule relative to protein) were collected (Figure A.11). As anticipated based on the HSQC results, garcinolic acid affected 3FY Med25 similarly to other H2 site ligands (*e.g.* ATF6 α (40-66) peptide) with perturbations of all four Tyr residues. However, not all residues shifted in an apparent dose-dependent manner. Y528 and Y432 behaved in a typical fashion for Med25 AcID ligands with incremental chemical shift perturbations as garcinolic acid was increasing added into 3FY Med25 AcID. The Y487/Y515 pair did not appear to share this typical behavior. These two resonances were slightly broadened at 0.1 and 0.5 eq. garcinolic acid but only Y487 demonstrated relatively minor (for this resonance) chemical shift perturbations. Then, starting at 1 eq. garcinolic acid, both the Y487 and Y515 resonances demonstrated large upfield perturbations. These results could represent two discrete binding modes for garcinolic acid interacting with Med25 AcID, indicating that garcinolic acid might adopt multiple orientations with the H2 site or that garcinolic acid might bind with a 2:1 stoichiometry at the H2 site.

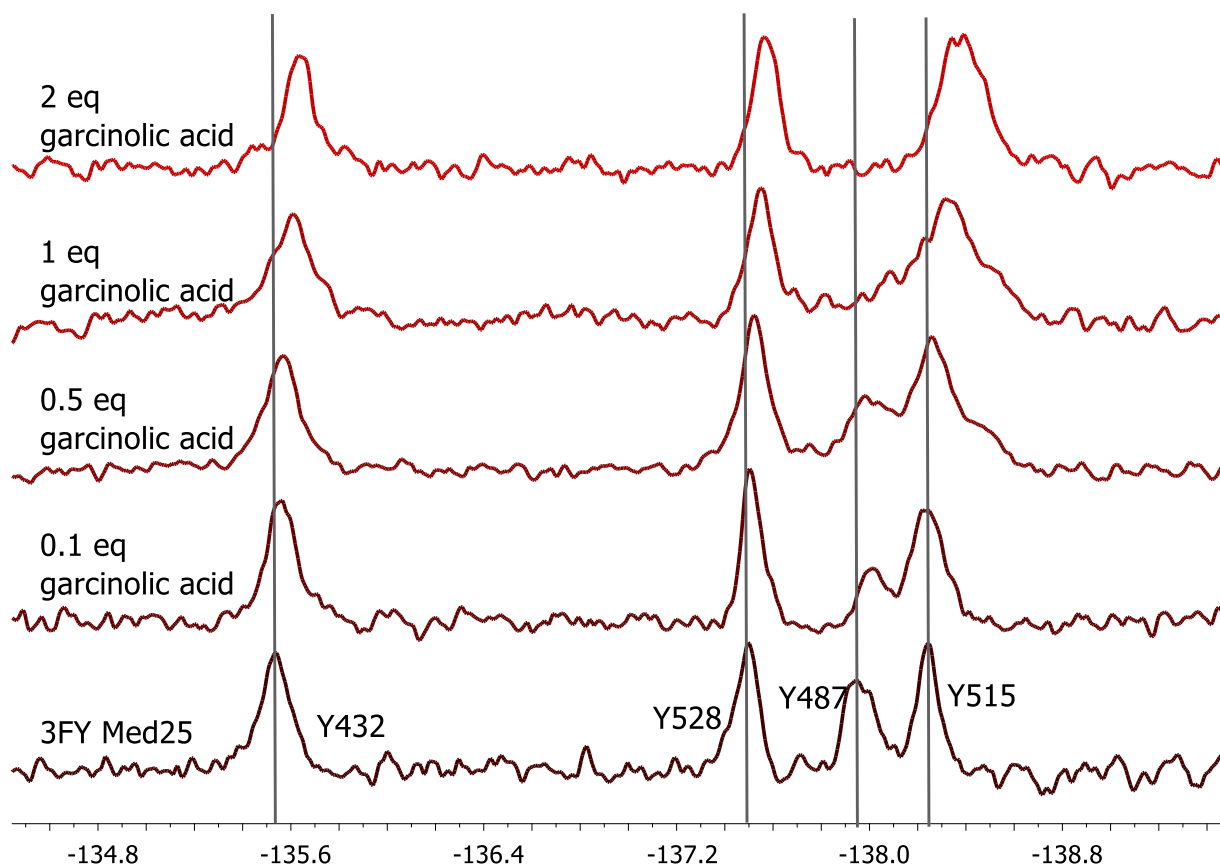


Figure A.11. PrOF NMR of 3FY Med25 AcID in complex with garcinolic acid. Spectral analysis of 3FY Med25 AcID in presence of increasing concentrations of garcinolic acid demonstrated that garcinolic acid behaves similarly to a H2 site peptide. However, differences in the dose-dependence of Y528/Y432 and Y487/Y515 suggest that two garcinolic acid molecules may bind a single Med25 AcID protein.

Together, HSQC and PrOF NMR of the Med25 AcID-garcinolic acid interaction suggested that garcinolic acid bound tightly and specifically to the H2 site of Med25 AcID. This would indicate that this molecule is capable of orthosteric inhibition of the H2 site. The ability of garcinolic acid to inhibit the Med25-VP16 H1 PPI is either a result of orthosteric inhibition of VP16 H1 in instances when this peptide is bound at the H2 site or allosteric inhibition of the H1 site. However, a lack of HSQC chemical shift perturbations in the H1 site makes the latter less likely than the former. Orthosteric inhibition of VP16

H1 at the H2 site would not be surprising considering mutagenesis experiments that suggested VP16 H1 bound at both the H1 and H2 sites.

Biochemical characterization of the CBP KIX-garcinolic acid interaction

Concurrent with the definition of the Med25-garcinolic acid interaction, similar experiments were performed to characterize the CBP KIX-garcinolic acid interaction. ^1H - ^{15}N -HSQC experiments were performed in which garcinolic acid was complexed with ^{15}N -labeled CBP KIX at 0, 0.25, 0.5, and 1.5 equivalents of small molecule relative to protein. This data provided dose-dependent chemical shift perturbations in resonances corresponding to several CBP KIX residues (Figures A.12, A.13, A.14). Peaks in each of the collected spectra were assigned to specific residues using a previously published NMR assignment¹⁶.

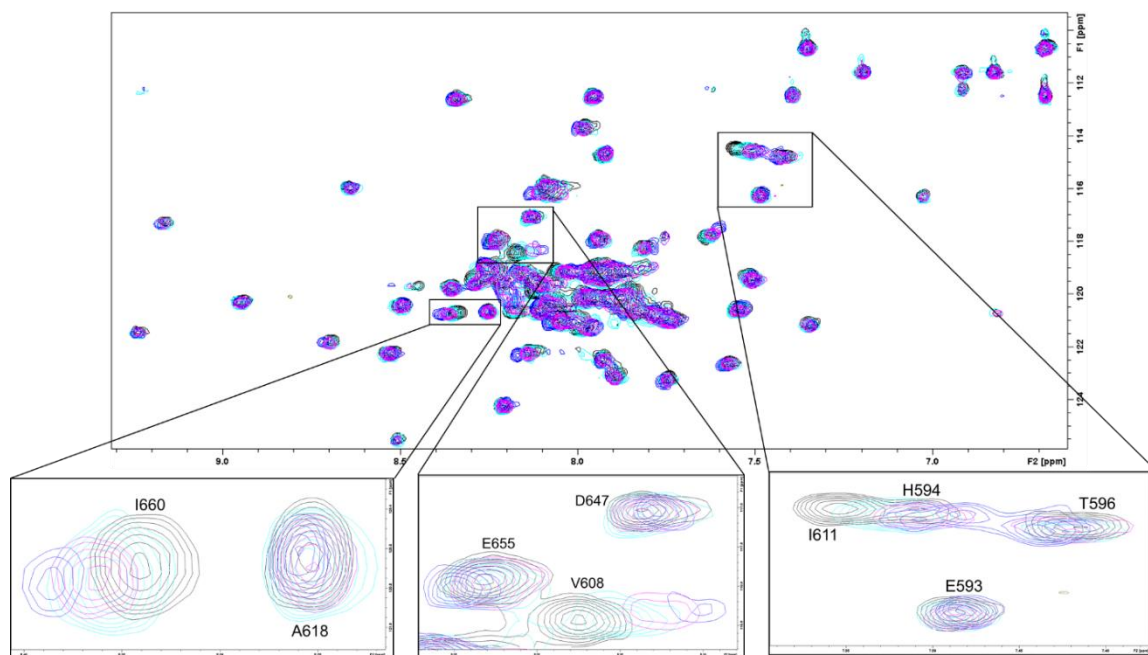


Figure A.12. ^1H - ^{15}N -HSQC NMR spectra of CBP KIX-garcinolic acid complexes. Overlay of the HSQC spectra of ^{15}N -labeled Med25 Acid with DMSO (black), 0.25 eq. of garcinolic acid (light blue), 0.5 eq. (light blue), and 1.5 eq. (black) is shown.

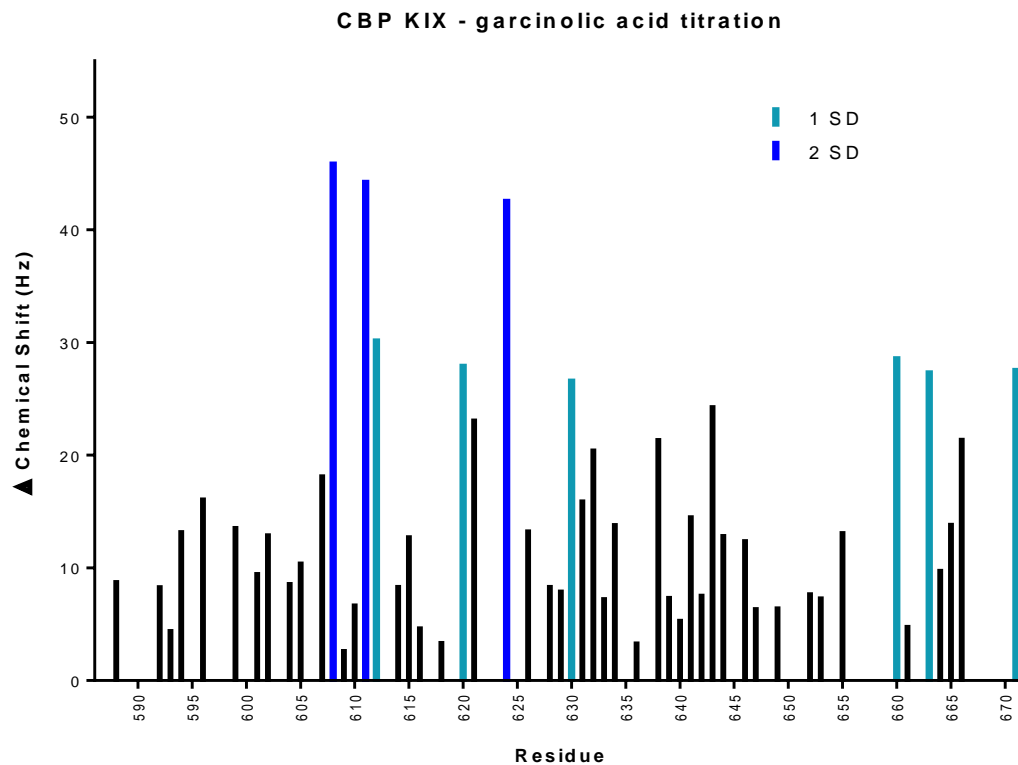


Figure A.13. Chemical shift perturbations within CBP KIX induced by saturating garcinolic acid conditions. The magnitude of chemical shift perturbations caused by complexation of ^{15}N CBP with 1.5 eq. garcinolic acid. Residues that shift 1-2 (light blue) and >2 standard deviations (dark blue) are significantly perturbed.

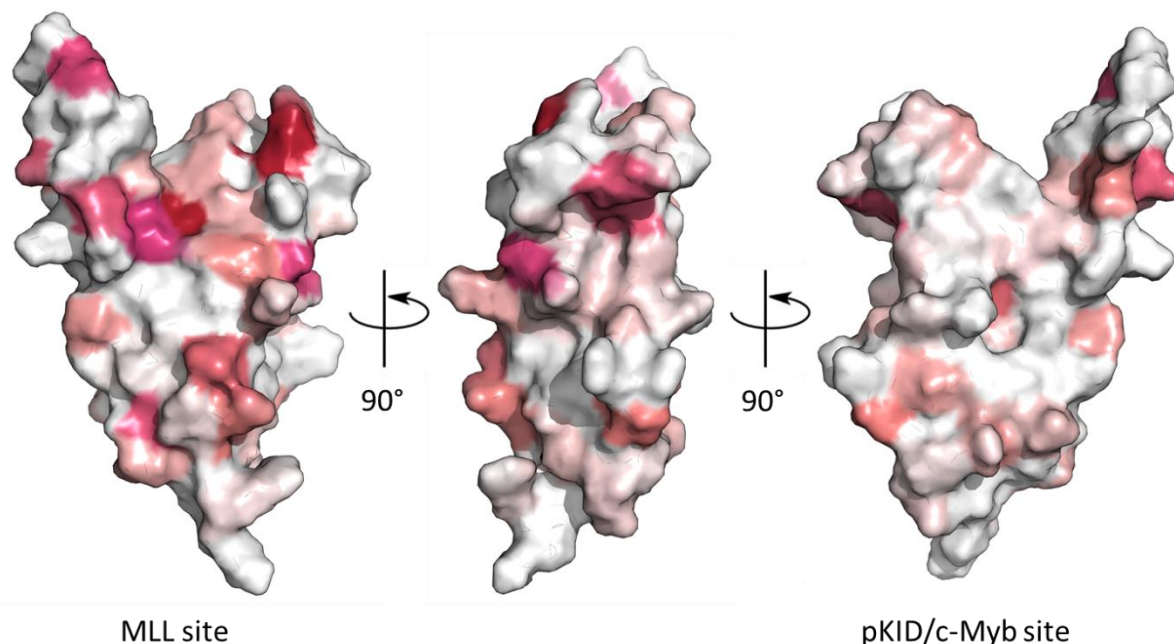


Figure A.14. Chemical shift perturbations induced by garcinolic acid mapped on CBP KIX. Mapped onto the structure of CBP KIX (2AGH) are chemical shift perturbations upon binding to 1.5 eq. garcinolic acid. Increasing shades of red indicate a gradient of increasing chemical shift perturbations. Garcinolic acid significantly affects residues within the MLL site and are 90° from the MLL site at a $\alpha1/\alpha2$ cleft

The HSQC NMR titration demonstrated that garcinolic acid induced significant chemical shift perturbations within the MLL site of CBP KIX (I611, F612, R624, I660, and E663). Critically, while there are minor chemical shift perturbations at the pKID/c-Myb site, zero residues within this site of CBP KIX are significantly perturbed. These data are consistent with garcinolic acid binding orthosterically at the MLL site. Interestingly, a few residues that are 90° from the MLL site at a cleft formed by $\alpha1$ and $\alpha2$ – V608, L620, and A630 – are also significantly perturbed at the highest tested garcinolic acid condition (1.5 eq. small molecule). These perturbations could be induced by allosteric or through-molecule effects induced by garcinolic acid at the MLL site. Alternatively, this region of CBP KIX could represent a second binding location. This would suggest either a 1:1 binding model in which both the MLL site and this binding site share a similar affinity for

garcinolic acid or a 2:1 binding model in which a second molecule binds at this site before, or after, a binding event at the MLL site.

PrOF NMR spectra of 3FY CBP KIX in complex with increasing concentrations of garcinolic acid (0, 0.1, 0.5, 1 and 2 equivalents of small molecule relative to protein) were collected (Figure A.15). 3FY CBP KIX contains five Tyr residues, all of which can be resolved in PrOF NMR spectra. Critically, for this protein-ligand interaction, only one of these Tyr residues, Y631, is in the proximity of the MLL site. Y631 is located on $\alpha 2$ of CBP KIX and sits near the base of the MLL site. In PrOF experiments, as expected, none of the other Tyr residues is affected by the presence of garcinolic acid, consistent with the molecule not binding near or within the pKID/c-Myb site. However, interestingly, garcinolic acid also did not perturb Y631 at 0.1 or 0.5 eq. relative to Med25 AcID and only provided a mild perturbation at 1 eq. molecule. At 2 eq. garcinolic acid, the chemical shift of Y631 was significantly perturbed. This delayed perturbation of Y631 could indicate that garcinolic acid either binds at the 'top' of MLL near the loop between $\alpha 1$ and $\alpha 2$ or at the 'third' site 90° from the MLL site at the cleft formed by $\alpha 1/\alpha 2$ (Figure A.16). Y631 is next to A630, one of the significantly perturbed residues in HSQC NMR experiments that residues within this alternative site. Note that the demonstrable loss in signal-to-noise observed in the PrOF NMR spectra of 3FY CBP KIX in complex with 2 eq. garcinolic acid is thought to have resulted from precipitation of protein during the experiment, which would thereby increase the relative ratio of garcinolic acid to protein as data was being collected.

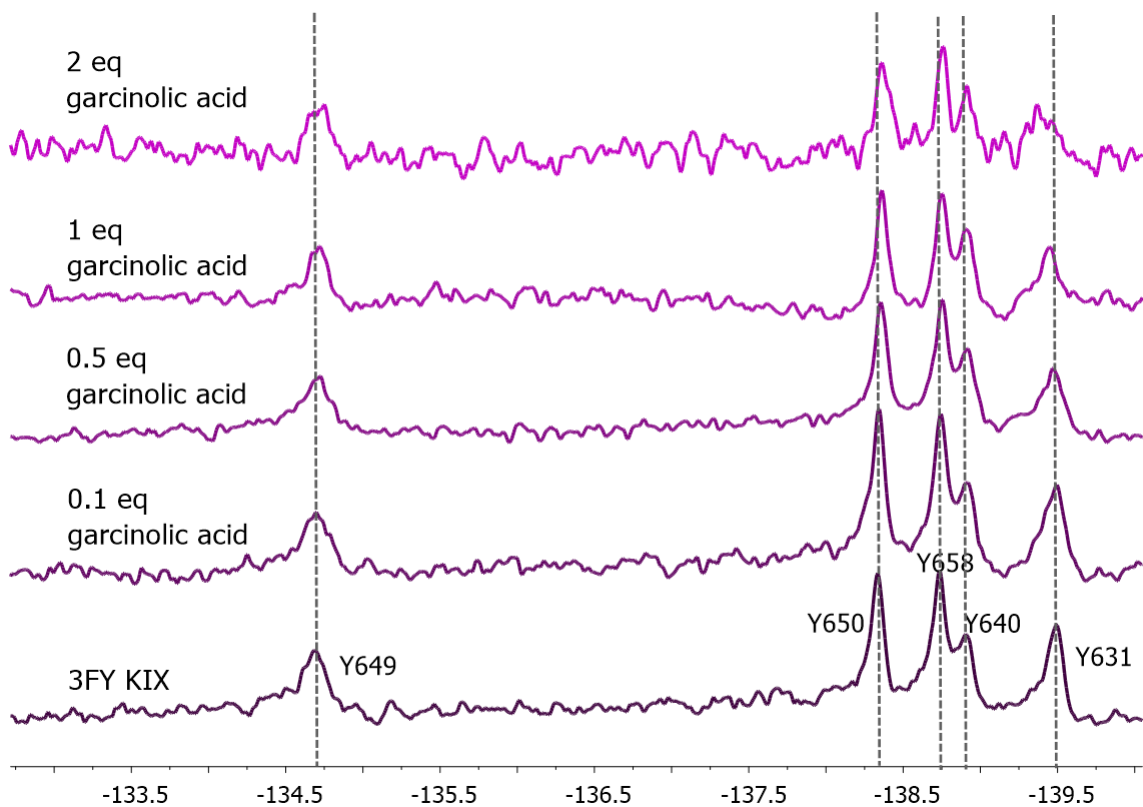


Figure A.15. ProOF NMR of 3FY CBP KIX in complex with garcinolic acid. Spectral analysis of 3FY CBP in presence of increasing concentrations of garcinolic acid demonstrated a significant, dose-responsive chemical shift perturbation of Y631 (located in proximity of the MLL site). None of the Tyr residues in proximity of the pKID site were perturbed, consistent with the HSQC NMR data.

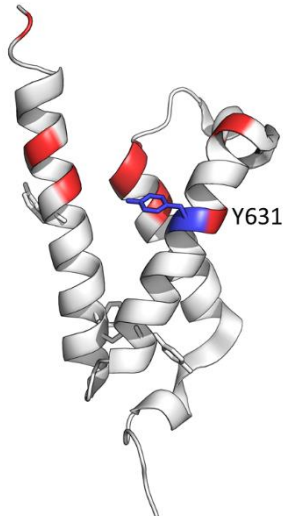


Figure A.16. Garcinolic acid likely binds near the MLL site within CBP KIX. NMR methodologies demonstrates that garcinolic acid causes significant chemical shift perturbations near the MLL site. Residues perturbed in HSQC NMR experiments are shown in red; Y631, the only 3FY residue perturbed in ProOF NMR, is depicted as sticks in blue.

The NMR experiments with CBP KIX and garcinolic acid demonstrated that the molecule binds to the protein at either the MLL site and that a second binding event could occur at the putative 'third' site located 90° from the MLL site in a cleft at $\alpha1/\alpha2$. This result suggests that garcinolic acid is an orthosteric inhibitor of the KIX-MLL PPI and an allosteric inhibitor of the KIX-cMyb PPI.

Conclusions

Garcinolic acid is a potent, single-digit micromolar inhibitor of the AcID domain of Med25 AcID and the KIX domain of Med15, CBP, and p300. Because these two domains are structurally divergent, the modes of recognition for garcinolic acid interactions were desired. Subsequent NMR data suggest that garcinolic acid likely interacts with unique sites of both Med25 AcID (H2 site) and CBP KIX (MLL site). However, these data also demonstrate that garcinolic acid likely binds both proteins in multiple orientations and/or

with >1:1 stoichiometry. These modes of recognition suggest that garcinolic acid, a rigid and negatively charged molecule, likely will not allow for selective inhibition of unique Med25 AcID functions in cellular experiments due to off-target effects and nonspecific binding interactions.

D. Follow-up of a Natural Product Extracts screen against Med25-ERM

Small molecules that target the coactivator Med25 AcID and its protein-protein interaction (PPI) are desired to allow for the study of Med25 AcID function in cellular and disease contexts. Natural products demonstrate, as evidenced by the examples of norstictic acid and the 34913 lipopeptide as described in this dissertation, a large class of molecules that exhibit chemical properties (e.g. conformational plasticity, structural complexity) that are useful in targeting coactivator-activator complexes that typically involve large surface areas and low binding affinity. To discover novel natural product inhibitors of this complex, two former graduate students in the Mapp lab, Steve Sturlis and Paul Bruno, designed a fluorescence polarization-based competition assay to screen the Med25-ERM PPI against a Natural Product Extracts (NPE) library (33,400 total Extracts) maintained by the Center for Chemical Genomics (Life Sciences Institute, University of Michigan). This highly diverse chemical library of partially fractionated extracts has been cultivated from a collection of sediments, cyanobacteria and sponges from across the world. Note that a single extract contains a majority of the organic matter produced by a single microbe (*i.e.* one extract \neq one compound). A primary screen of the full NPE library gave a Z' score of 0.78. Obvious false positives (previously known reactive/fluorescent extracts) were eliminated from the initial hits prior to subjecting those initial hits to a dose-response assay and a selectivity filter designed to eliminate compounds that inhibited unrelated PPIs, other activator-coactivator PPIs, and protein-DNA interactions. At the conclusion of this screening strategy, 332 natural product extracts were validated hits that required further study.

Secondary confirmation of inhibitory activity of validated hit extracts

Prior to isolation of the inhibitory molecules-of-interest, validated hit extracts must be reproduced for secondary confirmation of their activity. This is necessary to confirm that the activity demonstrated in the primary screen was not a result of degradation of the sample and that the inhibitory molecule-of-interest can be reproducibly biosynthesized by the producing microbial strain.

Table A.2. Natural Product Extracts selected for initial follow-up after the NPE primary screen. (Table prepared by Steve Sturlis)

	Strain	CCG Identifier	% ERM•AcID Inhibition	Parallel Fluorescence	% Fluorescence Quenching	% Gal4(DBD)•DNA Inhibition	% MLL•KIX Inhibition	Promiscuity Filter
A	06131R	SID-142998	56.3	35430	-6.1	-47.7	-7.9	2
B	12587-2Z	SID-143065	83.2	37498	3	-32.8	9.1	5
C	32294-H1Z	SID-142868	82.1	35766	3.1	-103.6	13	5
D	34908-2Z	SID-142867	83.2	35799	-3.7	-108.6	8.2	2
E	54916-1C	SID-141597	75	38438	-26.3	-101.4	7.9	4
F	78874R	SID-143056	65.5	36958	-6.5	-10.1	9.9	3
G	91085R	SID-142997	85.2	35887	-8.6	30.6	7.1	4
H	PAN101-7I	SID-32305	74.1	38049	-20.4	-88.2	9.1	5
I	41445-N3I	SID-31523	80.4	39056	-13.9	-28.7	13.3	8
J	44293-N1N	SID-33128	77.8	38368	-21.9	-90.4	-0.9	8
K	71961N	SID-69043	70	38711	-14.3	-53.4	3.4	5
L	41429-N1I	SID-68148	82.3	39516	-28.6	-85.4	4.1	4
M	39040-1I	SID-27645	64.4	39972	-15.1	-68.2	1.7	6
N	68157N	SID-32195	55.1	36047	-3.1	-20.7	-1	3
O	36180-2N	SID-31830	57.4	37403	-10	-16.4	3.9	4
P	49546-N4I	SID-68085	52	39949	-14.7	-52.7	-4.3	8
Q	52245-N2N	SID-33188	101.7	35559	-18.2	11.9	20	5
R	58236N	SID-140604	79.9	33193	-0.3	-7.9	9.3	5
S	65440-N1N	SID-68121	70	36498	-10.3	-34.5	6.5	3
T	71747Z	SID-142274	81.2	38212	-16.8	-74	10.8	4
U	86815-N2Z	SID-143008	102.5	38773	-8.9	-19.8	40.1	4
V	5538-A2N	SID-33057	86.2	38027	-19	-54.9	7.1	7
W	18163-N13Z	SID-142848	96.6	33242	3.9	-66.3	27.3	4
X	24815-H2Z	SID-142871	90.4	33750	32.7	-33	24.1	4
Y	55270-N4N	SID-68851	73.7	39860	-18.4	-60.5	2.8	4
Z	74604-N1I	SID-140915	74	38202	-18.3	-45.9	6.1	3
AA	82349-N4I	SID-140914	73.6	37721	-13.3	-39.7	7.2	2
BB	20731-H2I	SID-18195	77	34656	-5.9	-4.5	2.2	10
CC	73401N	SID-140641	57	36386	-10.6	-46.6	5.1	2
DD	67360-N9N	SID-68685	70.1	35517	-3.6	-18	11.4	4
EE	84215-1I	SID-141865	100.5	35290	-4.5	-33.1	16.7	3

Of the 332 inhibitory extracts obtained from the screening strategy, thirty-six were selected for initial follow-up (Table A.2). This subset was chosen to maximize potential biological diversity as related to location of the collection (i.e. Red Sea, Costa Rica, etc.), the culture medium required for the organism to produce secondary metabolites, and the

degree of inhibitory activity against the Med25 PPI interface. Additionally, preference was given to extracts that had been rarely, if ever, identified previously in other high-throughput screening efforts against this Extracts library. For each of the thirty-six selected extracts, the producing microbial strain were individually re-grown in an identical manner (number of days, temperature, media conditions) as the original sample that gave a validated hit in the primary screen (Figure A.17). These microbial growths all started from frozen spore stocks maintained by Pam Schultz and the Sherman lab. Using the spore stocks, microbial strains were streaked onto oatmeal plates for 3-5 days before transferring the microbe to 3 mL ISP2 media for 5-7 days. These cultures were then transferred to 100 mL of media for growth and secondary metabolite production (8-30 days at 37 °C. At the end of the growth, microbial strains were centrifuged and XAD-16 resin was added to the supernatant. After incubation with the supernatant, the XAD-16 resin, impregnated with all of organic material produced by the microbe, was sequentially extracted with two solvent systems – 50:50 methanol:acetone, and dichloromethane. Of the thirty-six selected strains, thirty-one were successfully re-grown and their organic material extracted; The other five microbial strains did not start to grow after initial streaking out on oatmeal plates.

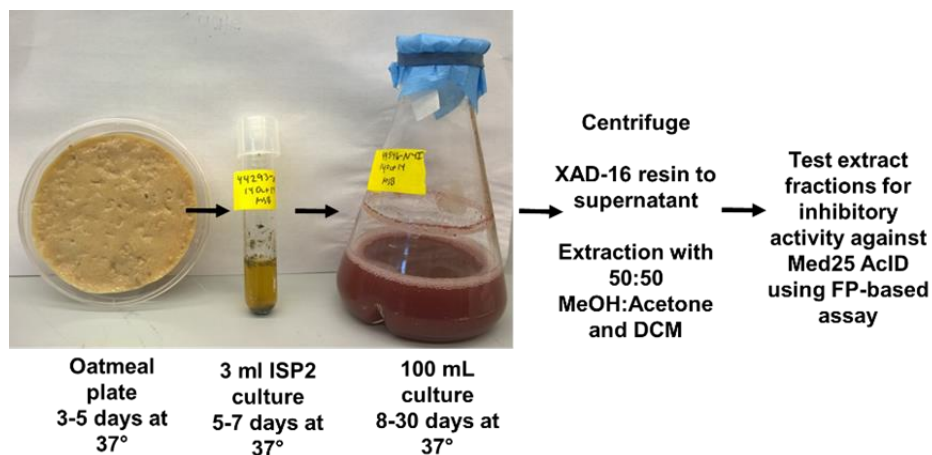


Figure A..17 Workflow for the re-growth of NPE strains from the primary screen.

After successful culturing and extraction of each microbial strain, a FP competition assay against Med25-ERM, as performed in the initial HTS, was performed. Additionally, a previously validated Med25-dependent luciferase reporter assay, as described in Chapter 4, was performed to test the ability of extracts to inhibit Med25 AcID function in a cellular context (Figure A.18). Collectively, these data demonstrated that fourteen of the originally chosen thirty-six unique extracts exhibit inhibitory activity *in vitro* and *in cellulo*. (Table A.3). These strains represented excellent starting points for large-scale growths and bioassay-guided fractionation to identify active compounds.

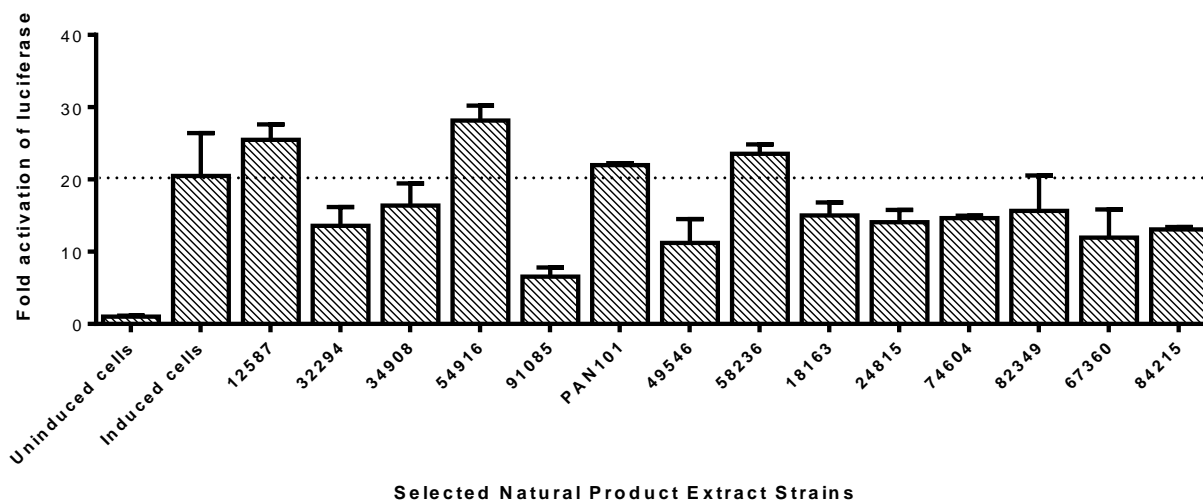


Figure A.18 Inhibitory activity of selected Natural Product Extract Strains in Med25-dependent luciferase assay. All successfully re-grown strains were tested in a Med25-dependent luciferase reporter assay; A selection of the data are shown above. The dotted line indicates the negative control; Notably, the NPR strain 91085 demonstrated excellent inhibitory activity. (Performed with Paul Bruno)

Table A.3 Analysis of inhibitory activity of re-grown NPE strains. Fourteen of thirty-one NPE, highlighted in yellow, demonstrated good inhibition *in vitro* (FP assays) and *in cellulo* (luciferase reporter assay).

NPE strain	Inhibition <i>in vitro</i>	Inhibition <i>in cellulo</i>
12587-2Z	Excellent	Good
52245-N2N	Excellent	
54916-1C	Excellent	
78874R	Excellent	Good
82349-N4I	Excellent	No inhibition!
84215-1I	Excellent	No inhibition!
20731-H2I	Above average	No inhibition!
24815-H2Z	Above average	
41445-N3I	Above average	Good
5538-A2N	Above average	Good
58236N	Above average	No inhibition!
71747Z	Above average	Good
71961N	Above average	Good
86815-N2Z	Above average	No inhibition!
91085R	Above average	Excellent

NPE strain	Inhibition <i>in vitro</i>	Inhibition <i>in cellulo</i>
06131R	Good	
18163-N13Z	Good	No inhibition!
32294-H1Z	Good	Good
34908-2Z	Good	Good
36180-2N	Good	
39040-1I	Good	
41429-N1I	Good	Good
44293-N1N	Good	Good
49546-N4I	Good	Good
65440-N1N	Good	
67360-N9N	Good	Good
68157N	Good	
73401N	Good	Good
PAN101-7I	Good	No inhibition!

Medium-scale growth and fractionation of selected microbial strains

Five of the microbial strains that demonstrated inhibitory activity *in vitro* and *in cellulo* following re-growth on small-scale were selected for medium-scale growth and subsequent bioassay-guided fractionation for isolation of active compounds (Table A.4).

Table A.4 NPE strains grown at medium-scale. Growth conditions are provided. Note that 91085 was co-cultured with Rhoddococcus after one day of microbial growth; 10 mL of Rhoddococcus liquid culture (high OD) was added per 1 L of 91085 culture.

NPE strain	Media conditions	Total growth time	Volume of culture
12587-2Z	A3M	8 days	8 L
33908-2Z	A3M	8 days	8 L
71961N	Nutrient poor	30 days	9 L
41445-N4I	ISP2	15 days	11 L
91085R	A3M	At Day 1 of 9, inoculated with Rhoddococcus	10.5 L

Near the end of microbial growth, on the penultimate day, XAD-16 resin bags (20 g per 1 L culture) were added to growing cultures. After the growth, these resin bags were extracted with three organic solvents – acetone, methanol, and dichloromethane – to remove the organic material contained within. Extracts were then subjected to fractionation using C18 column chromatography. A stepwise gradient of water:acetonitrile (100:0, 90:10, 75:25, 60:40, 45:55, 30:70, 15:85, 0:100) was used to collect eight fractions that were subsequently subjected to FP inhibition assays (Table A.5).

Table A.5 Inhibitory activity of C18 fractionated NPE strains. FP assays were performed to test the activity of C18 fractions of each strain grown on medium-scale to inhibit the Med25-ERM PPI. Fractions were tested at three concentrations of organic material (1.5 mg/mL, 0.75 mg/mL, 0.38 mg/mL) in duplicate. Shown below are the average percent inhibition at 0.75 mg/mL organic material.

	100:0	90:10	75:25	60:40	45:55	30:70	15:85	0:100
12587 DCM	6.07%	1.66%	18.43%	24.72%	26.71%	28.37%	15.45%	36.20%
34908	-72.41%	101.10%	25.83%	38.52%	42.16%	26.16%	4.53%	4.97%
71961	0.88%	17.55%	16.89%	25.83%	15.78%	29.47%	8.17%	0.77%
41445	13.33%	96.47%	59.92%	13.10%	3.33%	-46.16%	27.57%	8.63%
91085	50.63%	45.88%	56.75%	46.35%	35.41%	-1.57%	21.29%	-4.59%

FP assays of C18 fractions demonstrated that discrete fractions of each NPE contained activity against Med25-ERM. In particular, the 90:10 and 45:55 fractions of NPE strain 34908 (101% and 42% inhibition, respectively, at 0.75 mg/mL), the 90:10 and 75:25 fractions of NPE strain 41445 (96% and 60% inhibition, respectively, at 0.75 mg/mL), and the 100:0, 90:10, 75:25, 60:40 fractions of NPE strain 91085 (51%, 46%, 57%, and 46%

inhibition, respectively, at 0.75 mg/mL) demonstrated sufficiently high inhibitory activity to encourage further purification by HPLC.

Analytical HPLC runs of each of the aforementioned C18 fractions were performed to assess the complexity/total number of potential compounds contained within. These analytical runs suggested that the 90:10 and 75:25 fractions of NPE strain 91085 could be readily separated to produce purified compounds. HPLC runs of the C18 fractions of 34908 and 41445 appeared to be complex enough that they were initially passed over to focus on purification of 91085. In addition to the relative lack of complexity within the HPLC analytical runs, the 91085 strain was prioritized because it was the most potent NPE strain in the Med25-dependent luciferase assay performed during the secondary validation of hits.

Investigation of NPE strain 91085

The medium-scale culture (10.5 L) of 91085 was further fractionated after C18 chromatography using HPLC. Many different HPLC methods and columns were attempted throughout the entirety of this investigation. To simplify the discussion, a small fraction of all attempted experiments are described below.

The C18 75:25 fraction was purified using a gradient of 10-30% acetonitrile over 15 min followed by 30-40% acetonitrile over 30 min (7 mL/min) using a C18 preparative column on a Beckman HPLC. Collected fractions were tested for inhibition against Med25 (Figure A.19) to discover that two peaks contained activity and were carried ahead into further purifications. As an example, Fraction 22 from that HPLC purification was further fractionated using a gradient of 15-17.5% acetonitrile (0.1% formic acid) over 20 min

followed by 17.5-35% acetonitrile (0.1% formic acid) over 10 min (4 mL/min) with a C18 semi-preparative column on a Beckman HPLC. (Figure A.20)

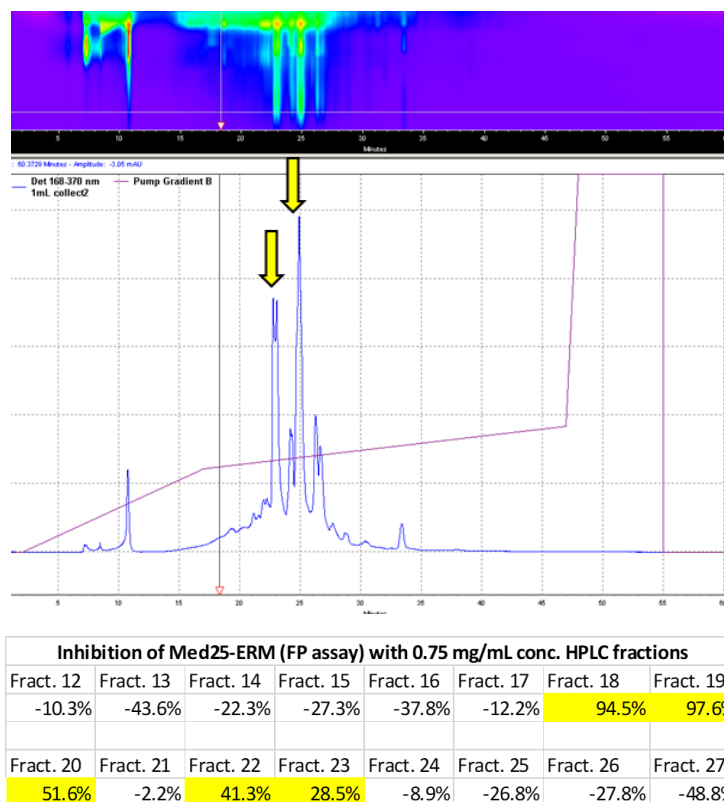
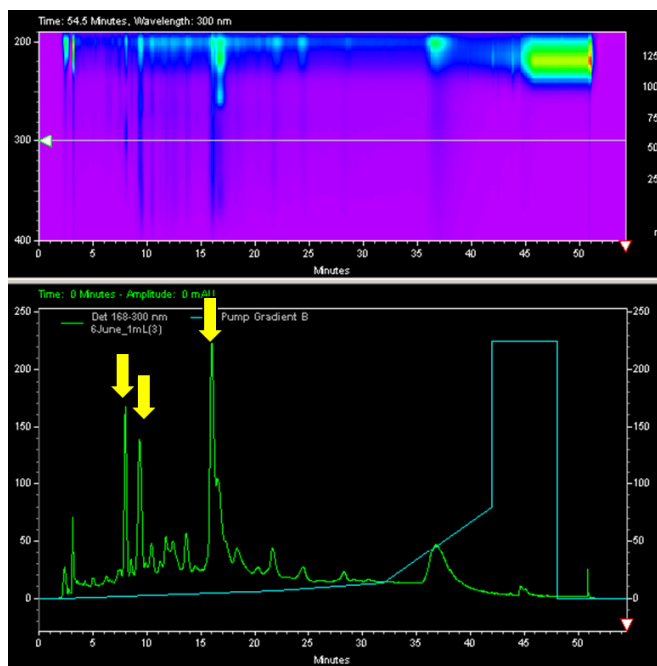


Figure A.19. HPLC purification of 91085 C18-75:25. Representative HPLC chromatogram of 91085 C18-75:25. Beckman HPLC; C18 preparative column; Gradient - 10-30% acetonitrile over 15 min followed by 30-40% acetonitrile over 30 min (7 mL/min); Peaks indicated by yellow arrows (Fract. 18-20 and 22-23) were active against Med25-ERM PPI, as demonstrated in the supplied table.



Inhibition of Med25-ERM (FP assay) with 0.75 mg/mL conc. HPLC fractions									
7.5 min	8 min	8.5 min	9 min	9.5 min	15 min	15.5 min	16 min	16.5 min	36-39 min
99.7%	60.8%	73.3%	74.5%	71.3%	81.9%	54.1%	67.9%	61.2%	-79.0%

Figure A.20. HPLC purification of 91085 C18-75:25/HPLC-22. Representative HPLC chromatogram of 91085 C18-75:25/HPLC-22 (Fraction 22 collected in Figure A.). Beckman HPLC; C18 semi-preparative column; 15-17.5% acetonitrile (0.1% formic acid) over 20 min followed by 17.5-35% acetonitrile (0.1% formic acid) over 10 min (4 mL/min); Peaks indicated by yellow arrows (8 min, 9 min, 15.5 min) were active against Med25-ERM PPI, as demonstrated in the supplied table.

As indicated in Figure A, the purification of 91085 C18-75:25/HPLC-22 produced three active peaks. Each of these was tested for inhibition in the Med25-dependent luciferase assay that had been previously utilized successfully against crude NPE extracts (Figure A.21). One of these partially purified fractions, termed “91085 C18-75:25/HPLC-22/HPLC-15.5 min”, demonstrated dose-responsive inhibition of Med25 function within this assay, suggesting that an active molecule was contained within this fraction. Unfortunately, at this stage, after a C18 purification and two sequential HPLC purifications, there was a very small amount of this partially purified material, much less than a milligram and not enough to collect a full suite of NMR data for structural

elucidation. In order to follow up this active fraction, it was necessary to grow more of the 91085 strain and on a much larger scale.

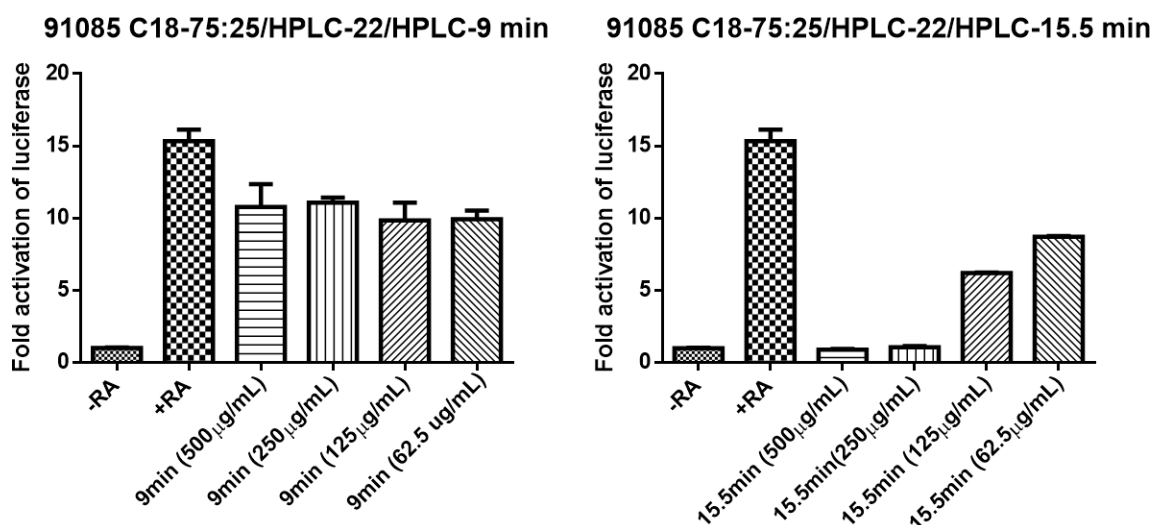


Figure A.21 Cellular activity of 91085 C18-75:25/HPLC-22/HPLC-15.5 min. Partially purified compounds from 91085 that have undergone C18 fractionation and two HPLC purifications were tested in a Med25-dependent luciferase assay. 91085 C18-75:25/HPLC-22/HPLC-15.5 min (See Figure A) demonstrated dose-dependent inhibition of luciferase production.

A 40 L growth was performed to generate more 91085 extract to enable isolation of active molecules in higher quantities. This growth was performed as before, although it is possible that there may have been slight differences in water composition due to seasonal variation. After the growth, extraction, and C18 fractionation, the 75:25 fraction from C18 was subjected to similar HPLC methods as had been previously used to purify 91085 C18 75:25. Unfortunately, the composition of the organic compounds within this C18 fraction appeared to be rather different than the same fraction from the medium-scale growth (Figure A.22). This suggested that the production of 91085 is not particularly reproducible and hinted that problems might lie ahead.

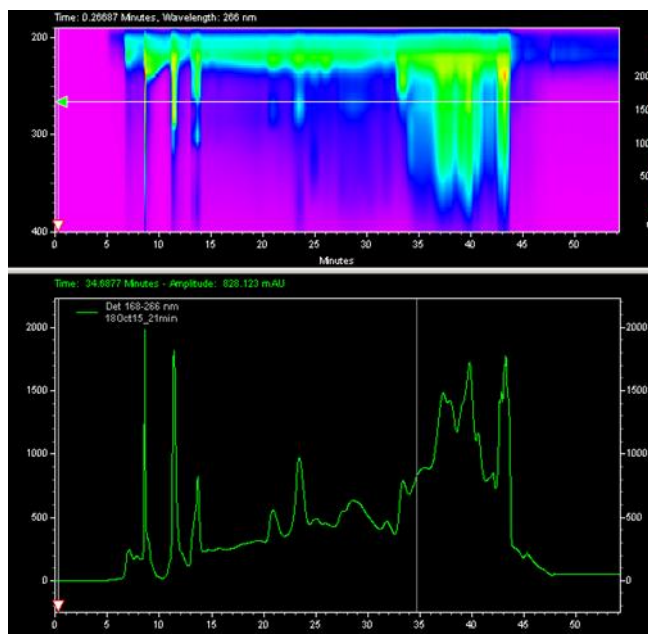


Figure A.22 HPLC purifications of 91085 C18-75:25 are not reproducible from one growth of 91085 to the next. 91085 was grown on large-scale (40 L) to acquire more material for compound isolation; HPLC analysis of 91085 C18-75:25 after this growth is *very* different than after first medium-scale (10.5 L) growth (See Figure A) Beckman HPLC; C18 preparative column; Gradient - 10-30% acetonitrile over 15 min followed by 30-40% acetonitrile over 30 min (7 mL/min);

Instead of focusing on the C18 75:25 fraction from the large-scale growth, further efforts sought to isolate active compounds from the C18 60:40 fraction. Additionally, to decrease the added sample complexity that was being demonstrated by the large-scale growth, all active C18 fractions were fractionated using size-exclusion chromatography (SEC) prior to continued HPLC purifications. Following this SEC purification, the C18 60:40 fraction from the large-scale was purified by HPLC. After several trials, this fraction was purified using an isocratic method (15% acetonitrile) with a C18 semi-preparative column on a Shimadzu HPLC. A large quantity of material (~18 mg) was partially purified as “28.5 min”. A subsequent HPLC purification of this peak using an isocratic method (35% methanol) with a C18 semi-preparative column on a Shimadzu HPLC provided a purified molecule, termed “91085 C18-60:40/HPLC-“28.5min”/HPLC-137” (Figure A.23).

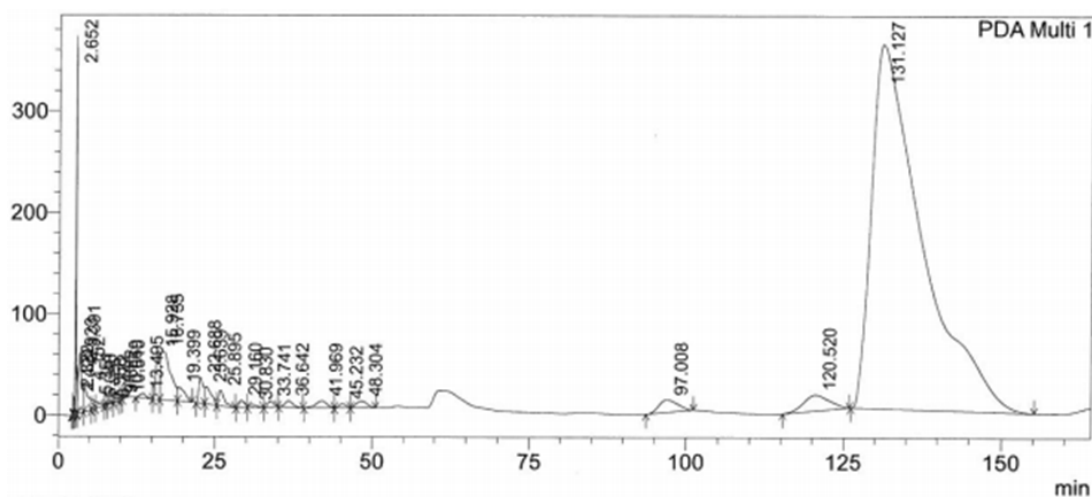
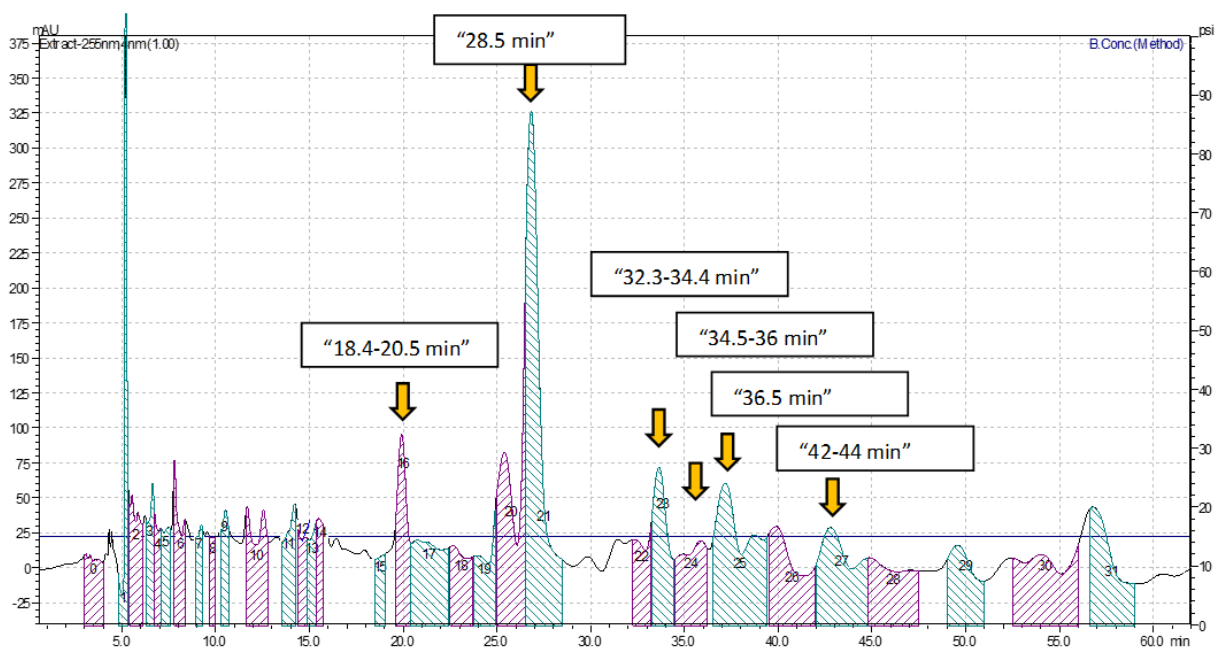


Figure A.23 Sequential HPLC purifications of 91085 C18-60:40. (A) Representative HPLC purification of 91085 C18-60:40. Isocratic method (15% acetonitrile) with C18 semi-prep column on Shimadzu HPLC. Active peaks are indicated by yellow arrows. (B) HPLC purifications of 91085 C18-60:40/HPLC-“28.5min” provided a pure molecule. Isocratic method (35% methanol) with C18 semi-prep column on Shimadzu HPLC.

The molecule was sufficiently pure and in high enough quantity to allow for a complete set of NMR data (^{13}C , ^1H , HSQC, HMBC, COSY) to be collected (Figure A. 24).

Unfortunately, however, this molecule was a poor inhibitor of the Med25-ERM PPI with

an IC_{50} of $818 \pm 129 \mu\text{M}$. At that point, the NMR data was left to be unanalyzed and different avenues were pursued to identify potent molecules from 91085.

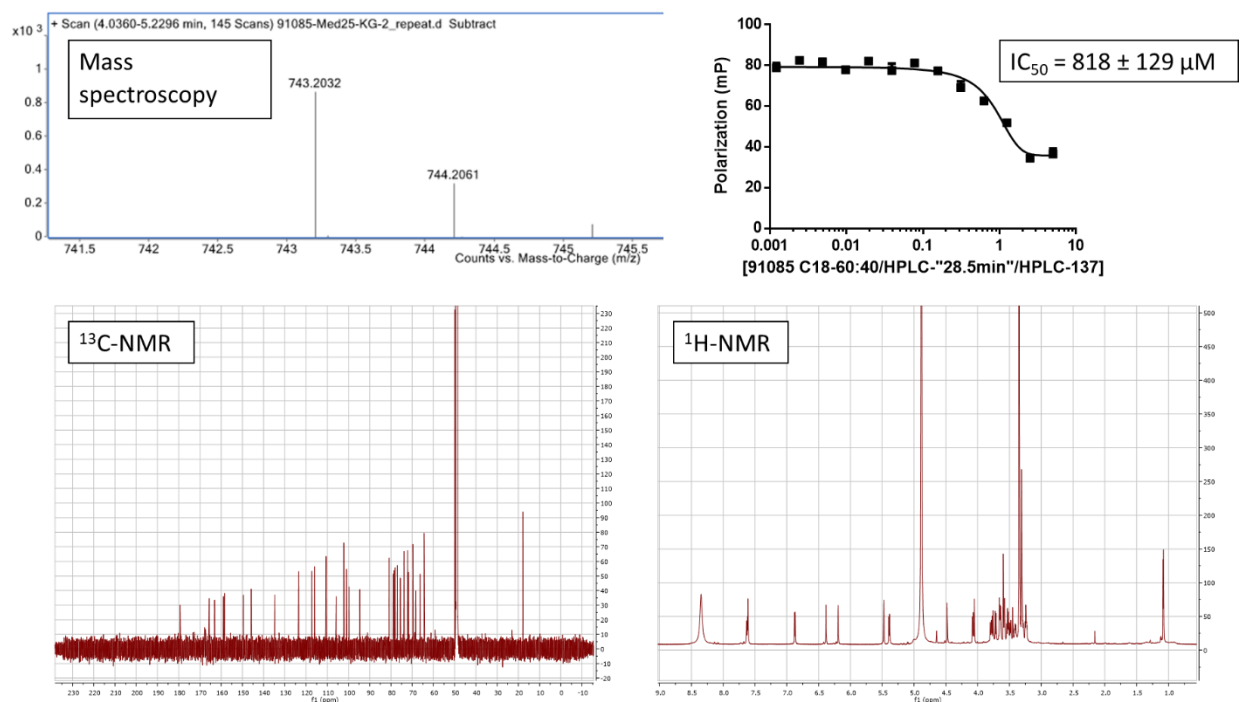


Figure A.24 Characterization of 91085 C18-60:40/HPLC-"28.5min"/HPLC-137. A pure molecule was identified; NMR and mass spectroscopy data was collected but not fully analyzed. This identified molecule demonstrated weak inhibition with an $IC_{50} = 818 \pm 129 \mu\text{M}$ against the Med25-ERM PPI.

The general story of 91085 C18-60:40/HPLC-"28.5min"/HPLC-137 played out two additional times. The exact reasons (*e.g.* PEG contamination of unknown origin) differed but the end result remained the same. The only identified molecules, of which four have been sufficiently purified, have proven to be poor inhibitors of Med25 Acid function. It should be noted that among those four molecules, complete NMR data sets and high resolution mass spectroscopy for three, termed 91085 C18-60:40/HPLC-"28.5min"/HPLC-137, KG-58, and KG-59, have been collected. Structural elucidation of these molecules could be incredibly beneficial in determining whether 91085 should be further pursued. It is possible that the discovered molecules are analogues of the actual

inhibitor(s) contained within Med25 Acid. To highlight this possibility, consider that norstictic acid is potent inhibitor of Med25 Acid ($IC_{50} \sim 2.5 \mu\text{M}$) but that a closely related compound, stictic acid, has no inhibitory activity against Med25 Acid ($IC_{50} \gg 250 \mu\text{M}$) (Figure A.25)

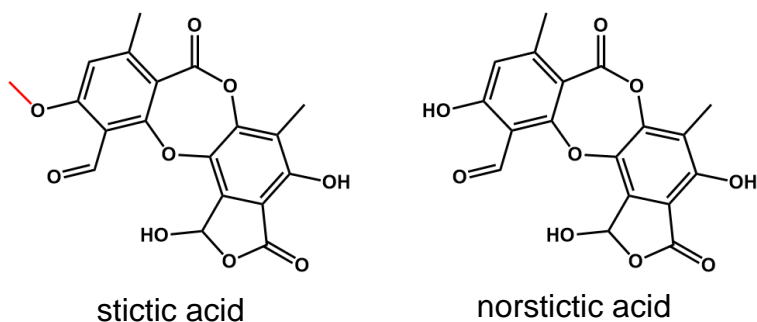


Figure A.25 Comparison of stictic acid and norstictic acid. Methylation of a phenol group is the only structural difference between a potent Med25 inhibitor (norstictic acid) and an inactive molecule.

References

1. Thakur, J. K., Yadav, A. & Yadav, G. Molecular recognition by the KIX domain and its role in gene regulation. *Nucleic Acids Res.* **42**, 2112–2125 (2014).
2. Radhakrishnan, I. *et al.* Solution Structure of the KIX Domain of CBP Bound to the Transactivation Domain of CREB: A Model for Activator:Coactivator Interactions. *Cell* **91**, 741–752 (1997).
3. Lee, C. W., Arai, M., Martinez-Yamout, M. A., Dyson, H. J. & Wright, P. E. Mapping the Interactions of the p53 Transactivation Domain with the KIX Domain of CBP. *Biochemistry (Mosc.)* **48**, 2115–2124 (2009).
4. Wang, F. *et al.* Structures of KIX domain of CBP in complex with two FOXO3a transactivation domains reveal promiscuity and plasticity in coactivator recruitment. *Proc. Natl. Acad. Sci.* **109**, 6078–6083 (2012).
5. Pinna, L. A. & Ruzzene, M. How do protein kinases recognize their substrates? *Biochim. Biophys. Acta* **1314**, 191–225 (1996).
6. Meggio, F. & Pinna, L. A. One-thousand-and-one substrates of protein kinase CK2? *FASEB J.* **17**, 349–368 (2003).
7. De Guzman, R. N., Goto, N. K., Dyson, H. J. & Wright, P. E. Structural Basis for Cooperative Transcription Factor Binding to the CBP Coactivator. *J. Mol. Biol.* **355**, 1005–1013 (2006).
8. Gao, Y. & Wang, H. -y. Casein Kinase 2 Is Activated and Essential for Wnt/beta-Catenin Signaling. *J. Biol. Chem.* **281**, 18394–18400 (2006).
9. Polakis, P. Wnt Signaling in Cancer. *Cold Spring Harb. Perspect. Biol.* **4**, (2012).
10. Jonker, H. R. A., Wechselberger, R. W., Boelens, R., Folkers, G. E. & Kaptein, R. Structural Properties of the Promiscuous VP16 Activation Domain †. *Biochemistry (Mosc.)* **44**, 827–839 (2005).
11. Vojnic, E. *et al.* Structure and VP16 binding of the Mediator Med25 activator interaction domain. *Nat. Struct. Mol. Biol.* **18**, 404–409 (2011).
12. Milbradt, A. G. *et al.* Structure of the VP16 transactivator target in the Mediator. *Nat. Struct. Mol. Biol.* **18**, 410–415 (2011).
13. Bontems, F. *et al.* NMR structure of the human Mediator MED25 ACID domain. *J. Struct. Biol.* **174**, 245–251 (2011).
14. Nishikawa, J. L. *et al.* Inhibiting fungal multidrug resistance by disrupting an activator–Mediator interaction. *Nature* **530**, 485–489 (2016).
15. Thakur, J. K. *et al.* A nuclear receptor-like pathway regulating multidrug resistance in fungi. *Nature* **452**, 604–609 (2008).
16. Wang, N. *et al.* Ordering a Dynamic Protein Via a Small-Molecule Stabilizer. *J. Am. Chem. Soc.* **135**, 3363–3366 (2013).